



<http://waikato.researchgateway.ac.nz/>

Research Commons at the University of Waikato

Copyright Statement:

The digital copy of this thesis is protected by the Copyright Act 1994 (New Zealand).

The thesis may be consulted by you, provided you comply with the provisions of the Act and the following conditions of use:

- Any use you make of these documents or images must be for research or private study purposes only, and you may not make them available to any other person.
- Authors control the copyright of their thesis. You will recognise the author's right to be identified as the author of the thesis, and due acknowledgement will be made to the author where appropriate.
- You will obtain the author's permission before publishing any material from the thesis.

**DIAGENETIC EVOLUTION OF SOME MODERN
AND ANCIENT COLD SEEP-CARBONATES FROM
EAST COAST BASIN, NEW ZEALAND.**

A thesis
submitted in partial fulfilment
of the requirements for the degree of
Masters of Science in Earth and Ocean Sciences
at the
University of Waikato

by

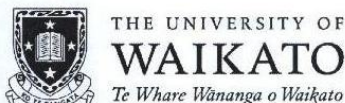
Sarah Maree Ewen



THE UNIVERSITY OF
WAIKATO
Te Whare Wānanga o Waikato

University of Waikato

2009



**DEPOSIT OF MASTERS THESIS , DOCTORAL OR MPHIL THESIS
IN THE UNIVERSITY OF WAIKATO LIBRARY**

| | | |
|--|---|--------------------------|
| Author: | Sarah Maree Ewen | |
| Title of thesis: | Diagenetic evolution of some modern and ancient cold seep-carbonates from the East Coast Basin, New Zealand | |
| Degree: | MSC | Year of submission: 2009 |
| An application to embargo has been made: | Yes | No (circle as required) |
| Termination date of the embargo: | | |

Declaration

I hereby deposit a print and digital copy of my thesis with the University of Waikato Library. I confirm that any changes required by the examiners have been carried out to the satisfaction of my primary supervisor and that the content of the digital copy corresponds exactly to the content of the print copy in its entirety.

This thesis is my own work and, to the best of my knowledge and belief, it contains:

- no material previously published or written by another person, except where this is appropriately cited through full and accurate referencing.
- no material which to a substantial extent has been accepted for the qualification of any other degree or diploma of a university or other institution of higher learning.

I have either used no substantial portions of third party copyright material, including charts, diagrams, graphs, photographs or maps in my thesis, or I have obtained permission for such material to be made accessible worldwide via the internet.

Conditions of use

From the date of deposit of this thesis or the cessation of any approved access restrictions, the conditions of use are as follows:

1. This thesis may be consulted for the purposes of private study or research provided that appropriate acknowledgement is made of its use;
2. The digital copy is made available via the Internet by the University of Waikato Library in downloadable, read-only format with unrestricted access, in the interests of open access to research information, provided that the thesis is not subject to an embargo. Should an embargo be in place, the digital copy will only be made available as set out above once the embargo has been lifted.
3. In accordance with Section 56 of the Copyright Act 1994, the University of Waikato Library may make a copy of this thesis for supply to the collection of another prescribed library on request from that library.

Signed: K.E.

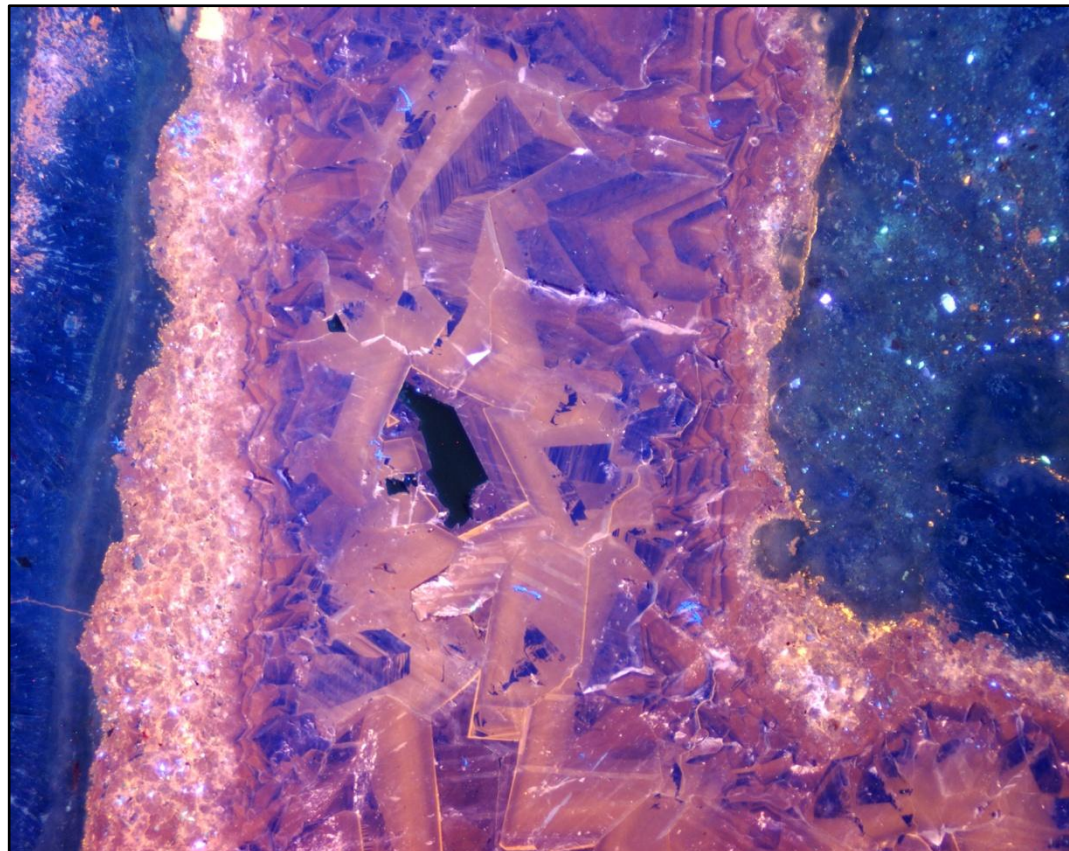
Date: 16/2/2009

I have seen and discussed the content of this form
The Chief Supervisor: C.S. Nelson

Signature: C.S. Nelson

Instructions for use of this form:

This completed and signed form should be bound into the copy of the thesis intended for the University of Waikato Library.



Cathodoluminescent image of a sparry late stage fill in a bivalve. The pink colouring is a result of the alteration of aragonite to calcite, aragonite is found either side of the vug.

The most beautiful experience we can have is the mysterious - the fundamental emotion which stands at the cradle of true art and true science.

Albert Einstein (1949)

Abstract

Cold seep-carbonates are the microbially mediated by-products of the anaerobic oxidation of methane (AOM) at seafloor cold seeps, and are widespread about modern continental margins and in the geologic record. Some modern and Miocene examples of cold seep-carbonates from the East Coast Basin, North Island, New Zealand have been analysed in this study, to characterise and determine their carbonate fabrics, elemental and mineralogical composition, and stable $\delta^{18}\text{O}$ and $\delta^{13}\text{C}$ isotope signatures, so as to provide insights into the diagenetic changes associated with the lithification and burial of seep-carbonates. The ancient samples were collected from the onshore middle Miocene Tauwhareparae (TWP) seep deposit, while the modern samples were obtained from the National Institute of Water and Atmosphere (NIWA) Cruise TAN0616 (November 2006) from Ritchie Ridge, offshore Hikurangi Margin.

A paragenetic sequence of diagenetic events involving early aragonitic phases, followed by late calcitic phases is defined for the seep-carbonates. This sequence likely has relevance for understanding the fluid-cement histories of seep-carbonates more widely. Two main carbonate mineralogies occur in each of the sample groups - modern samples are aragonitic or dolomitic, while the ancient ones consist dominantly of either aragonite or calcite. Thus, aragonite common to both sample groups, and is interpreted to represent the initial primary carbonate precipitate in hydrocarbon seep provinces under specific fluid flux and local pore-water chemistry conditions. Aragonite morphologies range from microcrystalline carbonate ('micarb'), to acicular aragonites that may form botryoids or spherulites. Dolomite occurs in those modern samples which appear to constitute exhumed remnants of a former subsurface 'seep plumbing system', and so are strictly not true seabed 'seep-carbonates', but instead are part of the larger hydrocarbon seep province. Calcite in the ancient samples is either a product of alteration and neomorphic transformation of aragonite, or derives from late stage cementation from burial fluids. As a result of their formation processes, the calcites are generally recrystallised and have equant or 'cellular' textures.

Stable $\delta^{13}\text{C}$ and $\delta^{18}\text{O}$ isotope cross-plots reveal a large spread of values for the sample groups. Ancient samples range from $\delta^{13}\text{C}$ -8 to -50‰ PDB and $\delta^{18}\text{O}$ -5.5 to +2‰ PDB. Modern samples have $\delta^{13}\text{C}$ values from -6 to -41‰ PDB and $\delta^{18}\text{O}$ values ranging from +2.6 to +6.7‰ PDB. The $\delta^{13}\text{C}$ values suggest the majority of the methane that formed these seep-carbonates is of thermogenic origin, although some mixing from other carbon sources may have occurred. The positive $\delta^{18}\text{O}$ signatures are suggestive of carbonate formation during dissociation of gas hydrates, while the negative values possibly indicate that some of the formation fluids were warmer than normal in the 17 – 30°C range.

Acknowledgements

First of all, I would like to thank my Whanau, both my friends and family who have given me love and support throughout this journey. Endless respect and thanks go to Cam Nelson, my primary supervisor. His wealth of knowledge and experience helped the whole project come together. Cam, you kept driving me and did a great job of editing, especially since I couldn't write "scientific" enough. Kathy Campbell, thank you for believing in both myself and my results; without your initial work I would have been blind down the microscope. Steve Hood, the mighty organiser of the cold seeps team, thanks for driving the CL machine, without which my results base would halve. Steph, thank you for everything, you have been my sounding board, my crying shoulder, my field buddy, my neutraliser and my big sister.

Mum and Dad, without you I would not be who I am, and would never have been able to get to where I am today. I will never find the words to say just how much you mean to me; you really should be joint authors. Amy, my best friend no matter what, and no matter where, thanks for the inspiration to keep on with my work as a geeky scientist. Grandy, you are one of my heroes, thank you for love and support, especially when times have been tough. Rob, thank you for your endless support, your motivational speeches and your love; thank you for cooking my food, washing my clothes and drying my tears; this study would not have been finished without you.

I would like to thank Dr Alan Orpin at NIWA Wellington for access to data, images and especially all the beautiful modern samples which made my thesis far more interesting! Thanks to the whole crew of NIWA cruise TAN0616 who collected the samples, especially Ashley Rowden, cruise leader. Thank you to Jens Greinert for advice and images. Early field work locating the paleo-seep sites was done by David Francis, who also provided indispensable help with field work and knowledge of the East Coast Basin. Thanks also go to Chris Hendy and Roger Briggs for discussion on geochemistry within the study.

A well deserved thank you to Xu Ganqing, Renat Radosinsky, Steve Cooke, Jacinta Pareeze, Annette Rodgers, Chris McKinnon, Glen Treweek, Ben Andrew and Barry O'Brien for technical support and lab analyses. A big thanks to Dave Francis, Stephanie Nyman, Kris Saether, Susan Nyman, Steven Hood, Cam Nelson, Dave Ewen, and Rob Bluett for field help. Sydney Wright has also been an amazing help with administration, printing and generally everything.

Funding from AusIMM was most appreciated, as well as the University of Waikato Masters Fees Award and Scholarship. Marsden Fund to the University of Waikato (V083) and to the University of Auckland (06-UOA-082) was the major fund for this project.

And lastly, to Brad, Tehani, Fi, Leah, Justin and Janine, I could not have survived the last two years without you. You are all my besties, thanks for being my rocks. Renee, Areta, Trace, Steph and Sarah, thanks for being there when I needed you; without some ‘normal’ people to talk to I wouldn’t have had a chance at finishing this study!

Table of Contents

| | |
|-------------------|------|
| Title page | |
| Frontispiece | v |
| Abstract | |
| Acknowledgements | vi |
| Table of contents | ix |
| List of figures | xiii |
| List of tables | xvii |

CHAPTER 1 *Introduction*

| | |
|---------------------------|---|
| 1.1 OVERVIEW | 1 |
| 1.2 AIMS OF STUDY | 3 |
| 1.3 COLD SEEP RESEARCH | 4 |
| 1.4 RELATED CONTRIBUTIONS | 5 |
| 1.5 STRUCTURE OF THESIS | 6 |

CHAPTER 2 *Cold Seep Systems*

| | |
|---|----|
| 2.1 INTRODUCTION | 9 |
| 2.2 COLD SEEP SYSTEMS | 10 |
| 2.2.1 Methane seepage | 10 |
| 2.2.2 Anaerobic oxidation of methane (AOM) | 11 |
| 2.2.3 Terminology | 12 |
| 2.3 COLD SEEP RELATED FEATURES | 12 |
| 2.3.1 Tubular concretions | 12 |
| 2.3.2 Mud volcanoes | 14 |
| 2.3.3 Pockmarks | 16 |
| 2.3.4 Gas hydrates | 18 |
| 2.4 COLD SEEP DISTRIBUTION | 19 |
| 2.4.1 Global occurrences | 19 |
| 2.4.2 New Zealand occurrences | 19 |
| 2.4.2.1 <i>Modern New Zealand cold seeps</i> | 20 |
| 2.4.2.2 <i>Ancient New Zealand cold seeps</i> | 21 |
| 2.5 IDENTIFYING COLD SEEPS | 24 |
| 2.5.1 Geometry and structures | 24 |
| 2.5.2 Biota | 26 |
| 2.5.3 Mineralogy | 28 |
| 2.5.4 Isotopic composition | 29 |

CHAPTER 3 *Physical Setting*

| | |
|-----------------------------|----|
| 3.1 INTRODUCTION | 31 |
| 3.2 EAST COAST BASIN | 33 |
| 3.2.1 Regional | 33 |
| 3.2.2 Structure | 34 |
| 3.2.3 East Coast Allochthon | 34 |

| | |
|---|----|
| 3.2.4 Hikurangi Margin | 35 |
| 3.2.5 Fluid flow | 36 |
| 3.2.6 Potential source rocks | 39 |
| 3.3 MIOCENE SEEP-CARBONATES – TAUWHAREPARAE | 40 |
| 3.4 MODERN SEEP-CARBONATES | 43 |
| 3.4.1 Builder's Pencil | 44 |
| 3.4.2 Rock Garden | 45 |

CHAPTER 4 *Methodology*

| | |
|---|----|
| 4.1 INTRODUCTION | 47 |
| 4.2 FIELD TECHNIQUES | 47 |
| 4.2.1 Onshore sampling | 47 |
| 4.2.2 Offshore sampling | 50 |
| 4.3 LABORATORY TECHNIQUES | 52 |
| 4.3.1 Rock sample preparation | 52 |
| 4.3.2 Plane polarised light (PPL) petrography | 53 |
| 4.3.3 Cathodoluminescent light (CL) petrography | 53 |
| 4.3.4 X-ray diffraction | 54 |
| 4.3.4.1 <i>Bulk mineralogy</i> | 54 |
| 4.3.4.2 <i>Component mineralogy</i> | 56 |
| 4.3.5 Stable isotope analysis | 57 |
| 4.3.6 Carbonate percentage determination | 58 |
| 4.3.7 Total organic carbon (TOC) | 58 |
| 4.3.8 Microprobe analysis | 58 |
| 4.3.9 Ultraviolet (UV) light | 59 |

CHAPTER 5 *Stratigraphy and Facies*

| | |
|-------------------------------|----|
| 5.1 INTRODUCTION | 61 |
| 5.2 FIELD RESULTS | 62 |
| 5.2.1 Site description | 62 |
| 5.2.2 Deposit structure | 65 |
| 5.2.3 Stratigraphic column | 66 |
| 5.2.4 Facies analysis | 66 |
| 5.2.4.1 <i>Facies 1</i> | 68 |
| 5.2.4.2 <i>Facies 2</i> | 71 |
| 5.2.4.3 <i>Facies 3</i> | 72 |
| 5.2.4.4 <i>Facies 4</i> | 73 |
| 5.2.4.5 <i>Facies 5</i> | 76 |
| 5.2.4.6 <i>Facies 6</i> | 77 |
| 5.2.4.7 <i>Facies 7</i> | 78 |
| 5.2.4.8 <i>Facies 8</i> | 80 |
| 5.2.5 Facies distribution map | 81 |
| 5.3 DISCUSSION | 82 |

CHAPTER 6 *Tauwhareparae Petrology*

| | |
|-----------------------------|----|
| 6.1 INTRODUCTION | 85 |
| 6.2 PETROGRAPHIC COMPONENTS | 86 |

| | | |
|--------|--|-----|
| 6.2.1 | Aragonitic microcrystalline carbonate (A1) | 86 |
| 6.2.2 | Acicular aragonite (A2) | 89 |
| 6.2.3 | Botryoidal aragonite (A3) | 90 |
| 6.2.4 | Spherulitic aragonite (A4) | 91 |
| 6.2.5 | Cellular calcite (C1) | 91 |
| 6.2.6 | Mottled calcite (C2) | 91 |
| 6.2.7 | Equant calcite (C3) | 93 |
| 6.2.8 | Siliciclastic calcite (C4) | 93 |
| 6.2.9 | Bioclasts (M1) | 95 |
| 6.2.10 | Pyrite (M2) | 96 |
| 6.2.11 | Scattered siliciclastics (M3) | 96 |
| 6.2.12 | Neomorphosed phases | 99 |
| 6.3 | PETROGRAPHIC BASED PARAGENETIC EVENTS | 102 |
| 6.3.1 | Early diagenesis | 104 |
| 6.3.2 | Late diagenesis | 106 |
| 6.4 | MINERALOGY | 108 |
| 6.4.1 | Bulk mineralogy | 108 |
| 6.4.2 | GADDs specific mineralogy | 109 |
| 6.5 | ELEMENTAL CHEMISTRY | 110 |
| 6.6 | STABLE ISOTOPES | 113 |
| 6.7 | CARBON CONTENT | 114 |
| 6.8 | HYDROCARBON INCLUSIONS | 114 |
| 6.9 | DISCUSSION AND INTERPRETATION | 116 |
| 6.9.1 | Paragenesis | 116 |
| 6.9.2 | Diagenetic pore fluids | 119 |
| 6.9.3 | Fluid flow considerations | 123 |

CHAPTER 7 *Ritchie Ridge Seep-Carbonates*

| | | |
|---------|---|-----|
| 7.1 | INTRODUCTION | 129 |
| 7.2 | DISTRIBUTION | 129 |
| 7.3 | HAND SPECIMENS | 132 |
| 7.4 | PETROGRAPHIC COMPONENTS | 137 |
| 7.4.1 | Aragonitic micarb | 137 |
| 7.4.2 | Acicular aragonite cement | 137 |
| 7.4.3 | Dolomite | 141 |
| 7.4.4 | Siliciclastic material | 143 |
| 7.4.5 | Bioclasts | 144 |
| 7.5 | MINERAL AND ELEMENTAL COMPOSITION | 145 |
| 7.5.1 | Bulk mineralogy | 145 |
| 7.5.2 | Component specific mineralogy | 145 |
| 7.5.3 | Carbon content | 146 |
| 7.5.4 | Elemental chemistry | 146 |
| 7.6 | STABLE ISOTOPES | 148 |
| 7.7 | HYDROCARBON INCLUSIONS | 149 |
| 7.8 | DISCUSSION AND INTERPRETATION | 151 |
| 7.8.1 | Bulk samples | 151 |
| 7.8.2 | Paragenesis and formation environments | 152 |
| 7.8.3 | Fluid flow considerations | 154 |
| 7.8.3.1 | <i>Stable $\delta^{13}\text{C}$ isotopes</i> | 154 |

| | |
|---|-----|
| 7.8.3.2 Stable $\delta^{18}\text{O}$ isotopes | 155 |
| 7.8.3.3 Implicating gas hydrates | 157 |

CHAPTER 8 *Synthesis and Conclusions*

| | |
|---------------------------------------|-----|
| 8.1 OVERVIEW | 159 |
| 8.2 MODERN VS ANCIENT | 160 |
| 8.2.1 Age | 160 |
| 8.2.2 Componentry | 160 |
| 8.2.3 Mineralogy | 162 |
| 8.3 SUBSURFACE METHANE MIGRATION | 163 |
| 8.4 SEEP-CARBONATE FORMATION | 164 |
| 8.4.1 Aragonite precipitation | 164 |
| 8.4.2 Alternate fluid flow scenarios | 167 |
| 8.4.3 Implicating gas hydrates | 179 |
| 8.4.4 Waning seepage and reactivation | 171 |
| 8.4.5 Calcite in seep-carbonates | 171 |
| 8.4.6 Dolomite formation | 177 |
| 8.5 SEEP-CARBONATES THROUGH TIME | 177 |
| 8.5.1 Modern seep-carbonates | 178 |
| 8.5.2 Miocene seep-carbonates | 181 |
| 8.6 CONCLUSIONS | 181 |
| 8.7 RECOMMENDATIONS FOR FURTHER STUDY | 183 |

REFERENCES

APPENDIX 1 *Sample Data*

| | |
|--|-----|
| A1.1 Sample list of TWP seep-carbonates | 201 |
| A1.2 Sample list of modern Ritchie Ridge seep-carbonates | 205 |
| A1.3 Sampling information for the modern Ritchie Ridge seep-carbonates | 205 |
| A1.4 Cruise data and sampling transects from NIWA Cruise TAN0616 | 206 |

APPENDIX 2 *Tauwharepareae Laboratory Data*

| | |
|---|-----|
| A2.1 Stable $\delta^{13}\text{C}$ and $\delta^{18}\text{O}$ isotope results | 207 |
| A2.2 Bulk mineralogy results | 219 |
| A2.3 GADDs component specific results | 212 |
| A2.4 Microprobe elemental content raw results | 215 |

APPENDIX 3 *Modern Laboratory Data*

| | |
|---|-----|
| A3.1 Stable $\delta^{13}\text{C}$ and $\delta^{18}\text{O}$ isotope results | 217 |
| A3.2 Bulk mineralogy results | 218 |
| A3.3 GADDs component specific results | 221 |
| A3.4 Microprobe elemental content raw results | 224 |

APPENDIX 4 *Additional Information*

| | |
|---|-----|
| A4.1 Additional known seep-carbonate deposits in the East Coast Basin | 225 |
| A4.2 Abbreviations used in the thesis | 227 |
| A4.3 Abstracts from presentations presenting data from this study | 228 |

List of Figures

| | | |
|--------------------|---|----|
| Figure 1.1 | A - NIWA Cruise TAN0616 remote operated vehicle image of seep-carbonate crust. B - Zone E at TWP. | 2 |
| Figure 1.2 | Map of New Zealand, with the study areas highlighted. | 4 |
| Figure 2.1 | Global map of cold seep distribution. | 9 |
| Figure 2.2 | A - Tubular concretions in Miocene mudstones, Whangaehu Beach. B - Tubular concretion in Miocene mudstones, TWP. C - Tubular concretion in shore platform, Whangaehu Beach. D - Tubular concretion, Herbertville Beach. | 14 |
| Figure 2.3 | A, B - Mud volcanism, Brookby gas seep, Hawkes Bay. | 15 |
| Figure 2.4 | Sidescan sonograph of pockmarks in Poverty Bay. | 17 |
| Figure 2.5 | A, B - Gas hydrate in seafloor sediments. | 18 |
| Figure 2.6 | A - Large oil seep at Waitangi, northwest of Gisborne. B - Smaller oil seep at Waitangi, northwest of Gisborne. | 21 |
| Figure 2.7 | A - Moonlight North seep-carbonate deposit. B - Bexhaven seep-carbonate deposit. C - Ngawaka seep-carbonate deposit. D - Wilder Road seep-carbonate deposit. | 23 |
| Figure 2.8 | A, B - NIWA Cruise TAN0616 remote operated vehicle image of seep-carbonate crust. | 25 |
| Figure 2.9 | A - Bathymodiolin mussel, TWP. B - Lucinid bivalve, Rocky Knob. | 27 |
| Figure 2.10 | A, B - Fossilised vestimentiferan (?) worm tube bed from Ugly Hill South. | 27 |
| Figure 2.11 | Diagram of relationship between isotopic composition and fluid source. | 30 |
| Figure 3.1 | Map of New Zealand, with important tectonic related features highlighted. | 31 |
| Figure 3.2 | Map of North Island and the Hikurangi Margin with seep-related phenomena highlighted. | 32 |
| Figure 3.3 | Structural map of the East Coast Basin, with TWP highlighted. | 34 |
| Figure 3.4 | Schematic diagram of the Hikurangi Margin, accretionary wedge and subducting Pacific Plate. | 35 |
| Figure 3.5 | A - Large oil seep at Waitangi. B - Close up of oil seepage and effusive bubbling. C - Waitangi-1 oil well. | 38 |
| Figure 3.6 | Tubular concretions in Miocene mudstones, Whangaehu Beach. | 38 |
| Figure 3.7 | Waipawa Black Shale outcrop at Porangahau, southern Hawkes Bay. | 39 |
| Figure 3.8 | Overview image of TWP and its surrounds, Raukumara Ranges. | 40 |
| Figure 3.9 | Geological map of TWP and its surrounding area. | 41 |
| Figure 3.10 | Tubular concretion in Pliocene mudstone, Tauwhareparae Rd. | 42 |
| Figure 3.11 | Stratigraphic column for East Coast Basin. | 43 |

| | | |
|--------------------|---|----|
| Figure 3.12 | Map of North Island, with cold-seep sites highlighted. | 44 |
| Figure 4.1 | Schematic outline of sampling zones at TWP. | 48 |
| Figure 4.2 | Field analysis - profiling Zone C. | 49 |
| Figure 4.3 | Field analysis - profiling Zone A. | 49 |
| Figure 4.4 | A - NIWA Wellington's RV Tangaroa research vessel. B, C, D - Dredge haul, aboard the RV Tangaroa. E - Cleaning seep-carbonate samples, aboard the RV Tangaroa. F - Large seep-carbonate sample, aboard the RV Tangaroa. G - Small faunal collection from seep-carbonate sampling, aboard the RV Tangaroa. | 51 |
| Figure 4.5 | A - Laboratory analysis, rock storage trays. B - Diamond bladed saw. C - Rock storage trays and slabs. D - Thin section grinder and saw. E - Rock storage trays and thin section blocks. F - Lap wheel polisher. | 52 |
| Figure 4.6 | Cathodoluminescence microscope. | 54 |
| Figure 4.7 | A - GADDs machine, University of Auckland. B - Close up of GADDs machine. | 56 |
| Figure 4.8 | A - Screen shot obtained from GADDs data collection. B - Image of fabric being analysed and position of laser. | 57 |
| Figure 4.9 | A - EPMA microprobe collection, University of Auckland. B - Screen data during data collection. C - Close up of stage where thin section is placed. | 59 |
| Figure 5.1 | Schematic outline of sampling zones at TWP. | 61 |
| Figure 5.2 | TWP carbonate deposit. | 62 |
| Figure 5.3 | Map of East Coast Basin with TWP highlighted. | 63 |
| Figure 5.4 | Aerial map of TWP seep-carbonate deposit. | 63 |
| Figure 5.5 | Zone C at TWP with varying carbonate morphologies identified. | 64 |
| Figure 5.6 | Zones A and E at TWP facing southwest. | 64 |
| Figure 5.7 | Faulting in Zone A at TWP. | 65 |
| Figure 5.8 | Stratigraphic column, from TWP. | 67 |
| Figure 5.9 | Facies relationships in Zone A and B. | 68 |
| Figure 5.10 | Facies relationships in Zone E. | 68 |
| Figure 5.11 | Mudstone contact between Zones A and B. | 69 |
| Figure 5.12 | Tubular concretion in basal mudstone at TWP. | 69 |
| Figure 5.13 | Nodular concretion in basal mudstone at TWP. | 70 |
| Figure 5.14 | Slabbed image of tubular concretion at TWP. | 70 |
| Figure 5.15 | Gradational contact between Facies 1 and 2. | 71 |
| Figure 5.16 | Slabbed image of nodular concretion from Facies 2. | 72 |
| Figure 5.17 | Facies 3 in deposit 'gut'. | 72 |
| Figure 5.18 | Close up of disjointed burrow in Facies 3. | 73 |
| Figure 5.19 | Zone A faulted section, image shows intensely brecciated and bioturbated nature of carbonate slab. | 74 |
| Figure 5.20 | Close up of internal brecciated and bioturbated fabrics in Figure 5.19. | 74 |

| | | |
|--------------------|---|-----|
| Figure 5.21 | Slabbed image of TWP-A/6. | 75 |
| Figure 5.22 | Slabbed image of TWP-A/5. | 76 |
| Figure 5.23 | Slabbed image of TWP-D/20. | 77 |
| Figure 5.24 | Slabbed image of TWP-E/8. | 77 |
| Figure 5.25 | Slabbed image of TWP-C/13. | 78 |
| Figure 5.26 | Bathymodiolin mussel at TWP. | 79 |
| Figure 5.27 | Slabbed image of TWP-D/1. | 79 |
| Figure 5.28 | Coralline siltstone from TWP. | 80 |
| Figure 5.29 | Facies distribution map for TWP. | 81 |
| | | |
| Figure 6.1 | A-F - Aragonitic micarb phases in TWP seep-carbonates (PPL and CL photomicrograph pairs). | 88 |
| Figure 6.2 | A-D - Aragonitic peloidal phases in TWP seep-carbonates (PPL and CL photomicrograph pairs). | 89 |
| Figure 6.3 | A-F - Acicular aragonite phases in TWP seep-carbonates (PPL and CL photomicrograph pairs). | 90 |
| Figure 6.4 | A-F - Aragonite phases in TWP seep-carbonates - (PPL and CL photomicrograph pairs). | 92 |
| Figure 6.5 | A-D - Late calcite phases in TWP seep-carbonates (PPL and CL photomicrograph pairs). | 93 |
| Figure 6.6 | A-F - Late calcite phases in TWP seep-carbonates (PPL and CL photomicrograph pairs). | 94 |
| Figure 6.7 | A-D - Cellular calcite phases in TWP seep-carbonates (PPL and CL photomicrograph pairs). | 95 |
| Figure 6.8 | A-F - Bioclastic material within TWP seep-carbonates (PPL and CL photomicrograph pairs). | 97 |
| Figure 6.9 | A-F - Worm tubes phases within TWP seep-carbonates (PPL and CL photomicrograph pairs). | 98 |
| Figure 6.10 | Initial and bioclastic neomorphism within TWP seep-carbonates (PPL and CL photomicrograph pairs). | 100 |
| Figure 6.11 | Bioclastic neomorphism within TWP seep-carbonates (PPL and CL photomicrograph pairs). | 101 |
| Figure 6.12 | Pervasive neomorphism within TWP seep-carbonates (PPL and CL photomicrograph pairs). | 102 |
| Figure 6.13 | Relative timing diagram for the paragenetic sequence observed in the TWP seep-carbonates. | 103 |
| Figure 6.14 | A-F - Varying petrographical features from within TWP seep-carbonates (PPL and CL photomicrograph pairs). | 105 |
| Figure 6.15 | A-F - Multiple phases from the paragenetic sequence identified in the TWP seep-carbonates (PPL and CL photomicrograph pairs). | 107 |
| Figure 6.16 | Graph of elemental composition of selected components from within TWP seep-carbonates. | 112 |
| Figure 6.17 | Close up of lower half of Figure 6.16, graph of elemental composition of selected components from within TWP seep- | 112 |

carbonates.

| | | |
|--------------------|---|-----|
| Figure 6.18 | Stable isotope cross plot for TWP seep-carbonate components. | 113 |
| Figure 6.19 | A-F - Hydrocarbon inclusions from selected components of the TWP seep-carbonates. | 115 |
| Figure 6.20 | Fe versus Mn content plot, from selected TWP seep-carbonate components. | 121 |
| Figure 6.21 | Sr/Ca ratio versus Mn content within selected TWP seep-carbonates. | 122 |
| Figure 6.22 | Sr/Ca ratio versus Mn content with water rock interaction information from Morse and Mackenzie (1990) superimposed. | 123 |
| Figure 6.23 | Calcite equilibrium graph from Friedman and O'Neil (1977). | 124 |
| Figure 6.24 | Aragonite equilibrium graph from Grossman and Ku (1986). | 125 |
| | | |
| Figure 7.1 | Map of Hikurangi Margin, North Island with major known cold-seep sites highlighted. | 130 |
| Figure 7.2 | A-F - Remote operated vehicle images from NIWA RV TANGAROA RESEARCH VESSEL Cruise TAN0616. | 131 |
| Figure 7.3 | A-D - Photo mosaic of slabbed aragonitic modern Ritchie Ridge seep-carbonates. | 135 |
| Figure 7.4 | A-D - Photo mosaic of slabbed dolomitic modern Ritchie Ridge seep-carbonates. | 136 |
| Figure 7.5 | A-D - Aragonitic micarb phases in modern Ritchie Ridge seep-carbonates (PPL and CL photomicrograph pairs). | 138 |
| Figure 7.6 | A-F - Acicular aragonite phases in modern Ritchie Ridge seep-carbonates (PPL and CL photomicrograph pairs). | 139 |
| Figure 7.7 | A-F - Acicular aragonite in modern Ritchie Ridge seep-carbonates (PPL and CL photomicrograph pairs). | 140 |
| Figure 7.8 | A-F - Dolomitic modern Ritchie Ridge seep-carbonates (PPL and CL photomicrograph pairs). | 142 |
| Figure 7.9 | A-D - Dolomite and dolomite rhombs in modern Ritchie Ridge seep-carbonates (PPL and CL photomicrograph pairs). | 143 |
| Figure 7.10 | A-D - Dolomitic modern Ritchie Ridge seep-carbonates (PPL and CL photomicrograph pairs). | 144 |
| Figure 7.11 | Graph of elemental composition of selected components from within dolomitic modern Ritchie Ridge seep-carbonates. | 147 |
| Figure 7.12 | Graph of elemental composition of selected components from within aragonitic modern Ritchie Ridge seep-carbonates. | 148 |
| Figure 7.13 | Stable isotope cross plot for modern Ritchie Ridge seep-carbonates. | 149 |
| Figure 7.14 | A-F - Photomicrographs of aragonitic Ritchie Ridge samples under ultraviolet light. | 150 |
| Figure 7.15 | Aragonite equilibrium graph from Grossman and Ku (1986). | 156 |
| Figure 7.16 | Dolomite equilibrium graph from Fritz and Smith (1990). | 157 |

| | | |
|--------------------|---|-----|
| Figure 8.1 | Schematic diagram for aragonite precipitation in cold seep systems. | 165 |
| Figure 8.2 | Relative timing diagram for 'early' seafloor diagenesis and precipitation of carbonate in cold seep systems. | 168 |
| Figure 8.3 | Schematic diagram for aragonite precipitation in cold seep systems, with varying fluid flow conditions. | 170 |
| Figure 8.4 | Schematic diagram for calcite precipitation in cold seep systems, with varying fluid flow conditions. | 173 |
| Figure 8.5 | Schematic diagram of the alteration of aragonite to calcite during diagenesis for seep-carbonates. | 174 |
| Figure 8.6 | Relative timing diagram for late diagenesis and alteration post burial in seep-carbonates. | 175 |
| Figure 8.7 | Schematic diagram for dolomite precipitation in the deep subsurface seep plumbing environment. | 176 |
| Figure 8.8 | A-D - Modern unaltered aragonitic Ritchie Ridge seep-carbonates (PPL and CL photomicrograph pairs). | 177 |
| Figure 8.9 | A-D - Ancient aragonitic seep-carbonates that are relatively unaltered, from D-group 1 (PPL and CL photomicrograph pairs). | 178 |
| Figure 8.10 | A-D - Ancient aragonitic seep-carbonates that have undergone moderate amounts of alteration, from D-group 2 (PPL and CL photomicrograph pairs). | 179 |
| Figure 8.11 | A-D - Ancient aragonitic seep-carbonates that have undergone extensive alteration, from D-group 3 (PPL and CL photomicrograph pairs). | 180 |

List of Tables

| | | |
|------------------|--|----|
| Table 2.1 | Methane sources in seabed sediments. | 11 |
| Table 2.2 | List of known ancient seep-carbonate deposits in the East Coast Basin. | 22 |
| Table 4.1 | Mineral and associated CL patterns. | 54 |
| Table 4.2 | Common d-spacings and 2θ values for XRD analysis. | 55 |
| Table 4.3 | Relative abundance scheme for XRD analysis. | 55 |
| Table 4.4 | Operating conditions for the GADDs machine. | 57 |
| Table 5.1 | List of facies found at the TWP seep-carbonate deposit. | |
| Table 5.2 | Summary of fossil taxa at TWP. | |
| Table 6.1 | Summary of petrographical components in TWP seep-carbonates. | |
| Table 6.2 | Mineral abundances in selected TWP seep-carbonates from XRD analysis. | |

- Table 6.3** Elemental content (ppm) for selected components from TWP seep-carbonates.
- Table 6.4** Range of stable isotopes for selected components from TWP seep-carbonates.
- Table 6.5** Carbonate content (%) of representative seep-carbonates from TWP.
- Table 6.6** Total organic carbon content (%) for selected TWP seep-carbonates.
- Table 7.1** Ritchie Ridge samples and respective sampling transects.
- Table 7.2** Descriptions of Ritchie Ridge seep-carbonate hand specimens.
- Table 7.3** Characteristics of aragonitic and dolomitic seep-carbonate hand specimens.
- Table 7.4** Mineral abundances in selected Ritchie Ridge seep-carbonates from XRD analysis.
- Table 7.5** Carbonate content (%) for selected Ritchie Ridge seep-carbonates.
- Table 7.6** Total organic carbon content (%) for selected Ritchie Ridge seep-carbonates.
- Table 7.7** Elemental content (ppm) for selected components from TWP seep-carbonates.
- Table 7.8** Stable $\delta^{13}\text{C}$ and $\delta^{18}\text{O}$ isotopic values for Ritchie Ridge seep-carbonates.
- Table 7.9** Summary of characteristic of Ritchie Ridge seep-carbonates as grouped by mineralogy.
- Table 8.1** Summary of components of seep-carbonates grouped by location.

CHAPTER 1

Introduction

1.1 OVERVIEW

In the past two decades, cold seep systems have become a topic of much interest for various researchers worldwide (Judd and Hovland 2007). One reason for this is their multi-faceted nature, necessitating a multi-disciplinary approach to their study across diverse fields of science such as geology, geophysics, biology, paleontology, biogeochemistry, oceanography, chemistry and microbiology. Commercial interests from energy and petroleum industries in relation to both hydrocarbon migration and gas hydrate formation also drive research programmes (Pecher et al. 2007).

Cold seeps are associated with focused fluid expulsion at the seafloor (Fig. 1.1A), typically hydrocarbons dominated by methane. The migration of these fluids through the subsurface leads to the formation of extreme environments at the seabed. These conditions are ideal ones in which chemosymbiotic communities and methanotrophic bacteria thrive at the seabed (Sibuet and Olu 1998; Hovland 2002). At these sites the anaerobic oxidation of methane is a biogeochemical driver for carbonate precipitation in the shallow subsurface (Boetius and Suess 2004). The carbonates formed at such sites become buried and eventually uplifted to form small, isolated outcrops of indurated, fossiliferous seep-carbonates (Fig. 1.1B).

Determining the paragenetic sequence of the different cements within seep-carbonate deposits affords insights about changing conditions within the seep system, including fluid source, duration of seepage and local pore water chemistries (Campbell et al. 2002). Furthermore, the identification of these seep-carbonates in the rock record can provide information about hydrocarbon seepage over time. Comparing samples from both modern and ancient settings reveals insights into the diagenetic changes that occur within the samples during their

shift from the seafloor into the shallow and deep subsurface burial environments (Greinert et al. 2001; Campbell 2006). These changes may include both mineralogical transformations and/or cementation from the passage of pore fluids of diverse origins.

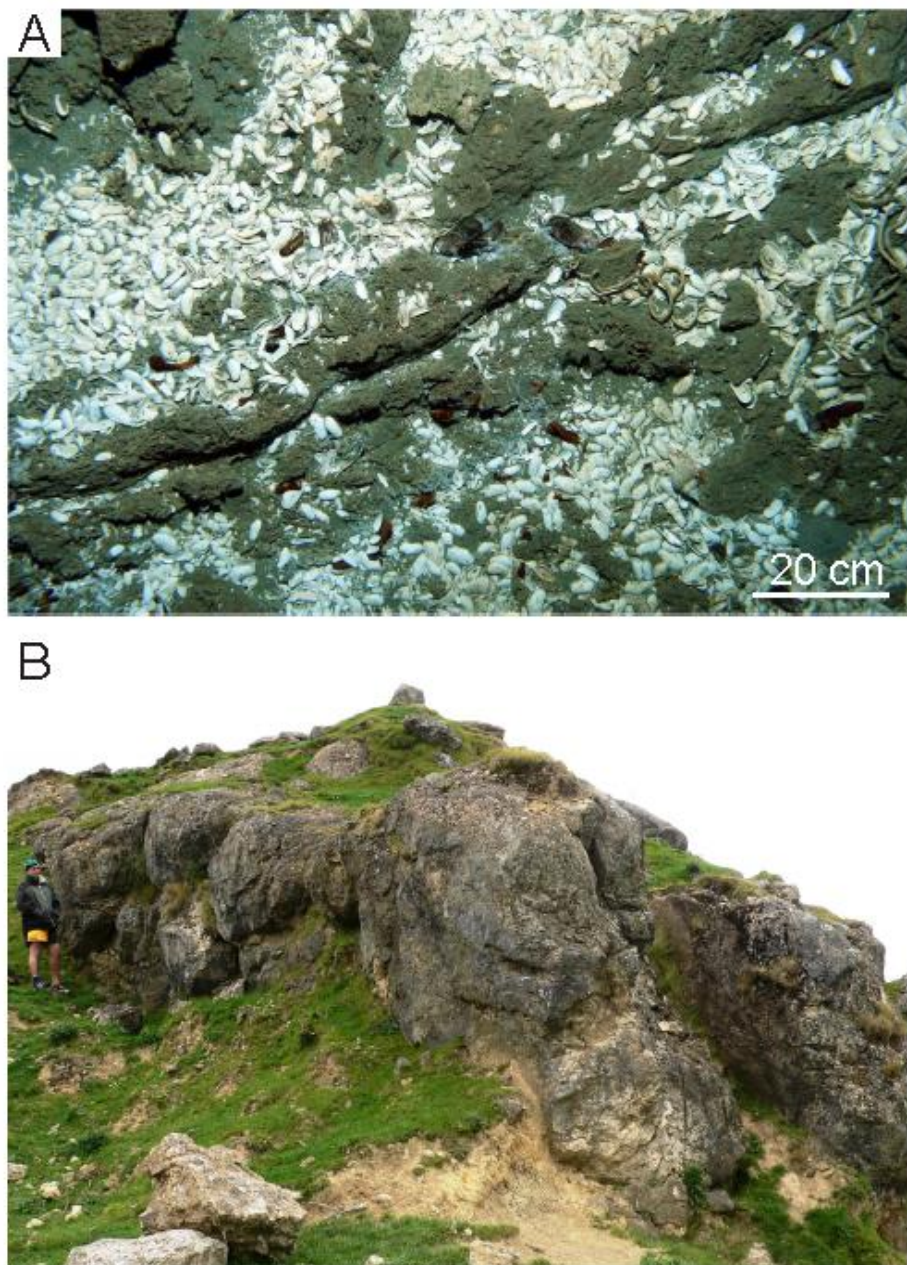


Figure 1.1: A – Remote operated vehicle (ROV) image of seep-carbonate slabs, scattered bathymodiolin mussels and dead *Calyptogena* sp. shells from offshore Hikurangi Margin (Image courtesy of NIWA, Wellington). B – Part of the ancient study site Tauwhareparae (TWP) Raukumara Peninsula. Note person for scale at bottom right.

1.2 AIMS OF STUDY

This study comprises field and especially petrological analysis of both modern (offshore) and ancient (onland) seep-carbonates from the Hikurangi Margin, New Zealand (Fig. 1.2).

The main aims include:

- Characterisation and determination of the paragenetic sequence within cold seep-carbonates at Tauwhareparae (TWP), a paleo-seep deposit of middle Miocene age in the onshore East Coast Basin.
- Characterisation and determination of the nature of modern cold seep-carbonates from Ritchie Ridge, offshore East Coast Basin.
- Development of some schematic diagrams documenting the processes and alterations acting on the cold seep deposits from the initial stages of carbonate precipitation (as in the modern offshore examples), through to their later stages of diagenetic alteration during burial (as in the ancient onshore examples).

To fulfil these aims, the following approaches were adopted:

- Mapping of the ancient onshore TWP deposit, including stratigraphic analysis, facies analysis and sampling.
- Description and sampling modern seep-carbonate samples from NIWA, Wellington for subsequent laboratory analysis.
- Laboratory analysis of both ancient and modern sample sets included detailed microscopy (both plane polarised light, or PPL, and cathodoluminescent light, or CL); stable $\delta^{13}\text{C}$ and $\delta^{18}\text{O}$ isotopes; XRD bulk mineralogy; GADDs mineralogy; EPMA elemental content; and ultraviolet (UV) light fluorescence.
- The data obtained from the above analyses were used to determine the order of precipitation and formation of the carbonate cements within the deposits (i.e. to develop a paragenetic sequence of diagenetic events).

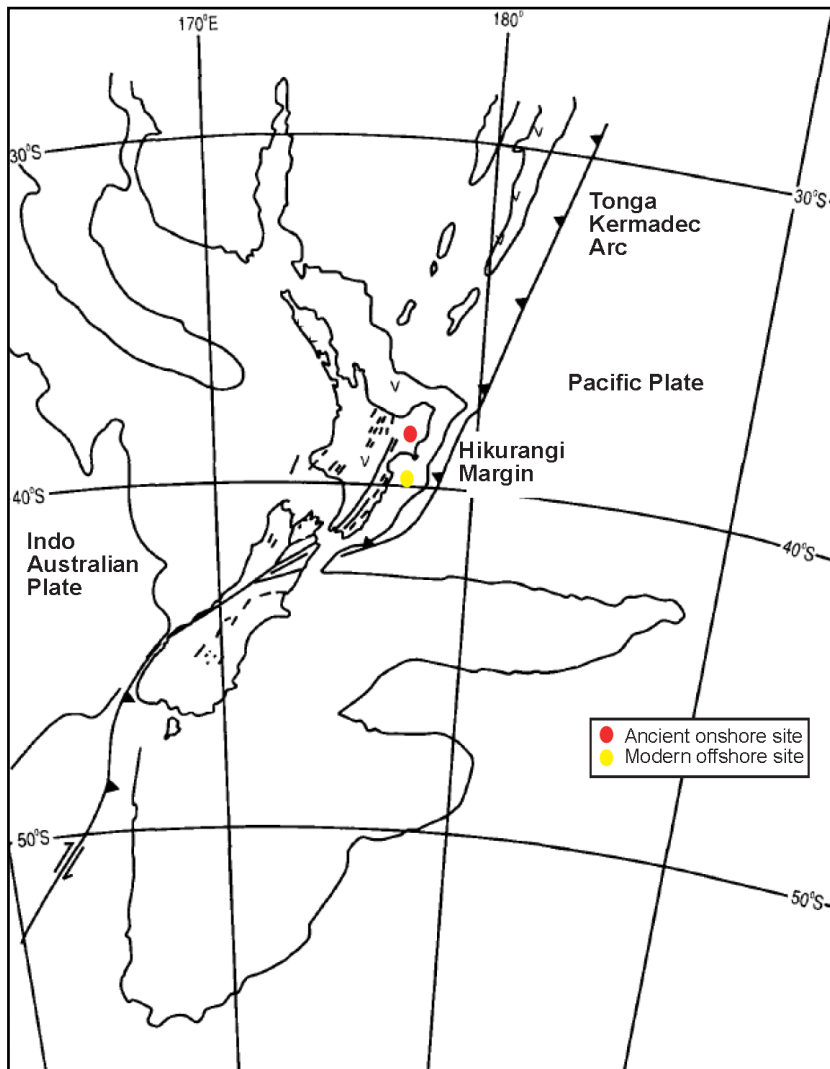


Figure 1.2: Map of New Zealand locating the middle Miocene onshore deposit studied in the Raukumara Ranges (red circle) and the offshore study sites at Ritchie Ridge (yellow circle). Image modified from King (2000).

1.3 COLD SEEP RESEARCH

This MSc thesis has been completed within a much wider Marsden funded research project on cold seep-carbonate systems in the East Coast Basin of North Island involving personnel mainly from The University of Waikato and The University of Auckland, with support and input from Dave Francis from Geological Research Limited, Lower Hutt and personnel at Geosciences Australia in Canberra; IFM-GEOMAR in Germany and NIWA in Wellington, New Zealand. Other student projects in the group are noted below.

- Stephanie Nyman – PhD Thesis – University of Waikato

“Tubular carbonate concretions from North Island, New Zealand: Evidence for hydrocarbon migration and the subsurface plumbing system of cold seeps.”

This study describes and characterises the occurrences of tubular concretions at four ancient seep sites in the North Island. The concretions are shown to demarcate subsurface seep plumbing networks and extensive use is made of stable isotopic trends to explain their origins.

- Kristian Saether – PhD Thesis – University of Auckland

“Miocene hydrocarbon seep deposits in New Zealand: Taxonomy and paleobiogeography”

Determination and identification of fossil seep fauna and their spatial and temporal relationships.

- Melissa Troup – MSc Thesis – University of Waikato

“Sedimentology and petrology of Miocene cold seep limestones in southern Hawkes Bay: Geologic evidence for past seabed hydrocarbon seepage.”

Characterisation of petrological properties of selected seep-carbonates occurring in the southern reaches of the East Coast Basin.

1.4 RELATED CONTRIBUTIONS

Some results from this study have been presented at annual conferences of the Geological Society of New Zealand, referenced below.

- Ewen, S.; Campbell, K.; Nelson, C.; Hood, S.; Francis, D. 2007: Petrology of some Miocene cold seep limestones in Raukumara Peninsula, East Coast Basin: Geologic evidence for past seabed hydrocarbon seepage. Geological Society of New Zealand Miscellaneous Publication 123A: 47.
- Ewen, S.; Nelson, C.; Hood, S.; Campbell, K.; Orpin, A. 2008: Petrology of some modern and ancient cold seep-carbonates, East Coast Basin, New Zealand. Geological Society of New Zealand Miscellaneous Publication 124A: 258.

[<http://www.victoria.ac.nz/geosciences08/symposia.html>]

- Hood, S.; Nelson, C.; Campbell, K.; Ewen, S.M. 2008: Insights into paragenetic complexities within Miocene hydrocarbon seep limestones in East Coast Basin, New Zealand. Geological Society of New Zealand Miscellaneous Publication 124A: 265.

[<http://www.victoria.ac.nz/geosciences08/symposia.html>]

1.5 STRUCTURE OF THESIS

This thesis has eight chapters followed by appendices.

Chapter 1 – This is an introduction to the thesis, noting the aims of the study and the relevance of studying cold seep-carbonate deposits.

Chapter 2 – This chapter is a general overview of some of the cold seep literature, explaining features typical of cold seep systems and their worldwide distribution.

Chapter 3 – Summary of the physical setting in which the seep-carbonate deposits in the East Coast Basin of New Zealand formed. The chapter also includes a brief description of other cold seep related features found in New Zealand.

Chapter 4 – Describes the methods used during the sampling and analysis of the cold seep-carbonates.

Chapter 5 – The observations and mapping results of the ancient TWP deposit are presented in order to elucidate their field nature and geological context.

Chapter 6 – All laboratory results from the TWP samples are provided herein, including a discussion of the results in relation to other documented laboratory results for cold seep-carbonates.

Chapter 7 – This serves as both a summary of observational data from the modern offshore areas and a description and interpretation of the results obtained from laboratory analysis of the modern samples.

Chapter 8 – Constitutes a synthesis of all laboratory and field observations and results, comparing and contrasting processes occurring in both sample groups, and suggesting some schematic models to explain and/or account for observed anomalies or patterns in the study. Conclusions and suggestions for further research are made at the end of this chapter.

Appendices are situated at the end of the thesis and are structured as follows:

Appendix 1: Complete sample lists for sample groups in this study and NIWA Cruise TAN0616 information.

Appendix 2: Tauwhareparae seep-carbonate laboratory results.

Appendix 3: Ritchie Ridge seep-carbonate laboratory results.

Appendix 4: Additional information, including a list of additional seep-carbonate deposit sites in the East Coast Basin, a list of abbreviations used in the thesis and the abstracts from two conference presentations.

The appendices disk contains all of the photomicrographs from the CL analysis of both modern and ancient seep-carbonate sample. Extra data from XRD and GADDS analysis can also be found on the disk.

CHAPTER 2

Cold Seep Systems

2.1 INTRODUCTION

Seep-carbonates form at the seabed as a consequence of diverse biogeochemical processes occurring on continental margins worldwide. Modern cold seep sites have been recorded around the world in all oceanic, geologic and tectonic settings (Fig. 2.1) (Roberts & Aharon 1994; Judd 2003; Campbell 2006). Evidence for modern seabed fluid-flow includes methane flares, carbonate crusts, chemosymbiotic communities and tube worms, pockmarks, mud volcanism, diapirs, strong BSRs and submarine slumping (Lewis and Marshall 1996; Judd and Hovland 2007).

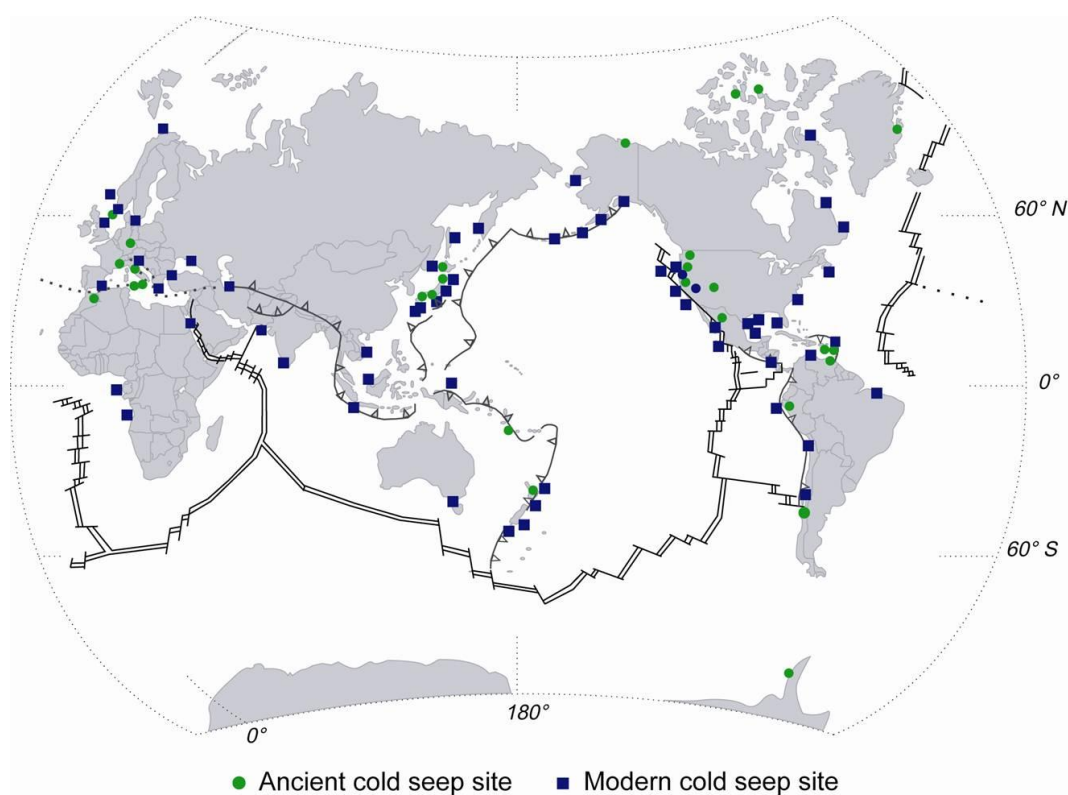


Figure 2.1 Distribution of modern and ancient cold seeps. From Nyman (2009) originally modified from Campbell (2006).

In order to elucidate the range of geologic products derived from cold seep formation, this chapter will introduce some other seep phenomena, as well as providing information about the processes which drive cold seep systems. A summary of some of the literature on cold seep systems includes examples from both modern settings and from the geologic record.

2.2 COLD SEEP SYSTEMS

A cold seep is an area of focused fluid expulsion at the seafloor. The fluids are commonly hydrocarbons, especially methane, and can also include hydrogen sulphide (Beauchamp and Savard 1992; Campbell et al. 2002). The buoyant fluids will migrate to the seafloor under pressure through paths of least resistance, typically along faults or zones of increased permeability (Judd and Hovland 2007). Broadly known as “seabed fluid flow”, this process is responsible for the seabed creation of complex chemosynthesis communities, geologic formations, prospective resources and potential hazards (Judd 2003; Judd and Hovland 2007).

2.2.1 Methane seepage

Three types of methane are commonly found in seafloor sediments: thermogenic, microbial and abiogenic. The latter is responsible for the formation of most of the methane found at hot vents (Judd 2003; Krüger et al. 2005). Table 2.1 identifies the key differences in the varying forms of methane. Although methane is the most common fluid known to expel from cold seeps, studies have shown that the amount of methane released from the seabed is only a fraction of the total amount of methane which originally migrated from depth due to uptake by microbes in the process of anaerobic oxidation of methane (AOM) (Boetius et al. 2000; Parnell 2002; Judd 2003; Boetius and Suess 2004; Peckmann and Thiel 2004). The discovery of AOM microbes has had major implications for understanding the global methane budget as they are a large methane sink (Boetius and Suess 2004; Krüger et al. 2005).

Table 2.1: Sources of methane in seabed sediments. Note that thermogenic and microbial (biogenic) methane are the most common fluids expelled from cold seeps. Adapted from Judd 2003; Krüger et al. 2005; Campbell 2006; Judd and Hovland 2007.

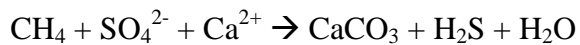
| Methane Type | Formation |
|--------------|---|
| Thermogenic | Burial and biogenic degradation of organic material at depth, to generate oil and gas, of which methane is the most abundant. Typically forms at greater burial depths relative to microbial methane. |
| Microbial | Methanogenic microbial activity is responsible for the decomposition of organic material. These processes generally occur at subsurface depths from the seafloor interface to 1 km depth, in anoxic environments with both relatively low temperatures and low sulphate concentrations. |
| Abiogenic | Normally found at hot (hydrothermal) vents; forms by the inorganic production of methane from magma degassing and/or cooling. Serpentinisation may also form methane. |

As fluids migrate up through seafloor sediment, the methane provides energy for chemosynthesis-based communities which develop at cold seep sites. The communities consist of tubeworms or bivalves such as mussels or clams, many of which have a symbiotic relationship with sulphide-oxidising bacteria.

2.2.2 Anaerobic oxidation of methane (AOM)

The anaerobic oxidation of methane (AOM) is the key biogeochemical process aiding and enabling the precipitation of methane-derived authigenic carbonate (MDAC) at cold seeps worldwide. AOM is microbially mediated as it is carried out by a consortia of Archaea and sulphate-reducing Bacteria (Boetius et al. 2000; Krüger et al. 2005). The consortia are responsible for the oxidation of methane, which provides energy for sulphide-oxidising communities of *Beggiatoa* sp. and *Acharax* sp. (Boetius et al. 2000; Boetius and Suess 2004; among others). Boetius et al. (2000) presented landmark findings of the first evidence of these microbial consortia and of the carbonate that they are producing. The consortia may appear

as aggregates and become incorporated into carbonate precipitates as shown in the reaction:



When bicarbonate is produced, alkalinity is increased which acts as a catalyst to encourage further carbonate precipitation (Savard et al. 1996; Boetius and Suess 2004; Luff et al. 2004; Reitner et al. 2005).

2.2.3 Terminology

It is difficult to find one exact definition or term to describe seep phenomena. Seep sites may be discussed as vents or seeps, and hot or cold, but parameters such as flow rate and temperature are only relative (Aharon 1994). In a recent review paper, Campbell (2006) proposed a definition for a hydrocarbon seep as: “..fluid discharge of varying rates and temperatures generated from the accumulation and burial of organic matter, its transformation to hydrocarbons, and their migration and release from sedimentary basins” (Campbell 2006, p. 384).

There is also cross-over and multiple terms used for the carbonate deposits which are precipitated at these sites. In fact some papers use ‘seep-carbonate’ and then describe the same deposit as a ‘seep limestone’ (Clari et al. 1994). The term limestone specifies the presence of over 50% carbonate material within the deposit. The name appears to be used more commonly when describing ancient examples that have been lithified and which have undergone varying degrees of diagenesis. Methane-derived authigenic carbonate, or MDAC, is also used, a term which has been developed from its formation mechanisms rather than its mineralogical content. Many examples of “seep-carbonates” have carbonate percentages ranging from below 50% to greater than 90% (cf. Campbell et al. in review), i.e. they contain varying amounts of siliciclastic components, effectively making them carbonate-cemented clastic sediments. This sedimentology is evident in both modern and ancient deposits. The term seep-carbonate will herein be used to encompass both modern and ancient MDACs.

2.3 Cold seep Related Features

2.3.1 Tubular concretions

Tubular concretions are interpreted to mark the subsurface plumbing systems or feeder pipes of cold seep systems and were found associated with some deposits of this study. Nyman (2009) defined a tubular concretion as "...a well-cemented body of rock within an otherwise less cemented host rock, typically siliciclastic mudstone". Like most seep-related phenomena, there are reports of both onshore and offshore occurrences. For example, tubular concretions or chimneys have been described along the Hikurangi Margin of the North Island (Orpin 1997; Nyman 2009), the Gulf of Cadiz in the Atlantic Ocean (Díaz-del-Río et al. 2003), Monterey Bay in California (Stakes et al. 1999; Aiello et al. 2001), and from the Eocene succession of Bulgaria (De Boever et al. 2006).

Offshore modern seep sites are often associated with tubular concretions. These may have been exhumed to litter the seafloor about the seeps, or they may be free-standing to form a positive relief on the seafloor. Orpin (1997) reported scattered tubes on the Otago Shelf, off South Island. Images from NIWA cruise TAN0616 along the central Hikurangi Margin reveal scattered tubes around Rock Garden Knoll, and samples from the cruise include both tubular and mushroom-like morphologies. Díaz-del-Río et al. (2003) described a vast field of chimneys in the Gulf of Cadiz. The chimneys reach up to 2 m in length and range in morphology from spiral or cylindrical, to mushroom or mound-like.

Nyman (2009) studied four major Miocene tubular concretion locations onshore North Island of New Zealand, including Cape Turnagain, East Cape, Taranaki and Rocky Knob. These sites host concentrated occurrences of tubular concretions which vary widely in morphology and size. Morphologies include doughnuts, tubes, cylinders, sinuous or tortuous pipes, bulbous, flower pots and stacked doughnuts (Fig. 2.2). Dimensions range from small tubes at Rocky Knob, 5 – 10 cm across, to large bulbous tubes at Taranaki which may be up to 10 m or more long (limited only by outcrop exposure). De Boever et al. (2006) recorded Eocene columnar concretions in Bulgaria which range in length from 1 – 8 m and are up to 1.5 m wide.

As can be seen from these observations, tubular concretions are common both onshore and offshore, and may vary greatly both in size and shape. However, presently the available literature focusing on these concretions is relatively minor compared to other forms of seep-carbonate.

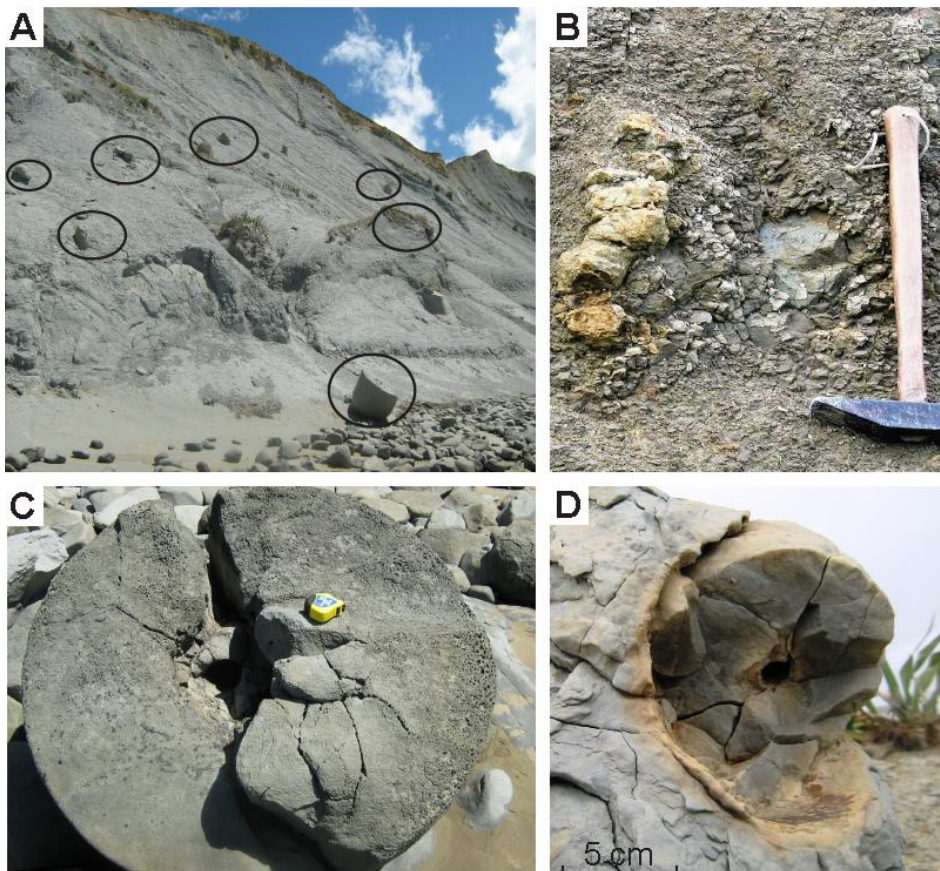


Figure 2.2 Tubular concretions from sites in the East Coast Basin, North Island. **A** – Large, bulbous concretions in Miocene mudstones at Cape Turnagain. **B** – Tubular concretion in basal mudstone at TWP. **C** – Large tubular concretion split through its centre, in shore platform at Whangaehu Beach, Cape Turnagain. **D** – Small pipe concretion with empty central conduit at Herbertville Beach, Wairarapa.

2.3.2 Mud volcanoes

Mud volcanoes associated with seep systems are found both onshore (e.g. Dashgil Mud Volcano, Azerbaijan, as discussed by Hovland et al. (1997)), and offshore (e.g. Hakon Mosby Mud Volcano, northeast Atlantic, as reported by Milkov et al. (2004b)). Judd and Hovland (2007, p. 197) proposed a definition for mud volcanoes as, “a topographically expressed surface edifice from which solid material (at least mud, but generally also breccias comprising clasts of solid rock

in a mud matrix) and fluid (water, brine, gas, oil) flow or erupt" (Fig. 2.3). Mud volcanoes are similar to cold seeps in that seepage may occur in many individual spots of one larger area at one time, this may vary temporally as well as spatially. They may also act to feed a cold seep system if they are a subsurface feature (diapir).

Mud volcanoes may preferentially form in basins with thick sediment successions, where the lower parts of the succession are characterised by plastic soft sediments (Judd and Hovland 2007). The Dashgil Mud Volcano in Azerbaijan is much like many mud volcanoes, which may have several zones of active seepage at one time. The plateau of the mud volcano has several areas of mud pools with active bubbling, plus a series of cones or gryphons where gas is expelled (Hovland et al. 1997). Mud volcanism in New Zealand and its relevance to hydrocarbon seepage and petroleum exploration is discussed briefly in Sections 2.4.2 and 3.2.5.

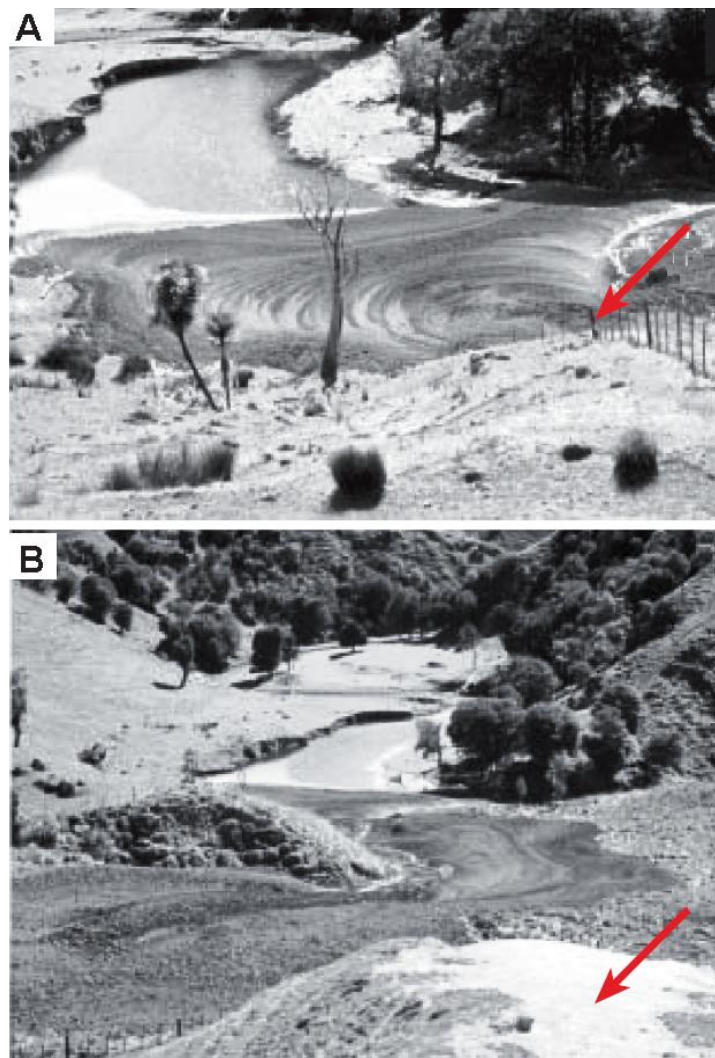


Figure 2.3 Mud volcanism at Brookby Gas Seep, Hawkes Bay, New Zealand. **A** – Epicentre of effusive activity denoted by red arrow. Debris accumulated in a talus pile down slope. **B** – Another view of activity and seepage at the site. Images from Pettinga (2003).

Offshore, mud volcanoes are large conduits for gas release and thus may be feeders for surface seeps. The volcanoes may host large and diverse chemosynthesis-based communities, which form zonation patterns similar to those found across cold seeps this is due to chemical gradients in the pore fluids decreasing away from the vent (Olu-Le-Roy et al. 2004; Léon et al. 2006). In some cases they may be areas of gas hydrate formation (Milkov et al. 2004b). The flanks of mud volcanoes grow by accretion of ejecta and the lower slopes may grow through the shedding of unstable build up of material by the rim (Milkov et al. 2004b; Léon et al. 2006). Léon et al. (2006) have demonstrated that mud volcanoes may exist in fields, associated with other seep features such as pockmarks and carbonate mound formation. Morphologies of the cones may also range from conical to oval to zones of vents in close proximity to one another, making parasitic vents or multi-cones (Léon et al. 2006).

Mud volcanoes are of great importance to the petroleum industry for two reasons. First, they may form a risk, as the ejecta or pressure of gas fluxes may disrupt pipelines or oil rigs. Second, the mud volcanoes may be a marker for source rocks from which the gas fluxes are draining (Milkov et al. 2004a; Judd and Hovland 2007).

2.3.3 Pockmarks

Pockmarks are one of the most common seep-related features, and are indicators of seabed fluid flow (Hovland et al. 2005; Judd and Hovland 2007). They are identified by shallow bowl-like depressions in the seafloor using side scan bathymetry, ROV or seismic imaging. In New Zealand they have been identified offshore along the Hikurangi Margin (Fig. 2.4) (Nelson and Healy 1984; Lewis and Marshall 1996) and also in fresh water such as Lake Rotorua (Chris Hendy pers. comm. 2007). Judd and Hovland (2007) provided a summary of pockmarks

studied worldwide, and it is evident that pockmarks are found in all oceanic settings.

Pockmarks have been reported to range in size from 1 to 190 m wide (Mazzini et al. 2006; Judd and Hovland 2007). The sediments in which they form appear to have some control on pockmark size, as there is an inverse relationship between grain size and pockmark dimension (Judd and Hovland 2007).

A suggested hypothesis for the formation of pockmarks invokes rising subsurface gases which cause seabed doming, which then expands until a critical point. At this stage a violent upward rushing of gas under pressure causes an explosive exhumation of sediments, leading to a scour bowl or depression (Judd and Hovland 2007). Pockmarks may also be associated with polygonal faults which can provide fluid pathways.

Pockmarks have been reported in isolation, but are more common in fields such as the TAYSO field in the Gulf Of Cadiz, Atlantic Ocean (Léon et al. 2006). They are reported to be conduits of fluid flow (Hovland 2003), and are often found in close proximity to mud volcanoes or diapirs (Léon et al. 2006; Judd and Hovland 2007). In many reports, seep-carbonate crusts or blocks are found exhumed or forming within the depressions (Hovland et al. 2005; Léon et al. 2006; Mazzini et al. 2006).

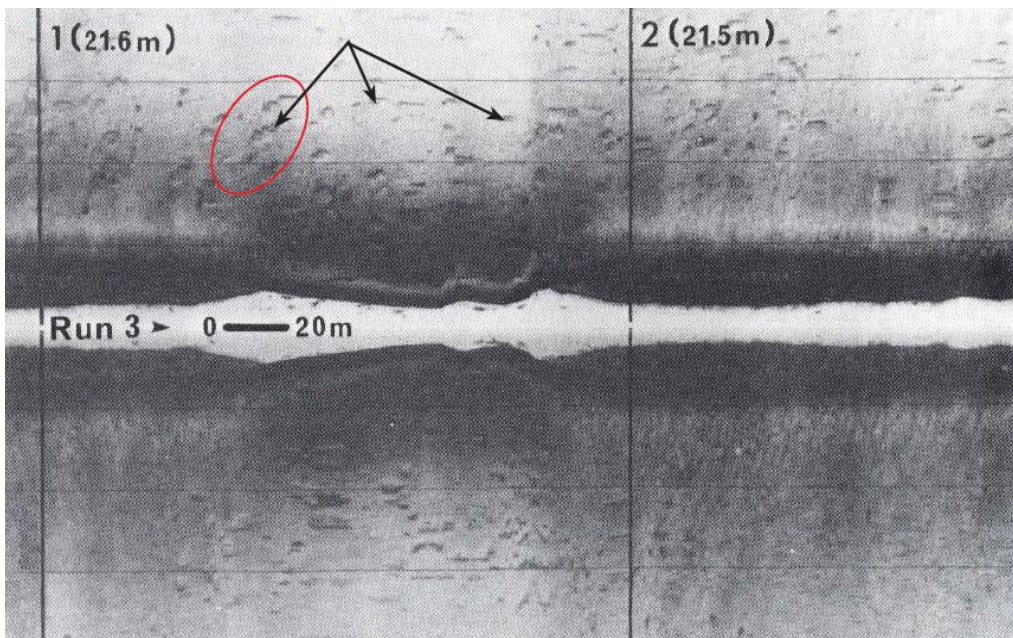


Figure 2.4 Side scan sonograph revealing extensive pockmarks in the northern Poverty Bay seafloor. The pockmarks are distributed extensively, rather than grouped together. Image from Nelson and Healy (1984).

2.3.4 Gas hydrates

Gas hydrates are frozen molecules of methane trapped between water molecules (Fig. 2.5) (Bohrmann et al. 1998; Trehu et al. 1999; Gorman et al. 2004; Judd and Hovland 2007). Gas hydrates form in a narrow stability field, and can only sustain their structure under very low temperatures, specific depths and pressure zones. A sustained input of methane must also be maintained for the hydrates to remain stable, and the pore fluids must be saturated in methane. These factors all contribute to the formation of a gas hydrate stability zone (or GSHZ), which may migrate up or down through host sediments (Trehu et al. 1999; Gorman et al. 2004; Milkov et al. 2004b; Judd and Hovland 2007).

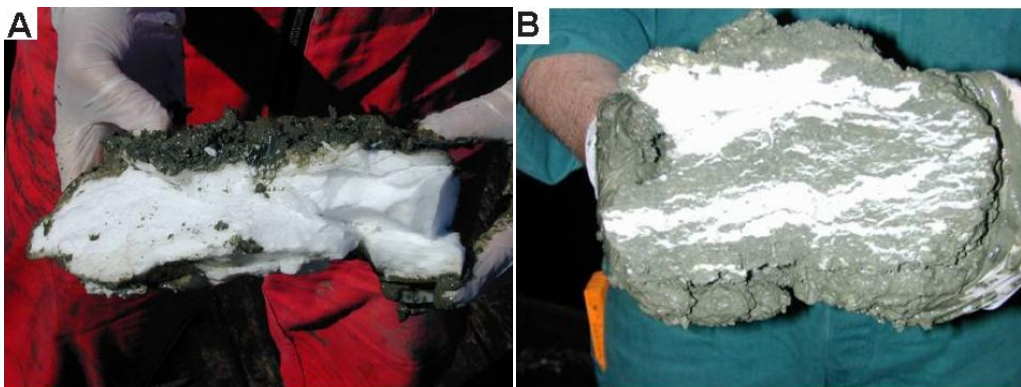


Figure 2.5 Frozen gas hydrate molecules in sediments sampled from cold seep sites. Image courtesy of IFM-GEOMAR, Kiel, Germany.

Several morphological variations have been identified in gas hydrates, the presence of which may affect seep-carbonate formation (Judd and Hovland 2007). In particular, the disssociation of gas hydrates may lead to the instability of host sediments (Pecher et al. 2004, 2005; Crutchley et al. 2007, in review; Ellis et al. in review).

Gas hydrates are identifiable in seismic imaging due to the hydroacoustic qualities of shallow gas accumulations, forming a bottom simulating reflection/reflector, or BSR (Gorman et al. 2004; Judd and Hovland 2007).

2.4. Cold Seep Distribution

2.4.1 Global Occurrences

As mentioned above, cold seeps are recorded worldwide (Fig. 2.1). In a review by Campbell (2006), 46 regions of ancient hydrothermal vents and hydrocarbon seep occurrences have been identified across the globe. Cold seep systems appear to be especially prevalent at convergent tectonic margins. Often they develop in these areas due to the compressive nature of the plate boundaries, which form thrust faults providing ample fluid pathways (Barnes et al. in review). Examples from such margins include the subduction margin of western North America (e.g. Campbell 1992; Bohrmann et al. 1998; Greinert et al. 2001; Goedert et al. 2003; Gieskes et al. 2005), New Zealand's Miocene to Recent East Coast (e.g. Kvenvolden and Pettinga 1989; Lewis and Marshall 1996; Campbell et al. 2008; Campbell et al. in review; Nyman 2009), Italian Apennine examples from the Miocene (e.g. Clari et al. 1994; Terzi et al. 1994; Cavagna et al. 1999; Conti and Fontana 1999, 2002, 2005; Peckmann et al. 1999; Barbieri and Cavalazzi 2005; Conti et al. 2007, 2008) and modern seeps offshore Japan (e.g. Han and Suess 1989; Han et al. 2008).

The Gulf of Mexico is an excellent example of a passive margin which has sustained vast fields of cold seeps because of sediment loading and salt tectonism (e.g. Carney 1994; Roberts and Aharon 1994; Orcutt et al. 2008). The Black Sea

is a unique environment where periods of varying salinity and oxygen availability in the water column have led to a stratified environment. Carbonates form both in the sediment as well as in positive relief on the sea floor (Peckmann et al. 2001; Reitner et al. 2005).

2.4.2 New Zealand Occurrences

It is now widely accepted that offshore of East Coast Basin, North Island, lies a prolific cold seep field along the Hikurangi Margin (Barnes et al. in review; Campbell et al. in review; Greinert et al. in review), and onshore there are many sites where Miocene paleo-seeps are marked by seep-carbonate deposits and plumbing features (Campbell et al. 2008; Nyman 2009). Unusual, scattered carbonates in deep marine mudrocks were first recorded in New Zealand by McKay (1877) and first described by Ongley and Macpherson (1928). However, an understanding of the origin(s) of these features has only recently begun to emerge in both the offshore (Lewis and Marshall 1996) and onshore (Campbell et al. 2008).

2.4.2.1 *Modern New Zealand cold seeps*

Cold seeps are currently active along the Hikurangi Margin offshore, and related seep phenomena are also found onshore. The Sponge Bay uplift of 1931 near Gisborne was documented by Strong (1933). A period of uplifting, which raised a shore platform above sea level, is one of the first documented diapiric or mud volcanism events in the Gisborne area. Pockmarks and mud volcanism were identified in the East Coast region of North Island by Nelson and Healy (1984). Side scan sonographs show the distribution and sizes of pockmarks in Poverty Bay (Fig. 2.4). Hydrocarbon seepage was linked to the formation of these phenomena (Nelson and Healy 1984).

Lewis and Marshall (1996) reported seafloor seepage of hydrocarbons along the Hikurangi Margin of New Zealand, listing at least 14 sites of active seepage in a convergent subductive margin, while also commenting on seep fauna. This paper was a landmark one identifying hydrocarbon rich fluid flow along the Hikurangi Margin. Sites identified and studied in this paper have provided a basis for subsequent studies, for example, Site 3 of Lewis and Marshall (1996) has become

the focus of more recent studies and is now known as ‘Rock Garden’ (Barnes et al. in review; Crutchley et al. in review; Ellis et al. in review; Netzeband et al. in review).

Orpin (1997) provided a possible model for seabed fluid expulsion off the Otago Coast, South Island, based on studies of dolomitic chimneys dredged from offshore. The chimneys are exhumed concretions that could be related to a former seep plumbing system (refer to Nyman 2009). Connections have also been made between gas conduits and gas hydrates on Ritchie Ridge, Hikurangi Margin (Pecher et al. 2004, 2005; Faure et al. 2006; Crutchley et al. 2008; Ellis et al. 2008) and in Fiordland (Crutchley et al. 2007).

As discussed in Chapter 3.2.5, mud volcanism occurs sporadically along the margin, and in particular in the Gisborne area where there are several active mud volcanoes (Nelson and Healy 1984; Francis et al. 2004) and oil seeps (Fig. 2.6) (Rogers et al. 1999). Pettinga (2003) also described events that took place when the Brookby Gas Seep went through a phase of mud volcanism in Hawkes Bay (Fig. 2.3).

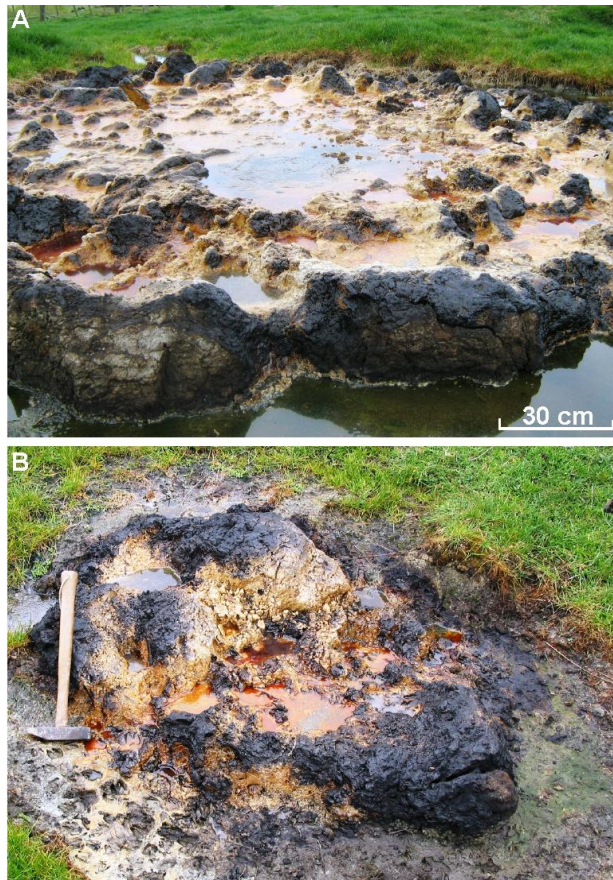


Figure 2.6 Oil Seeps at Waitangi (grid reference Y17 E2938359/N6306206). **A** – Largest seep, active at time of visit (November 2008). **B** – Smaller seep, 50 m south of seep in A.

2.4.2.2 Ancient New Zealand cold seeps

The first descriptions of what are now known as ancient seep-carbonates in the Raukumara region were made by Ongley and MacPherson (1928). Two sites, Tauwhareparae and Becks Haven (Bexhaven) were described as Tertiary limestone composed almost wholly of mussel fossil, *Modiolus* sp. These sites are also recorded on maps from the same survey in areas of known gas wells and gas seeps (Ongley and Macpherson 1928). One example of ancient seep-carbonate at Rocky Knob was described by Kamp and Nelson (1988) to be a small limestone, which was chiefly composed of disarticulated bivalves; it was named Moonlight Limestone. While these deposits were identified as a type of limestone, the authors noted that they were atypical compared to most New Zealand temperate shelf limestones. Mazengarb et al. (1991) mapped these deposits as either the Bexhaven or Moonlight Limestone - lenses of fossiliferous limestone characterised by specific bivalve types and a foetid smell.

Over the last decade the increased knowledge gained to identify cold seeps and their associated deposits has led to the New Zealand Miocene examples now being classified as methane derived authigenic carbonates, or MDACs (Campbell and Francis 1998; Campbell et al. 1999). The sites, listed in Table 2.2, have been included in a study of 14 ancient seep-carbonate deposits which span the East Coast Basin of North Island (Campbell et al. 2008). The carbonate deposits range in both morphology and size (Fig. 2.7), and in some cases subsurface plumbing is exposed (e.g. Karikarihuata and Rocky Knob). For a full table of information on these sites refer to Appendix 5.1.

Table 2.2 List of 15 ancient seep-carbonate deposits in East Coast Basin, including the 14 sites of Campbell et al. (2008).

| Site | Code | Grid Reference |
|-----------------------|-------|-----------------------|
| <i>Northern Sites</i> | | |
| Bexhaven | BXH | Y16 2955810E 6333127N |
| Karikarihuata Stream | KKH | Y16 2965700E 6335100N |
| Moonlight North | MLN | Y16 2943343E 6314003N |
| Rocky Knob | RKN | Y16 2941200E 6310300N |
| Tauwhareparae | TWP | Y16 2946283E 6324166N |
| Totaranui | TTN | Y16 2960605E 6319160N |
| Turihaua | TRH | Y18 2958065E 6274500N |
| Waiapu | WPU | Z15 2991680E 6365369N |
| Waapiro Stream | WPR | Z16 2976260E 6339430N |
| <i>Southern Sites</i> | | |
| Haunui | HAU | U23 2807322E 6104425N |
| Ngawaka | NGW | V23 2803946E 6107468N |
| Ugly Hill North | UGH-n | V23 2809905E 6107090N |
| Ugly Hill South | UGH-s | V23 2809402E 6107203N |
| Wanstead | WAN | U23 2813331E 6111065N |
| Wilder Road | WLD | V23 2806268E 6102668N |

Other geologic evidence of paleo-seep systems along the margin includes the relatively widespread occurrence of tubular concretions in Miocene slope mudstones, which have been interpreted to mark the focused migration pathways of methane rich fluids through past seep systems (Nyman 2009). Major sites include Cape Turnagain, East Cape, Taranaki Basin and Rocky Knob (Fig. 2.2).



Figure 2.7 Representative ancient seep-carbonate deposits in the East Coast Basin.
A – Moonlight North outcrop. **B** – A seep-carbonate boulder at Bexhaven. **C** – Ngawaka deposit in southern Hawkes Bay. **D** – Scattered boulders at Wilder Road.

2.5 Identifying Cold Seeps

Certain diagnostic characteristics can be used to help recognise certain carbonates as seep-related (Beauchamp and Savard 1992; Campbell 1992; Campbell and Bottjer 1993; Cavagna et al. 1999). Some features may be identified in the field, with further support from laboratory analyses such as plane polarised light (PPL) and cathodoluminescent light (CL) petrography. Faunal, elemental, mineralogical

and stable isotopic compositions can be especially important for providing positive identification of seep-carbonates. Campbell and Bottjer (1993) developed a sampling and exploration scheme based on work at Jurassic to Pliocene sites across the western U.S. continental margin. The work was undertaken by identifying common characteristics and fauna found at modern cold seeps. Most of the unique features of seep-carbonates develop as a result of AOM occurring during the formation of seep carbonates and the dynamic fluid flow regime to which they are exposed (Conti et al. 2007). The following section discusses seep-carbonate identification and their key facies attributes.

2.5.1 Geometry and structures

Seep-carbonates generally occur as isolated blebs, nodules, lenses or pods within clastic sediments (Greinert et al. 2001; Pecker et al. 2007). Undersea video or images reveal that modern seepage sites, both active and remnant, appear as “oases” of rock slabs and biota (Fig. 2.8 and Fig. 7.2), surrounded by vast regions of mud and seafloor sediment (Carney 1994). The prevalence of methane seepage in these areas is spatially restricted, and both the fauna and rock substrate distribution change in a gradient away from focused expulsion sites (Carney 1994). Associated structures may include pockmarks, diapirs and polygonal faults, the presence of which may be identified by seismic interpretation, swath bathymetry and undersea video obtained by remotely operated vehicles (ROV).

Ancient seep-carbonates appear to take several morphological forms. Blebs, nodules, boulders, slabs, pavements, pillars and mounds are typical, depending on their degree of induration and tectonic setting (Cavagna et al. 1999; Conti et al. 2007). Often they occur in isolated pods or nodules, and hence locating them may be serendipitous. Due to their relative resistance to weathering compared to the fine-grained clastic rocks in which they are found, seep-carbonates may appear as knobs or mounds above a weathered topography (Beauchamp and Savard 1992).

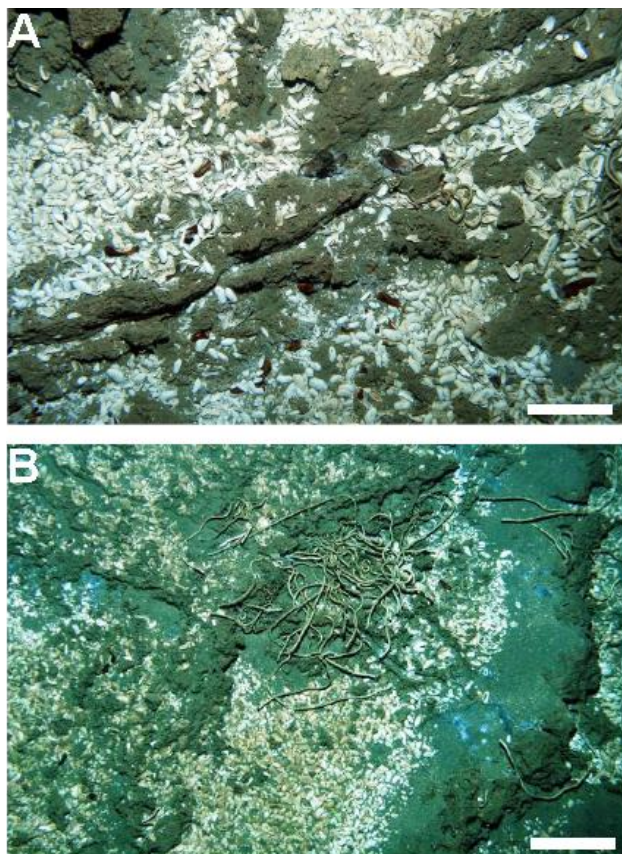


Figure 2.8 Photos from remote operated vehicle taken on NIWA Cruise TAN0616, scale bars are 20 cm in length. **A** – Dark brown carbonate slabs overlain by white *Calyptogena* sp. shells and scattered bathymodiolin mussels. **B** – Seep-carbonate crusts with *Calyptogena* sp. shells and vestimentiferan worm tubes. Images courtesy of NIWA, Wellington.

Brecciation is a common structure found in ancient seep-carbonates (e.g. Conti and Fontana 2002), which is a result of the dynamic fluid regime, cementation and potential gas hydrate influence on seep systems (Greinert et al. 2001). Hydrofracturing affects carbonate build up, and may be explosive or progressive. Slumping also occurs due to the build up and collapse of unstable fluid-laden sediments or the disassociation of gas hydrates (Pecher et al. 2004, 2005; Faure et al. 2006; Crutchley et al. in review; Ellis et al. in review). This dynamic setting typically forms carbonates which appear blocky and fragmented (Greinert et al. 2001).

2.5.2 Biota

Cold seep sites provide habitats for chemosynthesis-based communities. These communities consist of free living bacterial mats (e.g. *Beggiatoa* sp.), epifaunal

bivalves and their symbionts such as chemolithotrophic or methanotrophic bacteria (Boetius et al. 2000; Campbell 2006). There are five main groups of bivalves commonly found in seep systems: Vesicomyidae, Mytilidae, Solemyidae, Thyasiridae, and Lucinidae (Sibuet and Olu 1998). Tube worms found in cold-seeps can generally be grouped into the family Siboglinidae (Judd and Hovland 2007).

Species diversity may range from site to site, and be dependent on factors such as seep fluid flux, pore fluid geochemistry and other local environmental influences. Mytilids, such as bathymodiolin mussels, need hardgrounds for attachment while thyasirids and lucinids burrow into soft sediments to exploit sulphide-rich pore fluids for their symbionts (cf. Campbell et al. in review). *Beggiatoa* spp. aggregate in microbial mats, and are described by Boetius and Suess (2004) as “giant sulfide-oxidising bacteria”. Sulphide-oxidising bacteria may also be found within the gills of clams, such as the vesicomyid *Calyptogena* sp. or the bivalve *Acharax* sp. (Aharon 1994; Boetius and Suess 2004).

A biological zonation exists across some cold seep systems. This is due to the variations in fluid flux and therefore changes in chemical gradients across some seep. In areas of intense fluid flow, bacterial mats are common (Boetius and Suess 2004). These are also associated with gas hydrates and may form ‘microbialites’. Where fluid flux is intermediate to slow, *Calyptogena* sp. and *Acharax* sp. bivalves are common, with the latter being a low-sulphide specialist (Boetius and Suess 2004; Campbell 2006). When seepage is terminated due to a change in reservoir or fluid diversion to other areas of venting, the carbonate crusts and empty shells of *Calyptogena* sp. or *Acharax* sp. are left behind, as the remnants of ephemeral hydrocarbon seepage (Boetius and Suess 2004). Campbell (2006) presented an overview of variations in zonation patterns across several cold seep systems and related this to the availability of methane and sulphide in the porewater. For example, typically *Acharax* sp. is found at distal margins due to an ability to burrow deeper in sediments to reach the sulphidic zone (Boetius and Suess 2004).

In the geologic record, fossils are key to positive identification of ancient seep-carbonates (Figs. 2.9 and 2.10). This is due to the specific nature of faunal assemblages now recognised as inhabiting modern seeps. At some sites there may be a paucity of shell material if seepage had been inactive for some time, or if this fluid flow was originally diffuse and ephemeral (Levin 2005). Other areas, however, may have been colonised by large communities of vesicomyid clams or bathymodiolin mussels (e.g. Figs. 2.9A and B). Genetic studies can link modern and ancient seep fauna, and in modern settings there are biogeographical differences in species (Campbell 2006). In ancient deposits, the zonation patterns mentioned above may be used to interpret past fluid-flow conditions which once typified a site.

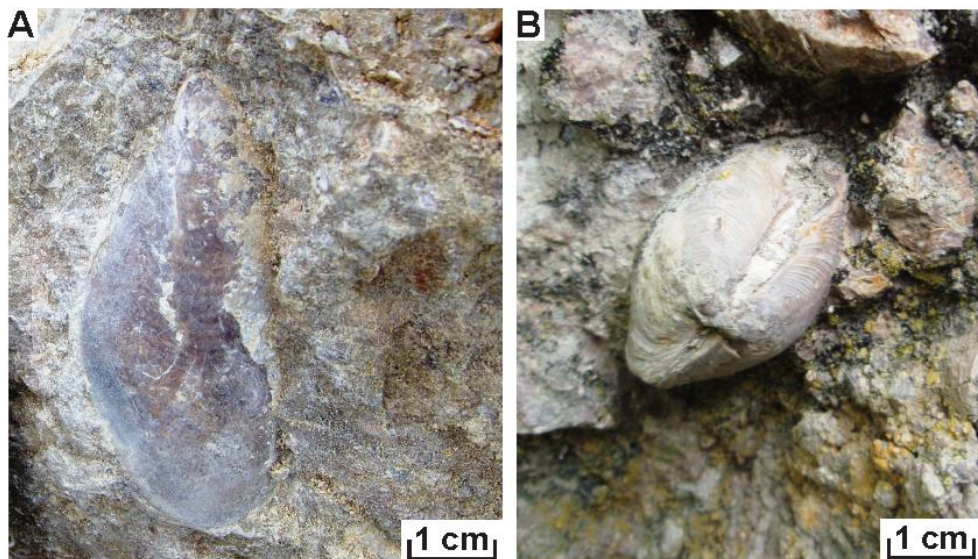


Figure 2.9: Fossilised seep-carbonate biota. **A** – Bathymodiolin mussel at TWP. **B** – Lucinid at Rocky Knob.

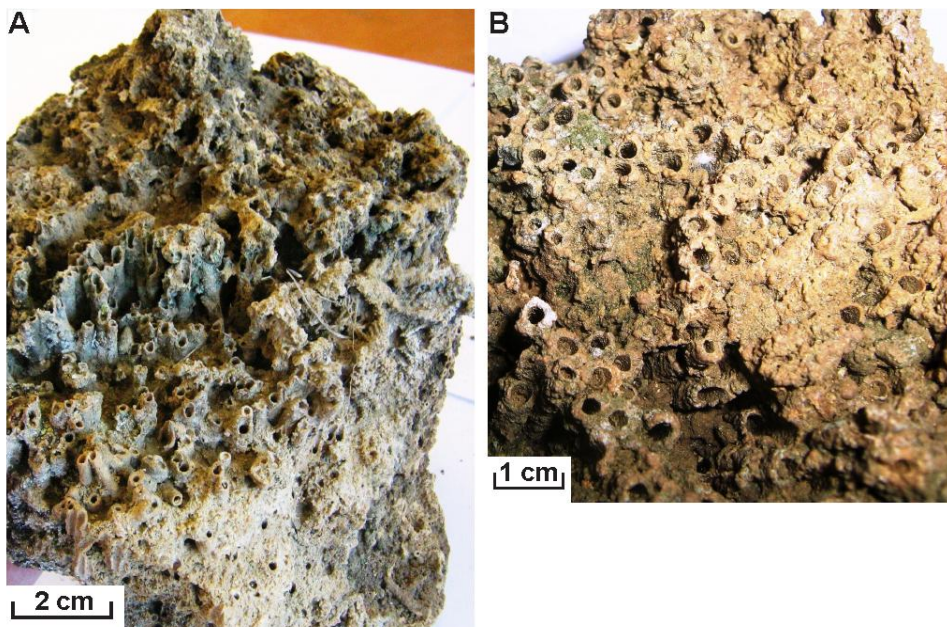


Figure 2.10: Fossilised bed of worm tubes from Ugly Hill, in the southern reaches of the Hawkes Bay. **A** – Fossilised bed, in orientation of sampling. **B** – Close up of tubes, the walls of which are laminar and have botryoidal layers of AOM cement.

2.5.3 Mineralogy

The mineralogy of seep-carbonates is complex and may vary among and within samples and sites. As carbonate is precipitated in the seabed by AOM, it incorporates siliciclastic sediment grains to form a carbonate-dominated deposit which becomes increasingly cemented and thus consolidated over time. The dominant carbonate minerals in seep-carbonates are calcite, aragonite and dolomite. Other associated minerals include pyrite, barite, gypsum and ankerite (Campbell et al. 2002; Campbell 2006; Judd and Hovland 2007). Various minerals preferentially precipitate depending on depth and temperature of formation, local pore water chemistry, fluid flux and availability of trace elements (cf. Burton 1993).

Calcite is a stable polymorph of calcium carbonate (CaCO_3). Calcite may appear as low magnesium calcite (LMC; <4 mol% MgCO_3) or high magnesium calcite (HMC; >4 mol% MgCO_3). In ancient seep-carbonates that have undergone extreme diagenetic alteration, calcite is the stable mineral product and is thus very common. In modern seeps, Greinert et al. (2001) reported a zonation of minerals which suggests that calcite is most commonly found in the central portions of seep systems, where fluid flow is slightly focused or diffuse. Aragonite is suggested to

precipitate in the uppermost area of seepage, at and directly beneath the seabed near the sediment-water interface in areas of advective fluid flow (Jørgensen 1992; Savard et al. 1996; Greinert et al. 2001, 2002; Aloisi et al. 2002). Aragonite is a metastable, orthorhombic polymorph of calcium carbonate (Korbel and Novak 1999). The significance of its presence and abundance in seep-carbonate is only just becoming recognised. Often aragonite is acicular or needle-like, or occurs in botryoidal bands. Aragonite and LMC are often found associated with one another (Naehr et al. 2007).

Dolomite is a carbonate mineral with equal proportions of Mg and Ca (50:50) $\text{CaMg}(\text{CO}_3)_2$. Dolomitic fabrics have been reported in several seep-deposits worldwide, generally as plumbing system concretions (Orpin 1997; Greinert et al. 2001; Nyman 2009). Typically both protodolomites (30 – 45 mol% MgCO_3) and pure dolomites (50 mol% MgCO_3) may be found together, but if a sample is dolomitic there is generally a paucity of either aragonite or calcite minerals in the carbonate. Dolomite has generally been observed in the deeper reaches of seep systems, and if sampled on the modern seafloor suggests that the dolomite may have been exhumed and exposed for some time (Rodriguez et al. 2000; Greinert et al. 2001; Naehr et al. 2007).

If pyrite is present in seep-carbonates, there is a link to the microbial processes occurring within the seep sediments (Barbieri and Cavalazzi 2005). Pyrite may be frambooidal in structure and is identified in modern Black Sea seep-carbonates (Peckmann et al. 2001) and Mesozoic Californian examples (Campbell et al. 2002). Siderite has been identified in carbonates from Hydrate Ridge, northeast Pacific Ocean, where siderite content in the sediment surrounding the cold seeps has also been linked to a stratified diagenetic zone (Naehr et al. 2000; Rodriguez et al. 2000). Barite is common in seeps from the Sea of Okhotsk (e.g. Derkachev et al. 2000), and in Devonian seep deposits of Nevada (Torres et al. 2003).

2.5.4 Isotopic composition

Cold seep-carbonates may be studied by their stable carbon and oxygen isotope composition ($\delta^{13}\text{C}$ and $\delta^{18}\text{O}$, respectively). Figure 2.11 is a diagram to show the

general ranges of $\delta^{13}\text{C}$ values and their carbon sources (Roberts and Aharon 1994).

It is well-documented that carbonates forming from methane-rich fluids generally are moderately to highly depleted in ^{13}C and so have quite to very negative $\delta^{13}\text{C}$ values (Gautier and Claypool 1984; Suess and Whiticar 1989). However, in seeps tapping a residual CO₂ (methanogenesis pool), $\delta^{13}\text{C}$ values may become enriched (Campbell 2006; Nyman 2009). A range of $\delta^{13}\text{C}$ values can result from different sources of methane (i.e. thermogenic or biogenic (Fig. 2.11) (see Section 2.2)), from different formative processes and from different degrees of mixing of fluid types (Campbell 2006).

On a fine scale, the isotopic signatures of individual cement phases or fabrics also may enable interpretation of the relative timing of cementation and the source of the fluids (Beauchamp and Savard 1992; Campbell et al. 2002).

Oxygen isotopes are generally indicative of water temperatures (Judd and Hovland 2007), and can thus indicate sources of water or the depth of burial a rock may undergo. However, diagenesis can also strongly alter oxygen isotope signatures (cf. Campbell 2006).

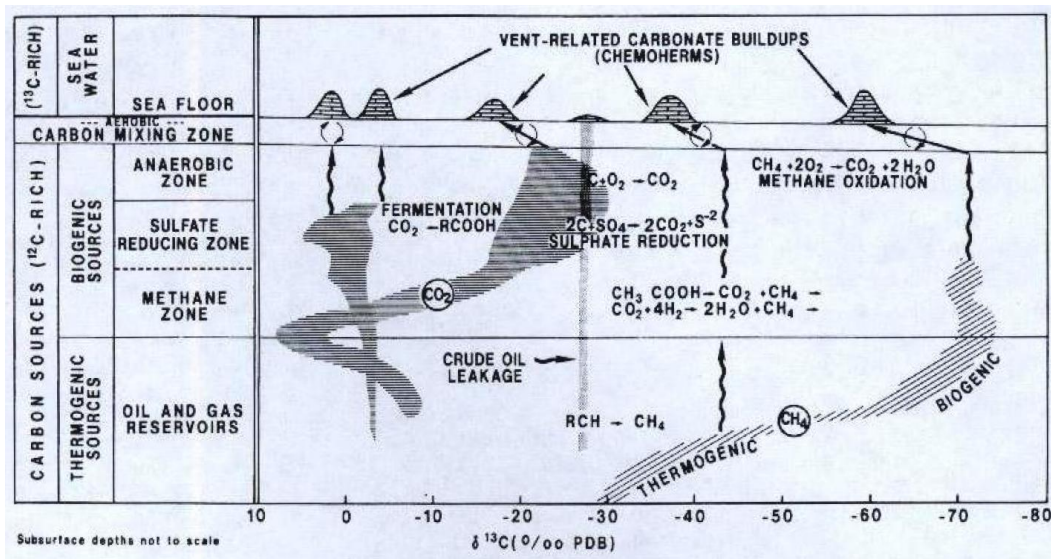


Figure 2.11 Diagram to show fluid source and resulting isotope values in cold-seep systems. Image taken from Roberts and Aharon (1994).

CHAPTER 3

Physical Setting

3.1 Introduction

This chapter serves as an introduction to the geological setting of the East Coast Basin and the Hikurangi Margin of eastern North Island (Fig. 3.1). It also briefly describes the physical, tectonic and geologic setting of the three sampling sites for this study, the principal onshore middle Miocene example at Tauwhareparae and the two comparative modern offshore localities at Builder's Pencil and Rock Garden, both of which are found on Ritchie Ridge (Fig. 3.2).

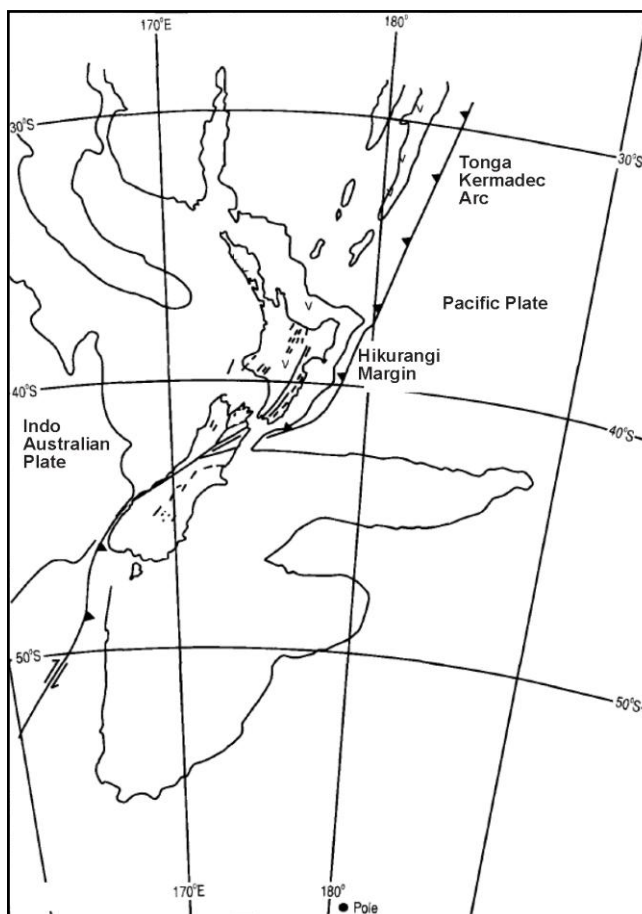
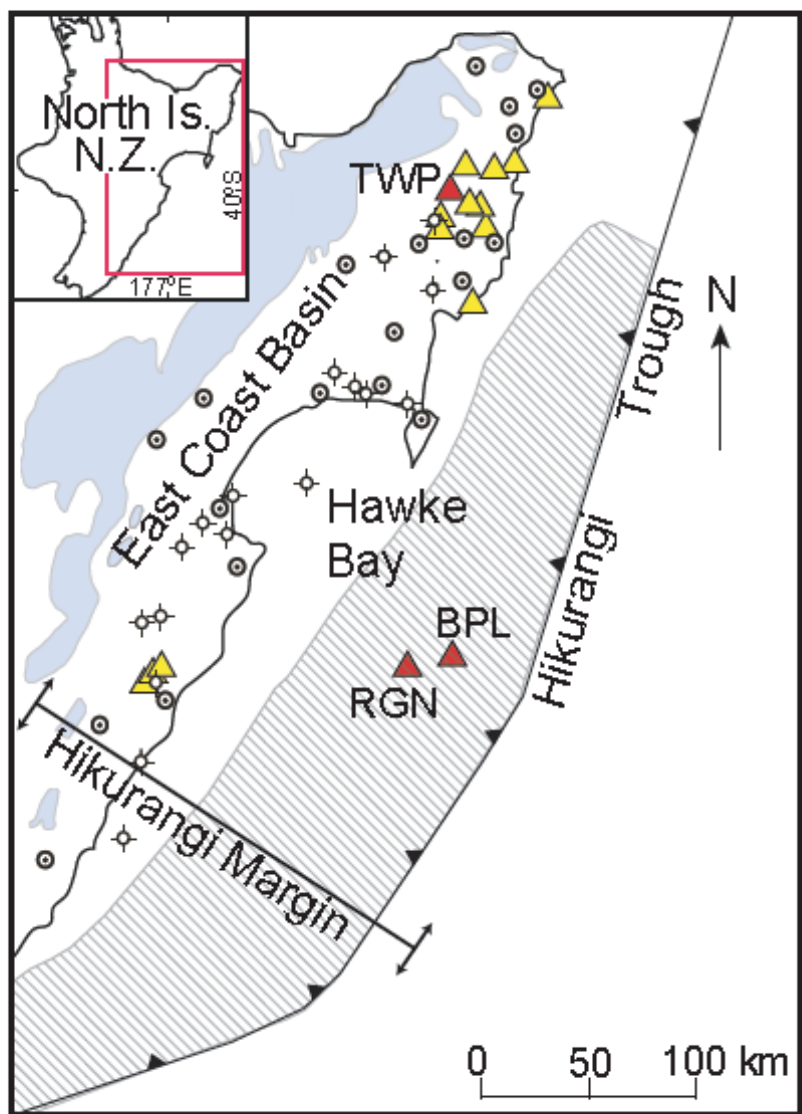


Figure 3.1 Subduction margin of New Zealand. In the north, the Pacific Plate is subducting beneath the Indo-Australian plate, while in the south the Indo-Australian plate subducts beneath the Pacific plate. Pole – pole of rotation of Pacific Plate with respect to Indo-Australian Plate. In the central zone plate movement is largely transform (Field et al. 1997). Image modified from King (2000).



- ▲ Miocene seep limestone localities
- ▲ Study sites
- Mesozoic basement rocks
- Well locations
- Known bottom simulating reflector (BSR)
- Active oil and gas seeps

Figure 3.2 Map of East Coast Basin and location of the main study sites, Tauwhareparae (TWP) onland, and offshore at Builder's Pencil (BPL) and Rock Garden (RGN) on Ritchie Ridge. Adapted from Nyman (2009).

Much of the onshore geology of the East Coast Basin has been extensively mapped and documented in a series of New Zealand Geologic Survey maps and Geological and Nuclear Sciences monographs (e.g. Mazengarb et al. 1991; Field et al. 1997; Francis et al. 2004). The seep-carbonate deposits in the area are an important part of the region's geologic history insofar as they are tangible records of fluid flow along the margin, presently and in the past. However, due to their relatively small outcrops in often isolated locations, they have only been mentioned briefly in most geologic publications, typically simply as limestone pods (in other words, until the late 1990's, their seep-carbonate origin was unknown).

3.2 East Coast Basin

3.2.1 Regional

The East Coast Basin of North Island has had a dynamic and complex history, strongly influenced by its position astride New Zealand's modern plate boundary (Fig. 3.1). The inception of this modern convergent plate boundary in the early Miocene (Waitakian – New Zealand Stage) marked the activation of thrust faults along the margin and formation of a substantial accretionary wedge (Field et al. 1997; King and Thrasher 1996; King 2000). The East Coast Basin is defined to extend from the Raukumara Basin offshore East Cape in the north, to Marlborough in the south, and is bounded to the west by the North Island's axial ranges (Fig. 3.2). In the east, the basin continues offshore as a forearc basin, bordered by the active Hikurangi Margin (Field et al. 1997).

Within the region there are several different basin types, including extensional rift basins, thrust-bounded basins and strike-slip basins (Field et al. 1997). These different basins are attributed to the dynamic changes in deformation throughout the Neogene, resulting in structural variations throughout the region.

Some literature suggests that areas within the East Coast Basin are currently undergoing uplift and sedimentation, with large amounts of over-pressuring affecting the drilling of certain formations for petroleum exploration (Darby and Ellis 2003). This over-pressuring is linked to fluid flow on the margin (Sibson and Rowland 2003). The presence of seep-carbonates in the East Coast Basin is

but one example of the evidence supporting a substantial history of subsurface fluid flow along the margin over time, other types of fluid flow include mud volcanoes and oil seeps (see Section 3.2.5).

3.2.2 Structure

The broad structure of the region was analysed by Moore (1988), who proposed two subdivisions based on facies and structure, the Eastern and Western sub-belts. In the northern reaches of the basin these were then divided into the Motu Block and the East Coast Allochthon (Fig. 3.3). Mazengarb (1993) further divided these blocks into five structural domains (D1-D5). Tauwhareparae is located in Domain 3 of Figure 3.3. Field et al. (1997) demonstrated that during the Early Cretaceous (Arowhanan – New Zealand Stage), D3 would have been part of the

imbricate frontal wedge, where faults and folding may have influenced fluid flow and expulsion. This shows that the site has been associated with the wedge, and thus overpressured fluid flow since then.

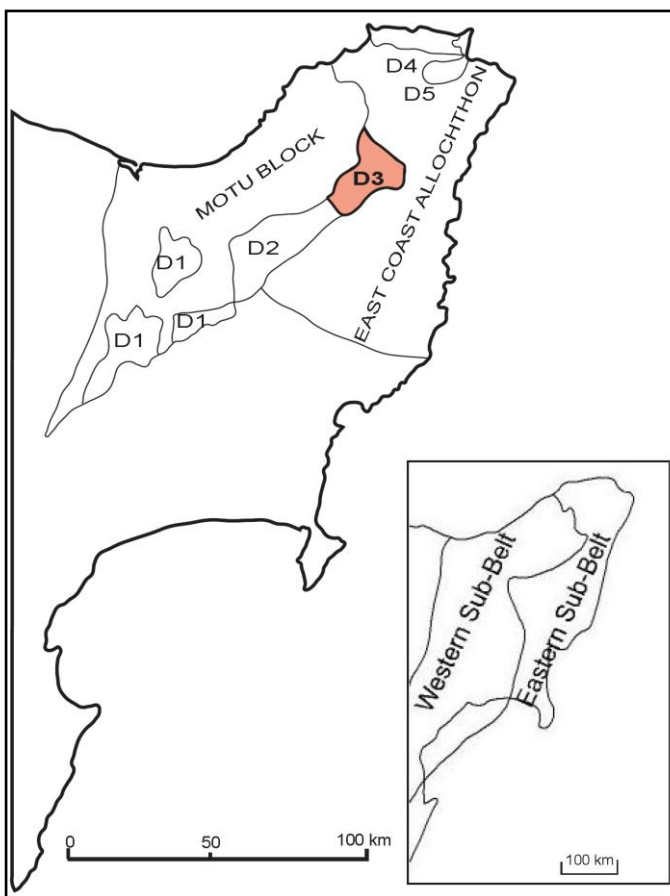


Figure 3.3 Structural divisions of East Coast Basin, North Island. Key: D1-D5 structural divisions from Mazengarb (1993). D3, the division in which TWP occurs is highlighted in red. Data and image modified from Moore (1988); Mazengarb (1993); Field et al. (1997).

3.2.3 East Coast Allochthon

The East Coast Allochthon (ECA) may be related to the Northland Allochthon and was emplaced across the northern reaches of the basin in the early Miocene (Field et al. 1997). The main mechanism by which the ECA was probably

triggered was the initiation of subductive processes occurring at the northern terminus of the Hikurangi Margin and Kermadec Arc system (Mazengarb et al. 1991; Field et al. 1997). Internal structure of the chaotic deposit is complex, including many fault and fold systems.

3.2.4 Hikurangi Margin

The Hikurangi Margin is the southern extension of the Tonga-Kermadec volcanic arc and marks the boundary between the Pacific and Indo-Australasian plates (Fig. 3.1). The margin likely has been active since about 40 Ma, but following a movement of the pole of plate rotation from 900 km south of New Zealand to 2100 km south nearly 22 Ma, the intensity of convergence and transpression increased (Lewis and Pettinga 1993). This led to inception of the modern plate boundary and onset of subduction and arc volcanism, as well as development of a forearc basin and associated frontal wedge (Fig. 3.4).

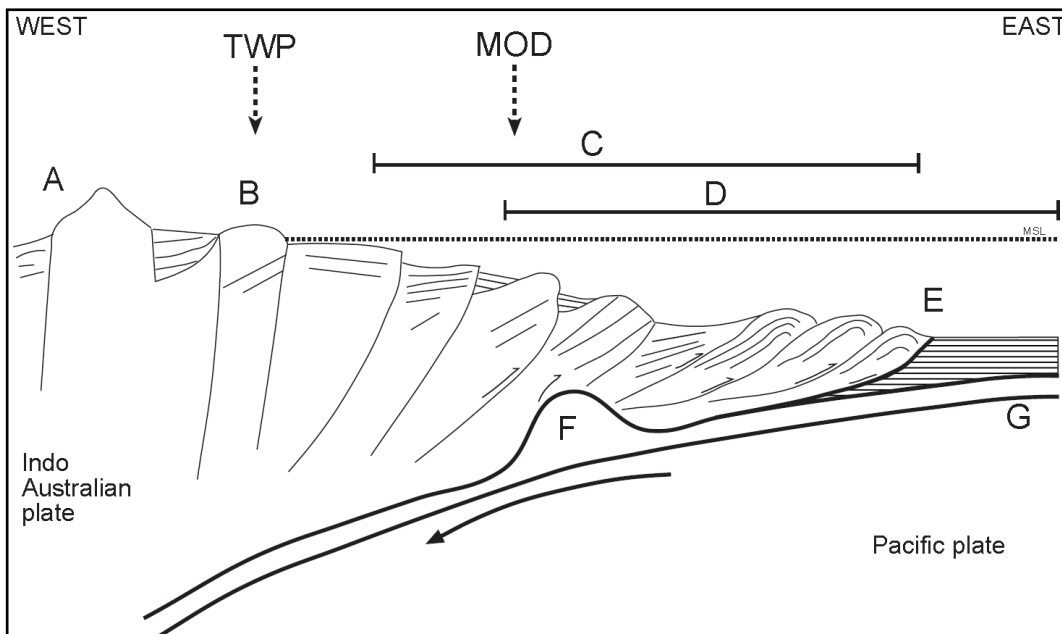


Figure 3.4 Generalised West to East diagram of Pacific plate subduction under East Coast Basin, North Island. The diagram is generalised, and is most like the mid-sector of the Hikurangi Margin, where the wedge is at its thickest. Key: **A**- Uplifted axial ranges; **B**- Backstop; **C**- Imbricate frontal wedge; **D**- Accreted trench fill; **E**- Deformation front; **F**- Subducting seamount; **G**- Subducting Pacific plate; **TWP**- Ancient seep-carbonate deposit at Tauwhareparae; **MOD**- Modern seep-carbonates, Ritchie Ridge. Scale not implied. Modified from Kvenvolden and Pettinga (1989); Lewis and Pettinga (2003); Lewis and Marshall (1996); Barnes et al. (in review).

In northern areas, plate movement is oblique convergent, while in the south motion is more transform (Lewis and Pettinga 1993; Barnes et al. in review). The ‘wedge’ is composed of sediments ranging from offscraped pelagic sediments and passive margin clinoforms, to slope basin infill and accreted ocean floor cherts, argillites and basalts (Lewis and Pettinga 1993). These sediments have been imbricately thrust together to form a substantial sedimentary wedge, with a backstop of highly indurated Mesozoic basement rock to the west. Regionally the wedge can be divided into three sectors - northern, southern and central. Both the northern and southern sectors have a limited accretionary front, and in the north there is evidence of re-entrance of subducted volcanic seamounts (Lewis and Pettinga 1993). The central sector of the wedge is especially prominent, and is up to 80 km wide and 7 km thick. Coastal hills onshore mark the highest of the imbricated ridges, exposing the Neogene sedimentary fill in the area (Lewis and Pettinga 1993).

The margin has been the focus of much scientific study, including bathymetric and seismic imaging offshore (Field et al. 1997; Barnes et al. in review) and stratigraphic mapping onshore. Submarine landslides and slumping are an important physical characteristic of the modern convergent margin (Barnes and Lewis 1991; Lewis and Marshall 1996; Faure et al. 2006; Barnes et al. in review). In some areas along the margin, gas hydrate instability is linked to such slumps (Pecher et al. 2004, 2005, 2007; Faure et al. 2006; Crutchley et al. in review; Ellis et al. in review).

3.2.5 Fluid flow

Once subduction was initiated and an accretionary wedge began to form during the early Miocene, overpressuring increased in the subsurface sediment pile, leading to dewatering of the sediments and activation of fluid flow (Darby and Ellis 2003). Currently, overpressure is thought to reach 300 m My^{-1} due to substantial subsidence (Darby and Ellis 2003). The manifestations of fluid flow in and around the margin since the inception of the plate boundary are many. Figure 3.4 is a generalised cross-section through the central sector of the margin. Note the relative position of the modern and ancient seep sites.

According to Lewis and Marshall (1996), there are three main geologic settings that foster the passage and expulsion of fluids on subduction margins, namely mid to upper slope ridges, shelf edges and canyon heads, and areas of slope collapse or slumping. Along the Hikurangi Margin, fluid is more likely to be expelled in the upper to mid slope because of faulting, permeable pathways and the presence of gas hydrates or clathrates (Lewis and Marshall 1996).

Mud volcanoes occur both onshore and offshore in the Hikurangi Margin region. They are the product of overpressured fluids rising through the subsurface, and expelling in sporadic and sudden bursts (Fig. 2.3). Within the East Coast Basin, mud volcanoes have been reported from both onshore (e.g. Brookby mud volcano described by Pettinga (2003)) and offshore (e.g. Sponge Bay uplift event of 1931 described by Strong (1933)).

Onshore, oil and gas seeps are widespread, from the well-known Te Puia Springs in the northern reaches of the basin, to the Waitangi Oil Wells around Gisborne that from 1910 – 1912 produced oil commercially (Fig. 3.6) (David Francis pers. comm. 2008). In the southern part of the basin, there are oil and gas seeps that have been analysed for lipids and biomarkers in an attempt to source individual seeps (Kvenvolden and Pettinga 1989; Rogers et al. 1999).

Offshore, cold seeps are now well-recognised to be a common feature along the Hikurangi Margin, and are generally associated with a strong basal seismic reflector (BSR) (Townend 1997; Gorman et al. 2004; Faure et al. 2006; Pecher et al. 2007; Barnes et al. in review).

Tubular concretionary structures, interpreted to mark cold-seep plumbing pathways, are found onshore at sites in East Cape, Cape Turnagain and Rocky Knob (Fig. 3.7) (Nyman 2009). Comparable plumbing features have been observed beneath the Karikarihuata and Tauwhareparae seep-carbonate deposits (see Section 5.3 and Campbell et al. 2008, in review).

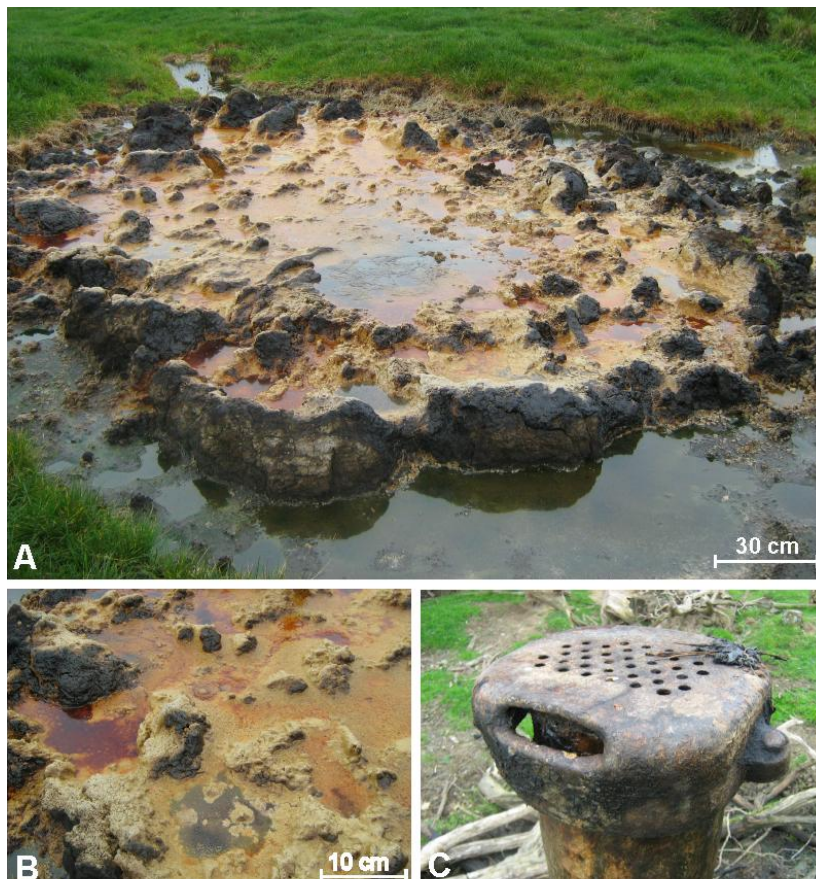


Figure 3.6 Waitangi Oil Seep, November 2008 (25 km northwest of Gisborne at grid reference Y17 E2938359/N6306206). **A** – Largest oil seep, 4 m across, actively bubbling. **B** – Close up shot of bubbling seep. **C** – Remnant Waitangi Well – 1, that was producing oil in 1910 (Dave Francis, pers. comm. 2008).



Figure 3.7 Tubular concretions (circled) in late Miocene mudstone cliffs, Whangaehu Beach, north of Cape Turnagain, Wairarapa (see Nyman et al. in review).

3.2.6 Potential source rocks

The East Coast Basin encompasses several potential hydrocarbon-bearing source rocks. In particular the Whangai and Waipawa Formations are known to be petroliferous (Field et al. 1997).

The Whangai Formation is a siliceous, in places calcareous mudstone occurring both onshore and offshore (Moore 1988; Mazengarb et al. 1991). In the north it crops out in many areas, especially in the vicinity of Ruatoria and Matawai, and in the south it is common in the Whangai Ranges and Wairarapa (Moore 1988). It is Late Cretaceous – Paleocene in age (Haumurian – Teurian NZ Stages) and is interpreted to have formed in shelf to basinal conditions (Leckie et al. 1995). Breccias, cherts and scattered greensands are found throughout the formation across the basin (Moore 1988). The formation is situated stratigraphically below the Waipawa Formation (Moore 1989; Field et al. 1997).

The Waipawa Formation occurs in outcrop from East Cape to Wairarapa (Fig. 3.8). It is quite similar to the Whangai Formation, that it is a siliceous mudstone, but its dark brown to black colour testifies to a typically high organic carbon content (2 to 6 % TOC, Field et al. 1997) (Moore 1988, 1989). The formation is Late Paleocene in age (Leckie et al. 1995), and is conspicuously leaking hydrocarbons at some locations (Field et al. 1997). The Waipawa Formation formed in a deep water environment (Leckie et al. 1995).



Figure 3.8 Waipawa Formation in outcrop at Porangahau, southern Hawkes Bay. The centre of the image shows a freshly exposed face of the shale, which is a black to dark grey colour. Photo courtesy of Susan Nyman.

These shales are most likely to be the source of many of the oil and gas seeps in the area, and may have originated methane for cold seep expulsion (Moore 1985; Field et al. 1997). The Waipawa black shale is considered to have the best potential for hydrocarbons in the area, although the Whangai Formation may be almost as worthwhile (Moore 1989; Field et al. 1997). However, Francis et al. (2008) has questioned whether these units could have been the source from the Miocene to the present day, considering that the shale oils may have become over-matured since the Miocene.

3.3 MIOCENE SEEP-CARBONATE - TAUWHAREPARAE

The ancient seep-carbonate deposit analysed in this study was sampled from one of several seep deposits in the Raukumara Ranges of North Island (Fig. 3.9). The site is known as Tauwhareparae (TWP) and is one of 15 presently known seep-carbonate deposits in the East Coast Basin, and one of the 12 found in the northern reaches of the basin (Fig. 3.2).



Figure 3.9 Photo of TWP in relation to its surroundings. It is found encased in mid-Miocene bathyal mudstones in the Raukumara ranges.

The Tauwhareparae paleo-seep deposit occurs in the northern extension of the East Coast Basin, astride the Tutamoe Syncline, which was probably a growth syncline developing throughout the Miocene (Fig. 3.10) (Dave Francis pers comm. 2008). The site lies on the northwestern limb of the syncline, about 1.5 km from its axis, and occurs within Neogene flysch-dominated sediments and

massive mudstone (Fig. 3.10) (Mazengarb et al. 1991). While geologic structures such as anticlines, synclines, faults and diapirs often provide fluid flow pathways for seep systems, the significance of the TWP deposit's relative proximity to the axis of a syncline is unclear. Despite local faults cutting through the mound at TWP at several elevations, the immediate area surrounding the deposit is not dominated by any major faults. However, the Arowhana Fault lies within 6 km of the site, and is a large fault which has been mapped in several major structural divisions (just north of the upper edge of Fig. 3.10) (Field et al. 1997).

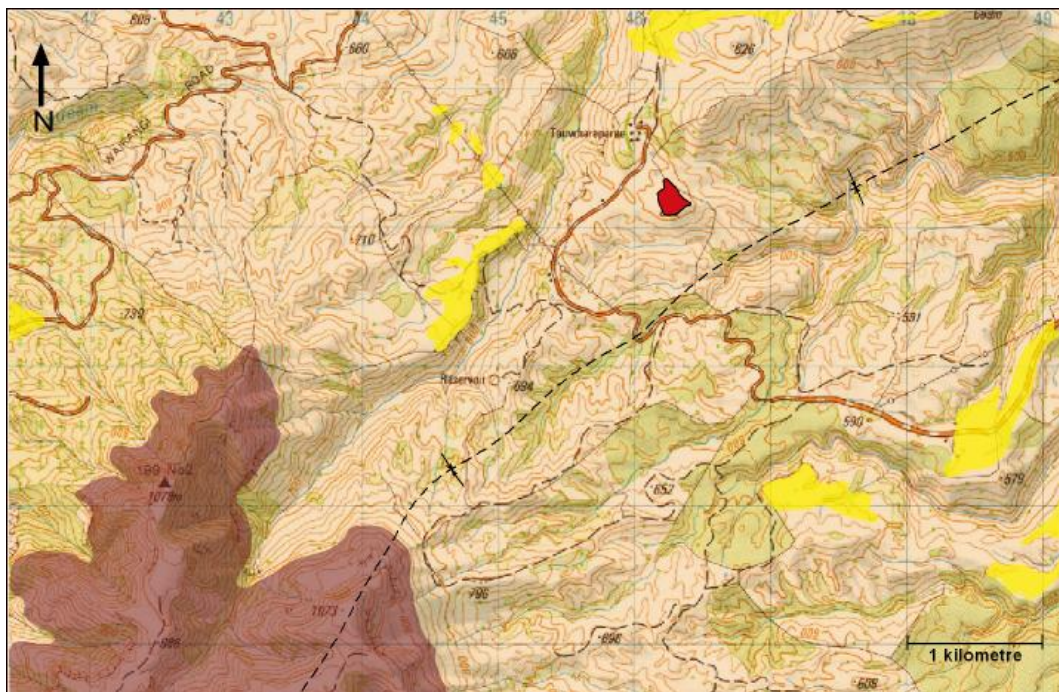


Figure 3.10 Tauwhareparae seep deposit and surrounding geology. Key – Purple-Areoma Sandstone on Tutamoe Plateau (synclinal outlier); Yellow – Gravel and silt terrace deposits, with various ash beds; Red – TWP paleo-seep site; Pale peach (background) – Host mudstone and flysch; Dashed line – Inferred position of the Tutamoe Syncline axis. Modified from Mazengarb et al. (1991).

Like most of the seep-carbonates in the region, the TWP example is encased within massive mudstones of middle Miocene (Lillburnian) age, which have an inferred thickness of at least 3000 m (Dave Francis pers. comm.). The mudstones are calcareous, massive to thin-bedded, and some contain interbedded sandstones (i.e. flysch). Seep-phenomena such as tubular concretions (originally known as ‘paramoudra’) have been recorded within the massive mudstones (Mazengarb and Francis 1985), and can be seen today along portions of Tauwhareparae Rd in road cuttings and slips today (Fig. 3.11) (grid reference Y16 E2956722/N6312137).



Figure 3.11 Tubular concretion in road cutting on Tauwhareparae Rd (grid reference – Y16 E2956722/N6312137). Concretion is one of four found in November 2008 in the same cutting. The host material is Ramanui Formation of Pliocene Age (i.e. much younger than the TWP example).

In terms of geological nomenclature, the northern seep-carbonates were once known as the Moonlight Limestone, but have since been renamed and are known as the Bexhaven Limestone. Names are taken from early observations of seep-carbonate occurrences on Bexhaven Station. This lithofacies falls within the Tolaga Group (Mazengarb et al. 1991). This group name was coined by Mazengarb et al. (1991) to encompass geologic formations in the area (inclusive of the seep-carbonates). Effectively the group formations or outcrops previously mapped by Ongley and Macpherson (1928), Black (1980), Mazengarb (1984) and Phillips (1985). The Tolaga Group is dominant on the NZGS Y16 geology map (Mazengarb et al. 1991). Tolaga Group rocks range from early to late Miocene (Otaian to Tongaporutuan – New Zealand Stage) and are characterised by bathyal mudstones and flysch with scattered limestones (Mazengarb et al. 1991; Field et al. 1997).

Figure 3.12 is a highly schematic stratigraphic column for the East Coast Basin demonstrating TWP's position relative to underlying source rocks and other ancient seep-carbonates in the basin. The TWP example is found in an area where others of middle Miocene age are located, with two examples of early Miocene age, and one of late Miocene age. Also note the typically massive slope mudstone encasing the deposits.

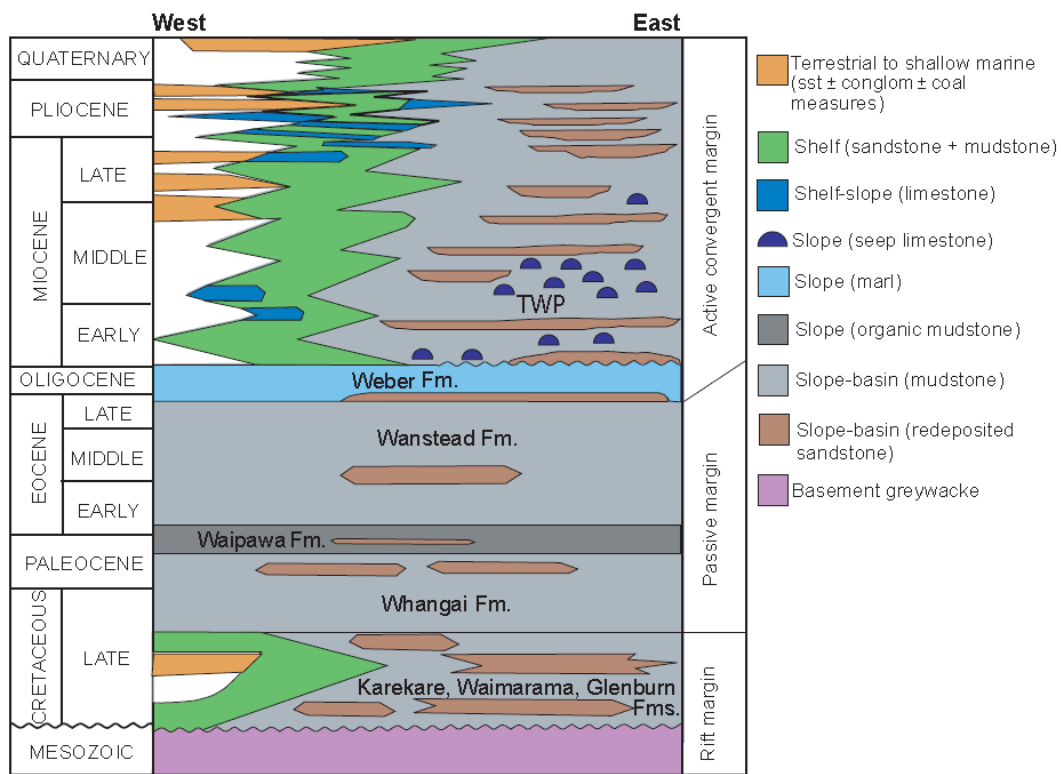


Figure 3.12 Highly schematic stratigraphic column for the East Coast Basin, showing the approximate level of Tauwhareparae (TWP) seep-carbonate deposit. Image modified from Nyman (2009), originally modified from Francis et al. (2004).

3.4 Modern Seep-Carbonates

Sampling of modern seep-carbonates was carried out on NIWA cruise TAN0616 in November 2006 (see Section 4.2.2). The samples obtained for this study were collected from two areas on Ritchie Ridge, offshore Hawke Bay, namely Builder's Pencil to the north and Rock Garden to the south (Fig. 3.13) (see Appendix 1.3 for latitude and longitude points across the sites). Ritchie Ridge is an elevated ridge across the imbricated wedge, one edge of which is reported to form a “backstop against the Pleistocene accretionary prism” (Pecher et al. 2004). Due to the water depth of the deposits (600 – 800 m) and resultant sampling methods (sled dredge), exact locations could not be pinpointed for individual samples, nor is *in situ* stratigraphic analysis available.

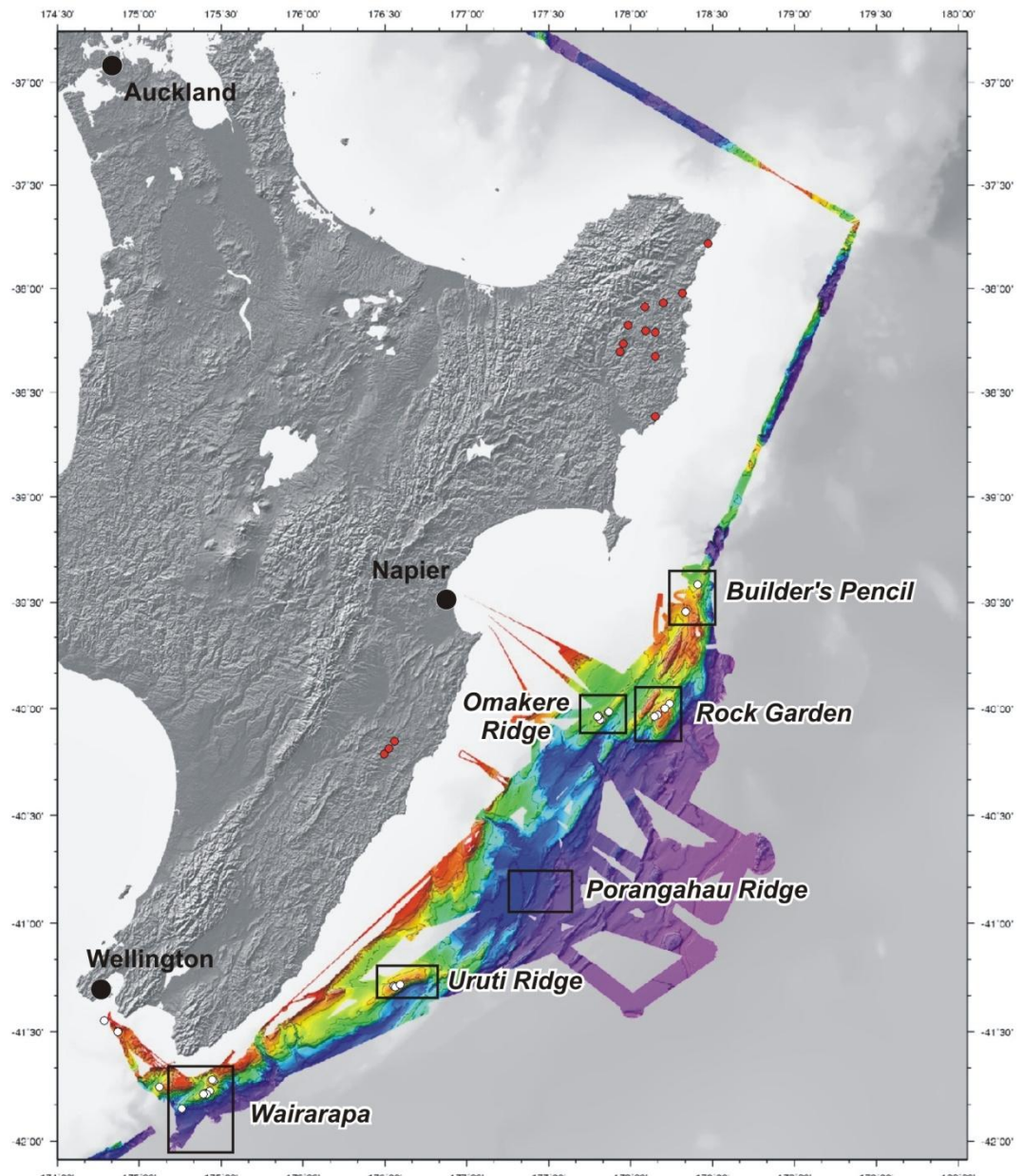


Figure 3.13 Hikurangi Margin, North Island and seep sites investigated on NIWA Cruise TAN0616. Builder's Pencil or (BPL) is the most northern site, and Rock Garden (RGN) is just south of it, although they are most geographically found on Ritchie Ridge. Figure courtesy of J. Greinert (RCMG, Ghent University, Belgium) and IFM-GEOMAR (Kiel, Germany).

3.4.1 Builder's Pencil (BPL)

Builder's Pencil (BPL) is a seep site on the landward flank of Ritchie Ridge that lies in 850 – 1250 m water depth (Fig. 3.13) (Barnes et al. in review). According to most recent observations, Builder's Pencil currently does not appear to be expelling fluids (Greinert et al. in review). Structurally, the site overlies a series of imbricate thrusts, and is underlain by an anticlinal fold, which is in turn

underlain by an active thrust fault (Barnes et al. in review). Stratigraphically it overlies a succession of Cretaceous-Paleogene foundation rocks, associated basin fill, and accreted trench turbidites (Barnes et al. in review). A strong BSR occurs in the subsurface and extends from near Rock Garden in the south to Ritchie Banks in the north (Pecher et al. in review).

3.4.2 Rock Garden (RGN)

Rock Garden (RGN) is a cold seep field on the southern portion of Ritchie Ridge that lies at water depths of 600 – 800 m (Fig. 3.13). Named informally by local fishermen who identified a rising plume of bubbles in their fish finder, the site has since been discussed in several papers (Lewis and Marshall 1996; Pecher et al. 2004; Faure et al. 2006; Barnes et al. in review; Campbell et al. in review; Crutchley et al. in review; Ellis et al. in review).

Bathymetric side scan sonar analysis by Faure et al. (2006) led to the identification of two northeast striking ridges, known as eastern and western Rock Garden. Morphologically, Rock Garden is characterised by a relatively flat-topped ‘plateau’ (Lewis and Marshall 1996; Barnes et al. in review) flanked by a series of slump features (Faure et al. 2006). Rock Garden is currently an active area of fluid expulsion, involving four active seepage zones: LM-3, Weka, Faure’s Site and Rock Garden Knoll (Lewis and Marshall 1996; Faure et al. 2006; Barnes et al. in review; Netzeband et al. in review). Pecher et al. (2007) reported gas flares at Rock Garden that were imaged on Cruise TAN0607. Rock Garden sits above a range of lithologies, including Cretaceous-Paleogene foundation rocks and Neogene accreted turbidites (Barnes et al. in review). In terms of seep-related fauna, the Rock Garden seafloor exposes scattered dead *Calyptogena* sp. bivalves and vestimentiferan tube worms, contrasting with some of the other seep sites in the area, such as Faure’s Site where large beds of live bathymodiolin mussels have been observed (Bialas et al. 2007).

A strong BSR (bottom simulating reflector) occurs beneath Rock Garden (Pecher et al. 2005; Barnes et al. in review; Crutchley et al. in review). The associated gas hydrate field recently has been linked to erosional processes in the vicinity of

Rock Garden. Several processes that ultimately lead to fluctuations in gas hydrate stability have been suggested to produce the observed erosional scars across the site (Pecher et al. 2004, 2005; Faure et al. 2006; Crutchley et al. in review).

Structurally, Rock Garden has formed as an uplift response to the subduction of a seamount beneath the area (Pecher et al. 2004, 2005; Faure et al. 2006; Barnes et al. in review). The two northeast trending ridges mentioned earlier are displaced by a NE-SW striking fault (Barnes et al. in review; Crutchley et al. in review). Faulting is linked to fluid flow processes in the area, and shallow faults have been mapped to enter the base of the BSR underlying Rock Garden (Pecher et al. 2004; Crutchley et al. in review; Greinert et al. in review).

CHAPTER 4

Methodology

4.1 Introduction

The techniques used in the analysis of seep-carbonates are slightly different from those used in a standard petrographical study of most limestones or sedimentary rocks. This is mostly due to the fact that the rocks themselves are complex. The transition from outcrop into hand sample, and from slab into thin section reveals an increase in complexity that can only be described as increasing in orders of magnitude. It arises due to the dynamic regime of fluid flow and changes in anoxic-oxic environments in which the seep-carbonates form. With this in mind, the analysis undertaken has been tailored to best analyse and unravel the paragenesis and multi-phase history of the seep-carbonates, the prime focus of this study.

4.2 Field Techniques

4.2.1 Onshore sampling

Field work at the onshore site at Tauwhareparae (TWP) was carried out over a week in November 2007. Objectives of the field study included both stratigraphic and facies analysis, mapping and profiling of the outcrop, and a comprehensive sampling regime. The deposit at TWP was divided into eight sampling zones, known as TWP-A through TWP-H (Fig. 4.1). These zones were based on physical groups of rock cropping out in the field and the morphology of the deposit.

Facies analysis of the seep-carbonate deposit at TWP was made difficult because the *in situ* outcrop, associated boulders and float material vary in appearance on a deca-metre scale or less. Significant lithologic changes are evident within boulders and even within hand samples. Consequently, the facies map and classification generated have been generalised so as to demonstrate only the major changes in lithological characteristics across the outcrop.

Traditionally, seep-carbonate outcrops have not lent themselves to a comprehensive stratigraphic analysis, partly because outcrops are relatively small in size. Also some deposits have undergone remobilisation and thus some degree of mixing of various facies. However, by combining several stratigraphic columns, an outline of general stratigraphy has been established at TWP that can be linked broadly to facies distribution.

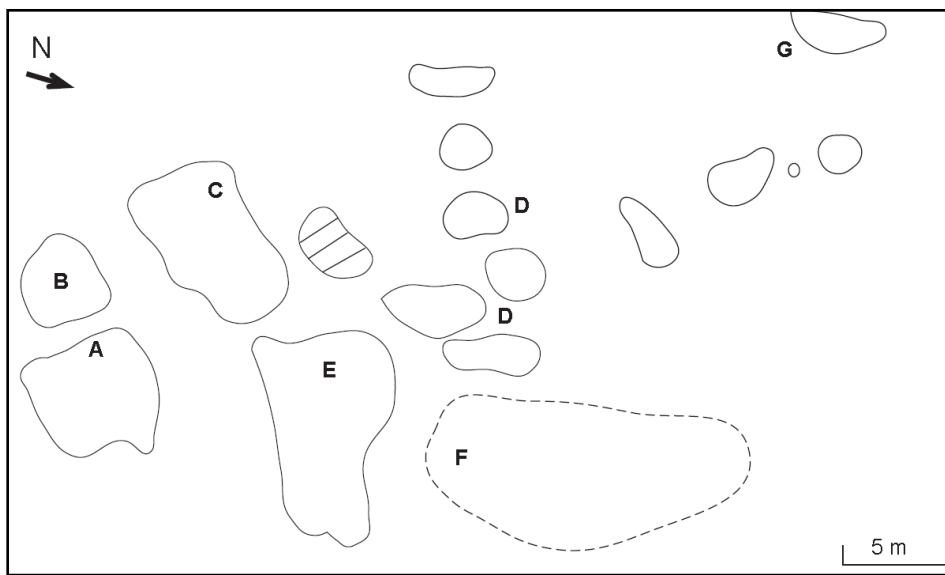


Figure 4.1 Outline of sampling zones A-G at TWP. Zone F is primarily float boulders and slabs along the flanks of the knoll. Note that Zone H is host mudstone and is found below the outcrop and further south on Tauwhareparae Road, and not included in this figure.

Hand samples were collected with a heavy-duty geologic hammer and sledge hammer, and ranged from 10 x 20 cm in size up to 30 x 50 cm blocks (Fig. 4.2). Numbering was organised in relation to the outcrop section from which the sample was collected, and was incorporated into the sampling scheme that has been established since the earliest field work began on the seep-carbonate research project (Collins 1999). Thus, samples were labelled TWP-section/sample number, so that for example TWP-A/16 is from zone A and was the 16th sample taken from that specific area. Samples were then described. A total of about 100 samples were collected. The full sample list is given in Appendix 1.1. Fifteen individual points of analysis in the form of profiles were created by choosing well-exposed longitudinal sections of outcrop to measure and sample (Fig. 4.3). For mapping, a base map was created by using an enlargement of the site from the NZMS Y16 1:50 000 topography map sheet. Grid references were established

using a GARMIN E-trex hand-held GPS instrument and were typically accurate to within about 5 m.



Figure 4.2 Profile construction, sampling and stratigraphic analysis of Zone C at TWP.



Figure 4.3 Stratigraphic logging and measuring of Zone A at TWP.

4.2.2 Offshore sampling

Modern offshore samples were collected on the NIWA RV Tangaroa research cruise, TAN0616 (Fig. 4.4). This leg was undertaken in November 2006 and ran between Wairarapa and Hawke Bay. Although the main objectives of the cruise were to undertake a biological study of seep-related fauna and flora, some large dredged samples of methane-derived authigenic carbonate (MDAC) were kept for future analysis. Dredging was mainly done with a rock dredge and basket (Fig. 4.4B-D). Once collected, samples were photographed but no further analysis was made. Following the cruise these dredge samples were stored at NIWA in Wellington.

Subsequently, Dr Alan Orpin (NIWA, Wellington) made the dredge samples available for petrological analysis within this carbonate-seep study. Hence, the material effectively provides the opportunity to take a uniformitarian approach to the study of the ancient TWP seep-carbonate deposit. The author visited NIWA Wellington in December 2007 to photograph, describe, and collect subsamples of the original material. For a full sample list, and cruise data, see Appendix 1.2-1.4.



Figure 4.4 **A** – NIWA's primary research vessel, RV Tangaroa; **B,C,D** – Rock dredge collection on the Tangaraoa; **E** – Cleaning hemipelagic mud off dredged samples; **F** – Seep-carbonate sample with shrimp; **G** – Small faunal specimens collected from carbonate rich dredge hauls; these are primarily encrusting benthic fauna. Images of Cruise TAN0616 courtesy of Alan Orpin, NIWA Wellington.

4.3 Laboratory Techniques

4.3.1 Rock sample preparation

Before any laboratory work could be done, all coherent samples were cut into slabs using a diamond bladed saw to reveal internal fabrics (Fig. 4.5). Subsequently the slabs were cut to a thickness of 1-2 cm for thin section preparation, while thin section blocks were made to fit upon a standard microscope slide (2.5 x 4 cm). Slab offcuts were powdered in a ring mill grinder for 45 seconds, producing powders for stable isotope analysis, X-ray diffraction (XRD), and carbonate determination.



Figure 4.5 A – Rock storage trays at the University of Waikato; B – Allegro diamond bladed saw for slabbing samples and cutting thin section blocks; C – Slabbed samples in storage trays; D – Grinding machine used to trim and grind thin sections; E – Thin section blocks in storage trays; F – Diamond lap wheels for polishing thin section blocks.

4.3.2 Plane polarised light (PPL) petrography

The block faces to be studied were polished for 5 – 10 minutes on a diamond lap wheel. If samples had integrity and strength, the blocks were mounted on frosted slides using standard procedures and Hillquist Epoxy resin. After mounting, the slides with blocks attached were ground down and polished.

Modern samples that were friable and moderately unlithified were block mounted and then cut and polished. Block mounts were made by cutting and polishing standard blocks, and then placing them in “box frames” constructed of tin foil and masking tape. These frames had a small amount of resin in the base, and after placing the block inside, the rest of the mount was filled with resin. After setting overnight, the samples were trimmed with a small saw blade and then polished and affixed to slides with normal mounting procedures.

When these processes were completed the thin sections were polished to (0.03 mm thickness) obtain a smooth and clean finish.

Standard petrography using an Olympus BH-2 binocular petrographic microscope was carried out to determine the fabrics and textures that make up the seep-carbonates. Measurements of mineral or crystal size were calculated and component-specific petrography was undertaken.

4.3.3 Cathodoluminescent light (CL) petrography

Cathodoluminescence (CL) petrography was used to determine variations in mineralogy and to further identify carbonate phases within thin sections. The analysis was carried out at the University of Waikato using a CITL MK5-1 Cathodoluminescence stage attached to a microscope with relatively consistent operating conditions involving a gun voltage of 16 kV and a current of 450 mA (Fig. 4.6). Images were taken using a Nikon camera DMX1200 and captured using Nikon’s ACT-1 software interface.

The CL colours produced are a result of luminescence created by energetic electrons being fired at the thin sections and their contained minerals (Pagel et al. 2003). Luminescence will change depending in particular on the content of Mn

and Fe within the thin section components (refer to Table 4.1 for a list of characteristic CL patterns). This may be used to help determine the geochemical environmental conditions under which the carbonates formed or were altered (Pagel et al. 2003).



Figure 4.6 Cathodoluminescence stage and microscope.

Table 4.1 Some common minerals and their associated CL patterns (adapted from Pagel et al. 2003)

| Mineral | CL pattern |
|-------------|--|
| Aragonite | dark blue, black (dull, non-luminescent) |
| Calcite | orange – yellow (brightly luminescent) |
| Dolomite | pink - red |
| K-Feldspar | bright blue |
| Plagioclase | bright green |
| Quartz | variations in colour |

4.3.4 X-ray diffraction (XRD)

4.3.4.1 Bulk mineralogy

Two methods of X-ray diffraction (XRD) analysis were undertaken during this study, namely bulk XRD and componentry XRD. Bulk analysis was run on a Philips (XPERT) XRD machine in the Department of Earth and Ocean Sciences at the University of Waikato. X-ray powder diffraction analyses were run from 0-40

$^{\circ}2\theta$, and the major mineralogy was determined from peak positions (see Table 4.2). A relative abundance of mineral types was assessed from peak intensities, using the procedure of Nelson and Cochrane (1970). This provided a qualitative scale for relative abundance (Table 4.3).

Table 4.2: Common Å spacings and 2θ values from (Nelson and Cochrane 1970).

| Mineral | d-spacings | 2θ |
|--------------------|------------|-----------|
| <i>Aragonite</i> | 4.21 | 21.1 |
| | 3.40 | 26.2 |
| | 3.27 | 27.2 |
| | 2.87 | 31.1 |
| | 2.73 | 32.8 |
| | 2.70 | 33.2 |
| | 2.48 | 36.2 |
| | 2.41 | 37.3 |
| <i>Calcite</i> | 3.86 | 23.0 |
| | 3.04 | 29.4 |
| | 2.85 | 31.3 |
| | 2.50 | 35.9 |
| | | |
| <i>Dolomite</i> | 4.03 | 22.1 |
| | 3.69 | 24.1 |
| | 2.89 | 30.9 |
| | 2.67 | 33.5 |
| | 2.54 | 35.3 |
| | 2.41 | 37.3 |
| | 2.19 | 41.2 |
| | | |
| <i>Quartz</i> | 4.26 | 20.85 |
| | 3.34 | 26.5 |
| <i>Plagioclase</i> | 3.31 | 26.0 |
| | 3.2 | 27.8 |

Table 4.3 Relative abundance scheme for XRD mineralogy.

| Symbol | Quantity |
|--------|----------|
| - | None |
| R | Rare |
| S | Some |
| C | Common |
| A | Abundant |

4.3.4.2 Component mineralogy

The SIEMENS GADDs (General Area Detector Diffraction system) machine (Fig. 4.7) at SGGES, The University of Auckland scans individual points on thin sections using a laser beam width of 0.5 mm. Operating conditions are shown in Table 4.4. An image is produced by a digital camera showing the position of the laser beam on the sample (Fig. 4.8). Using a scan time of 120 seconds, a series of detectors collect x-ray beams that are fired at the material within the point being analysed. This produces an image that consists of points varying in size and colour depending on the intensity of the x-ray reflection, which is influenced by crystal size, orientation and mineralogy (Fig. 4.8). From this, Chi analysis is done on the data, identifying key peaks in intensity. Using EVA Software the mineralogy is determined by matching peaks with their corresponding mineral types, similar to normal XRD analysis.

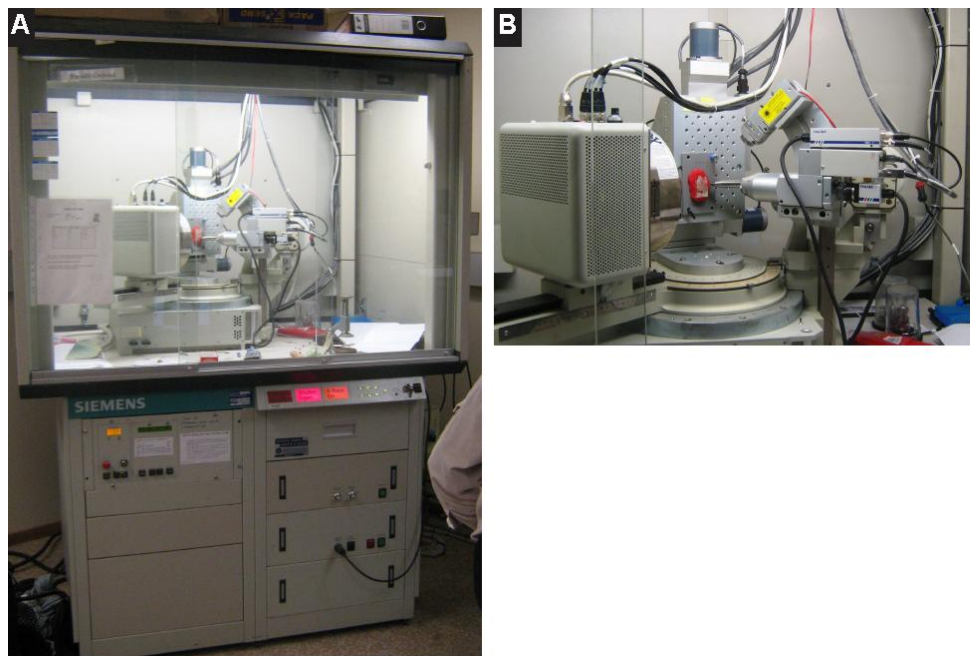


Figure 4.7 GADDs data collection. **A** – GADDs machine with X-ray screen; **B** – Close up of thin section and laser point.

The GADDs machine is a new technique as applied to cold seep-carbonate research and was used in this project to evaluate mineralogical changes suspected on a fine microscopic scale first detected using CL and PPL microscopy, and therefore confirmed the hypothesised paragenesis.

Table 4.4. Operating conditions for the GADDs machine.

| Operation Settings |
|---------------------------|
| 40kV 30mA |
| 2θ 40 |
| Omega 20 |
| 0.5mm Collimator |
| 120sec Count |
| 0.01 deg Integration |

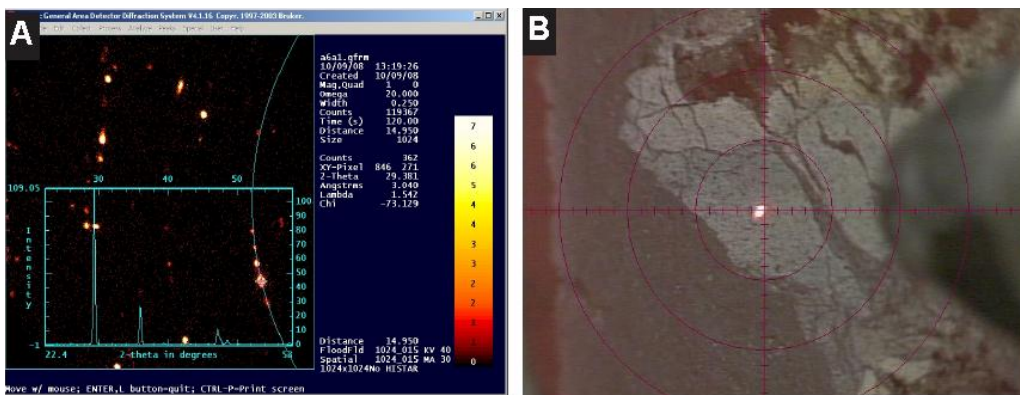


Figure 4.8 A – Screen image photographed during data collection, with peak graph superimposed; B – Photo of thin section surface and laser point for analysis.

4.3.5 Stable isotope analysis

Microdrilling was carried out with a Dremel drill and drill bits to extract powders for component-specific stable oxygen and carbon isotope analysis of the ancient Tauwhareparae samples. Powdered samples from drilling ranged in weight from 0.05-0.146 g. Five main components were drilled: background micarb; sparry or fibrous aragonite phases; late detrital fill; and fossilised shells. Modern Ritchie Ridge samples were powdered in bulk for isotope analysis due to their more uniform fabrics. Prior to any isotope analysis, bulk XRD was carried out on all samples to determine the dominant mineralogies present in order to decide acidification times for isotope analysis.

Stable isotope analysis was carried out in the Department of Earth and Ocean Sciences at University of Waikato. Samples were run either as calcite/aragonite- or dolomite-rich. For the first group, samples were reacted in 105% orthophosphoric acid at 70°C for 10 minutes in a Europa CAPS (Carbonate Automatic Preparation System) and the evolved CO₂ introduced into a Europa 20/20 mass spectrometer. For the second group of samples (dolomite rich) the acidification time was changed to 2 hours rather than 10 minutes so as to ensure complete dissolution of this more stable carbonate phase.

Isotope values are given in delta (δ) notation per mille (‰) deviation of the $^{18}\text{O}/^{16}\text{O}$ or $^{13}\text{C}/^{12}\text{C}$ ratio of the sample relative to the VPDB standard in relation to repeated analyses of the international standard NBS-19 and internal standard

WCS. Instrument precision is $\pm 0.05\text{\textperthousand}$ for both $\delta^{18}\text{O}$ and $\delta^{13}\text{C}$. Analytical precision is 0.05 to 0.1%.

4.3.6 Carbonate percentage determination

Carbonate percentage was determined using the LECO titration machine in the Department of Biological Sciences, University of Waikato. Bulk powders were measured out at 25 mg and burnt off at 900°C. The weights were then compared to standards of quartz and pure carbonate.

4.3.7 Total organic carbon (TOC)

Total organic carbon (TOC) was analysed in 15 representative samples at GEOMAR (Kiel, Germany). The instrument used was a Carlo Erba NA 1500 elemental analyser, which utilised samples 10-20 mg in weight that had previously been combusted to CO₂ at a temperature of 1050°C in a tin cup.

4.3.8 Microprobe analysis

Microprobe analysis was carried out at the SGGES, University of Auckland, using an Electron Probe Micro Analyser (1987 JEOL JSM 840A) (Fig. 4.9). The equipment has been rebuilt to JXA-840A EPMA specifications. Moran Scientific (Bungonia, NSW, Australia) supplied the hardware and software interfaces for the X-ray detectors. Analysis was carried out on selected points (2 μm across) to confirm and quantify commonly occurring elements such as calcium, magnesium, iron, strontium, manganese, silica, aluminium, potassium, and sodium. Counts were taken over 100 seconds using a probe current of 0.8 nA.

Thin sections were polished and then carbon-coated (to absorb electrons), and small black rings were circled to identify areas of interest. Images were located using a microscope and then analysed with the microprobe.

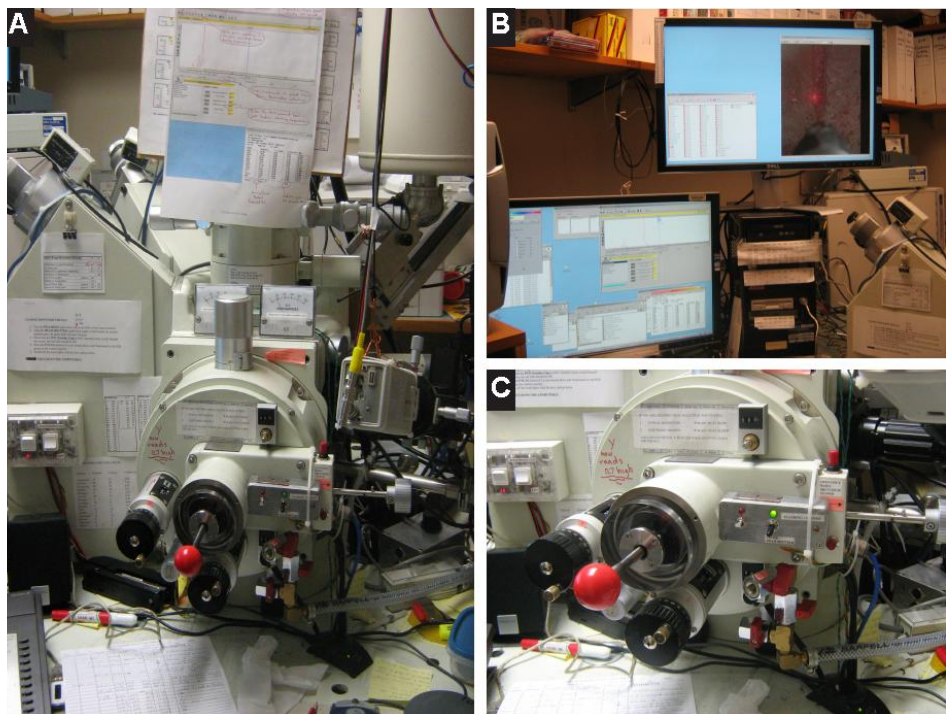


Figure 4.9 EPMA for microprobing at the University of Auckland. **A** – overview image of EPMA system; **B** – imaging of thin section in top right, screen below shows peak analyses of elemental composition; **C** – close up of stage for thin section stage.

4.3.9 Ultraviolet (UV) light

Polished thin sections were analysed under ultraviolet light in the Department of Biological Sciences, University of Waikato. The UV ‘block’ attachment has the following specifications: excitation type – UV; excitation filter – BP 340 – 380 nm; Dichromic mirror – 400 nm; Supression filter LP 425. Images were captured through a Leica Olympus microscope and Olympus data software.

The UV light excites organic material to glow a green – yellow tinge, while surrounding material did not fluoresce. Images produced are therefore a good indicator of where material with an organic source, and possibly hydrocarbons, are located in the carbonate phases (Hood 2000; Campbell et al. 2002).

CHAPTER 5

Stratigraphy and Facies

5.1 Introduction

This chapter summarises field work and related observations at the middle Miocene Tauwhareparae seep-carbonate locality. A site description provides the morphology and layout of the deposit, while a stratigraphic column and a facies map serve to portray the lithological features of the carbonate. For the physical and geologic setting of the paleo-seep, refer to Chapter 3. Analytical results from laboratory analysis on the carbonates are presented in Chapter 6. During field work, the deposit itself was divided into a series of “zones”: A-G (Fig. 5.1), each morphologically distinct from one another around the mound. Specifically, faulting has divided the mound into three portions, and the other zones were designated by erosional differences, forming areas with more rock than others. Sampling according to these zones was also carried out. An eighth zone, known as Zone H, is included as the host mudstone that was sampled at the site and at a road cutting 100 m south of the outcrop.

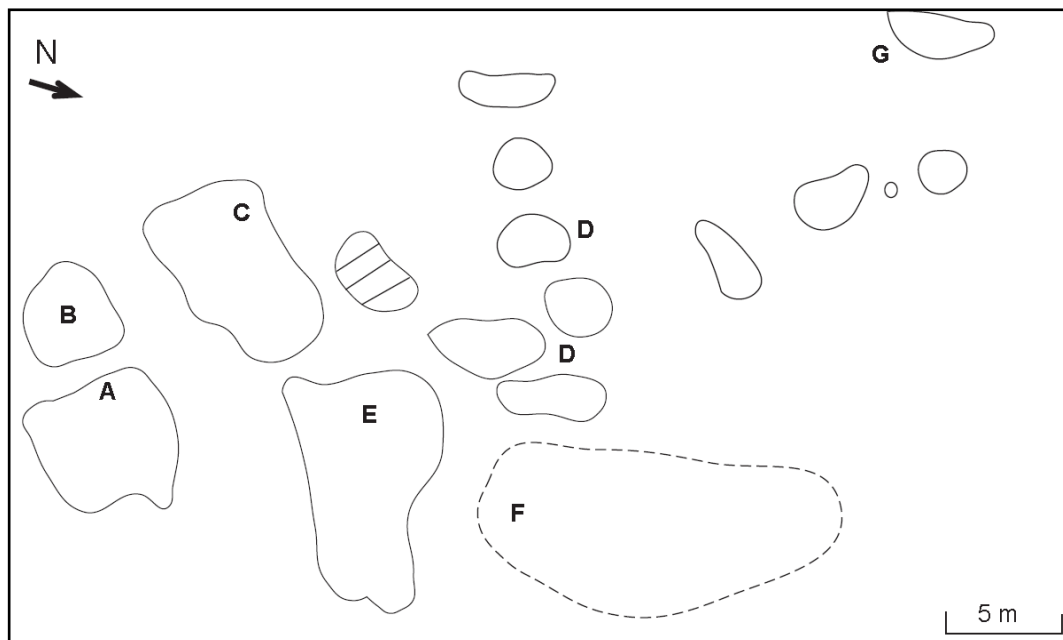


Figure 5.1 Outline of sampling ‘zones’ at TWP. Note that sampling zone H is not included on this map, as it is positioned further south than the mound. The three portions of the deposit separated by faulting are A; B; and C-E.

5.2 Field Results

5.2.1 Site description

The Tauwhareparae (TWP) seep-carbonate deposit (Fig. 5.2) is located at NZMS 260 Map Grid 1:50 000 Y16 (2946283E/6324166N) (Fig. 5.3). Access to the outcrop is obtained by a four-wheel drive track once used by local farmers who quarried the carbonate. This track winds around the knoll and stops near the summit. The seep-carbonate sits above a massive mudstone unit of middle Miocene age (Lillburnian NZ Stage – 15.1 to 12.7 Ma) (Campbell et al. 2008). A high point in the surrounding area, the mound reaches 653 m in elevation, and is situated 2.8 km southeast of the Tauwhareparae trig station.



Figure 5.2 Tauwhareparae seep-carbonate mound. Photo taken on southwestern flanks facing north. Note large amount of float material scattered downhill.

Spatially TWP has been divided into eight sections, labelled Zone A through H (as seen in Figure 5.1). Zones A to E are distinct areas of outcropping rock which progress around the knoll in a clockwise circular pattern, while Zone F refers to float rock, considered in the field descriptions only. Zone G comprises a series of boulders 100 m to the south, which appear as a separate outcrop. Samples known as TWP-H are host mudstones collected both in the mudstones directly below the mound and at a mudstone outcrop 300 m south, along Tauwhareparae Road.

Figure 5.4 is an aerial photo of the mound, that shows the actual carbonate outcrop to be limited to the top 40 m of the hill, although several areas of float blocks are found at lower elevations. At its widest point the knoll reaches 100 m across, not necessarily as solid outcrop but rather including also a series of disjointed slabs and boulders. The carbonate blocks take on several morphologic

forms in outcrop, including slabs, boulders, blocks and smoothed pavements (Fig. 5.5). At one stage the mound probably existed as a larger more solid outcrop. However, weathering, quarrying and cattle activities have decimated the size and integrity of the outcrop.



Figure 5.3 Location of TWP in the Raukumara Ranges. Image modified from MapToaster.

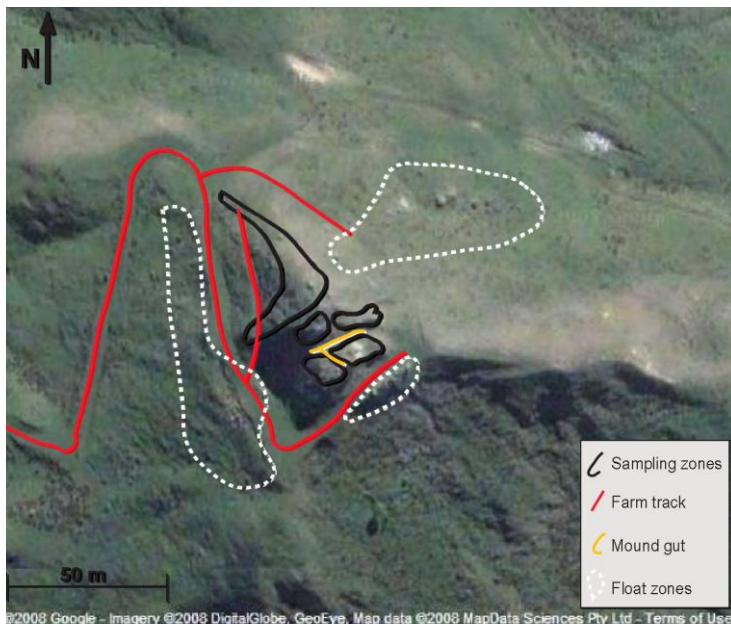


Figure 5.4 Aerial photograph of the Tauwharepareae seep-carbonate mound and surrounding fields. As can be seen in the image, the actual amount of outcrop is restricted to the top 40 m of the knoll, although large zones of float material are found on the lower flanks of the hill. Image modified from Google Earth.

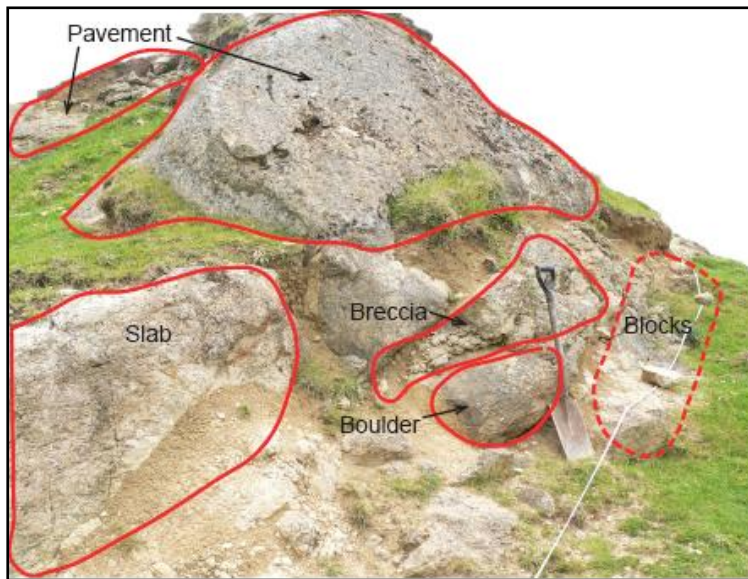


Figure 5.5 Image of Zone C, facing north. Range of carbonate morphologies seen at TWP. Note spade for scale. In general the smoothed pavements are found stratigraphically above other forms of carbonate.



Figure 5.6 View of TWP seep-carbonate deposit looking northwest. Sampling zone boundaries are marked in yellow, with relevant labels. Mudstone contacts are marked in red, and are variable across the photo. People for scale.

Three vertical metres of weathered mudstone form the base of the exposed mound. This is interspersed with disseminated carbonates nodules and subsurface plumbing features (Fig. 5.6). Above the mudstone–carbonate contact, boulders and slabs make up the outcrop, with individual slabs in places reaching 3 m in size. Float boulders range from small chunks (20 cm across) to large slabs up to 2 m wide. Some float boulders near Zone A can be “fitted” into the outcrop visually from where they are likely to have toppled.

5.2.2 Deposit structure

The paleoseep-carbonate outcrop has the erosional morphology of a mound, with a reasonably gradational change over 1.5 m from the mudstone below into the carbonate proper. Structurally, the mound is both faulted and brecciated; both are common processes in seep systems. Faulting combined with the anthropogenic effects of quarrying have led to the division of the mound in half by a 15 m long x 1 m wide gut. Faulting appears to run in a series of parallel sets through the mound, striking 250° northwest (Fig. 5.7), with joint sets also along the same strike. Faulting has led to the stripping of “upper” facies off “lower” facies from upthrown blocks in the southeastern section.

At its maximum, the carbonate succession reaches 30 m in thickness, but this varies significantly about the mound due to faulting and mass-wasting of rock material. Erosional processes are evidenced by large amounts of carbonate blocks strewn down the knoll on which the mound rests.

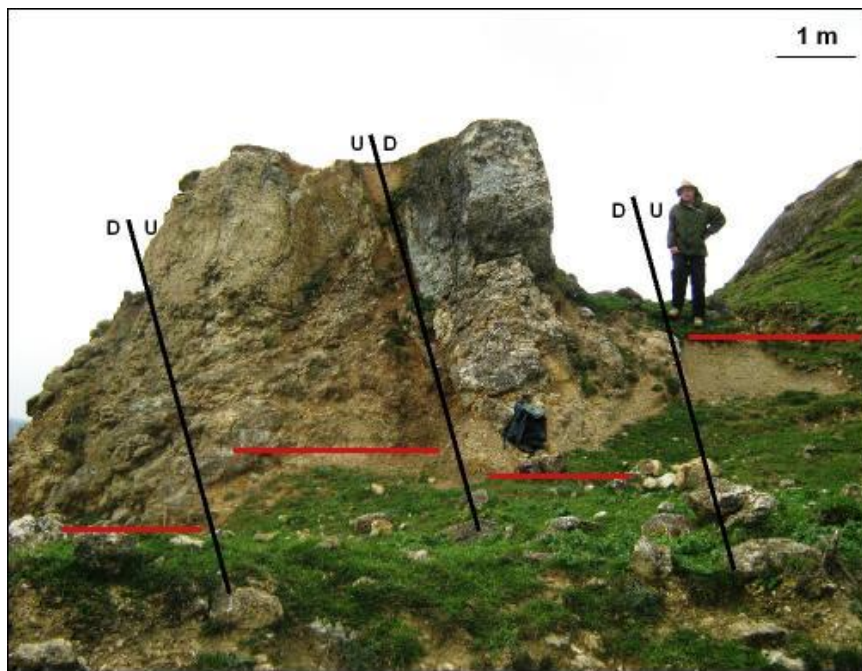


Figure 5.7 Faulting through Zone A at TWP. Faults have led to varied mudstone elevations across the deposit, and may be responsible for the gut formation between zones A, B and C.

5.2.3 Stratigraphic column

The composite stratigraphic column produced here shows 30 m of discontinuous outcrop. The maximum thickness at one location is 25 m, while in general the extent of outcrop at any one position may only reach 6 m thickness. The column itself has been created using composites of sections across the mound. Locations where these descriptions have been made are marked on the outcrop map (Fig. 5.8). Refer to Section 5.2.4 for further analysis of the key facies present at Tauwhareparae.

5.2.4 Facies analysis

The facies map provided is a generalisation of the main facies found within the mound. This map, much like the stratigraphic column, has been constructed from a summary of the diverse geology around the mound, and is a result of the wide range of dynamic processes occurring within the seep system. Figures 5.9 and 5.10 illustrate some of the facies in the field and their relationship to one another. At the end of this section a generalised map (Fig. 5.29) showing the relative abundance and distribution of the eight facies within the outcrop. Table 5.1 names each facies type with a brief description of their attributes.

Table 5.1 List of and description of each facies at TWP.

| Facies Type | Key Attributes |
|------------------------------|---|
| 1 Basal mudstone | Massive calcareous mudstone with scattered tubular and nodular concretions. |
| 2 Transitional deposits | Transition from Facies 1 into Facies 3, gradational change into a chaotic brecciated zone, includes talus zones of shedding material. |
| 3 Brecciated mudstone | Horizon of brecciated and burrowed mudstone. |
| 4 Rehealed carbonate slabs | Massive slabs of brecciated micarb, rehealed by thick fibrous veins marking fluid pathways. |
| 5 Fibrous aragonite deposits | Zones of extensive aragonite and calcite cementation, may be associated with microbial laminae. |
| 6 Worm-tube rich carbonate | Zones of lithified worm-tubes in all orientations, often associated with mussel rich carbonate. |
| 7 Bivalve-rich carbonate | Bathymodiolin mussel rich facies, with various infills, mostly occurs in upper reaches of outcrop. |
| 8 Coral-rich siltstone | Fine grained siltstone in several areas across the deposit with beds of <i>Caryophyllidae</i> sp. coral. |

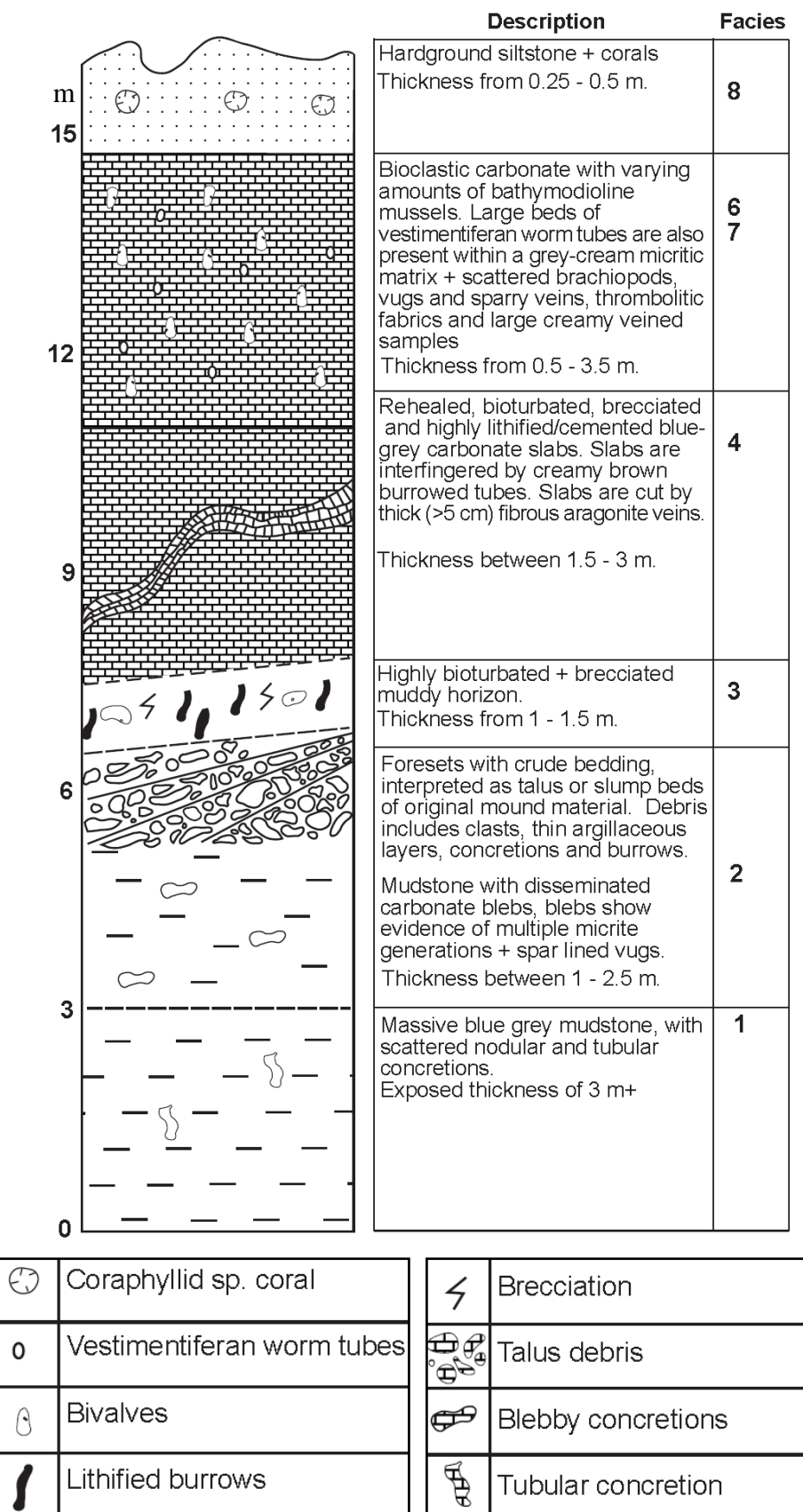


Figure 5.8 Composite stratigraphic column for TWP seep-carbonate outcrop. Key is underneath column.

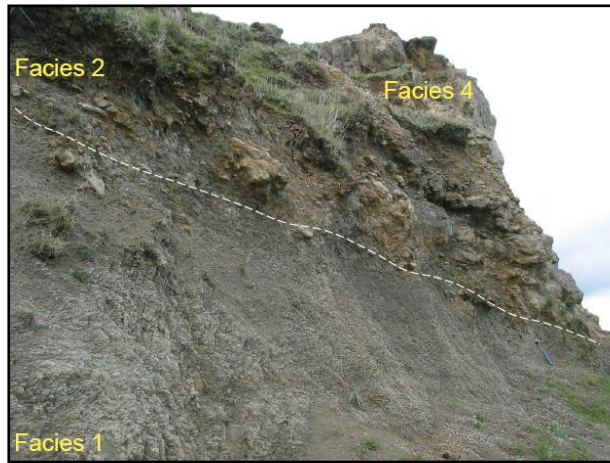


Figure 5.9 Gradational contact between basal mudstone (Facies 1) and transitional deposits (Facies 2). Facies 4 lies stratigraphically above the two.

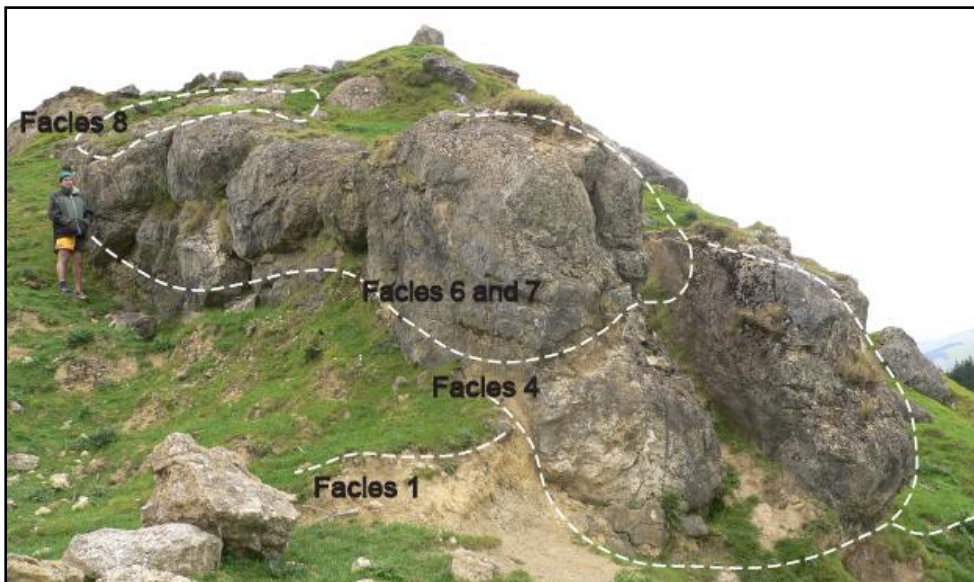


Figure 5.10 Zone E at TWP comprises several facies types. The mudstone below has nodular concretions exposed. Facies 8, a siltstone with coral thickets, is an indurated slab between zones C, D and E.

5.2.4.1 *Facies 1: Basal mudstone with scattered concretions*

The base of the mound lies on a massive blue-grey mudstone that is middle Miocene (Lillburnian) in age (Campbell et al. 2008). Due to faulting the mudstone occurs at several different elevations across the outcrop, and is overlain by three different facies. Below Zones A and B, Facies 2 overlies the mudstone (Fig. 5.11), whereas in a separate faulted block below Section E, Facies 4 lies directly above the mudstone. In the gut of the mound, the mudstone appears to grade transitionally into Facies 3.



Figure 5.11 Mudstone contact between Zones A and B. Note gradational contact inferred between Facies 1 and 2. Red dashed lines indicate crude bedding interpreted as shedding of Miocene talus slopes.

Sampling of the mudstone below Zone B revealed a single colonial coral. At several points in the mudstone, nodular and tubular concretions are exposed (Figs. 5.12 and 5.13); these are interpreted to represent parts of a seep plumbing system. The tubes are concretionary and have central conduits. There are also scattered varieties of other concretions, mainly appearing as large nodules rather than discrete tubes, although most still have conduits through them.



Figure 5.12 Tubular concretion from below Zone B. The concretion appears nodular, but is actually brecciated and broken up.



Figure 5.13 Nodular concretion from below Zone E. Morphologically it is sinuous and is composed of many concretionary blebs. Black line denotes length of concretionary blebs.

Figure 5.14 shows a slabbed tubular concretion found within the mudstone at TWP. The central conduit can clearly be identified, as well as a crystalline lining around the conduit.



Figure 5.14 Slabbed image of a tubular concretion from near the contact between Facies 1 and 2 in Zone B. Note the dark fracture veins within the core concretion, and the crystalline lining around the central conduit.

5.2.4.2 Facies 2: Transitional deposits

Facies 2 represents the transition from massive mudstone with scattered concretions (Facies 1) into a horizon of breccia and mudstone (Facies 2). The major feature within Facies 2 is that 0.5 – 1 m slabs of carbonate are interspersed with broken concretions and a chaotic mix of brecciated carbonate (Fig. 5.15).

A crude cross-bedding below Zone A is apparent (Fig. 5.11), which may represent middle Miocene talus slopes about parts of the original mound, reflecting a shedding effect of overburden. Between the beds of disturbed material are thin argillaceous layers, which may be indicative of periods of shedding followed by periods of non-activity. This facies is best represented in Zones A and B, particularly in the faulted section of Zone A.

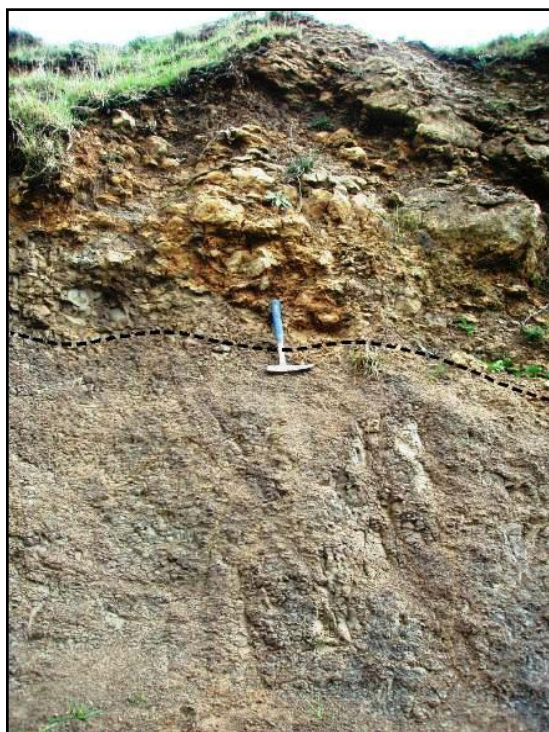


Figure 5.15 Contact between Facies 1 and 2. Large slabs of concretions and carbonate are characteristic of the transitional nature of Facies 2.

Sample TWP-B/6 is a nodular shaped concretion from the basal mudstone. There are several small crystal lined vugs, which appear to be joined throughout the sample (Fig. 5.16). Small fractures or growth veins mark the inner surface of the concretion, lined with a fine dark material. The sample was found near the

contact between Facies 1 and 2, in an area where several nodular concretions were protruding from the mudstone (Fig. 5.10).

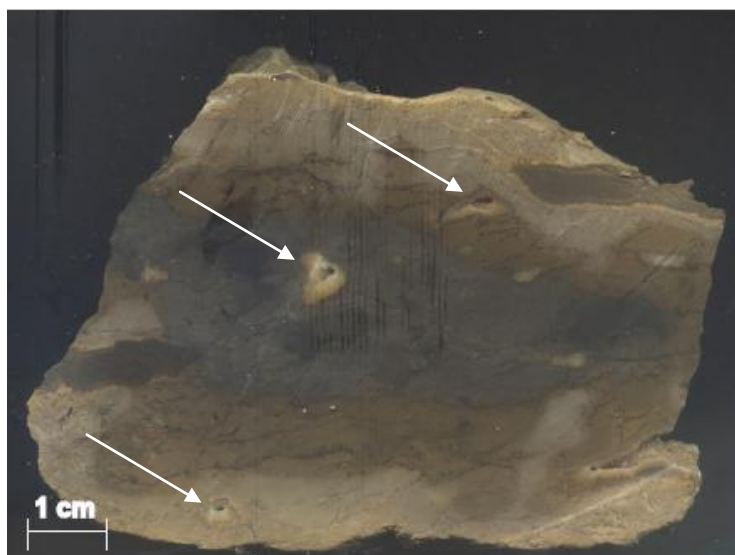


Figure 5.16 Concretion from Facies 2. Although there is no central conduit, spar-lined vugs occur across the sample (white arrow).

5.2.4.3 *Facies 3: Brecciated mudstone*

This facies is most abundant where it is exposed along the walls of the gut that cuts through the mound, and appears to have a matrix of muddy-silty material, which includes abundant burrows, concretions and brecciated clasts dispersed throughout (Fig. 5.17).



Figure 5.17 Image of Facies 3, as seen in the mound gut. The deposit is chaotic and is composed of burrowed and brecciated mudstone. Although abundant burrows and bleb shaped concretions are found in this horizon, no tubular examples were noted.

The burrows range in size from 3 – 10 cm long and 0.5 – 3 cm thick. They appear as chestnut – rust brown and vary in morphology from sinuous to linear tubes with

no apparent preferred orientation. In places, individual burrows are broken and appear as a series of disjointed tubes (Fig. 5.18).



Figure 5.18 Disjointed burrows from Facies 3. These burrows are abundant, and found both intact and broken up.

Concretions reach up to 15 cm in length and, in general, are nodular with no discernable conduits or distinct morphologies; no tubular concretions have been noted. The lower boundary of Facies 3 is gradational, while the upper boundary is inferred to be more abrupt, mostly due to the fact that Facies 4 comprises large concretionary slabs lying directly above this bed.

5.2.4.4 *Facies 4: Healed carbonate slabs*

This facies comprises an indurated series of slabs lying above Facies 1, 2 and 3 at different localities around the mound. Zone A provides the best place to view the internal structure of this facies, as a large 2 m – size block has fallen from this location (Fig. 5.19).

Facies 4 generally consists of blue-grey carbonate blocks that have been brecciated or disturbed and rehealed by thick fibrous aragonite veins. The external surfaces of the slabs appear as blue and cream-grey blebs dominated by bioturbation of alternating colours (blue – host, cream – burrows) (Fig. 5.20). Within the slabs, it is apparent that each block is made up of a series of rehealed clasts and nodules, representing different phases of fluid flow through the carbonate. The appearance and abundance of Facies 4 varies due to faults dissecting the section, with at least one fault cutting straight through the largest slab in Zone A.



Figure 5.19 Internal fabrics of Facies 4 in Zone A. The effects of bioturbation are prevalent. At the base of the slab there is evidence of preferential weathering between the burrows. See Figure 5.20 for a close up of bioturbated pattern.



Figure 5.20: Close up of previous image, showing an example of the bioturbation seen at TWP. Characteristic colour zonation emphasises bioturbation in slabs from Facies 4, particularly so in the faulted area of Zone A. The blue colouring is interpreted to be the host sediment, while the cream is the lithified burrows.

TWP-A/6 is from the highly faulted area in Zone A. The sample is strongly veined and altered with multiple stages of cementation including pink, grey, brown, yellow and black fabrics. No bioclastic material is present, although

foraminifera are present within the siliciclastic veins. Fibrous creamy cements are present, and the slab is also fractured and micro-brecciated (Fig. 5.21).

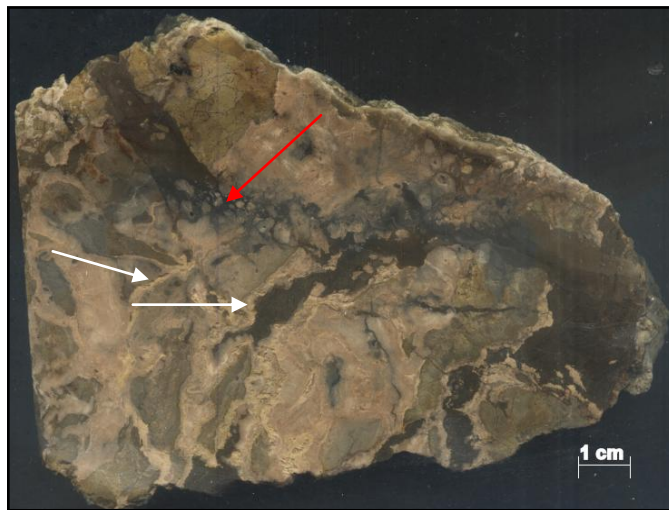


Figure 5.21 Slabbed example from TWP-A/6, Facies 4. Note the variations in colour through the different carbonate phases. Microbrecciation is apparent in the dark vein that runs through the centre of the sample. White arrows highlight creamy, carbonate crusts, while red arrow denotes zone of Microbrecciation.

Another common fabric within Facies 4 is the combination of brecciated mud clasts of different sizes and shapes, and various generations of laminar fibrous aragonite. The aragonite veins are responsible for healing the slabs and cementing them together to form a brecciated lithology. One such sample is TWP-A/5 shown in Figure 5.22, where the red arrow indicates brecciated clasts while the creamy fabric between is the aragonite re-healing the clasts. This aragonite also traps impurities, fluids and hydrocarbons in its crystal structure. Vugs are common in this facies, particularly when samples have been slabbed to reveal the inner structures of the rocks. In sample TWP-A/5, a drusy vug through the cement exposes a crystalline lining through the void. The brecciation represented by the mud clasts may occur on a macro scale, as is seen in this sample, or on a microscale, revealed by microscopy.

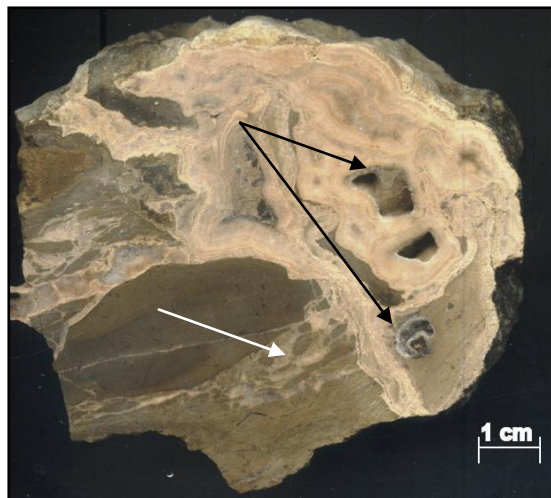


Figure 5.22 Slabbed example from Facies 4 (TWP-A/5) showing brecciation and re-healing by thick fibrous aragonite veins. Two features on this slab are noteworthy; the crystalline vugs which cut across the whole original sample (e.g. black arrows), and the micro-brecciation in the lower section of the slab (e.g. white arrows).

5.2.4.5 *Facies 5: Fibrous aragonite deposits*

This facies, along with Facies 6 and 7, is scattered through the outcrop, in some areas being dominant and in others showing only minor development. The fabrics found within these rocks are generally full of thick creamy aragonite, and small zones of micro-brecciation or siliciclastic veins. Subsequent analysis has shown that this facies is intimately linked with thrombolitic textures in hand specimen (cf. Figure 4D in Campbell et al. 2008), and microbial laminites in thin section. These creamy fabrics may be interspersed with worm tubes or bivalves. Microbial mats may be laminar, as are the mats associated with sample TWP-D/20, which is characterised by an alternating pattern of pink and white cements, with minor dark detrital injections dispersed through the rock (Fig. 5.23). These collectively represent successive generations of botryoidal aragonite and microbial laminae, which have been injected with veins of sediment.

Sometimes Facies 5 also includes micritic samples with thick fibrous bands which have altered to a powdery creamy vein. Sample TWP-E/8 provides an example of this fabric. As is evident in Figure 5.24, various periods of aragonite growth are common, while micro-brecciation is also found amongst the veins.

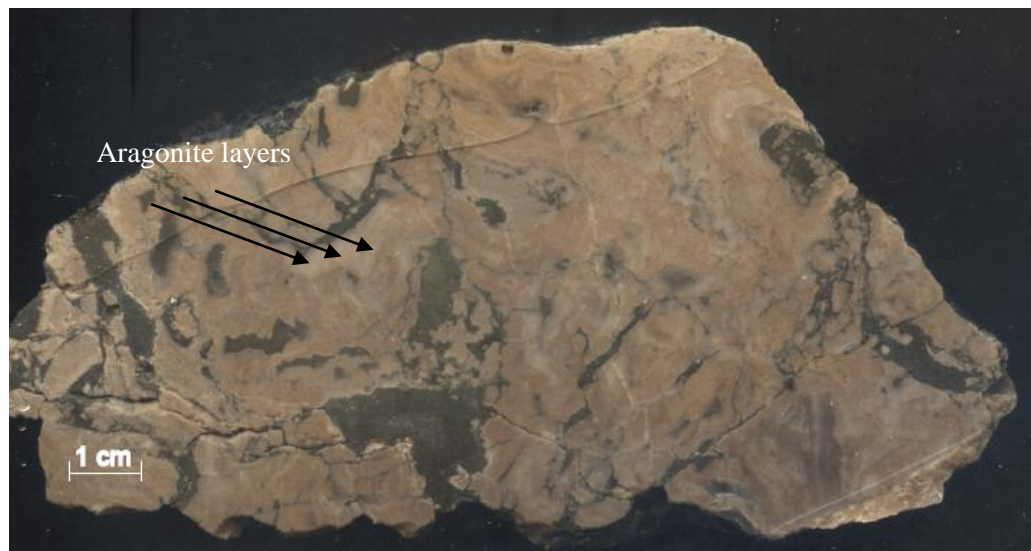


Figure 5.23: Slab from sample TWP-D/20, Facies 5. It is dominated by fine pink aragonitic laminae (e.g. arrows) and detrital injection veins. Characteristic of thick aragonite deposits, with microbial laminae along the boundaries.

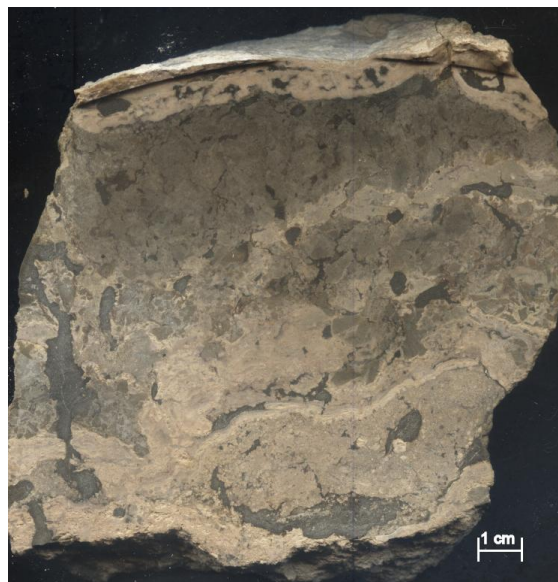


Figure 5.24: Slabbded example of Facies 5 from sample TWP-E/8, showing possible thrombolitic textures.

5.2.4.6 *Facies 6: Worm tube-rich carbonate*

Facies 6 is the dominant lithology found in Zone C. It comprises varying micarb fabrics that are dense with worm tubes (Fig. 5.25). Varied fills are present, as well as different orientations of tube morphology. While Facies 6 is dominant within Zone C, it is also found in parts of Zones D and E.

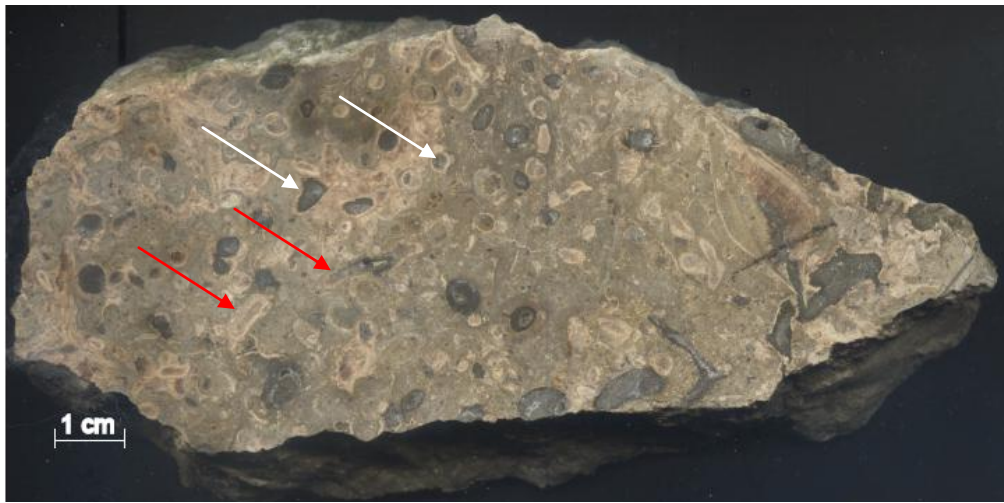


Figure 5.25 Slabbed example of Facies 6 from TWP-C/13, typical worm tube (WT) rich components. The arrows shown illustrate both longitudinal (e.g. red arrows) and latitudinal (e.g. white arrows) cross sections of worm tubes, indicating there is no preferred orientation.

Hand specimens of Facies 6 are cream–pink–grey in colour, and contain vestimentiferan worm tubes which range in length from 1 – 10 cm, and in width from 4 – 12 mm. Tube fills range from glassy pink spar, to white carbonate crusts to dark detrital sediment. In some areas they are found concurrently with bathymodiolin mussels (e.g. TWP-D/2), while in other examples the tubes themselves are dominant (e.g. TWP-C/13). Where the tubes are exposed in the outer edges of boulders they stand out, as the seep-carbonate preferentially weathers out around them. As is evident in Figure 5.25, there is no specific orientation in which the tubes are aligned.

5.2.4.7 Facies 7: Bivalve rich carbonate

Much of the carbonate mound at Tauwhareparae is fossiliferous and incorporates one dominant group: namely bathymodiolin mussels. In some areas of brecciation or faulting the shells are disarticulated, while in major shell beds within Sections D and E the fossils are well preserved (Fig. 5.26).



Figure 5.26 Bathymodiolin mussel from Facies 7 in Zone D.

A typical sample from this facies is shown in Figure 5.27, a fossil-rich carbonate from near the top of the carbonate mound. The sample shows limonite or weathering patterns around the bivalve shells. Some shells have dark fills in them while others have a pink crystalline cement. In specific areas burrows are present, as well as various disarticulated bivalves.

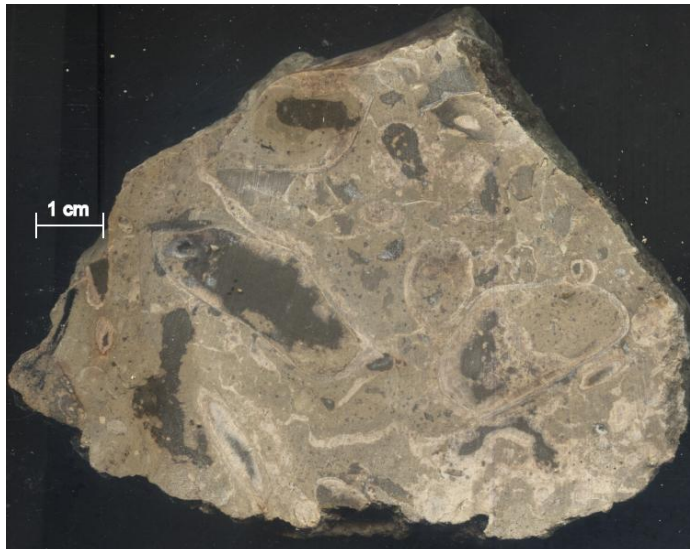


Figure 5.27 Fossiliferous slabbed example from Facies 7, sample TWP-D/1. Note the varying fills within the mussels.

Generally carbonate with dense bathymodiolin beds (such as boulders in the upper area of Zone D) display no preferred growth orientation or placement of the

mussels. Rather they exist as a chaotic orientation of shells, although in most zones they are articulated.

5.2.4.7 Facies 8: Coral rich siltstone

This is a dark brown fine grained siltstone with beds of *Caryophyllidae* sp. coral (Fig. 5.28) (Campbell et al. 2008). It typically occurs near the highest points of the exposed outcrop but is relatively rare in distribution, likely due to erosion of the siltstone.



Figure 5.28 Coralline siltstone from upper facies at TWP. This is only exposed in a few areas, where it has not been eroded. Figure taken from Campbell et al. (2008).

5.2.5 Facies distribution map

Figure 5.29 is a facies distribution map for TWP. Note that the map only infers an underlying basal mudstone, and does not infer the outcrops or facies that have been identified to underlie the knoll. The map only presents boulders or outcrops that can be seen at the surface.

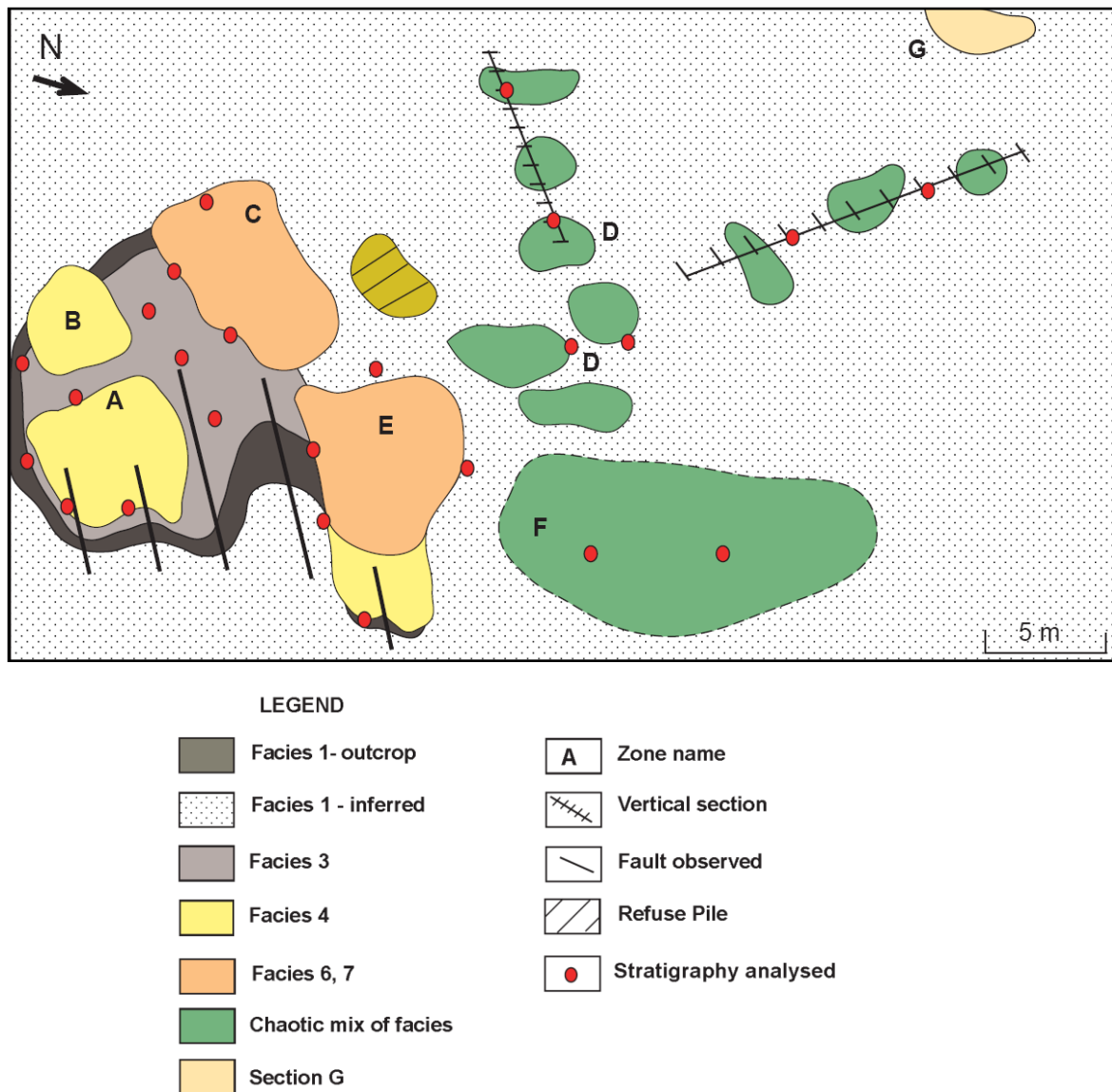


Figure 5.29 Facies distribution map at TWP. Facies distributions have been grouped into the dominant facies in individual areas. Red circles are areas where stratigraphy of the area has been studied and described.

Facies 1 is the basal mudstone and appears in outcrop on the eastern edge of the mound. The mudstone has been exposed from mass wasting processes such as slumping and creep. It is exposed under zones A and B as well as below the

eastern track where further concretions can be identified. In areas of faulting the mudstone has been exposed at several heights (see Section 5.2.1.1). Faulting has also influenced whether subsequent facies have been uplifted and thus exposed, the result of which has lead to a different stratigraphic sequence of facies exposed on the eastern side of the outcrop compared to the western. Hence, in the eastern section of the mound (zones A and B) Facies 1, 2 and 4 constitute the dominant outcrops, while Facies 3 is exposed through the central gut which splits the east from the west. The western sector of the deposit is interpreted to be stratigraphically higher in the system and is where Facies 6, 7 and 8 are dominant.

5.3 Discussion

Tauwhareparae is the site of a hydrocarbon paleo-seep. In outcrop, eight general facies exist within an area of ~ 100 m by 50 m. These facies range from authigenic carbonate with abundant crystalline generations, to bioclastic micrites, to a basal mudstone with scattered tubular and nodular concretions. Specific facies are found in separate zones around the site, the current positions of which may be structurally controlled through subsequent faulting and erosion, or as a by-product of differences in original ephemeral fluid flow dynamics when the cold-seep was active. In general the seep-carbonates are extremely varied in cements, fills and amount of bioclasts. This is reflected in the facies distribution map.

Through studies of modern day active seeps and comparisons to older paleo-seep sites worldwide, it is likely that the TWP seep was active for a relatively long period of time (Campbell 2006). This assumption is based on the rich faunal assemblage at TWP and the sheer volume of carbonate at the site. The presence of talus slopes in Zone A also suggests the carbonate deposit reached a size significant enough to experience mass wasting. The diverse lithologies found at the sites and the presence of corals in the upper siltstone also confirm periods of cementation, precipitation and exhumation as hardgrounds at the seafloor interface.

The presence of the fossiliferous carbonate as an isolated pod or lens within a succession of Lillburnian mudstones up to 3 km thick (Campbell et al. 2008) is characteristic of the ‘oasis’ factor seen in seeps offshore today (Carney 1994).

The presence of a seep plumbing system below the deposit is confirmed by the presence of both nodular and tubular concretions in the lower mudstone (cf. Nyman 2009).

Faunal assemblages at TWP have been reported in Campbell et al. (2008). Table 5.2 has been modified from the paper, and serves as a summary of the diversity of fauna at the site. As well as a diverse range of macrofossils there are many trace fossils.

Table 5.2 Summary of fossilised fauna found at TWP paleo-seep. Table modified from Campbell et al. (2008).

| Fossil Taxa | |
|---------------|--|
| Bivalvia | Bathymodioline mussels |
| | <i>Modiolus</i> cf. <i>M. areolatus</i> |
| | <i>Diplodonta?</i> sp. |
| | Teredinid |
| Gastropoda | <i>Leptella?</i> sp. |
| Polychaeta | Vestimentiferan worm tubes |
| Brachiopoda | 3 terebratulides (<i>Liothyrella?</i> , others) |
| Cnidaria | cf. <i>Goniocorella</i> |
| Trace fossils | Roughly cylindrical to clavate borings |

It has been suggested in the literature that the spatial zonation patterns of faunal assemblages within the seep sites may be indicative of varying periods of fluid flow, due to certain niches and chemical tolerances (Campbell 2006; Jenkins et al. 2007). Field work at TWP reveals a higher concentration of macro fossils in Facies 6 and 7, and a lack thereof in Facies 1, 2 and 3. This may be a function of formation, i.e. position of the carbonate, subsurface versus seafloor settings. However, apart from a stratigraphic split of occurrences there does not appear to be a strong zonation of fauna across the deposit.

In comparison to other seep-carbonate sites in the northern East Coast Basin, TWP is the second largest in exposed outcrop size after Rocky Knob. The facies found at TWP are similar to those reported from Karikarihuata and Rocky Knob

(Collins 1999) and other examples in the region (Campbell et al. 2008). Both Rocky Knob and Karikarihuata also display evidence of a basal plumbing system (Collins 1999).

One main observation reported elsewhere is the overwhelming diversity of fabrics within samples from the same deposits (Conti and Fontana 1999; Campbell et al. 2002). This has been attributed to the dynamic and ephemeral nature of seep systems, stemming primarily from changes in fluid flow rates, composition and fluxes.

The effects of brecciation are reported at most substantial seep sites. At TWP, carbonate mud clasts rehealed with aragonitic cements are common in Zones A and B. In Campbell et al. (2008), hand specimens similar to those seen in the above zones are illustrated and explained as the result of fluid over pressure and brecciation, with subsequent cementation by acicular aragonite.

Seep-carbonate sites in the southern East Coast Basin are currently under analysis (see Section 1.3), but initial field data suggest the sites all share similarities with TWP, although examples from Ngawaka and Haunui are more siliciclastic rich than at TWP.

Field observations from ancient seep-carbonates worldwide yield many of the same general characteristics. These may include: the isolated nature and relatively small volume of carbonate compared to the siliciclastic host mudstone; diverse yet distinct faunal assemblages of chemosynthetic organisms; foetid smell of rocks when struck with hammer; extensive veining ranging from thick isopachous cements to fine undulating veinlets; evidence of fossilised tube worms and thrombolites; association with tubular concretions or oil-seeps (Beauchamp and Savard 1989; Campbell 1992; Campbell and Bottjer 1993; Cavalazzi et al. 2007; Conti et al. 2007). During field work at TWP, the presence of all the above characteristics were confirmed at or near the site.

CHAPTER 6

Tauwhareparae Petrology

6.1 Introduction

In order to gain insight into the mechanisms of formation of the Tauwhareparae paleo-seep carbonate deposit and its subsequent diagenetic alterations, detailed petrographic analysis was undertaken on thin sections of samples representative of the different field facies and internal cement components. The combination of both plane polarised light (PPL) and cathodoluminescent light (CL) thin section petrography of thin sections offers a unique perspective into the mineralogical changes within the seep-carbonates. The use of CL is especially helpful, as the technique also picks up structural and zonation detail within samples that cannot be seen in PPL. Other laboratory methods used in the analysis of the Tauwhareparae seep-carbonates included microprobe, UV light analysis, carbonate percentage determinations, XRD mineralogy, and stable carbon ($\delta^{13}\text{C}$) and oxygen ($\delta^{18}\text{O}$) isotopes. Aims of this analysis were as follows:

- Classify componentry (i.e. identify different textures, cements and colours)
- Use CL to clarify diagenetic changes
- Determine mineralogy of components
- Identify elemental variations within fabrics and components

With these data it is possible to estimate the degree of alteration a rock has undergone and combine that information with basic geological principles, such as cross-cutting relationships, to determine a relative timing of major paragenetic events, including early cementation phases and late diagenetic alteration phases. This chapter reports the results from the above listed laboratory techniques; for methods refer to Chapter 4. See appendices 2.1 through to 2.4 for full laboratory results for the TWP samples.

6.2 PETROGRAPHIC Components

The following section describes the components identified in the TWP seep-carbonate samples. Table 6.1 summarises the components and their characteristics. The aragonitic fabrics are characteristic of early formation, while the majority of calcites are associated with diagenetic alteration of pre-existing fabrics, resulting in mild to extreme overprinting. Eight major carbonate phases (A – Aragonitic or C – Calcitic), three minor groups of components (M – Minor) and three phases of neomorphism (N – Neomorphic) are described, for a total of 14 paragenetic events or phases.

6.2.1. Aragonitic microcrystalline carbonate (A1)

A1 constitutes a microcrystalline carbonate cement, characterised by its brown–grey colour and clotted, dirty appearance (Fig. 6.1A). Because the original definition of ‘micrite’ (a contraction of the term microcrystalline calcite) implied a calcite composition (Folk 1959, 1962; Reid et al. 1990), the term “micarb” is used here for the microcrystalline carbonate (A1) in this study, which is dominantly aragonitic. The micarb occurs in nearly all samples as a primary cement, although not generally within confined pores such as bivalve shells or worm tubes. In other words, it appears as the general “background” matrix. While it has a brown–grey colour in PPL (Fig. 6.1C and 6.1E), the micarb luminesces a dark blue to lilac colour under CL (Fig. 6.1B and 6.1D), and contains scattered siliciclastic, sand-sized grains such as quartz and feldspars. The micarb “matrix” is full of peloids; some are well-rounded and others are cut by later veins. The peloids may occur as geopetal fills or as islands within the micarb (Fig. 6.2A-B). Under plane light the peloids share the same texture as the micarb, but may be surrounded by volumetrically minor areas of acicular or spherulitic aragonite crystals. Under CL the peloids are blue to lilac in colour (Fig. 6.2C-D). In places extensive alteration affects both micarb and peloids by a change in fabric to a microspar, and mineralogy (aragonite to calcite). CL colours also change from a lilac to ultimately a deep cerise or burgundy colour (Fig. 6.10A-B and 6.10E-F).

Table 6. 1 Petrographic components in TWP seep-carbonates.

| Phases | Code | Petrographic character | Crystal size (µm) | CL Character |
|--|------|---|---|--|
| Aragonitic micro-crystalline carbonate (micarb) | A1 | Light - dark brown, mottled fuzzy microcrystalline carbonate ± siliciclastic grains, peloidal and clotted fabrics. Develops concurrently with colonisation by macroinvertebrates. | | Ranges from dark blue, light blue to lilac; peloids take on a slightly more purple sparkly luminescence; siliciclastics appear as bright blue and green grains (feldspars) |
| Acicular aragonite | A2 | Translucent - grey array of acicular needles, generally lie perpendicular to growth surface and display undulose extinction ± pale green u.v. fluorescence | Needles may grow up to 250 - 2 mm in length | Dark blue - non luminescent |
| Botryoidal aragonite | A3 | Botryoidal mamelons of aragonite appear as bundles or as cones, commonly show fine laminae within and around edges. Found with dark laminae. Laminae appear clotted and dark and range in size from 0.01 - 0.05 mm thick. | 300 - 750 | Dark blue - non luminescent, although after neomorphism the laminae between mamelons may preferentially turn a cerise - purple colour |
| Spherulitic aragonite | A4 | Spherulitic acicular aragonite, may exist as full or 3/4 rosettes of growth, and are normally found in groups of spherulites. Generally form in cavities and pore spaces, and may nucleate off micarb 'islands'. May appear circular or as ovoid folds. Undulose extinction | 500 - 800 | Dark blue - non luminescent |
| Cellular calcite | C1 | Appears morphologically similar to plant cells; rounded crystal faces. | 50 - 120 | Burnt orange |
| Mottled calcite | C2 | Light coloured, mottled cement in small veins or lining shells. | 10 - 20 | Bright yellow, mottled colouring |
| Equant calcite | C3 | Equant blocky crystals with some zonation developed. | 250 - 700 | Peach, cerise or red - orange hues |
| Siliciclastic calcite | C4 | Grey cement with abundant siliciclastic grains. | | Very bright yellow, with bright blue and green speckles |
| Neomorphism 1 | N1 | Microspar, sugary crystalline fabric with large blocky equant crystals with twinning. | | Cerise or red - purple colour |
| Neomorphism 2 | N2 | Internal cement fabric of shells with blocky, equant crystals with fragmented extinction | | Colour halos appear through shell or tube wall structure and 'flame' patterns overprint the crystals |
| Neomorphism 3 | N3 | Varies from large equant spar to an overprinted acicular bundle. | | All fabrics take on a burnt orange - yellow colour, A1 appears as a cerise - purple colour |
| Bioclasts (includes bivalve shells, worm tubes and foraminifera) | M1 | Internal fabrics have varying extinction patterns, ranging from equant crystals to original texture | 200 - 4 mm | Depends on original mineralogy and degree of alteration; may range from purple-blue to orange-yellow |
| Pyrite | M2 | Dark rinds around shell edges | 100 - 200 | Non luminescent |
| Scattered siliciclastics | M3 | Varies from quartz (black to grey) to feldspars , in places twinned | 50 - 250 | Varies, most commonly bright blue and green for feldspars |

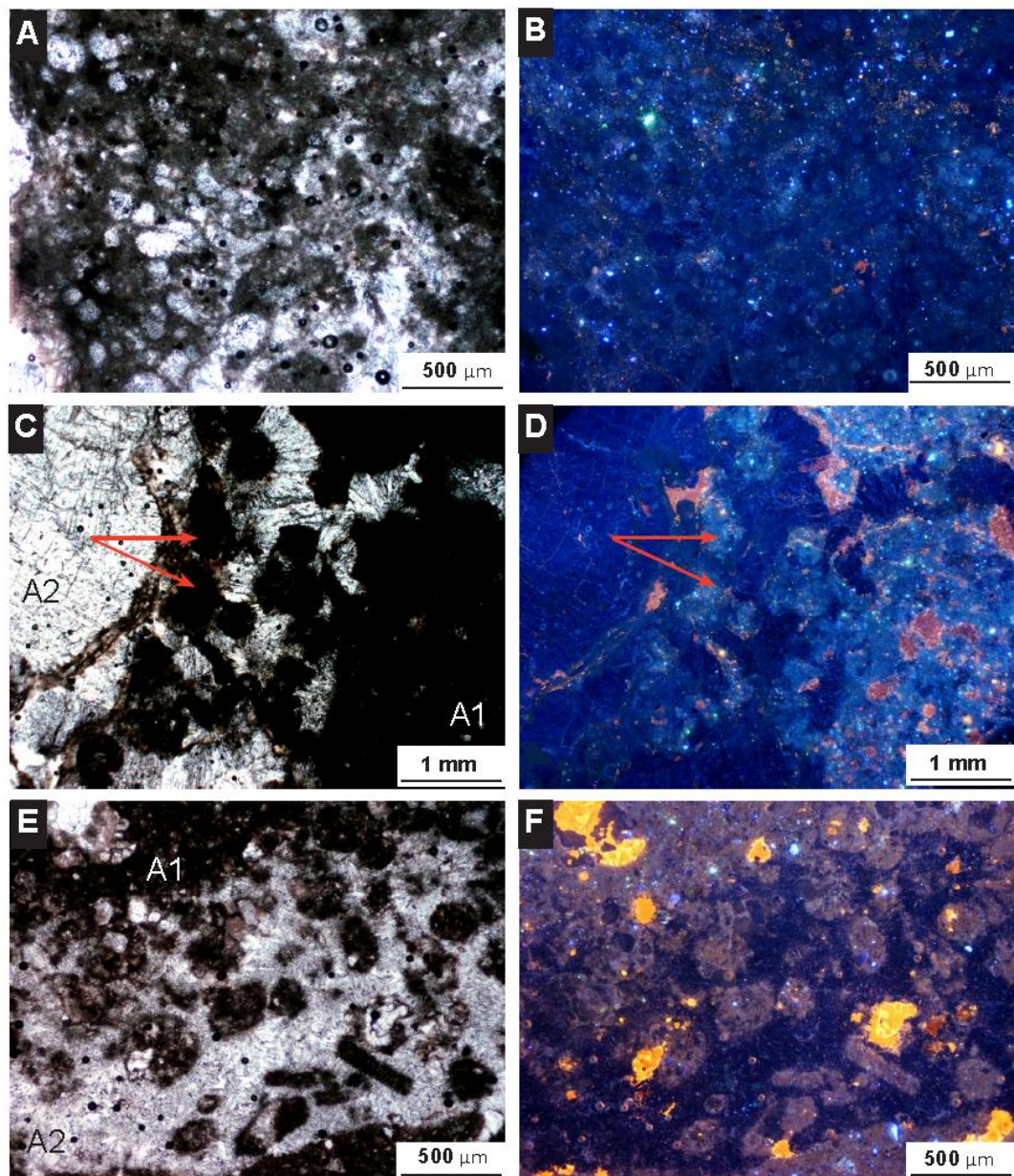


Figure 6.1 Photomicrographs of aragonitic micarb (A1) (PPL – A, C, and E; CL – B, D, and F) in TWP seep-carbonates. **A** and **B** - Micarb with minor acicular aragonite phase. **C** and **D** - Brecciated micarb (A1) with acicular aragonite (A2) growing in pore spaces. The brecciated micarb clasts (e.g. red arrows) are darker than the acicular aragonite. **E** and **F** - Disseminated blebs of micarb (A1) within a pore space filled with acicular aragonite (A2). Yellow patches are a late calcite phase.

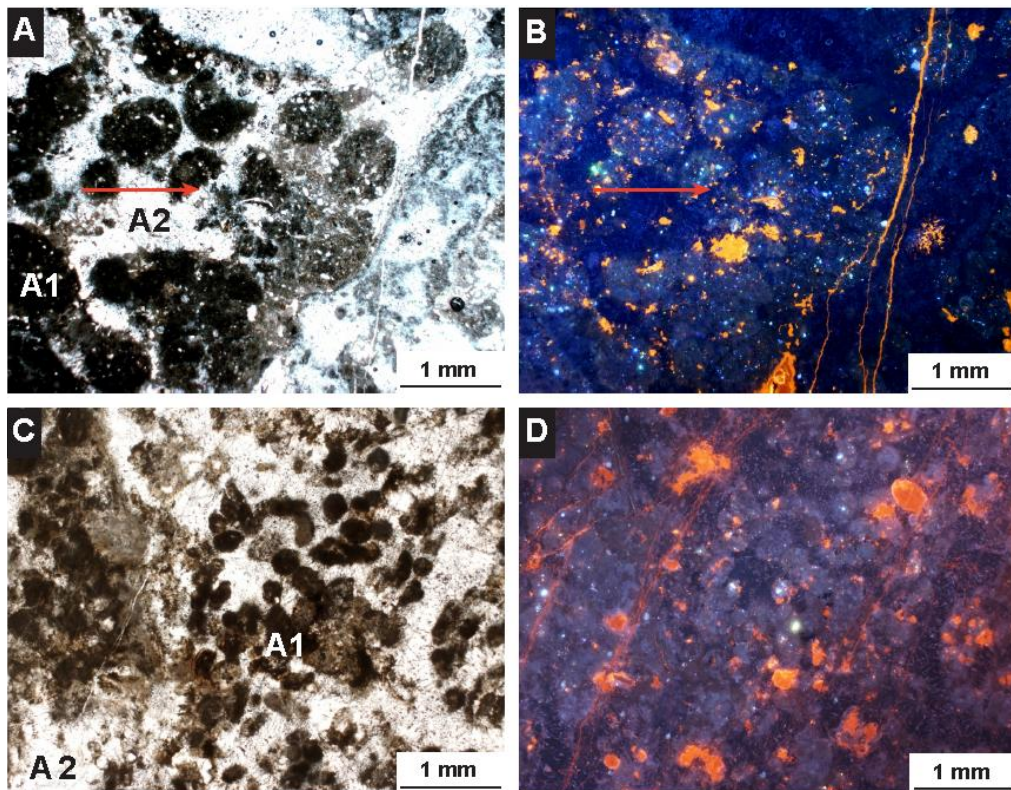


Figure 6.2 Photomicrograph pairs of peloidal fabrics (PPL – A and C; CL – B and D) in TWP seep-carbonates. **A** and **B** - Fresh unaltered peloids in a matrix of aragonitic micarb (A1, e.g. yellow arrow) and acicular aragonite (A2). The bright yellow patches are small blebs of late calcite beginning to form. Note that several peloids (e.g. red arrow) are cut in half. **C** and **D** – Peloids from a sample that has undergone some diagenetic alteration; hence, some of the peloid structures have turned orange. Note all peloids are well-rounded and contain scattered siliciclastic grains.

6.2.2 Acicular aragonite (A2)

Acicular aragonite crystals grew from 300 μm - 2 mm in length from the edges of bioclastic material (Fig. 6.3A-B), and brecciated clasts. While some needles appear to have nucleated in radiating splays, others grew perpendicular to the nucleating surface (cf. Fig. 6.3A-B and 6.3E-F). In general, the aragonite is a clean sparry cement, although some splays are riddled with dark speckled fluid inclusions (Fig. 6.3C) which are interpreted to be hydrocarbons (see Section 6.8). The acicular aragonite is translucent to clear under PPL and does not luminesce strongly under CL (Fig. 6.3D and 6.3F), where it is dark blue in colour. During diagenetic alteration, this fabric appears to be somewhat resistant to neomorphism, and generally changes CL colour only after all other fabrics have undergone some degree of change. In these cases the dark blue CL pattern changes into a cerise or pink colour (Fig. 6.4C-D).

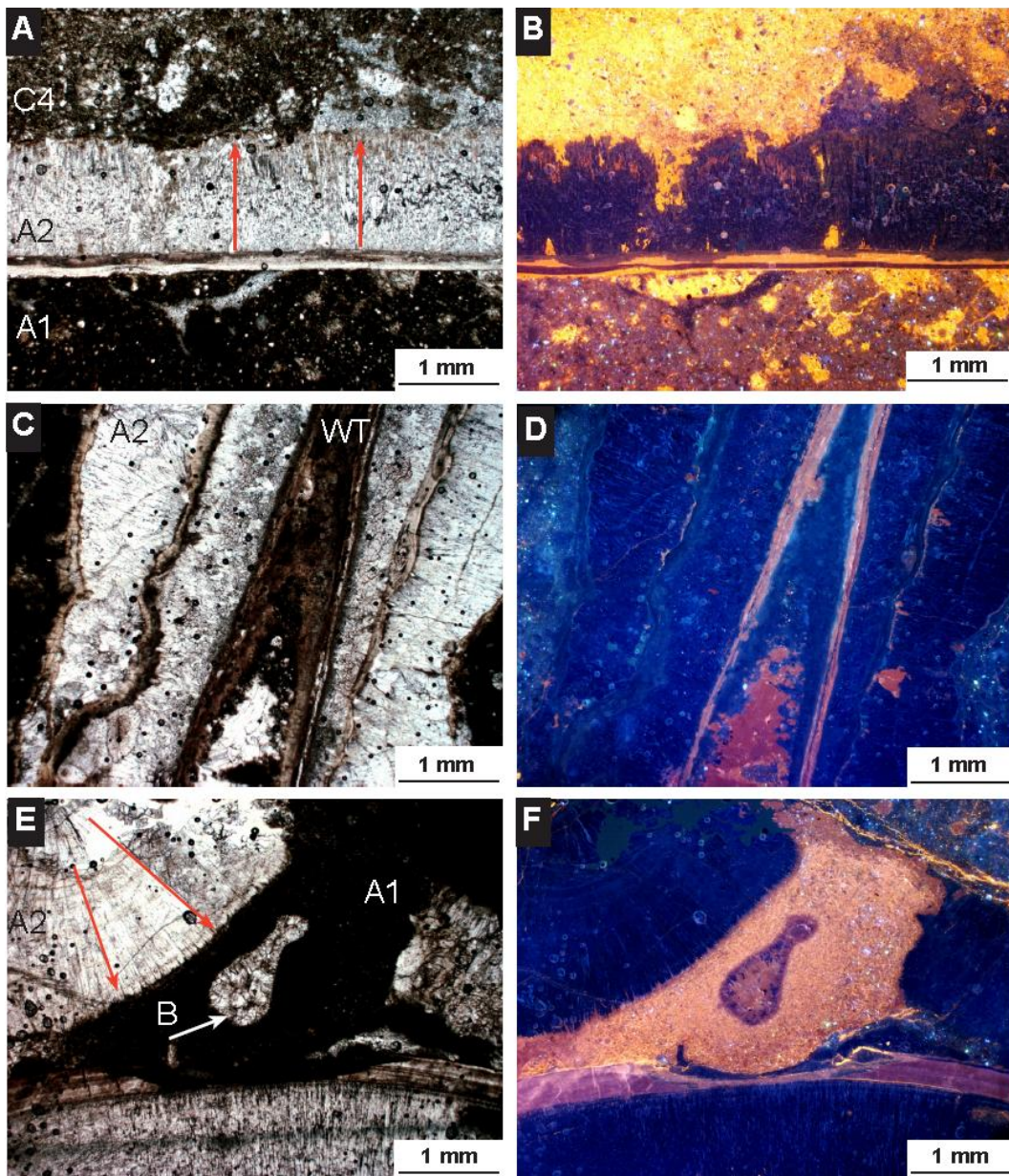


Figure 6.3 Photomicrographs of acicular aragonite (PPL – A, C, and E; CL – B, D, and F) in TWP seep-carbonates. **A** and **B** – A bivalve acts as a nucleating surface for growth of needles of acicular aragonite (A2). The final fill within the bivalve is a siliciclastic-rich vein cemented by late calcitic orthospar (C4). **C** and **D** – Interior worm tube (WT) walls act as a nucleation surface. Acicular aragonite (A2) has formed, filling the tube worm cavity with an elongated splay. Note that there are several phases of aragonite that have precipitated within the sheltered structure. **E** and **F** – Multiple splays of acicular aragonite (A1) and a boring (B) within a neomorphosed microspar. There is evidence of an early phase of acicular aragonite within the burrow, which itself is situated within an altered microspar, this is indicative of different periods of seepage where a hardground formed before reactivation of cementation.

6.2.3 Botryoidal aragonite (A3)

In some thin sections, mamelons (dense cone-shaped splays of crystal growth) of botryoidal aragonite fill cavities. The botryoids appear as multi-generational growths in one principal direction (Fig. 6.4E-F). Some botryoids grew

simultaneously with microbial laminates and appear as alternations of aragonite and fine dark laminae (10 – 500 µm thick) of a black (organic rich) clotted carbonate material. Within the internal structure of individual aragonite botryoids, fine laminae of brown, pink and cream bands may be evident (Fig. 6.4E).

6.2.4 Spherulitic aragonite (A4)

This phase of aragonite differs from the other aragonites as it appears to have formed in larger cavities where entire rosettes could grow, as opposed to the discrete surfaces from which the acicular aragonite developed. Spherulites that were not fully formed are more common than rosettes that developed in a full sphere (Fig. 6.4A-D). In general the spherulite needles have smaller aspect ratios than the fine needle splays in acicular aragonite, and many smaller spherulites may fit into the same area that one large acicular splay may occupy.

6.2.5 Cellular calcite (C1)

In TWP-C/9, the dominant phase found in the veins of a remnant micarb matrix is a “snake skin” or “cellular” fabric (Fig. 6.7A-B). This appears to be restricted to the veins and may be an expression of fine-scale autobrecciation ± recrystallisation (Fig. 6.7C-D). This fabric is found in several samples, all from different zones and facies in the outcrop but all related to veining. The characteristic “cells” themselves are irregular in size and range in length from 50 – 120 µm.

6.2.6 Mottled calcite (C2)

In places a layer of mottled calcite separates some components, such as between worm tubes or bivalve shells (Fig. 6.5B and 6.11B) and micarb. These layers are typically thin, from 10 – 20 µm, and cannot be identified easily in PPL. But under CL the fine layers are distinctive (bright CL) and appear to exploit pre-existing boundaries or discontinuities (i.e. between shell and carbonate matrix). It also appears that if enough space was available (e.g. a vug lining or drusy pore), this minor calcite may have then developed into large blocky calcite crystals (Fig. 6.5C-D).

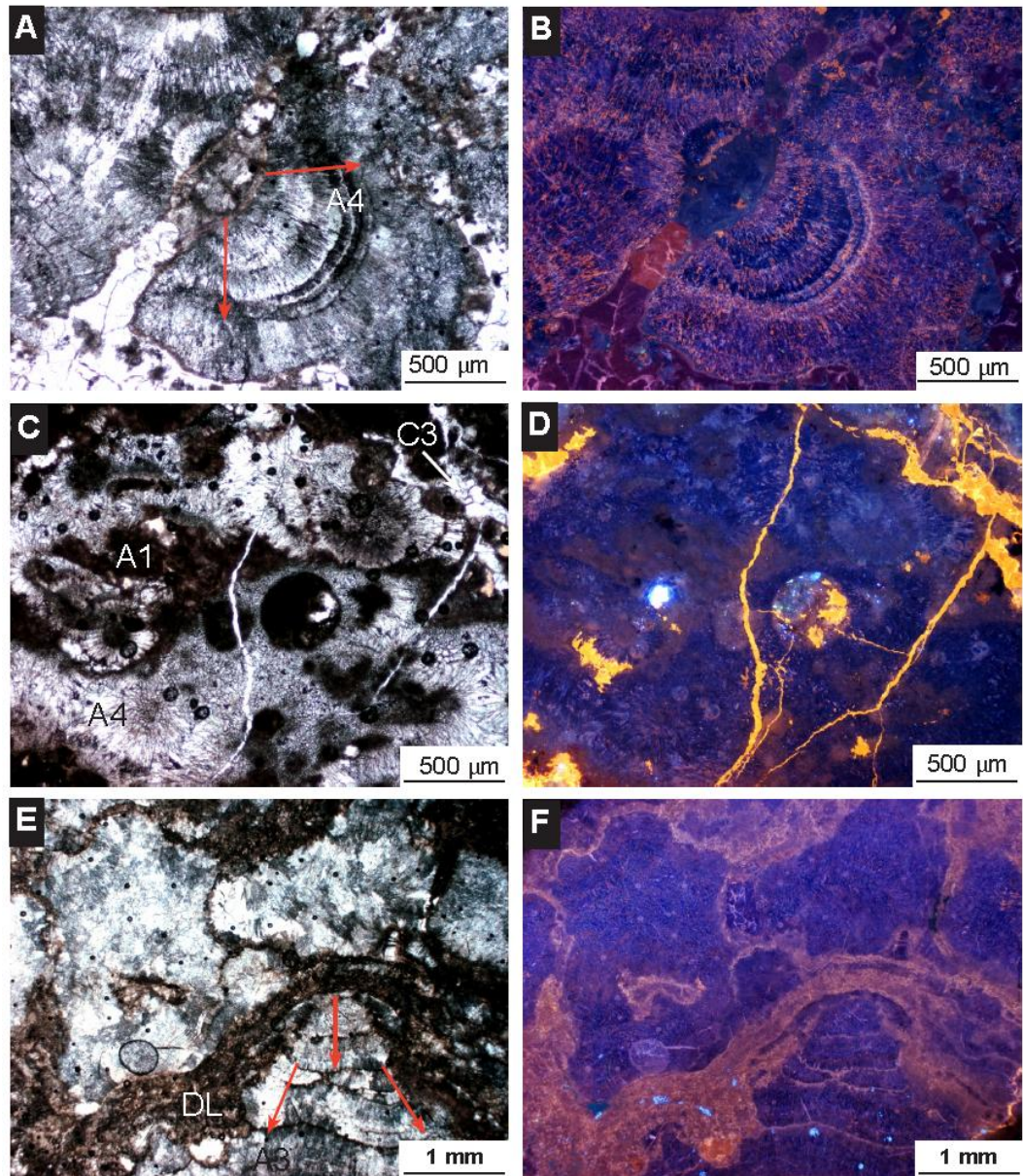


Figure 6.4 Photomicrographs of cavity-filling aragonite phases under PPL (left side) and CL (right side) in TWP seep-carbonates. Red arrows indicate direction of crystal growth. **A** and **B** – Large spherulite undergoing initial neomorphism. **C** and **D** – Occluded pore with fill of spherulitic aragonite (A4) and patches of micarb (A1), the surrounding cavities of which are A4 filled. The void is cut by late yellow calcite veins and fenestrae (C3). **E** and **F** – Laminated mamelons of botryoidal aragonites (A3) interspersed with dark microbial laminae (DL).

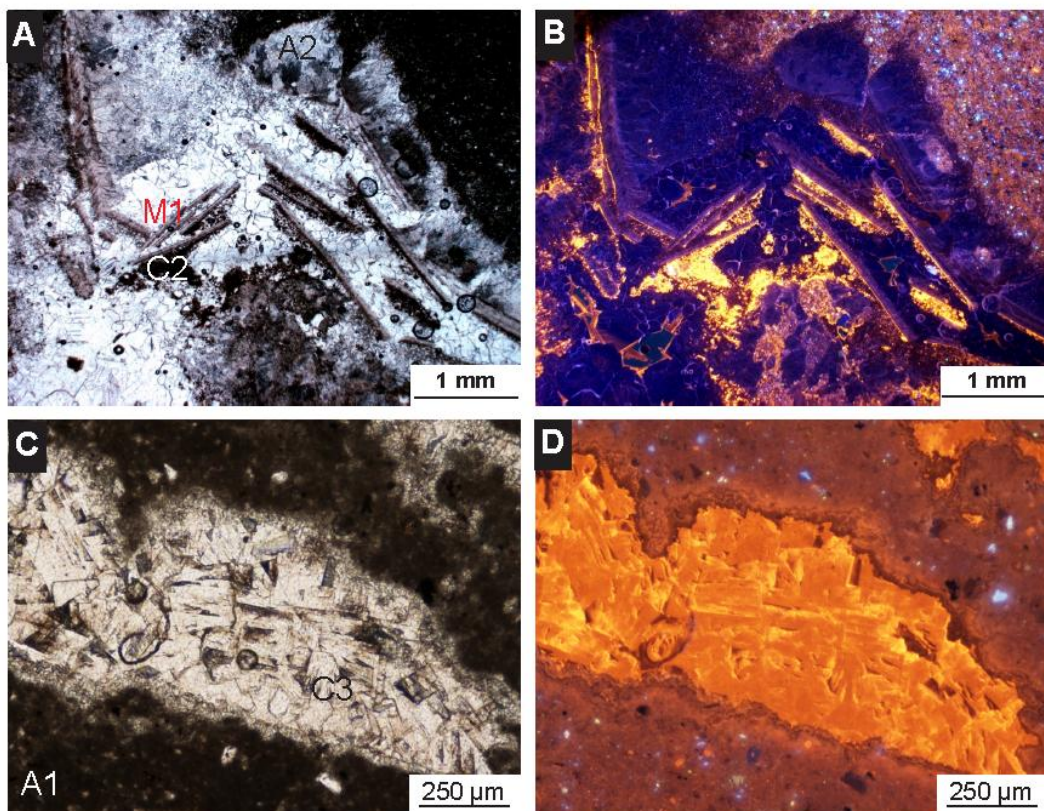


Figure 6.5 Photomicrographs displaying two different calcite phases from representing late stage diagenesis in the TWP seep-carbonates (PPL – left side and CL – right side). **A** and **B** thin layers of mottled calcite (C2) are growing on the diffuse boundaries of bivalve bioclasts (M1). **C** and **D** recrystallised late equant calcite (C3) in a fracture vein cutting through a mass of micarb (A1).

6.2.7 Equant calcite (C3)

This calcite may be zoned or twinned (Fig. 6.6C-F). In places it is dentate at the tips of crystals, generally in altered fabrics where aragonite has developed into calcite. Often equant calcite is the central, final phase in a spar filled vug or pore. Individual crystal sizes range from 70–250 µm, but in aggregates the crystal bundles may be spread throughout a vug up to 4 mm across.

6.2.8 Siliciclastic calcite vein (C4)

These are zones of siliciclastic material that have been cemented by late (burial) fluids saturated in calcite. It is a common fabric and is easily identified in both hand specimen and thin section. Under CL the vein appears as very bright yellow, with a great amount of green and blue grains (Fig. 6.15C-D), this CL pattern illuminates calcite cement and siliciclastic grains. In hand specimen, the veins are generally connected to the last fill in the pore spaces such as worm tubes and fossilised shells.

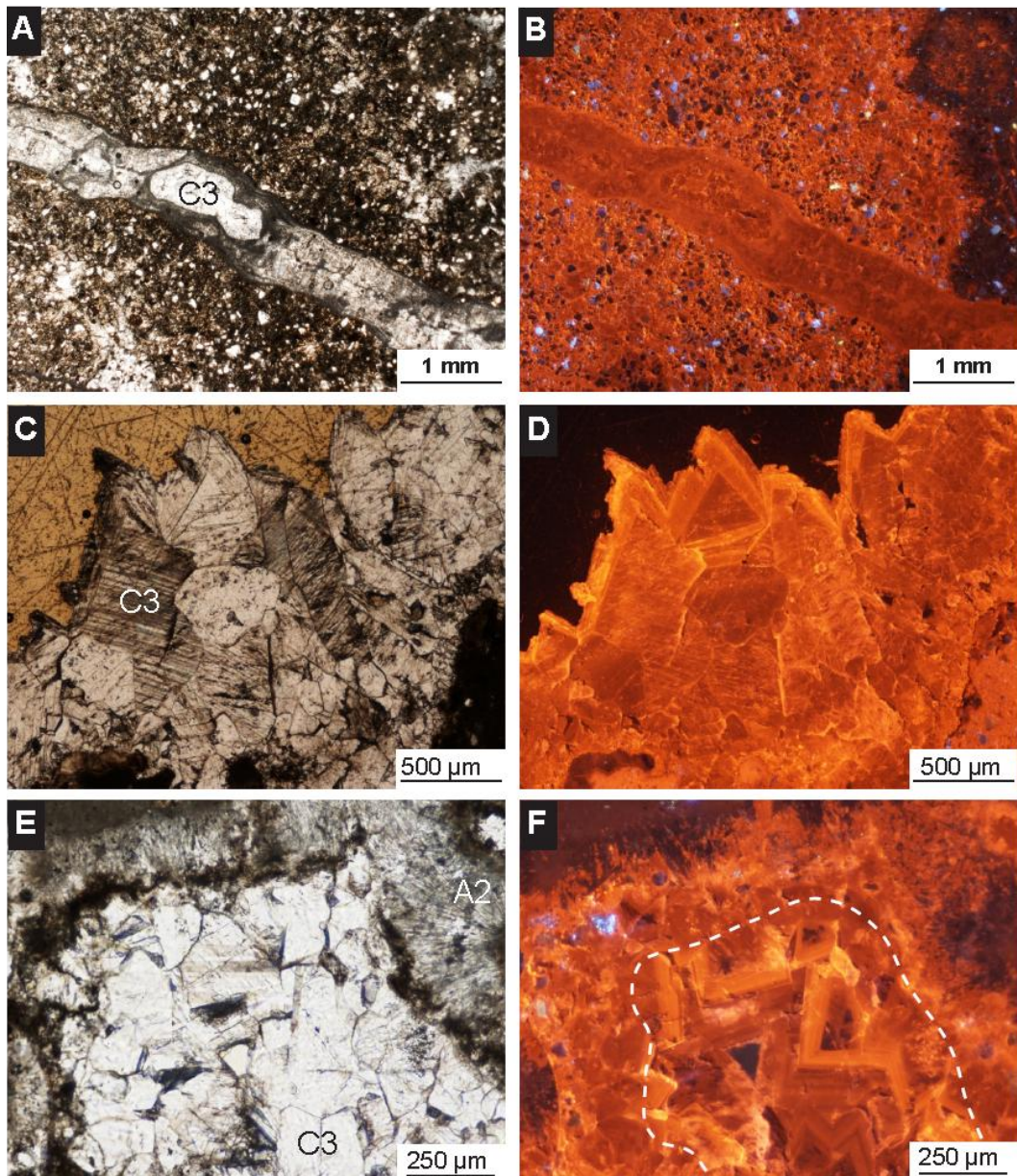


Figure 6.6 Photomicrographs of calcite phases from late stage diagenesis in the TWP seep-carbonates (PPL - left side and CL - right side). **A and B** – Cross-cutting vein of recrystallised equant calcite (C3). **C and D** – Equant calcite (C3) as last fill in a vug. **E and F** – Zoning in a recrystallised calcite (e.g. within white circle). The acicular aragonite (A2) phase near the edge of the image would have originally lined the void.

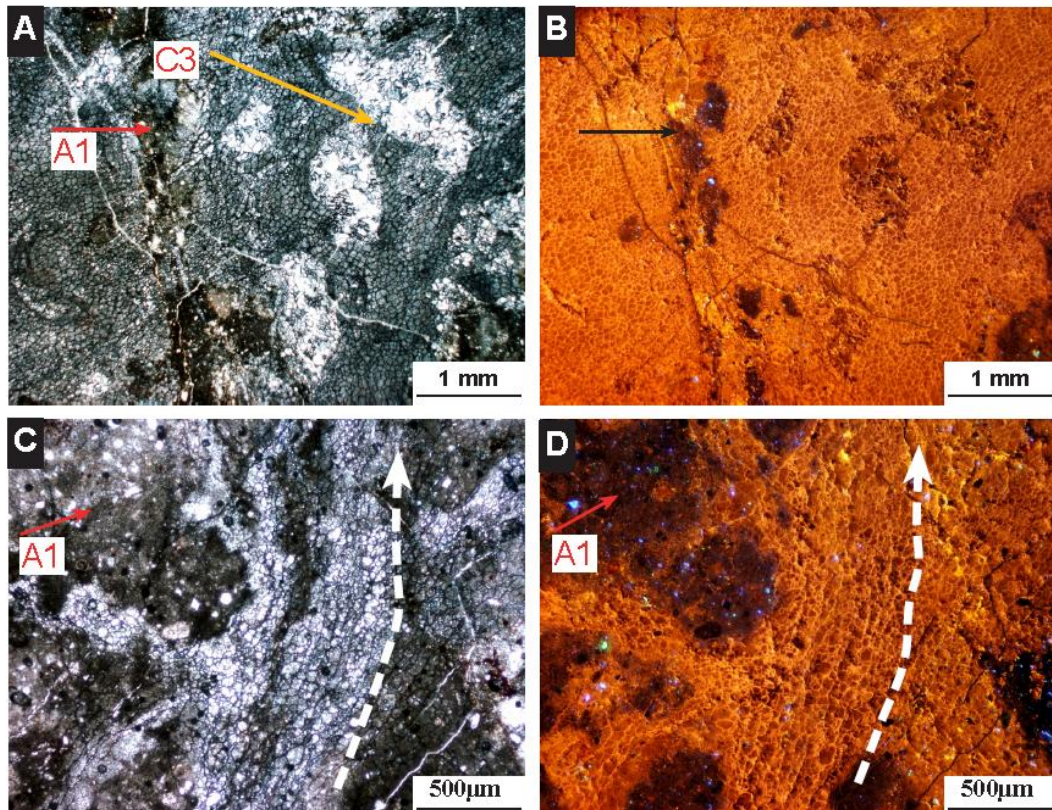


Figure 6.7 Photomicrographs of “cellular” calcite phase from the late stages of diagenesis in the TWP seep-carbonates (PPL – left side and CL – right side). **A** and **B** – General image of phase, including several sparry remnant aragonite veins. **C** and **D** – Detail of cellular pattern to show individual “cell” crystal structures. The recrystallised “cells” follow a ‘stretched’ vein like morphology, which may be fluid flow related. Several blebs of remnant micarb (A1) are highlighted.

6.2.9 Bioclasts (M1)

Both whole and disarticulated bivalve shells occur within the TWP carbonates. In thin section these range from large, unaltered bioclasts to fine broken disseminated pieces within slump facies. In general bioclasts are more common in facies that occur higher in the stratigraphy (see Section 5.2.4). Based on CL characteristics it appears that neomorphism has had relatively minor effects on the shell fabrics.

Large, cerise, equant crystals in the ultimate fill of a mussel shell is indicative of neomorphism within the structure of the shell (Fig. 6.10E-F). Figures 6.8C and 6.8D display a gastropod undergoing neomorphism both in the shell and within its cavity fill. As pores, shells provide a nucleus for different phases of carbonate precipitation and can also provide a sheltered diagenetic environment. In some

cases, micarb peloids have formed within sheltered shells, or large blocky calcites occur within shell clasts (Fig. 6.8A-B).

Worm tubes occur in all field sampling zones and are dominant in Zone C (see Section 5.2.4.6). The fossilised remains appear as small 300 – 800 µm wide tubes, up to 5 cm long. Tube infills range from a simple fill of acicular aragonite to places where a distinct and complex paragenesis exists across a few millimetres. Sample TWP-C/2a is an example of the latter case (Fig. 6.15C-D), showing a worm tube lined with acicular aragonite, followed by a fine microspar along the borders of this aragonite and then blocky equant orthospar filling the remaining central pore space. In some worm tubes, geopetal infills are common including some rife with peloids. The least common tube fill is a siliciclastic rich cement with minor glauconite. Figure 6.9A–6.9E shows a range of tube worm morphologies in thin section view. Note that Figure 6.9A-B is a longitudinal view through a worm tube.

Both planktic and benthic foraminifera occur within the TWP samples, although most are present within zones of siliciclastics (Fig. 6.8E-F).

6.2.10 Pyrite (M2)

While abundant pyrite has been reported from seep-carbonates worldwide (e.g. Beauchamp and Savard 1992; Peckmann et al. 2001; Campbell et al. 2002), it appears to be only a minor component within TWP samples. Pyrite is present in several samples as rinds or as globules in between shell material. The pyrite is mainly frambooidal in habit and revealed a mostly dark rust colour in PPL.

6.2.11 Scattered siliciclastics (M3)

A common feature in many thin sections is siliciclastic grains which are associated with many other fabrics. In some cases the zones are full of moderately rounded quartz, feldspar, mica and zircon grains (50–250 µm in size) and in others the veins may be rich in both planktic and benthic foraminifera (Fig. 6.8E-F). Commonly clasts composed of disarticulated shell material are found within the siliciclastic areas. CL patterns of the veins depend on the timing of vein emplacement, i.e. early or late diagenesis. This likely reflects the changing

fluid sources that passed through the fractures, and precipitated the carbonate cements. Glauconite also may be common in these veins, ranging from nascent to highly evolved (Middleton 2003).

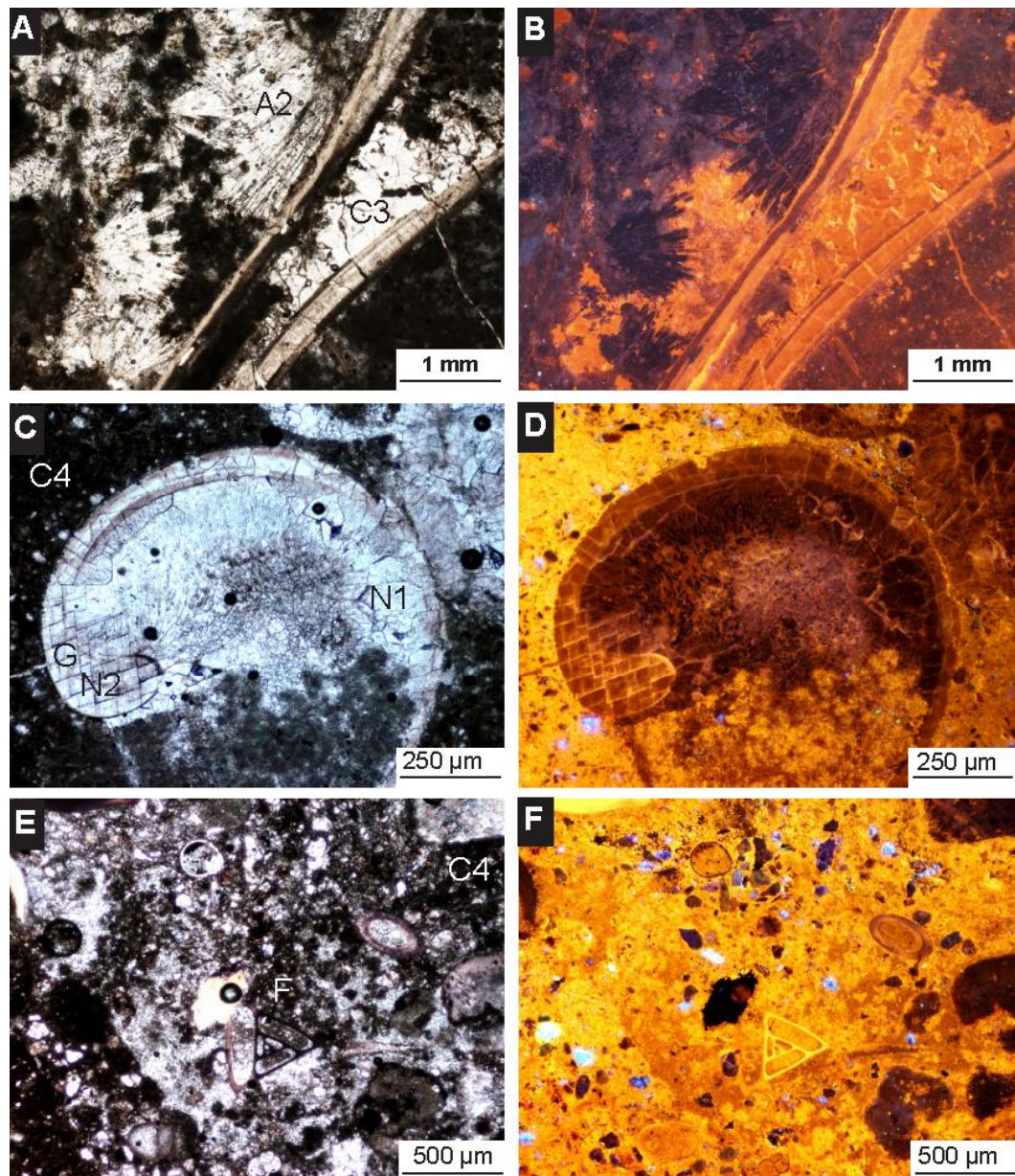


Figure 6.8 Photomicrographs of bioclasts in thin section under PPL (left side) and CL (right side) in TWP seep-carbonates. **A** and **B** – At the boundary between two bivalve shells, an equant calcite (C3) phase precipitated. **C** and **D** – Gastropod in calcitic matrix. The gastropod shell has undergone bioclastic neomorphism (N1), and the cavity fill has undergone initial neomorphism (N1) within the central pore space. **E** and **F** – Siliciclastic vein cemented by calcite microspar (C4); foraminiferal test (F) is also calcitic.

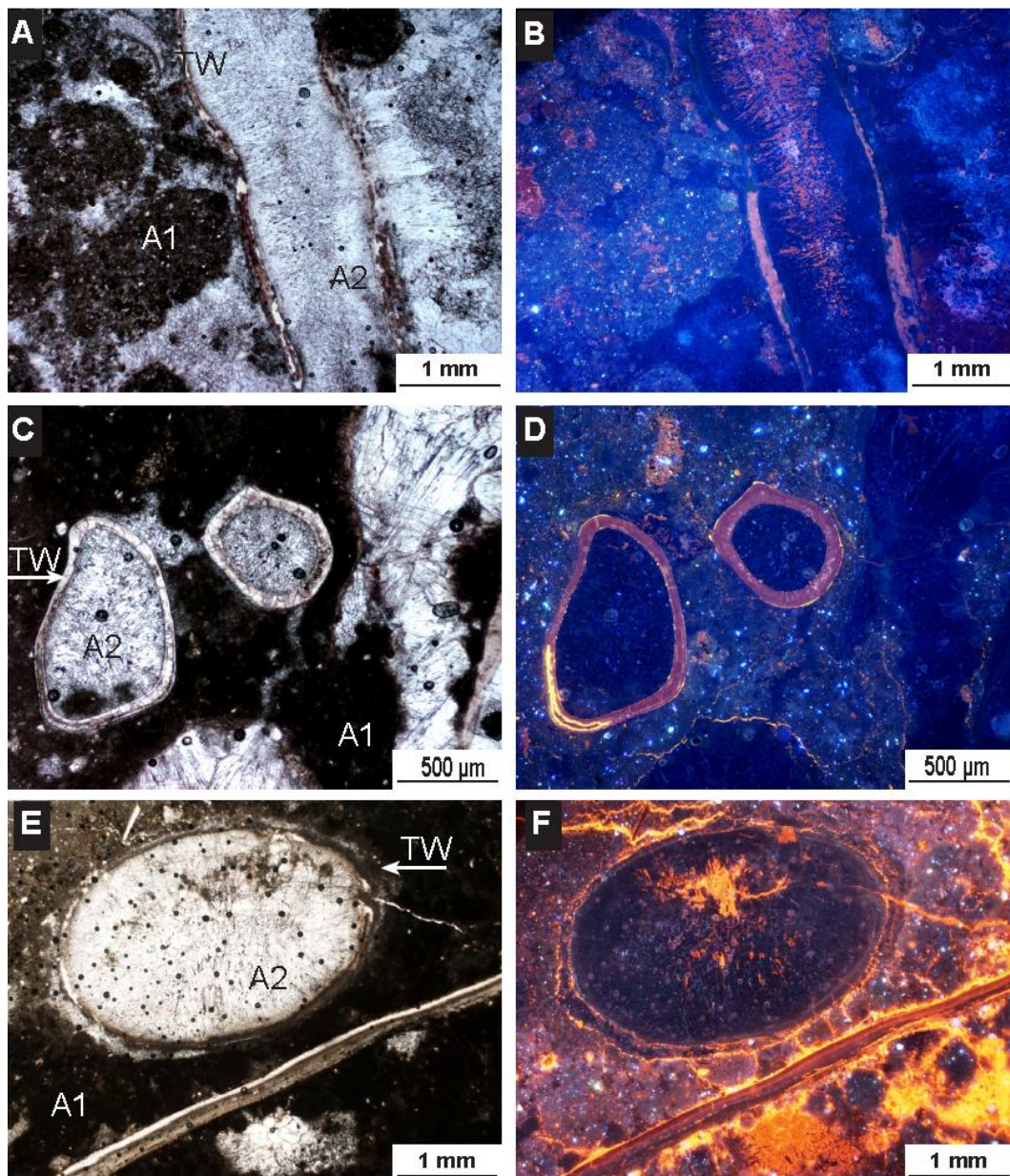


Figure 6.9 Photomicrographs of vestimentiferan worm tubes under PPL (left side) and CL (right side) in TWP seep-carbonates. **A** and **B** – Longitudinal section of worm tube, with acicular aragonite needle splays. Worm tube is in matrix of aragonitic micarb. **C** and **D** – Section through vestimentiferan worm tubes. The walls preferentially altered earlier than the surrounding micarb matrix. **E** and **F** – Bioclasts with minor calcite phase (C2) forming in the diffuse boundaries.

6.2.12 Neomorphosed phases

Neomorphic fabrics represent late diagenetic overprinting of the TWP seep-carbonate deposit. The term “aggrading neomorphism”, originally coined by Folk (1956), and further developed by Bathurst (1975), is used to broadly encompass processes of both recrystallisation and polymorphic transformation during carbonate diagenesis. Under CL, specific colour patterns identify these changes and associated features, such as neomorphic fronts, which were also confirmed with mineralogic assessment.

Early cements within pore spaces, such as bivalve shell cavities, worm tubes or vugs, show evidence of initial neomorphism (Neomorphism 1), by sharp to gradual changes in their crystal morphology, evident in PPL, or changing CL colours from dark blue into cerise red (Fig. 6.10E-F). Primary structures may include micarb, peloids, spherulitic aragonite and the original boundaries between botryoids. The most common textural end results of neomorphism 1 overprinting/recrystallisation is either a fine microspar which is pink under CL, or a blocky equant calcite with a cerise CL colour (Fig. 6.14A-B and Fig. 6.10E -F respectively).

PPL may reveal some effects of bioclastic neomorphism (Neomorphism 2), such as alteration of the internal structure of bivalve shells or worm tube walls from a finely laminated or massive structure to a more crystalline and blocky mass. Under CL, a worm tube wall which has undergone N2 alteration may display a concentric ring pattern of alternating colours, ranging from blue to yellow to pink hues (Fig. 6.11A-D).

A feature of pervasive neomorphism (Neomorphism 3) is the recrystallisation of fabrics such as acicular aragonite. N3 can be identified in both PPL and CL as it appears as extensive overprinting and damage to the fabrics. Figures 6.12A-B and 6.12C-D show photomicrograph pairs from altered zones of TWP-A/6 in which there is evidence of remnant acicular aragonite that changed morphology under PPL, as well as in CL from dark purple to bright orange. One feature noted in N3 is a “cellular” texture of calcite involving recrystallised, subangular to rounded

crystals from 50 to 120 µm across (Fig. 6.12E-F). The CL colour most commonly seen for these fabrics is dull yellow to orange.

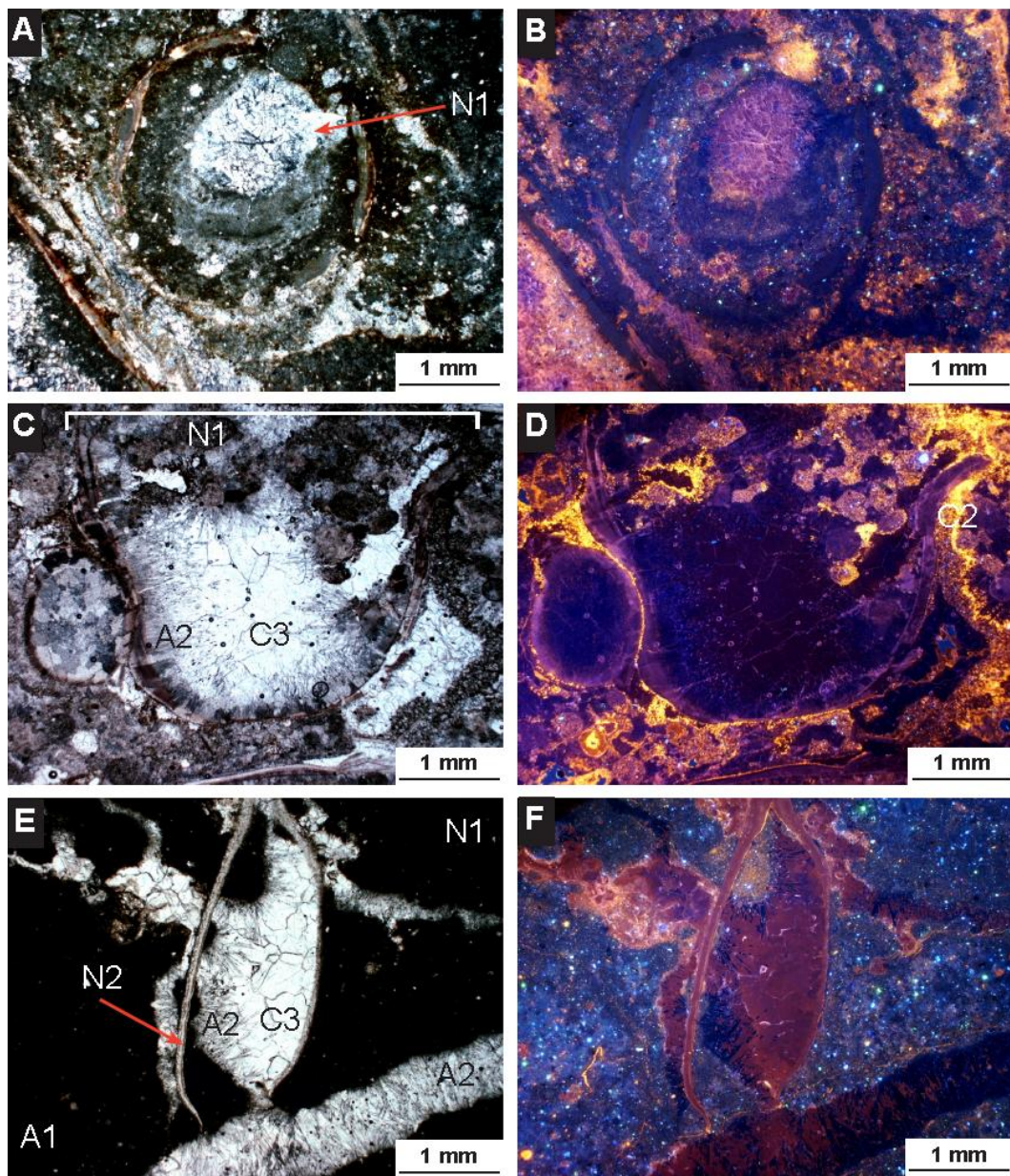


Figure 6.10 Photomicrographs featuring zones of initial and bioclastic neomorphism (N1 and N2 respectively) under PPL (left side) and CL (right side) in TWP seep-carbonate thin sections. **A** and **B** – Worm tube with internal cavity fill undergoing initial neomorphism (N1). **C** and **D** – Bivalve shells forming boundaries for a zone of initial neomorphism (N1). Note that acicular aragonite (A2) lining is transforming to an equant or blocky calcite in centre. Also featured in this image is mottled calcite (C2) developing in a thin layer between discrete shell boundaries. **E** and **F** – Bivalve undergoing both initial and bioclastic neomorphism (N1 and N2). The test of the mussel has been structurally altered, and the inner cavity fill of acicular aragonite (A2) has changed to an equant crystal that is cerise in CL and calcitic in mineralogy. The shell is situated within a matrix of relatively unaltered micarb (A1).

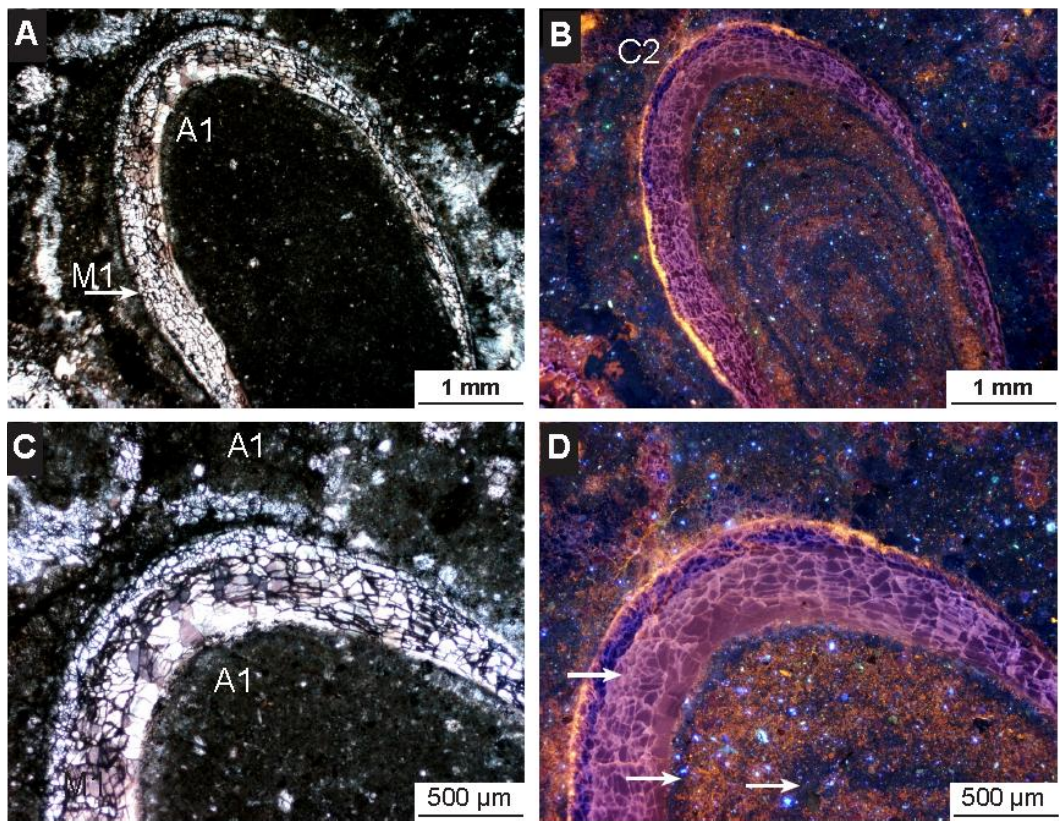


Figure 6.11 Photomicrographs of bioclastic neomorphism of tube worms from a TWP seep-carbonate thin section under PPL (left side) and CL (right side). **A** and **B** – Worm tube bioclast (M1) surrounded by micarb (A1). Worm tube walls are being replaced, and the resulting crystal is altering into a ‘flame’ structure. The internal fill displays changes in colour, reflective of changes in pore fluid history. **C** and **D** close up of **A** and **B** in which the changes in crystal structure are more clearly evident. White arrows point to varying colour zones within the worm tube.

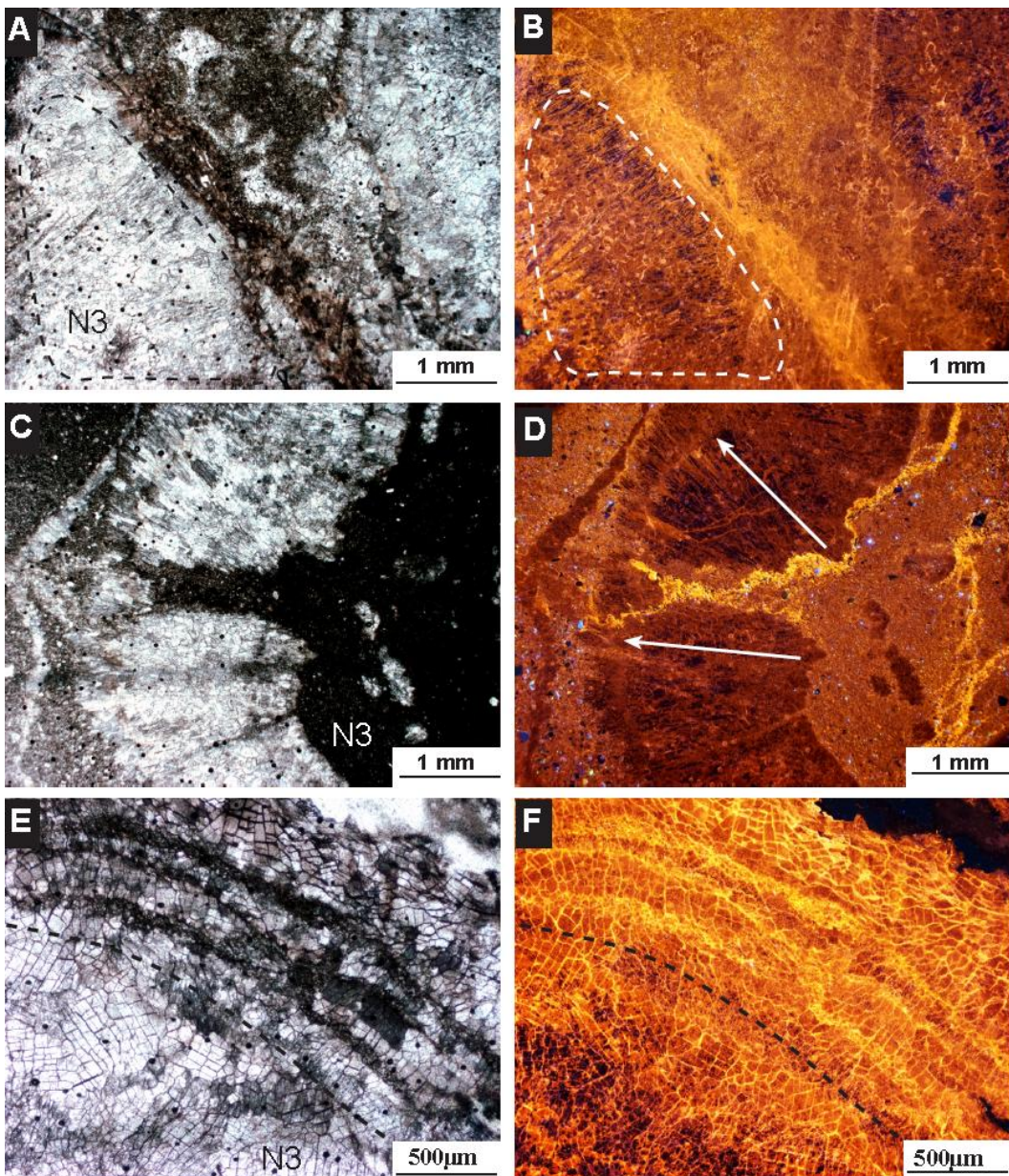


Figure 6.12 Photomicrographs of pervasive neomorphism under PPL (left side) and CL (right side) in TWP seep-carbonate thin sections. **A** and **B** – Zone of remnant acicular aragonite identified by fabric morphology and GADDs (as circled) which has undergone extensive neomorphism (N3). **C** and **D** – Splay of remnant acicular aragonite that had been neomorphosed. The white arrow indicates original direction of needle growth. Under CL a small amount of purple colour remains in the crystals. **E** and **F** – Recrystallised fabric of neomorphosed aragonite and recrystallised cellular calcite.

6.3 Petrographic based paragenetic events

The paragenesis described for the TWP seep-carbonates is necessarily generalised because diagenetic features do vary across the mound, likely related to relative proximity to main vent sites and thus to the extent and degree of alteration. It is also clear that patchy diagenesis occurred within the original carbonates. The proposed paragenesis for the TWP seep-carbonates has been subdivided into 14

phases or events within two broad temporal groups, namely early and late diagenesis. These are summarised in Figure 6.13, a schematic diagram illustrating the relative timing of each paragenetic event involved in the formation and subsequent diagenetic alteration of the TWP seep-carbonate.

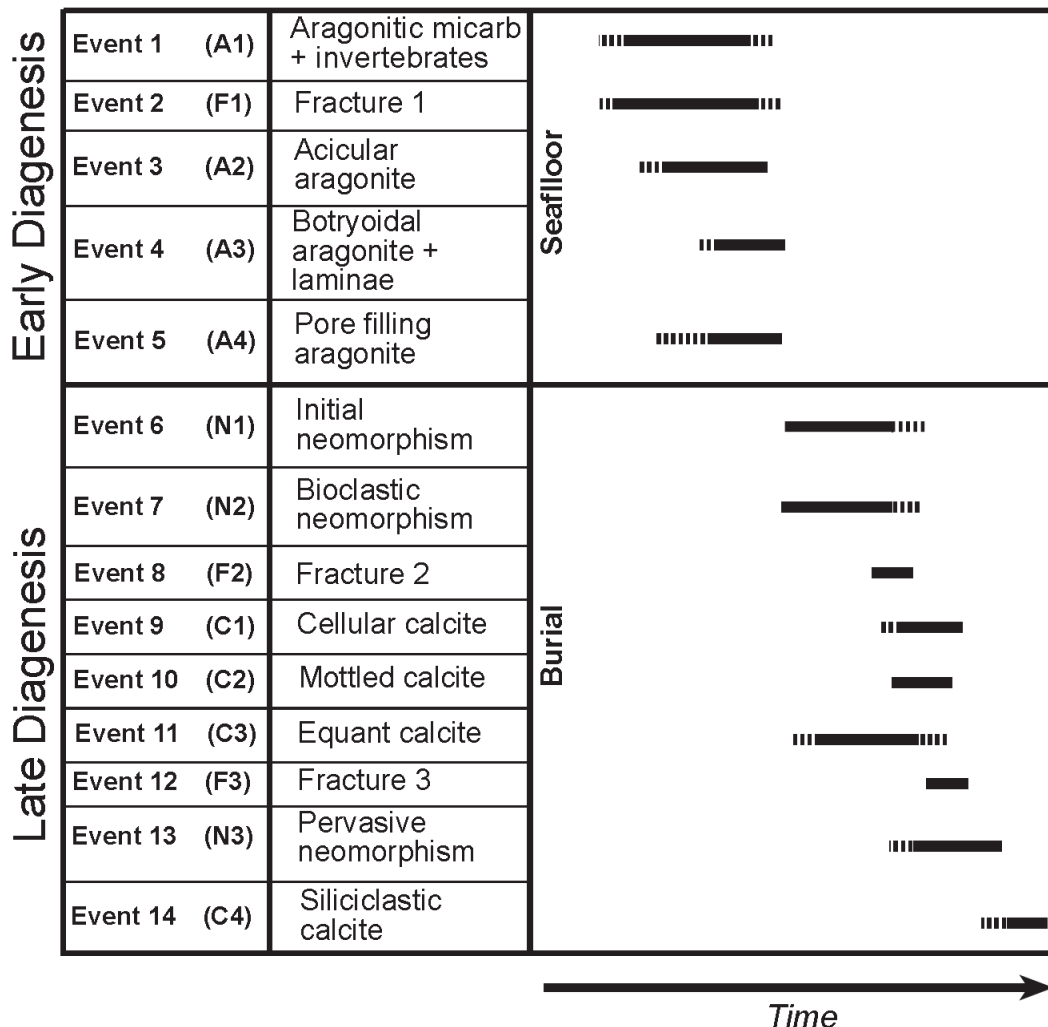


Figure 6.13 Relative timing diagram for paragenetic sequence of seep-carbonates at TWP. The top section of the diagram represents the initial formation of the deposit, and cement fills occurring at or near the seafloor during AOM. The lower section represents a burial situation during late diagenesis, with pore or vein filling phases. Solid black lines indicate the most likely timing when events were dominant, while dashed lines imply periods of time when the event might have occurred as a minor phase. The 14 events are discussed in Section 6.2 and 6.3; minor events M1-M3 are excluded from this diagram. This is despite the minor phases co-occurring with some of the major events. The minor events are generally interpreted to be associated with seafloor precipitation in general and are thus present throughout early diagenesis.

6.3.1 Early diagenesis

Relatively unaltered aragonitic micarb (A1) is seen in many TWP carbonates and is the primary cement phase within most samples – i.e. it forms the carbonate matrix of most outcrops. The precipitation of this cement occurred at much the same time as chemosynthesis-based communities were flourishing on the paleo-seabed, as evident from the encased fossil macro-invertebrates such as bathymodiolin mussels, worm tubes and vesicomyid clams. This aragonitic micarb is dark blue to purple under CL, also suggestive of an early phase (see Section 7.4).

The first fracturing event (F1) is interpreted to have occurred early in the deposit's growth, providing open areas upon which various crystalline aragonite phases could precipitate. While this is recorded in the paragenetic sequence diagram (Fig. 6.13) as one event, it may have been repetitive or cyclical depending on changes in fluid dynamics within the seep-system (see Section 6.3). During this event the aragonitic micarb (A1) was brecciated (F1). It is evident that this early phase of micarb is closely associated with a series of aragonite cements, some filling cavities and others lining brecciated micarb clasts, and filling in the voids amongst these individual clasts. Evidence for worm tubes being present in the system from the onset of seepage can be seen in Figures 6.9A-F. These images of worm tubes show that all interior fills are lined by acicular aragonite (A2).

In some cases borings into the acicular aragonite (A2) or micarb, are filled with early cements and constitute evidence for local hardground development during the early stages of paragenesis (Fig. 6.3E-F). Hardgrounds support seep-carbonate formation close to or at the sediment-seawater interface (Campbell et al. 2008).

The occurrence of botryoidal aragonite (A3) intercalated with dark clotted microbial laminae, (inferred as microbial in origin, cf. Cavagna et al. 1999; Campbell et al. 2002) suggests that microbial activity was not limited to within chemosymbiotic bivalve gills or worm tubes, but also formed mats that may have lined areas of advective fluid flow.. This may be an adaptation to fully exploit the fluids migrating through the system.

Scattered siliciclastic zones appear to have formed within the pore or cavity spaces created by tectonism during early diagenesis. This may have been due to changes in the seep dynamics, possibly associated with local destabilisation and slumping of the carbonate deposit. The veins introduced and trapped foraminifera, siliciclastic grains and disarticulated shell material.

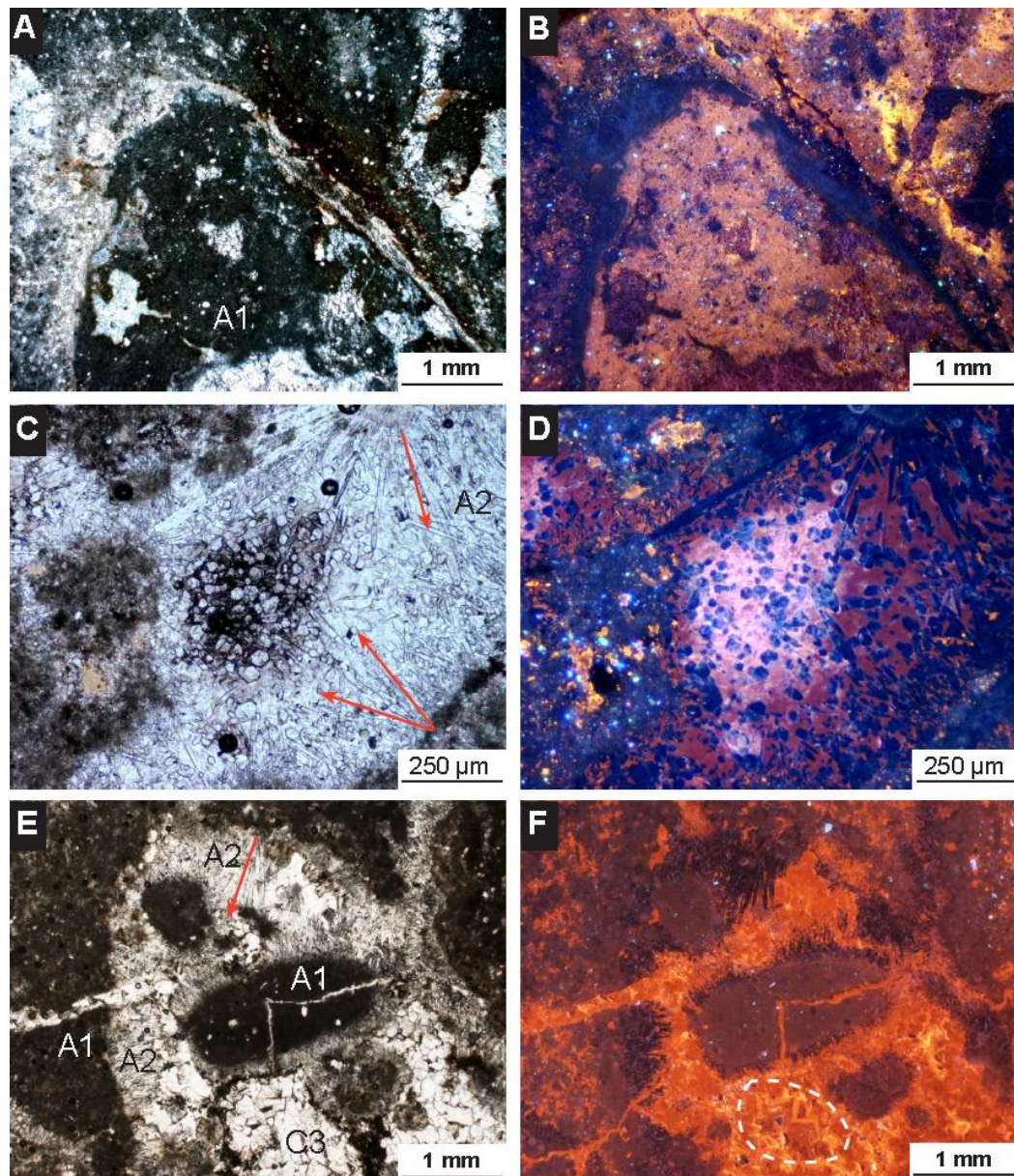


Figure 6.14 Photomicrographs displaying various features within the TWP seep-carbonate under PPL (left side) and CL (right side). **A** and **B** – Neomorphosed micarb (A1) within a worm tube is a pink colour under CL. **C** and **D** – Acicular aragonite (A2) undergoing neomorphism to a more equant crystalline habit. Note that in the centre of the image, the hexagonal blue rhombs are the terminations of the aragonite needles in cross-section, lighter material surrounding the crystals may be microbial or an intermediate cement during alteration. **E** and **F** – Micarb peloid (A1) is split by an equant calcite vein (C3) that has developed zoning (e.g. within white dashed circle). Acicular aragonite (A2) lines the cavity.

After early colonisation by mussels and clams, the shells provided micro-environments for the accumulation of micarb peloids as geopetal infills, and were then also cemented into the deposit, and trapped or focussed burial fluids during selective diagenesis or alteration. Worm tubes also acted as secondary fluid pathways, enabling the passage of methane-rich fluids and the subsequent precipitation of fibrous aragonite phases (Fig. 6.15C-F).

6.3.2 Late diagenesis

The paragenetic events recorded during late diagenesis for the TWP carbonates are similar to those described by Campbell et al. (2002) for the paragenesis of Mesozoic seep-carbonates from the Californian convergent margin, mostly due to the fact that they occurred mainly in voids or fracture veins (Fig. 6.15A-B) and can be identified by the degree of neomorphism or alteration occurring in the carbonates. Late diagenesis effectively occurs after seafloor seepage has ceased, and during or following burial of the seep-carbonates (Campbell et al. 2002).

Neomorphism within the TWP seep-carbonates can be divided into three main types; initial-, bioclastic-, and pervasive- (N1, N2 and N3 respectively). These types have been assigned to describe both the scale and degree of alteration that has occurred and the structures that have actually been neomorphosed. Both initial (N1) and bioclastic neomorphism (N2) are restricted to specific fabrics. Initial neomorphism has occurred in pores, veins and cavities bordered by shells (Fig. 6.10A-B). Bioclastic neomorphism (N2) altered the inner structure of the shell fill or the shell itself (Fig. 6.11A-B). These neomorphic phases were initiated during the earliest stages of late diagenesis and may have continued concurrently throughout most of the remainder of the paragenetic sequence.

Fracturing was also an important process, as it created space for the precipitation of various late diagenetic cements. Both fracture events F2 and F3 appear to be related to local tectonic movements that extended the carbonate deposit and enabled the passage of burial fluids that were saturated in calcite.

The precipitation/neomorphic events during late diagenesis are recorded by calcites (C1, C2 and C3) that have yellow CL patterns and often large equant crystals. Some appear dentate (see Figure 6.6E-F), while others are blocky in morphology. Minor veins with the same CL colour appear to have exploited the boundaries between shelly biota and the matrix in which they were embedded.

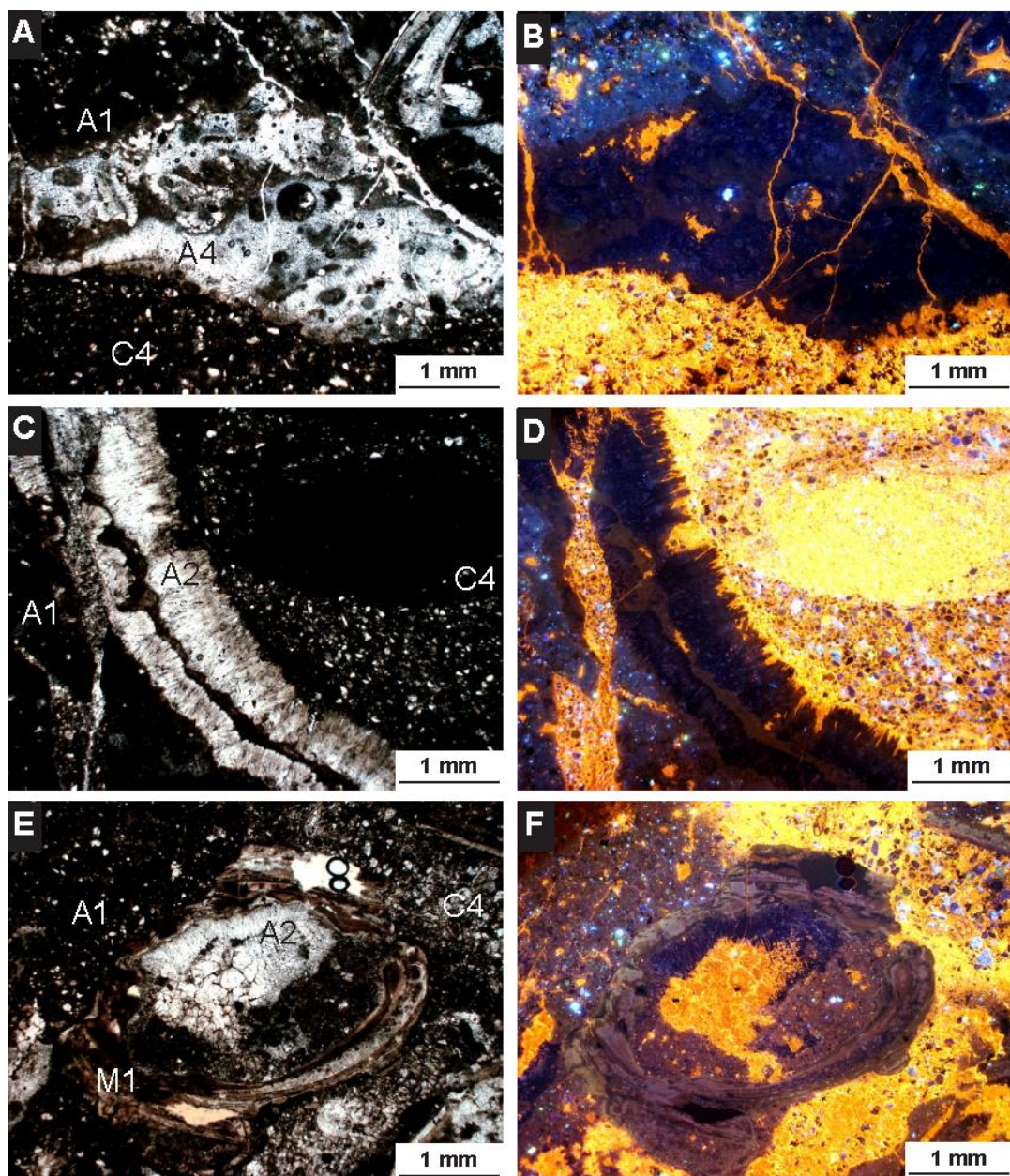


Figure 6.15 Photomicrographs displaying multiple phases from the paragenesis of TWP seep-carbonate under PPL (left side) and CL (right side). **A** and **B** – Zone of spherulitic aragonite (A4) originally surrounded by aragonitic micarb (A1). This phase was cross-cut by a late siliciclastic-rich, calcitic orthospar (C4). **C** and **D** – Worm tube in micarb (A1) at base, lined by acicular aragonite (A2). The tube likely acted as a fluid pathway and was subsequently cemented by a late calcite (C4). **E** and **F** – Bioclast with sheltered

paragenetic sequence within structural boundary of worm tube (acicular aragonite; altered pink/lilac microspar; late calcite).

A late phase in the late diagenetic sequence is pervasive neomorphism (N3) (Fig. 6.12E-F). This stage may have begun as early in the sequence as during the formation of the mottled or blocky calcite phases. Where it is present, pervasive neomorphism appears to have overprinted all other fabrics which formed before it, and aggrading neomorphic fronts are relatively common.

In the ultimate stage of diagenesis, dark siliciclastic veins (C4), which appear bright yellow under CL and are dense with detrital grains, injected through the paths of least resistance within the carbonates (bright yellow material in Figures 6.15A-F). This phase may have lead to precipitation of dark calcitic veins within worm tubes, bivalve shells and other pore spaces. This event supplied sediment and burial fluids to an otherwise closed paragenetic system.

6.4 Mineralogy

The bulk mineralogy of TWP seep-carbonate samples was determined using XRD, while micro-scale changes in mineralogy across individual cement phases were analysed using GADDs and confirmed using CL (for methodologies refer to Section 4.3).

6.4.1 Bulk mineralogy

A summary of the bulk mineralogy at TWP is shown in Table 6.2. The dominant minerals are the carbonate polymorphs, aragonite and calcite. Aragonite is dominant in relatively unaltered samples that have undergone less diagenesis than the calcite dominated samples. The calcite is almost exclusively low-Mg calcite (<4mol% MgCO₃) except for small amounts of possible high-Mg calcite (>4mol% MgCO₃) in a couple of samples. No dolomite was present at TWP, and the siliciclastics included mainly quartz, plagioclase feldspar and clays in varying abundances.

Table 6.2 Relative mineral abundances in representative samples from the TWP seep-carbonate. Table Key: Arag. – aragonite; LMC – low-Mg calcite; HMC – high-Mg calcite; Qtz. – quartz; Plag. – plagioclase feldspar; Clay – undifferentiated clay minerals; A – abundant; C – common; S – some; R – rare; (-) – absent. Note that amounts are relative abundances only (see section 4.3.4). For all XRD peaks and graphs, refer to Appendix 2.1.

| Sample | Arag. | LMC | HMC | Qtz. | Plag. | Clay |
|----------|-------|-----|-----|------|-------|------|
| TWP-A/10 | S | A | - | C | S | R |
| TWP-A/12 | R | A | - | S | R | S |
| TWP-A/14 | C | C | - | C | S | R |
| TWP-A/16 | C | C | - | C | C | R |
| TWP-A/17 | C | A | - | R | R | C |
| TWP-A/4 | - | A | - | A | R | R |
| TWP-B/1 | S | A | - | C | R | S |
| TWP-B/9 | C | A | S | S | S | S |
| TWP-C/1 | A | A | - | S | R | S |
| TWP-C/13 | A | C | S | S | S | R |
| TWP-C/14 | A | C | - | S | R | R |
| TWP-C/17 | A | C | - | S | S | R |
| TWP-C/18 | A | A | - | C | S | S |
| TWP-C/2 | A | C | - | C | S | C |
| TWP-C/5 | A | C | - | C | R | |
| TWP-C/7 | C | C | - | C | C | R |
| TWP-C/9 | C | A | - | S | C | R |
| TWP-D/1 | A | C | - | S | R | - |
| TWP-D/15 | - | A | - | C | S | S |
| TWP-D/16 | A | C | - | S | S | - |
| TWP-D/20 | C | A | - | C | S | - |
| TWP-D/4 | A | C | - | S | R | - |
| TWP-E/14 | C | A | - | R | - | - |
| TWP-E/4 | R | A | - | R | - | - |
| TWP-E/8 | C | A | - | S | S | R |

6.4.2 GADDs specific mineralogy

The use of GADDs proved important for confirming the mineralogy and paragenesis established (by bulk XRD, PPL and CL) for the TWP seep-carbonate

deposit, especially over small spatial scales. The instrument yields mineralogical results on a 0.5 mm scale. These data, when combined with thin section images showing the actual positions of mineral phases, confirmed several stages of the interpreted paragenetic sequence (Fig. 6.13).

Firstly and most importantly GADDs verified the mineralogic interpretations made with CL petrography. In particular, the yellow patterns are calcite, the blue patterns are aragonite and the intermediary purple red (cerise) colours are an alteration product of mixed mineralogy.

Secondly, GADDs aided in the interpretation that neomorphism is occurring in patches at specific locations and in specific fabrics that are identifiable with CL. It is also occurring to different degrees in the samples. For example the cerise red is a calcite mixed with minor aragonite; whereas, the completely diagenetically overprinted fabrics are bright yellow and orange, and comprise only calcite.

6.5 Elemental Chemistry

Spots of known mineralogy (identified by XRD, GADDs and/or petrography) were analysed on the microprobe, so that elemental compositions could be ascertained (see Section 4.2.8). Table 6.3 shows the results reported in parts per million (ppm). Figures 6.16 and 6.17 are a summary of the averaged values for selected carbonate phases from the TWP thin sections. Figure 6.16 is the average elemental composition for all phases analysed. Because of overwhelming predominance of calcium, Figure 6.17 is drawn to emphasise the variations amongst the other analysed elements.

The average Sr value for acicular aragonite is 5664 ppm, while the highest value is 10951 ppm. Both aragonitic peloids probed gave Sr and Mn values below detectable limits, but SiO₂ values exceeded 17 000 ppm, likely because the spot also incorporated was evaluating siliciclastic grains.

Fe, Mn, and Mg values are considerably lower in samples with high Sr (averages of 575, 77 and 2599 ppm, respectively) compared to samples with low Sr (3436,

589, and 5500 ppm, respectively), again supporting the mainly aragonitic versus calcitic mineralogies, respectively.

All but one example of the late calcites had Sr values that were below detectable limits, and the equant calcite (neomorphosed aragonite) had an elevated Sr value of 14003 ppm, presumably remnant Sr from the original acicular aragonite fabric.

Table 6.3 Elemental content values (ppm) as determined by EPMA analysis for selected components of TWP seep-carbonates. Note b.d = below detectable limits.

| SAMPLE | Carbonate Phase | Si | Al | Fe | Mn | Mg | Ca | Sr | Na ₂ | K ₂ |
|-------------|-------------------------|-------|-------|------|------|------|--------|-------|-----------------|----------------|
| TWP-C/1 1 | Acicular aragonite | b.d | b.d | b.d | 310 | 4945 | 389440 | 539 | 1632 | 747 |
| TWP-C/1 2 | Acicular aragonite | b.d | 53 | 1088 | 387 | 241 | 389787 | 10951 | 2226 | 498 |
| TWP-C/2b 1a | Acicular aragonite | b.d | b.d | b.d | b.d | b.d | 380721 | 7989 | 2893 | 332 |
| TWP-C/2b 1b | Detrital calcite | 7293 | 1905 | 5052 | 1007 | 4945 | 365998 | b.d | 890 | 1577 |
| TWP-C/2b 1c | Detrital calcite | 1730 | 529 | 4353 | 1007 | 4764 | 379220 | b.d | 742 | 1079 |
| TWP-C/2b 2a | Detrital calcite | b.d | b.d | 1010 | 232 | b.d | 383865 | 9604 | 1410 | 415 |
| TWP-C/2b 3a | Arag micarb peloid | 17718 | 13706 | 4353 | b.d | 1749 | 339268 | b.d | 742 | 5063 |
| TWP-C/2b 3b | Arag micarb peloid | 20383 | 11748 | 4975 | b.d | 2352 | 323044 | b.d | 2522 | 4814 |
| TWP-C/9b 1 | Cellular calcite | 28658 | 12648 | 4975 | 929 | 4584 | 323974 | b.d | 2374 | 3071 |
| TWP-C/9b 2 | Equant calcite | b.d | b.d | 155 | b.d | 362 | 348702 | 14003 | 1484 | 747 |
| TWP-D/4b 1 | Acicular aragonite | b.d | b.d | b.d | b.d | 603 | 393085 | 10592 | 2226 | 498 |
| TWP-D/4b 2 | Microspar (initial neo) | 2431 | 1270 | 2487 | b.d | 7478 | 378862 | b.d | 74 | 1328 |
| TWP-D/4b 3 | Neomorphic front | b.d | b.d | 1943 | 1007 | 6875 | 387224 | b.d | 74 | 581 |
| TWP-D/4b 4 | Equant cerise | b.d | b.d | 389 | 387 | 6936 | 391799 | 449 | b.d | 498 |
| TWP-D/4b 5 | Burrow | b.d | b.d | 233 | b.d | 2654 | 387868 | 2424 | 890 | 83 |
| TWP-D/4b 8 | Aragonitic micarb | b.d | 20851 | 700 | 77 | 1327 | 355206 | 10322 | 2077 | 1909 |
| TWP-D/4b 6 | Acicular aragonite | b.d | b.d | 855 | b.d | 6936 | 383365 | 1526 | 371 | 913 |
| TWP-D/4b 7 | Aragonitic micarb | b.d | b.d | 1088 | b.d | b.d | 393514 | 8348 | 1929 | 747 |
| TWP-D/20 1 | Botryoidal aragonite | b.d | 212 | b.d | b.d | 3317 | 386796 | 987 | 1113 | 249 |
| TWP-D/20 2 | Detrital calcite | b.d | 159 | 2565 | b.d | 7298 | 386081 | 2154 | 74 | 747 |
| TWP-D/20 3 | Acicular aragonite | b.d | b.d | 1788 | b.d | 5971 | 398088 | 2962 | b.d | 498 |
| TWP-A/6a 1 | Cellular calcite | b.d | 53 | 233 | b.d | 5910 | 392156 | b.d | 1113 | 332 |
| TWP-A/6a 2 | Pervasive neomorphism | 15147 | 8150 | 3265 | b.d | 4161 | 358708 | b.d | 1039 | 2573 |
| TWP-A/6a 3 | Pervasive neomorphism | b.d | b.d | 1399 | b.d | 5247 | 369015 | 539 | 668 | 83 |

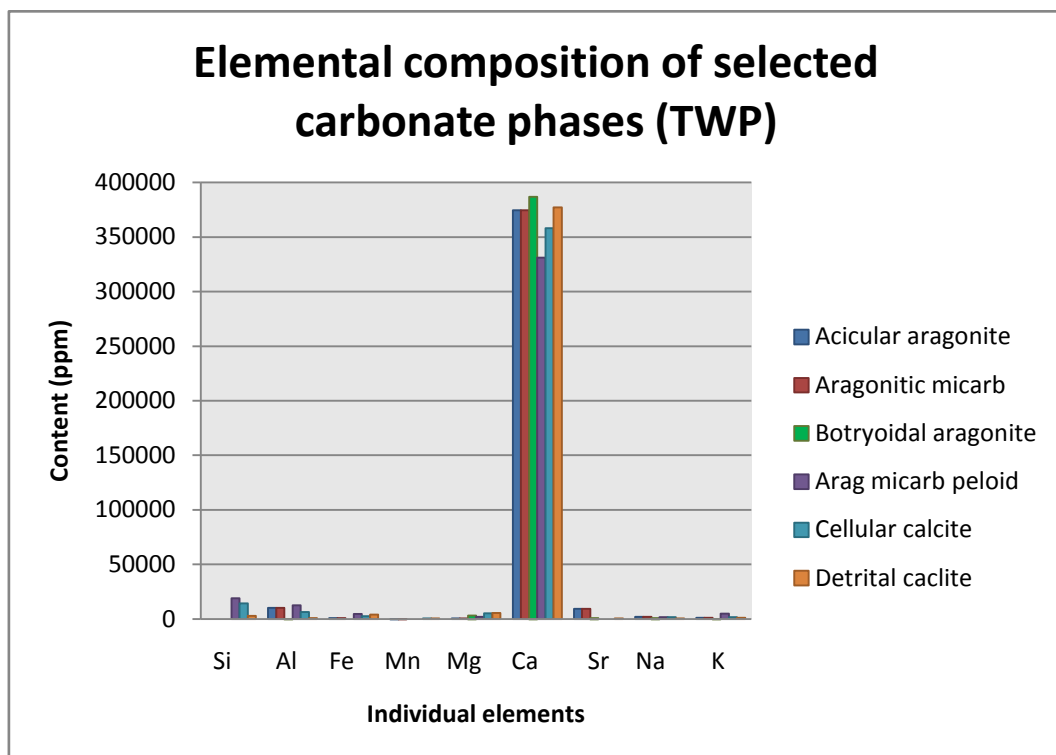


Figure 6.16 Histogram of varying elemental compositions (ppm) in selected carbonate phases of the TWP seep-carbonates.

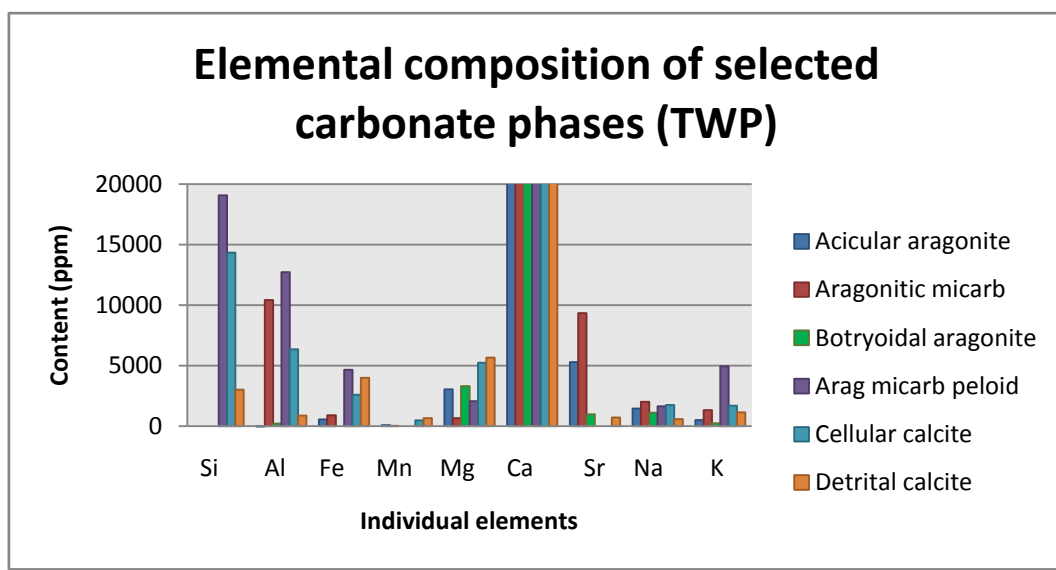


Figure 6.17 Detail of lower half of Figure 6.16 emphasising changes across selected carbonate phases at TWP in elements other than calcium.

6.6 STABLE ISOTOPES

Selected fabrics within the TWP seep-carbonates were micro-drilled for stable isotope analysis. Aragonitic fabrics (Group 1) have $\delta^{18}\text{O}$ values ranging from +2

to $-5\text{\textperthousand}$ PDB and $\delta^{13}\text{C}$ values ranging between -32 and $-50\text{\textperthousand}$ PDB. The calcite fabrics (Group 2) have $\delta^{18}\text{O}$ values that range from $+2$ to $-5.5\text{\textperthousand}$ PDB and $\delta^{13}\text{C}$ values ranging between -8 to $-50\text{\textperthousand}$ PDB. The isotope values vary among fabrics (refer to Table 6.4). Figure 6.18 is a graph of $\delta^{18}\text{O}$ versus $\delta^{13}\text{C}$ for selected components from the seep-carbonates from TWP. There is one major outlier within the data range, this is a late siliciclastic rich calcite (C4) that has a $\delta^{13}\text{C}$ value of $-8\text{\textperthousand}$ PDB, making it anomalously high (Fig. 6.18).

Table 6.4 Stable isotope range for components analysed at TWP. Note that Section 6.9.3 refer to these ‘isotope groups’. For full list of results see Appendix 2.1.

| Group | Phase | $\delta^{13}\text{C} \text{\textperthousand}$ PDB | $\delta^{18}\text{O} \text{\textperthousand}$ PDB |
|-------|------------------------|---|---|
| 1a | Aragonitic micarb | -44.50 | -39.20 |
| 1b | Acicular aragonite | -50.00 | -40.00 |
| 1c | Botryoidal aragonite | -37.45 | -32.23 |
| 1d | Pore filling aragonite | -46.68 | 1.45 |
| 2a | Neomorphosed calcite | -50.00 | -36.24 |
| 2b | Siliciclastic calcite | -42.34 | -8.97 |

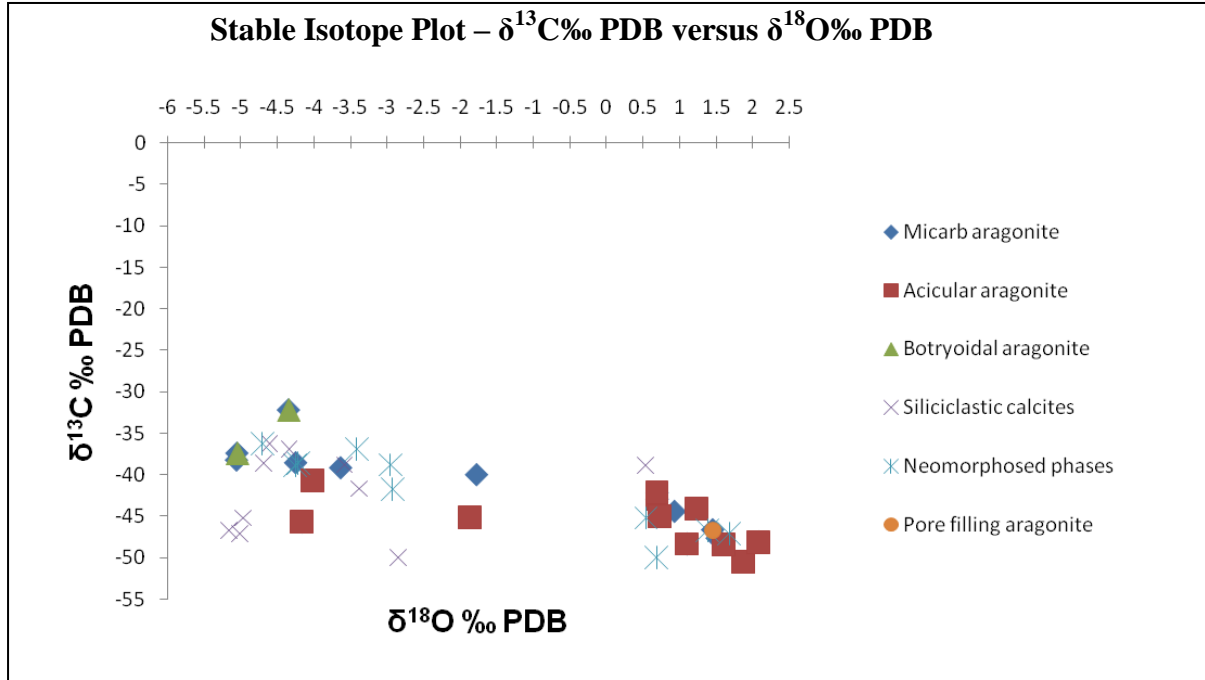


Figure 6.18 Cross plot of stable isotope analysis for TWP seep-carbonates.

6.7 CARBON CONTENT

The TWP seep-carbonates range in composition from 44 to 90% carbonate (see Table 6.5). The variation in carbonate percentage is reflective of the fabrics within the samples, and on a larger scale, the field facies to which they belong. For example, TWP-A/17 is predominantly composed of fibrous aragonite cements, while TWP-B/8 is mostly composed of host calcareous mudstone clasts, with small zones of aragonite crusts. As is evident from Table 6.6, TOC for the TWP samples range from 0.1315 – 1.0245 %.

Table 6.5 Carbonate content (%) for representative samples from TWP seep-carbonates.

| Sample | Carbonate (%) |
|----------|---------------|
| TWP A/10 | 68 |
| TWP A/12 | 68 |
| TWP A/16 | 71 |
| TWP A/17 | 90 |
| TWP B/1 | 62 |
| TWP B/9 | 73 |
| TWP C/9 | 68 |
| TWP C/13 | 62 |
| TWP D/1 | 58 |
| TWP D/20 | 55 |
| TWP E/4 | 44 |
| TWP E/8 | 52 |
| TWP E/14 | 81 |

Table 6.6 Total organic carbon content (%) for representative samples from TWP seep-carbonates.

| Sample | TOC % |
|----------|--------|
| TWP-A/12 | 0.3275 |
| TWP-A/17 | 0.173 |
| TWP-B/1 | 0.261 |
| TWP-B/9 | 0.233 |
| TWP-C/2 | 0.1315 |
| TWP-C/9 | 0.245 |
| TWP-D/4 | 1.0245 |
| TWP-D/20 | 0.416 |
| TWP-E/14 | 0.3045 |

6.8 HYDROCARBON INCLUSIONS

A range of thin sections with significant acicular aragonite (A1) and some other crystal phases were analysed with UV light to determine whether the dirty fluid inclusions and dark zones within many of the crystals were of organic origin (Campbell et al. 2002). Figures 6.19A-F show a range of fluorescent patterns obtained from the analysis. In some situations the acicular aragonite fluoresced white both within the crystals, and around the terminus of the crystals (Fig. 6.19A-B). In other images it is evident that the major fluorescing material is

found as inclusions within the crystals (Fig. 6.19E-F). Other phases were viewed under the UV light, but they failed to fluoresce.

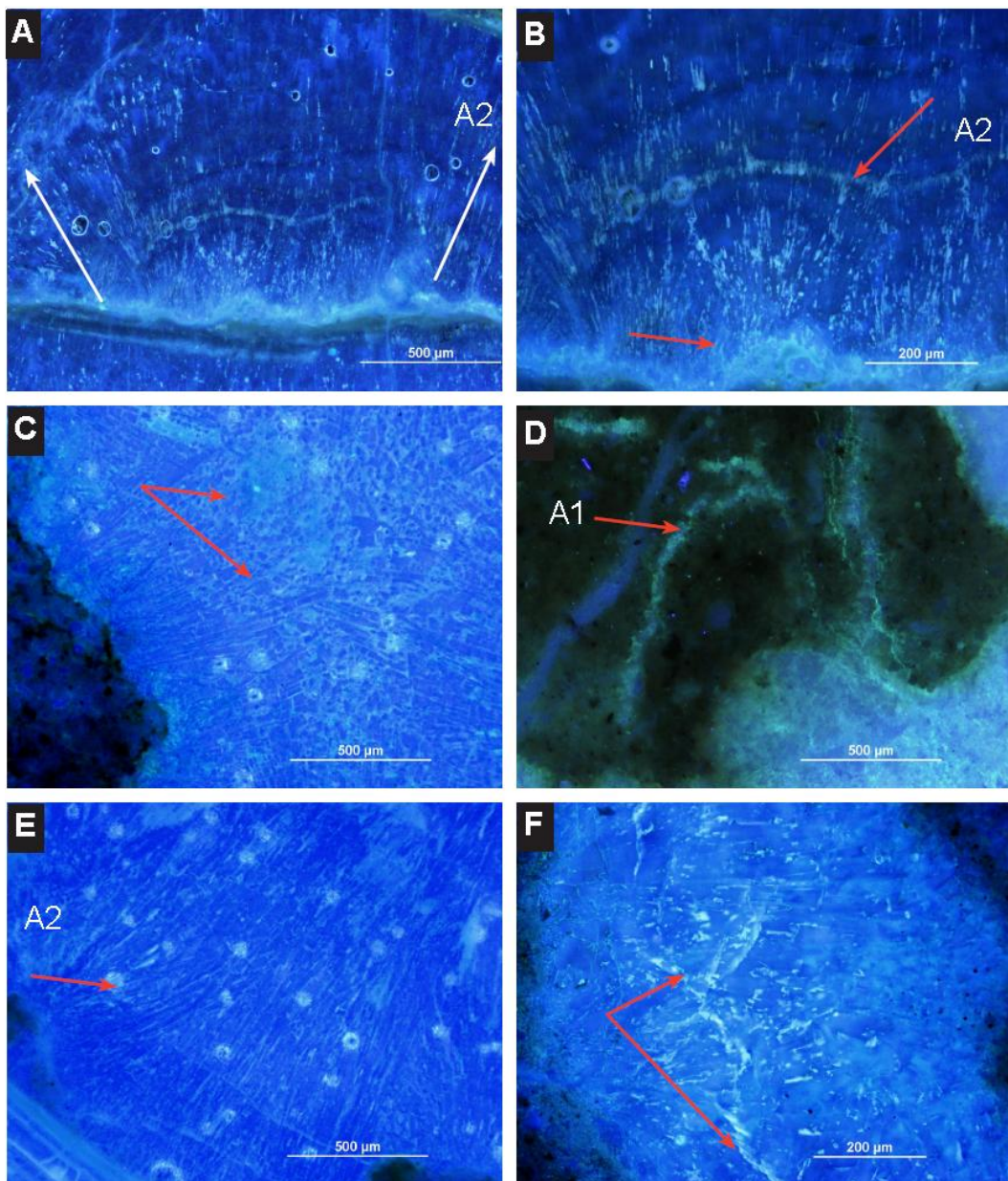


Figure 19: Photomicrographs of TWP thin sections under UV light. Where present organic hydrocarbons fluoresce a very pale green colour. **A** and **B** – Thin section image from sample TWP-D/4, **A**- a general overview and **B**- close up of a vein filled with acicular aragonite (A2). In these images the hydrocarbons are both present within the sparry crystals and in bands between splays. **C** and **D** – Sample TWP-B/9, which is an early micarb (A1) breccia, rehealed by large bands of acicular aragonite (A2). Hydrocarbons are found both between crystals and bordering the aragonitic micarb. **E** and **F** – Further images of hydrocarbons between aragonitic crystal boundaries.

6.9 Discussion and Interpretation

The TWP seep-carbonates are one example of a paleo-seep deposit amongst at least 15 others in the East Coast Basin of the North Island (Fig. 3.2). The

following discussion serves as an analysis of the laboratory results obtained from the detailed petrography and petrology of representative samples from the site. As mentioned in Section 2.1, seep-carbonates have only recently begun to have been studied in detail, and their paragenesis in particular has become the focus for several researchers (Beauchamp and Savard 1992; Savard et al. 1996; Campbell et al. 2002; Buggisch and Krumm 2005; Himmeler et al. 2008). In general, within the TWP seep-carbonates analysed, primary aragonite is the dominant phase in relatively unaltered samples, while calcite and altered aragonite are dominant in samples that have been variably and often extensively altered during diagenesis (Fig. 6.13).

6.9.1 Paragenesis

Early seafloor hydrocarbon seepage was a dominant factor contributing to the colonisation of free-living bacteria and Achaea and chemosymbiotic taxa at the TWP cold-seep in the middle Miocene. The presence of free microbes in near seafloor sediment is evidenced by the aragonitic micarb forming the primary cement in samples from the site. This fabric is characterised by a clotted dark appearance under PPL, and is associated with peloidal structures with the same apparent mineralogy as the micarb (cf. Teichert et al. 2005; Leefmann et al. 2008).

Peloidal structures are commonly associated with bacterial precipitation. Chafetz (1986) suggested that often the nuclei of peloids are in fact clusters of bacterial clumps. Cavagna et al. (1999) presented evidence for the presence of both dolomitic and calcitic peloids in the Miocene Marmorito Limestone in Italy, inferred as microbial in origin. The presence of peloids within seep-carbonates is now routinely linked to microbial structures (Campbell et al. 2002; Cavalazzi et al. 2007; Jenkins et al. 2007). Perry et al. (2007, p. 160) proposed the term ‘organomineral’ to include “any minerals precipitated by interaction with organopolymers, bio(organic) and/or non-biological organic compounds but without evidence of direct skeletal, intracellular or extracellular biological control.” This seems to be a fitting description for the primary micarb cement of this study, the precipitation of which is a result of microbial interactions (see

Section 2.2.2), thus interacting with ‘bio-organic compounds’ but without any structure to control the precipitation.

The presence of acicular aragonite (A1) in seep-carbonates, both ancient and modern, is well documented (Savard et al. 1996; Jørgensen 1992; Campbell et al. 2002, 2008; Buggisch and Krumm 2005; Peckmann et al. 2005; Himmler et al. 2008). The splays of needles are interpreted to precipitate during periods of advective fluid flow along discrete boundaries of components such as brecciated clasts or shell material. The acicular aragonite (A2) found at TWP is often concentrated in bands up to 5 cm thick and over 1 m long. These veins are normally constructed from multiple generations of aragonite, and appear to split large slabs and boulders. Within the TWP carbonates, several forms of acicular aragonite are present (see Section 6.2), either nucleating off brecciated clasts or as pore filling cements. Leefmann et al. (2008) provided lipid biomarker data which link varying aragonite morphologies to different degrees of interactions with microbes, i.e. the varying appearances of aragonite phases is related to the role of bacteria in the rocks. Variations in morphology can be linked to more or less indirect interaction with microbes in the subsurface.

As the migration of hydrocarbons through the subsurface progressed, sporadic or continuous bursts of strongly advective flow, perhaps structurally controlled, were responsible for brecciation processes. Brecciation commonly occurred within the TWP deposit and is a widely reported process from cold seep systems globally (Conti and Fontana 2002; Buggisch and Krumm 2005). The precipitation of early cement phases or the presence of gas hydrates in the shallow subsurface could have initially blocked fluid flow (Nyman 2009) until fluid pressures built up, leading to hydro-fracturing of portions of the carbonate body. In areas of constant flow, carbonate clasts could originate from breakage of slabs. Constant jostling of these clasts would lead to the gradual rounding of their angular edges through autobrecciation. If fluid conditions changed, these clasts may have become remobilised or incorporated into new carbonate crusts as intraclasts.

The onset of late diagenesis associated with burial likely heralded changing conditions in local tectonism, regional subduction, fluid flow dynamics,

sedimentation rates, fluid seepage depths and/or gas hydrate formation (Campbell 2006; Nyman 2009).

One form of diagenetic alteration in carbonates is described as ‘neomorphism’ (Folk 1959; Bathurst 1975). Recrystallisation and alteration of metastable aragonite to calcite has been documented in seep-carbonates from Mesozoic to Miocene age (Savard et al. 1996; Buggisch and Krumm 2005; Himmeler et al. 2008). Aissaoui (1985) presented a model for the partial and complete calcitisation of marine botryoidal aragonites from reef deposits of Miocene and Pleistocene age. The model appears to fit well for those samples from TWP that have undergone pervasive neomorphism. This alteration process may or may not leave remnants of the original aragonite material. Furthermore, an explanation of the varied but consistently blocky morphology of replacement calcite is made, and in that the calcites effectively refill dissolution voids (e.g. from migration of H₂S) by precipitating small crystals into these areas (Aissaoui 1985). Alteration of metastable aragonite to calcite was an important diagenetic process during the history of the TWP seep deposit, an observation well-supported by evidence from CL petrography, XRD and GADDs analyses.

Initial neomorphism (N1) appears to have occurred in the earliest stages of late diagenesis, and then continued to varying extents and intensities throughout the diagenetic history of the carbonate deposit. Primary micarb (A1) was altered and recrystallised into a fine-grained microspar or to large blocky, equant crystals. Mineralogically, these phases were changing from aragonitic to a mix of calcite and aragonite, depending on the degree of alteration.

The mottled calcite (C2) precipitated as a result of burial fluids, saturated in calcite and migrating through the system, and exploiting pre-existing boundaries such as worm tube and shell edges. Equant and cellular calcite forms from the recrystallisation of aragonite as it was being altered into calcite. The cellular calcite may have been in a more vigorous flow system, leading to the morphology of a jostled vein network. Visually, the hand specimens that later reveal these internal fabrics appear as if they have multiple coloured zones and fabrics (e.g.

Fig. 5.21), and when compared to unaltered samples, they seem to have less primary cement, and are more visually heterogeneous.

The siliciclastic calcite (C4) phase is considered to be the last event in the paragenetic sequence of the TWP seep-carbonate (Fig. 6.13). While it may occur concurrently with the final late stage of pervasive neomorphism, there is no evidence that the neomorphism altered this late calcite. The phase itself is characterised by siliciclastic grains, bound by orthospar cement, which under CL appears bright yellow, and in fact has the brightest luminescence of all fabrics studied. It occurs in micro-veins and fenestrae at the thin section scale, and in hand specimen it is identified as the dark fill of many voids and pores, such as fossilised shells and tubes. In some examples the phase cross-cuts earlier fabrics, and in some examples it cuts across fabrics which have undergone pervasive neomorphism. The emplacement of the veins into a solid mass of carbonate was presumably enabled by tectonic extension of the deposit (F3) (Greinert et al. 2001). When this tectonism occurred, cavities and fractures created space for the injection of siliciclastic material and subsequent cementation by late-stage, calcitic burial fluids.

6.9.2 Diagenetic pore fluids

Spatially, the changes in dominant mineralogy vary across the deposit. The carbonate has undergone patchy diagenesis, in which some areas or cement phases have been diagenetically altered to a greater extent than others. This is evidenced by the large degree of variation in lithologic character across the carbonate deposit.

Elemental data obtained by spot probe analysis provided further confirmation of the observations from CL petrography and GADDs analysis. These data also provide a link between the elemental composition of the different carbonate phases at TWP compared to other studies on seep-carbonate petrography. Savard et al. (1996) and Buggisch and Krumm (2005) presented CL, probe and isotopic data for seep-carbonates, and attempted to explain the relevance of aragonite transformation in seep-carbonates. Observations included remarks on the alteration of aragonite and its diagenetic replacement with a late phase of blocky

calcite. In Savard et al. (1996), variations between acicular needles and equant crystals under PPL and CL are consistent with the disparity between the acicular aragonite and equant calcite phases in the paragenetic sequence for TWP. Buggisch and Krumm (2005) summarised elemental compositions found in several Paleozoic seep studies, and the relationship to different alteration stages of aragonites. They generally found an enrichment in Sr in aragonites relative to calcites, and remnant Sr in altered aragonites. Savard et al. (1996), Buggisch and Krumm (2005) and Kelly et al. (1995) reported similar patterns of high Sr values in aragonites relative to late burial calcite phases, excluding recrystallised calcites which appear to have remnant strontium.

Kelly et al. (1995) reported Sr values for fibrous cements which were less than those listed in Savard et al. (1996) and Buggisch and Krumm (2005) a maximum of 1240 ppm, with an average of 640 ppm perhaps because they were dealing with recrystallised calcite with some remnant Sr. They also reported elemental data (ppm) for a void-filling sparry cement much like the TWP phase of equant calcite (C3). The relative amounts of both Fe and Mn are lower than in the TWP equivalent phase, although in relation to Sr values, they do share similar patterns of lower Sr associated with higher Fe and Mn.

Figure 6.20 is a scatter plot of iron vs manganese concentrations from different carbonate phases in the paragenetic sequence at TWP. The results show similar patterns to those reported by Campbell et al. (2002) for seep-carbonates from the Mesozoic. The earlier cements show a shift towards lower Fe contents, while the later cements are more enriched in Mn relative to Fe. Figure 6.21 is a plot of the Sr:Ca ratio vs Mn as modelled in Morse and Mackenzie (1990) and discussed in Campbell et al. (2002). The results also are similar to those in Campbell et al. (2002), where early cements are relatively high in Sr/Ca associated with low Mn, while later cements shift to the lower right of the graph, with lower Sr/Ca and higher Mn content. According to the diagenetic trend diagram as given in Figure 7.41 in Morse and Mackenzie (1990 p. 365), this pattern of elemental compositional changes is consistent with increased rock-water interaction.

Morse and Mackenzie (1990) demonstrated that certain diagenetic trends may exist during the loss of Sr or Mg to circulating pore waters during diagenesis. In open systems with relatively low rock-water interaction, Sr/Ca ratios should decrease due to loss of the strontium to surrounding pore waters. This will contrast with closed systems experiencing higher water rock interaction where the Sr/Ca ratios should be closer to the original fabrics being altered (Morse and Mackenzie 1990). The pore water conditions during late diagenesis at TWP were likely reducing, as Mn increases in the late calcite phases (Fig. 6.21), a known co-precipitate during recrystallisation processes in late diagenesis.

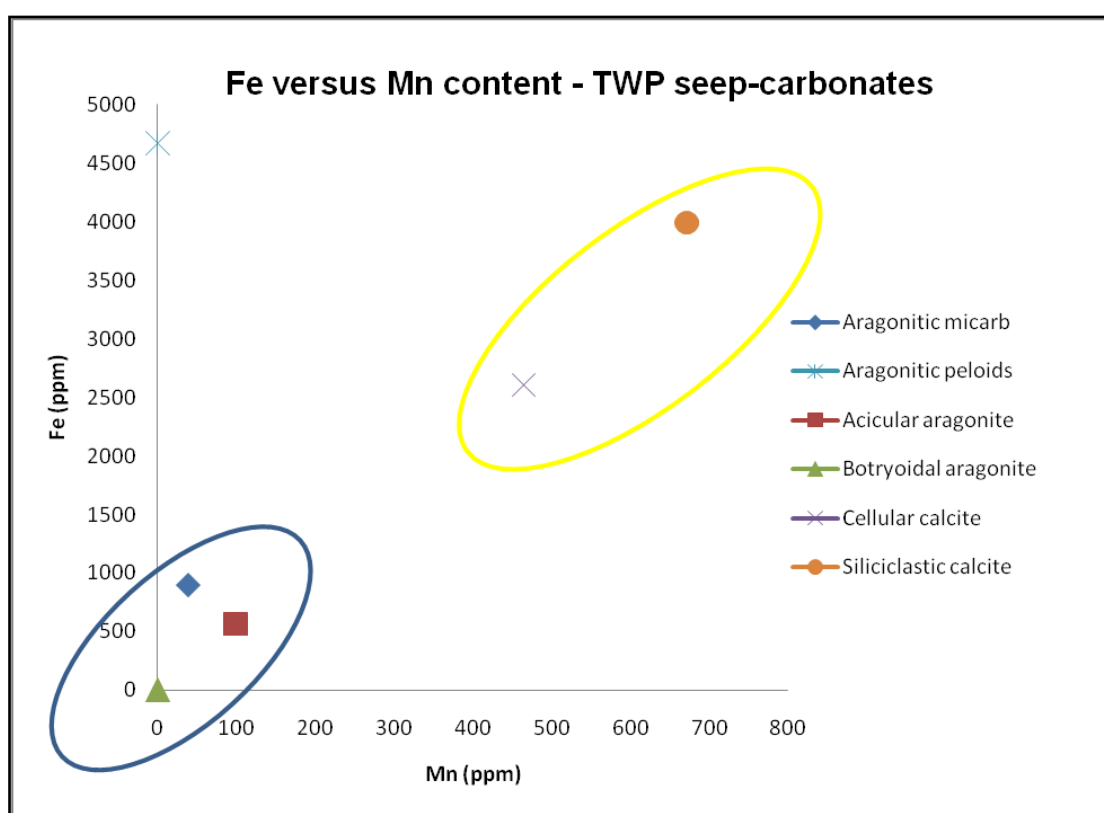


Figure 6.20: Scatter plot of iron vs. manganese (ppm) averages from selected components in the TWP seep-carbonates. The blue ring encircles the aragonitic samples that form a similar group; the yellow ring encircles the calcitic samples.

By combining elemental data, CL observations, Figure 6.22 (Morse and Mackenzie 1990) and an assumption of progressive stabilisation of metastable carbonate phases during diagenesis, it is possible to make some inferences about microenvironmental conditions during diagenesis of the TWP seep-carbonates. Variations in Sr, Mg and Mn content in both original and replacement phases indicate there were two distinct diagenetic groupings in the samples analysed. As

noted above, carbonates from an open diagenetic system will typically have relatively depleted Sr values compared to those in a closed system.

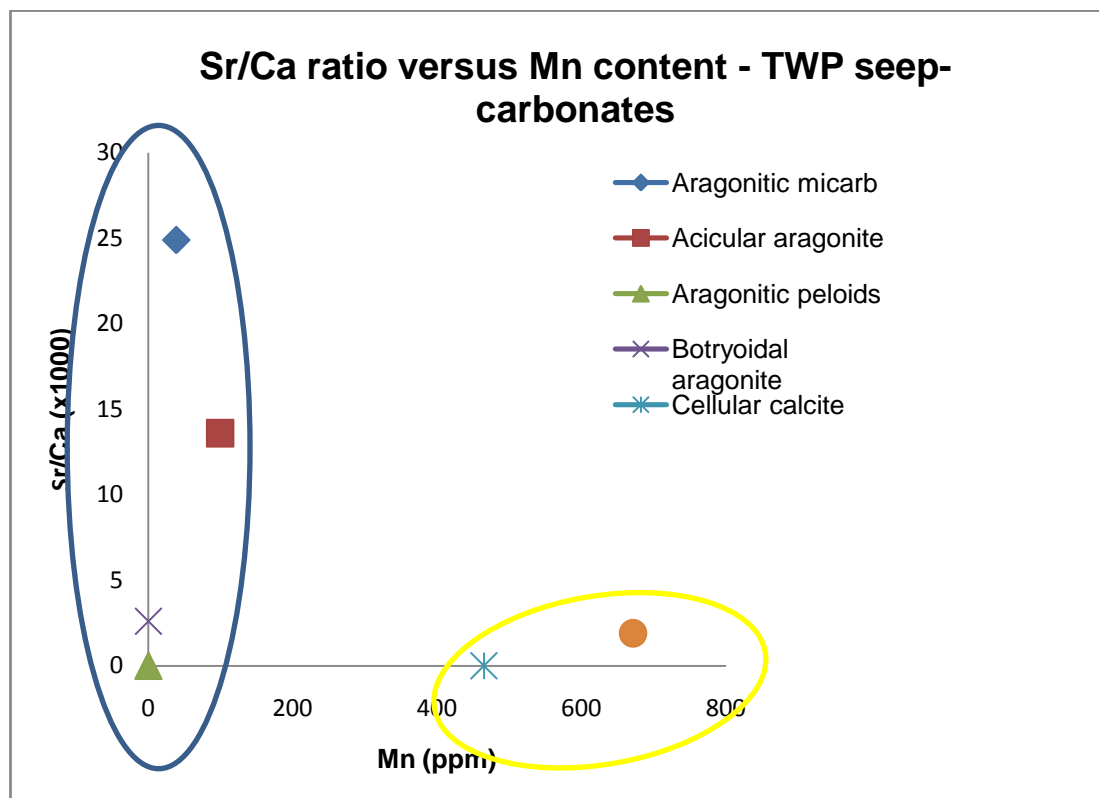


Figure 6.21 Scatter plot of the strontium to calcium ratio vs. manganese (ppm) from selected components within the TWP seep-carbonates. Blue ring encircles the aragonitic samples; the yellow ring encircles the calcitic samples. This is related to water rock interactions during diagenesis (Morse and Mackenzie 1990; Campbell et al. 2002).

Assuming that metastable phases such as aragonite will transform until they reach a stable equilibrated phase, such as calcite, then a diagenetic system will remain ‘open’ until that diagenetic transformation has fully occurred. Considering that at TWP there are aragonite rich samples that are relatively unaltered as well as samples that have undergone complete calcitisation or neomorphism, two distinct diagenetic groupings can be inferred. Those that have not fully transformed would have been subjected to a more open system, with Sr values depleted relative to the original fabrics. Those in a closed system that have completely recrystallised to calcite have remnant Sr values that are closer to the original components. These findings are comparable with the geochemical data and interpretations made by Campbell et al. (2002).

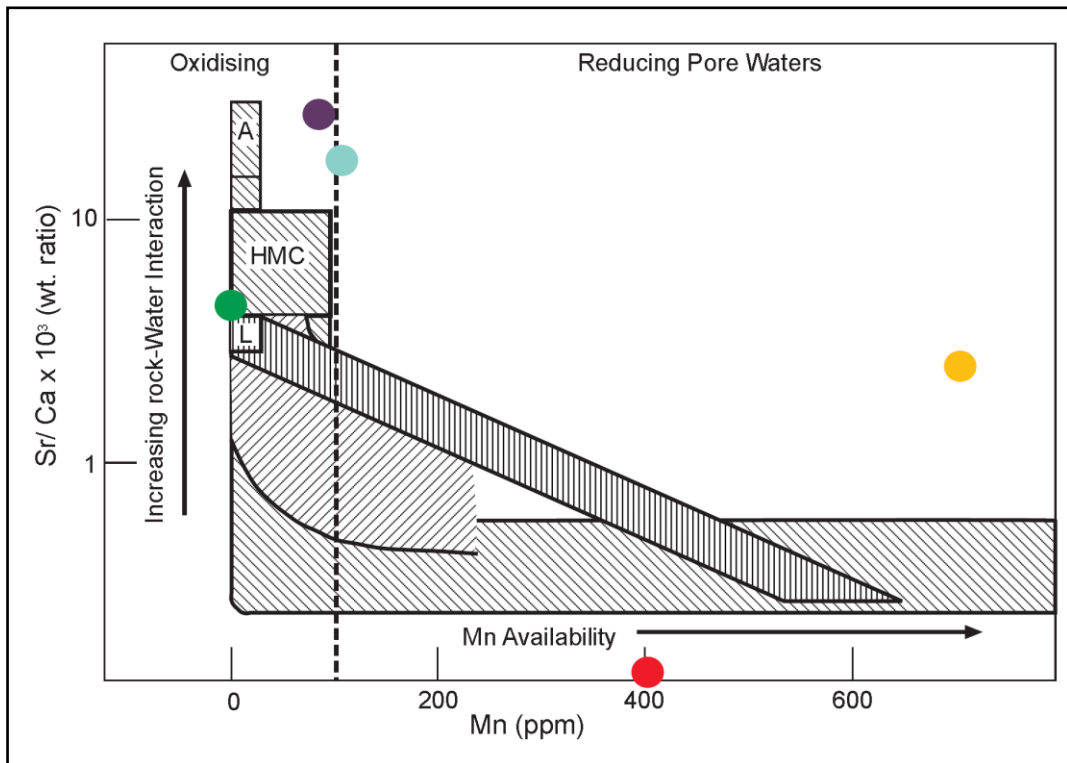


Figure 6.22 Water-rock interaction in diagenesis. Adapted from Morse and Mackenzie (1990). Key: A – Aragonite – L – low Mg calcite; HMC – high Mg calcite; Purple – micarb; Blue – acicular aragonite; Green – botryoidal aragonite; Yellow – siliciclastic calcite; Red – cellular calcite.

6.9.3 Fluid flow considerations

In conjunction with the depleted $\delta^{13}\text{C}$ values, the UV light analysis indicates that fluids with an organic origin, likely methane hydrocarbons, were a dominant driving force in the formation of the TWP seep-carbonates. The acicular aragonite has acted as a ‘freeze frame’ mechanism to trap and thus record a fraction of the fluids migrating through the system. Under PPL the needles appear sparry and transparent, but have varying amounts of dark fluid inclusions within them. Under UV light it is evident that these fluid inclusions are of organic origin, and are probably hydrocarbons (Fig. 6.19). The inclusions are trapped in the acicular needles, as well as in bands around the terminus of bundles of aragonitic splays. Campbell et al. (2002) also provided UV light analysis of organic inclusions, noting the same pattern in the needles and around the boundaries of splay zones. Hood (2000) utilised the technique to identify hydrocarbon inclusions in studies of the Tikorangi Formation Limestone in Taranaki Basin.

The $\delta^{13}\text{C}$ values from TWP range between -8 to -50‰ PDB. Excluding the -8 ‰ PDB outlier, this then provides a range of values between -24 and -50‰ PDB. These values are likely to have come from a fluid source of thermogenic methane (refer to Fig. 2.11) (Irwin et al. 1977; Roberts and Aharon 1994), although mixing with a minor source of microbial methane cannot be ruled out.

Stable $\delta^{18}\text{O}$ isotopes for the TWP seep-carbonate components analysed range from -5.5 to +2‰ PDB. These values can help constrain the temperature of carbonate precipitation.

If the carbonate cements precipitated from Miocene New Zealand sea water (-0.7 to -0.5‰ PDB, Feary et al. 1991), with slope bottom water temperatures between 5 and 10°C (Ridgway 1969), then the $\delta^{18}\text{O}$ of calcite precipitated would range between -0.5 and +1‰ PDB (light blue rectangle in Fig. 6.23; Friedman and O’Neil 1977) and the $\delta^{18}\text{O}$ of aragonite between -0.5 and +1.5‰ PDB (blue rectangle in Fig. 6.24; Grossmann and Ku 1986).

The aragonite (Group 1) cements with $\delta^{18}\text{O}$ values that fall between -1.5 and -5‰ PDB could have formed in temperatures ranging from 15 – 35 °C (Fig. 6.24). These warmer temperatures are typically indicative of deeper burial, e.g. depths of 500 – 1000 m (with a geothermal gradient of 23°C/km, Field et al. 1997). However, this is an unlikely depth for the precipitation of aragonite, a cement which is more likely to precipitate within shallow, porous sediments, with a high influx of sulphate to the surrounding pore waters (Savard et al. 1996; Greinert et al. 2001).

One scenario which may explain the negative values of the oxygen within the aragonitic fabrics could be the upward migration of warmer fluids (between 15 and 30°C) from depth to the seafloor. Rapid ascent of the fluids through the subsurface would not have allowed for sufficient cooling, resulting in increased temperatures relative to the surrounding seafloor environment (and ‘anomalously’ depleted oxygen isotope values).

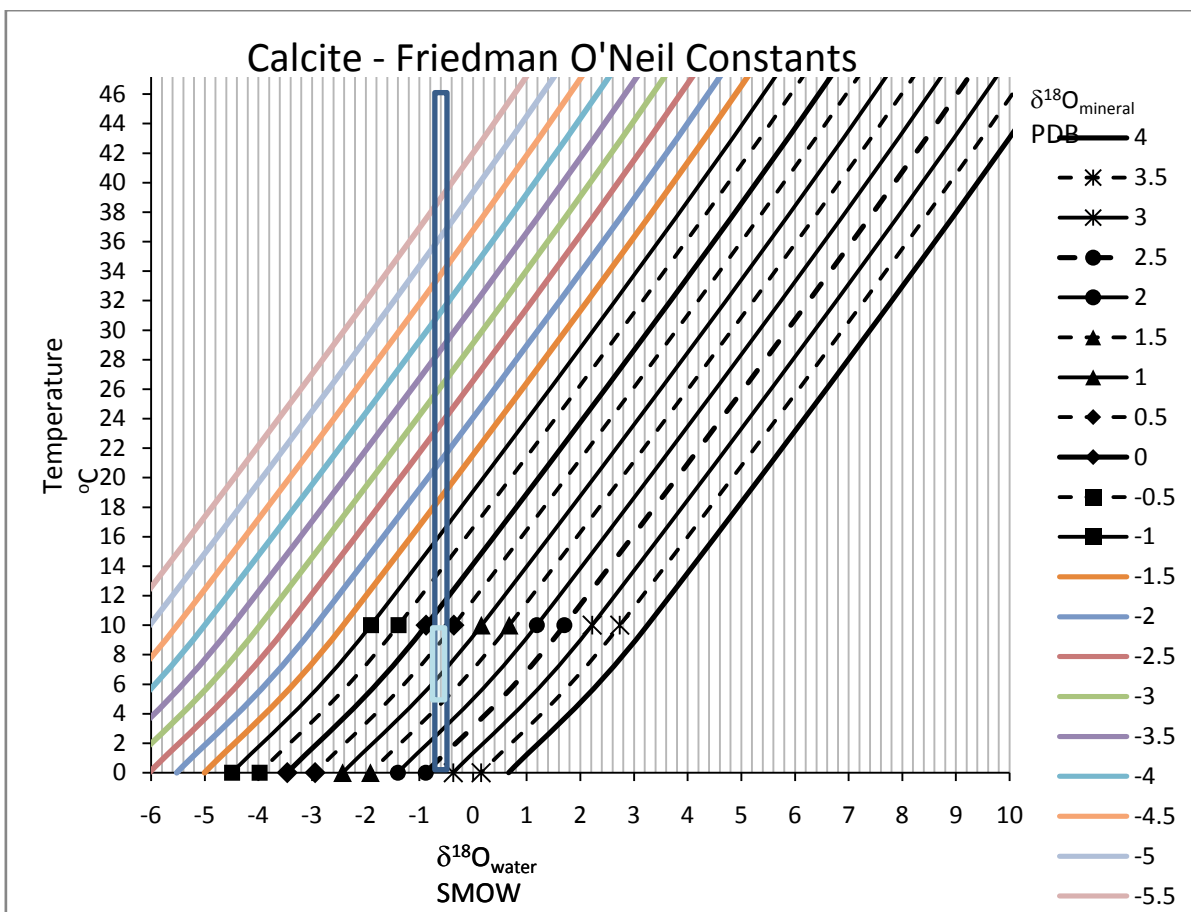


Figure 6.23 Calcite equilibrium equations from Friedman and O'Neil (1977). Long dark blue rectangle encompasses the range of possible PDB and SMOW values and their associated temperatures of formation. Small, blue rectangle is the likely range based on calculated $\delta^{18}\text{O}$ values of estimated Miocene New Zealand sea waters (Fearn et al. 1991).

During fluid ascent, if methane encounters the gas hydrate stability zone (GSHZ), then methane hydrate may form, incorporating the heavy oxygen into the clathrate molecule (Davidson et al. 1983; Ussler and Paul 1995). Incorporation of heavy oxygen into the hydrate molecule results in anomalously ^{18}O -depleted pore waters, another factor leading to the observed $\delta^{18}\text{O}$ values of the aragonites in addition to warmer fluids (albeit, temperatures need not have been so high). Some fluids continued to migrate to the seafloor and were anaerobically oxidised, and utilised in the formation of aragonite cements, such as aragonitic micarb, acicular aragonite and botryoidal aragonite.

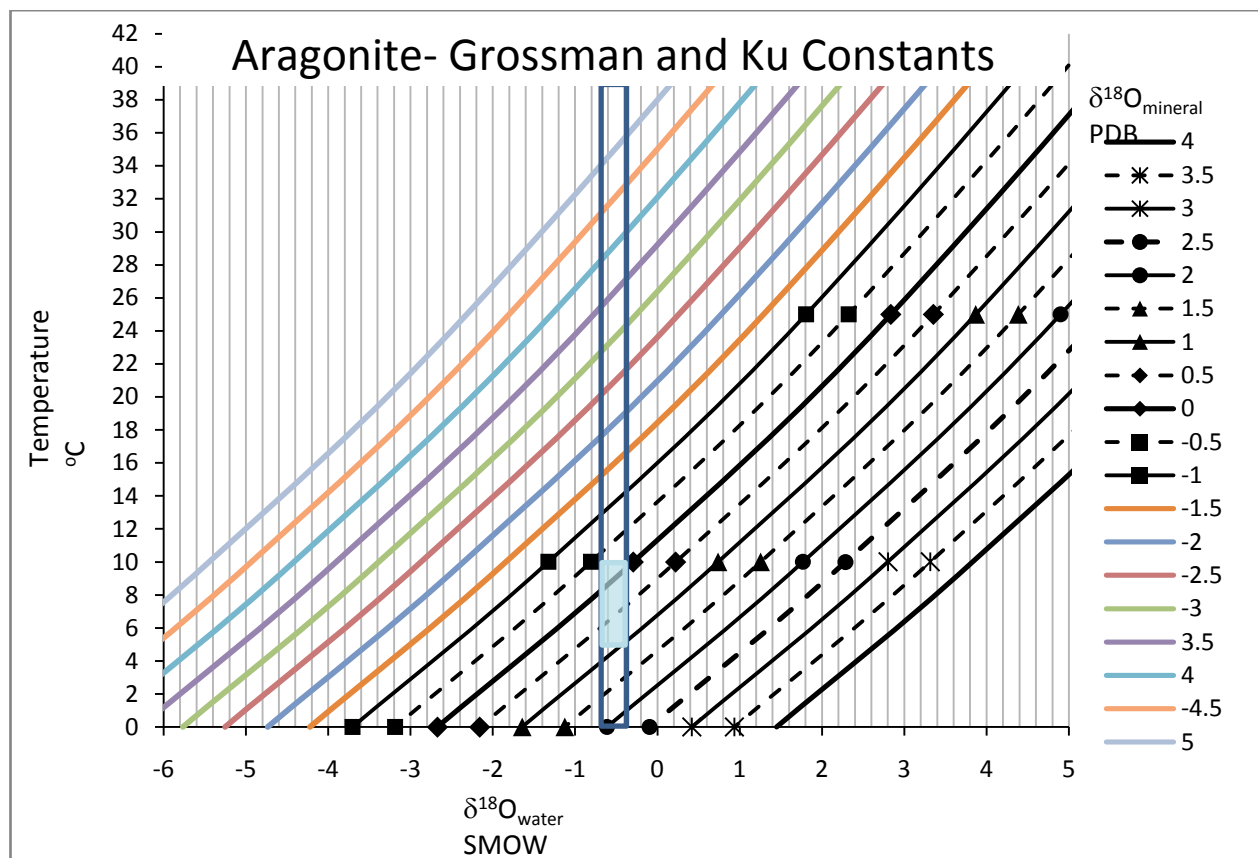


Figure 6.24 Aragonite equilibrium graph from Grossman and Ku (1986). Long dark blue rectangle encompasses all possible SMOW and PDB values for cements with their corresponding temperatures of formation. Small blue rectangle encompasses likely values calculated from estimated $\delta^{18}\text{O}$ values of Miocene New Zealand seawaters (Feary et al. 1991).

Based on equilibrium calculations, the aragonite cements with positive oxygen isotopes values ($\delta^{18}\text{O}$ between +1 and +2.5‰ PDB), would have precipitated at temperatures between 0 and 4°C. Such temperatures are unlikely to be found at the seafloor, or within shallow burial depths where aragonite is likely to form, therefore the $\delta^{18}\text{O}$ values are interpreted as being enriched from estimated Miocene New Zealand seawater.

Alternatively, the enriched oxygen isotope values could be caused by gas hydrate dissociation. During hydrate dissociation, methane and water are released from the clathrate molecule into the pore waters. As heavy oxygen is preferentially incorporated into the clathrate molecule during formation, would thus be released back into the pore waters causing ^{18}O -enrichment (Davidson et al. 1983; Ussler and Paul 1995; Naehr et al. 2000; Hein et al. 2006). The consequence of this

process is that carbonates precipitated from these fluids (e.g. Groups 1a-b) would be enriched in $\delta^{18}\text{O}$.

Based on calcite equilibrium calculations (Fig 6.23, Friedman and O'Neil 1977) $\delta^{18}\text{O}$ values between +0.5 and +1.5‰ PDB would have precipitated from Miocene New Zealand marine waters (slope temperatures between 5 and 10 °C). The calcite (Group 2) cements range from -5.5 to -2.5‰ PDB. Based on calcite equilibrium calculations (Fig. 6.24, Friedman and O'Neil 1977), such values are indicative of fluid temperatures between 22 and 40°C. These temperatures are associated with burial depths between 550 and 1200 m (based on a geothermal gradient of 23°C/km, Field et al. 1997). This seems a reasonable estimation of depth, especially since Group 2 fabrics are interpreted from petrographical analysis to be late stage burial fabrics. However, warmer fluids could also encountered the near seafloor environment due to their rapid ascent.

CHAPTER 7

Ritchie Ridge Seep-Carbonates

7.1 INTRODUCTION

The modern seep-carbonates analysed in this study were supplied by Dr Alan Orpin from the National Institute of Water and Atmospheric Research (NIWA) in Wellington, New Zealand. The samples were collected from water depths of 700–819 m during NIWA Cruise TAN0616 in November 2006 by sleds which traversed several transects across Builders Pencil (BPL) and Rock Garden (RGN) (Fig. 7.1), two sites in the Ritchie Ridge area (see Section 4.2.2) on the Hikurangi Margin.

This chapter summarises observations from the sampling cruise, as well as the results obtained from petrological analyses of the seep-carbonates. It concludes with a synthesis of results and makes some comparisons with other studies of modern seep-carbonates. For laboratory methods refer to Section 4.3 and for detailed laboratory results and images refer to Appendices 3.1 – 3.X.

7.2 Distribution

It is now well-known that the Hikurangi Margin is a zone of active subsurface fluid flow and expulsion, with several cold-seep locations and areas of gas hydrates (see Section 3.2.4). MDAC forming at the seafloor in the region have been reported along the margin at several seep sites ranging from Ritchie Ridge in the north to Cook Strait in the south (Fig. 7.1). While seep-carbonate samples collected on NIWA Cruise TAN0616 came from several scattered localities across the margin, this study focuses only on those specimens collected from Ritchie Ridge at the Builders Pencil and Rock Garden sites.

Cold seep systems generally are oases of productivity in fine-grained muds (Carney 1994). Typically sampling is carried out by dredging along transects, and occasionally from donated specimens collected by local fishermen (Lewis and Marshall 1996). This is the situation for the modern Ritchie Ridge samples.

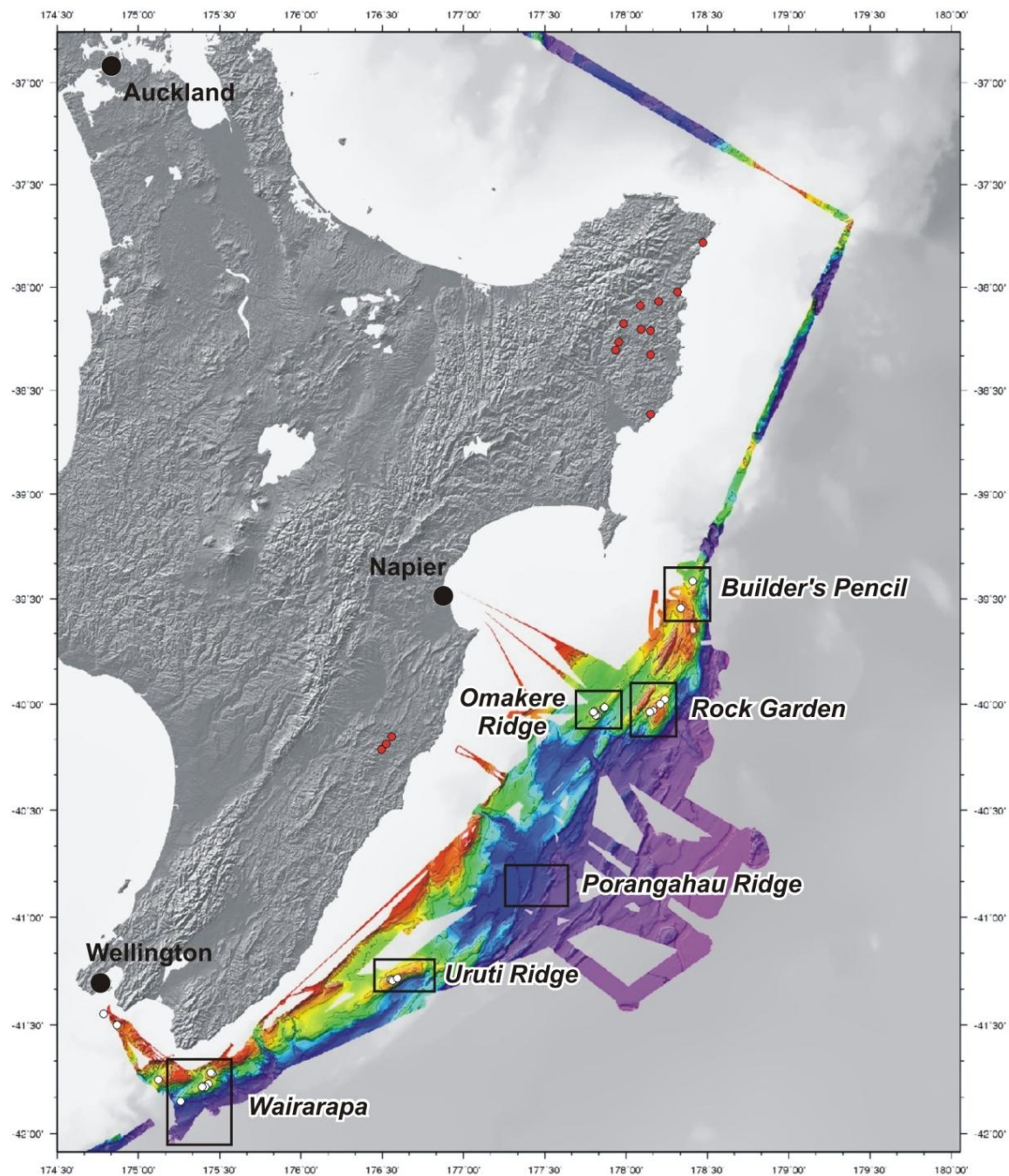


Figure 7.1 Map of Hikurangi Margin, North Island, bathymetry and known seep sites. From North to South they are, Builders Pencil and Rock Garden (on Ritchie Ridge), Omakere Ridge, Porangahau Ridge, Uruti Ridge and Wairarapa sites. Red circles are onshore seep-deposits, and white circles are offshore seep-sites. Figure courtesy of J. Greinert (RCMG, Ghent University, Belgium) and IFM-GEOMAR (Kiel, Germany)

Due to the sled dredge collection technique used on the cruise, the precise locations of dredged samples are not known. Table 7.1 shows available sampling information for the Builders Pencil and Rock Garden. Note that some slabs may not have been sampled *in situ* and because they had been exhumed by erosion and

exposed at the seafloor. Indeed, the broader regional tectonic setting of the margin is dynamic and characterised by slips and slumps capable of exposing such carbonates (see Section 3.4.2) (Faure et al. 2006). Figure 7.2 is a collection of images of the seafloor around the seeps from Cruise TAN0616 taken with a remotely operated vehicle. Note that many seep-carbonate crusts and bacterial mats are observed.

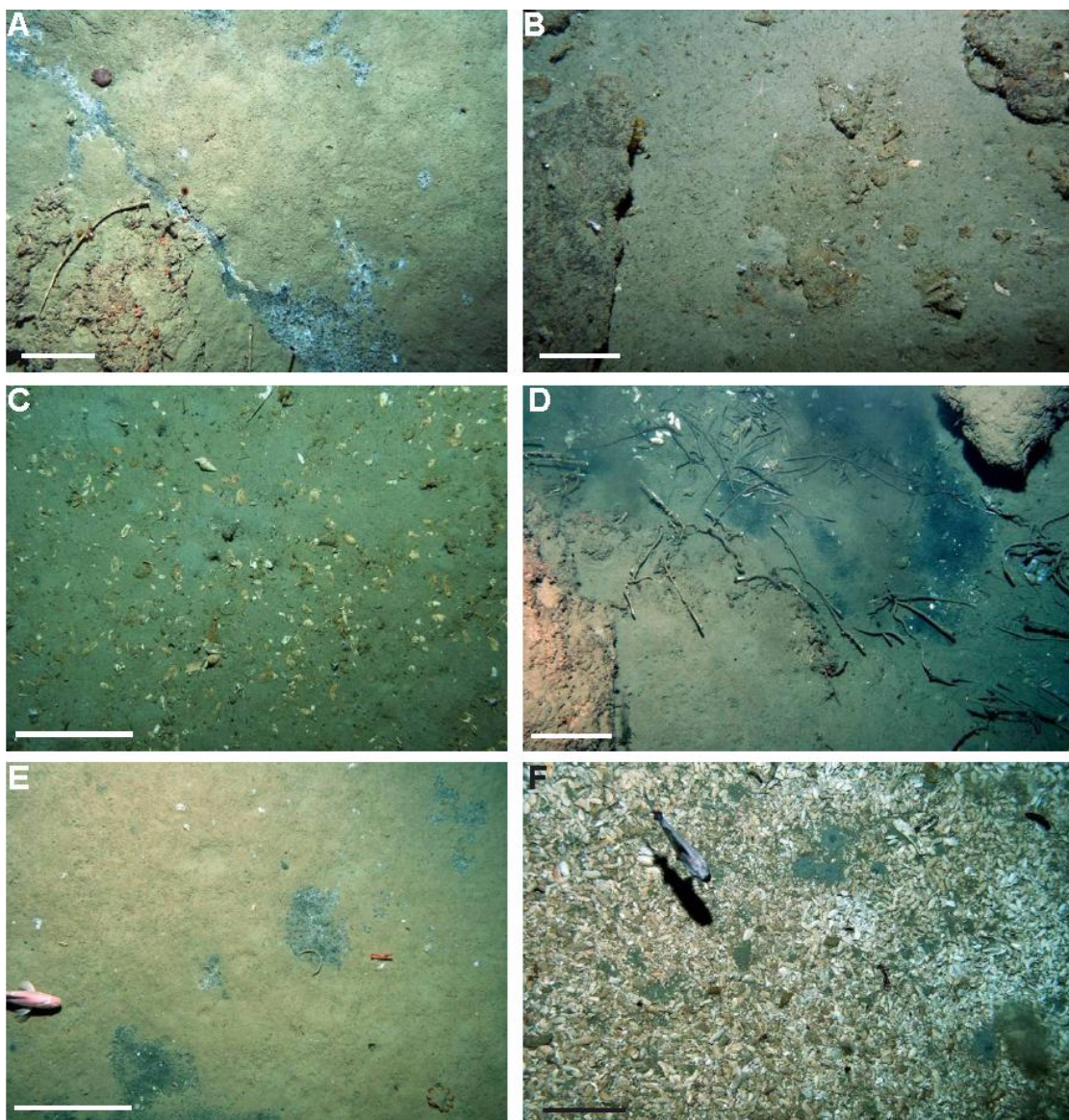


Figure 7.2 Montage of remote operated vehicle images from NIWA Cruise TAN0616, scale bars are 20 cm long. **A** – Seep pores in muddy seafloor sediments, some exposed seep-carbonate crusts. **B** – Exposed, manganese stained carbonate crusts and boulders. **C** – Shelly debris in seafloor muds. **D** – Dark black patches are bacterial mats, note long tube worms scattered within area of exposed carbonate crusts. **E** – Bacterial mats in seafloor mud. **F** – Large amount of scattered, dead *Calyptogena* shells on the seafloor, remnant seep area(?) (from Orpin et al. 2007). **Images courtesy of NIWA....**

The modern specimens were collected from four separate sampling transects (Table 7.1). In all cases the samples were collected using a sled mechanism. Depths reached by the sled were relatively consistent, ranging from 786-819 m across Builders Pencil and 700-787 m across Rock Garden. Thus all of the samples analysed came from a water depth of 700-819 m. MOD-1 is anomalous because it was sampled by a fisherman in a private fishing boat; it is believed to have been sourced from around Builders Pencil. There are no data available for MOD-10 due to a lost sample number between the cruise and storage.

Table 7.1 Location of individual modern samples.

| Sample | Location | Transect station | Depth range (m) |
|---------------|-----------------|-------------------------|------------------------|
| MOD-1* | Builders Pencil | - | - |
| MOD-3 | Builders Pencil | 38 | 815-819 |
| MOD-4 | Rock Garden | 12 | 749-787 |
| MOD-5 | Rock Garden | 12 | 749-787 |
| MOD-8 | Rock Garden | 10 | 700-760 |
| MOD-9 | Builder Pencil | 38 | 815-819 |
| MOD-10 | - | - | - |
| MOD-11 | Builders Pencil | 25 | 786-810 |

While grid references cannot be recorded for each individual sample, Appendix 1.3 shows a full list of latitude and longitude points for the start and end points of the sampling tracks, as well as other data collected from the cruise.

7.3 Hand Specimens

Initial observations of the seep-carbonate specimens show they vary in colour, morphology, fabric type, texture, biotic components and apparent porosity. Table 7.2 provides descriptions for each sample analysed, while Figures 7.3 and 7.4 illustrate cut hand specimens, determined to be dominated by aragonitic and dolomitic mineralogies, respectively.

Table 7.2 Summary table of Ritchie Ridge hand seep-carbonates

| Sample | Description |
|--------------------------------|--|
| MOD-1 (Fig. 7.5A) | Coquina of <i>Calyptogena</i> sp. bivalves, some disarticulated and others whole, encased in a silty mud matrix. |
| MOD-3 (Fig. 7.6A) | Grey-cream muddy micrite, with common tubular conduits. Micro-borings on outer surface are variably iron stained which extends into borings or conduits. Common epifauna on exterior surface, especially corals and attached scattered brittle stars. |
| MOD-4 (Fig. 7.5D) | Small white blebs of carbonate precipitated into grey beige mudstone. Scattered whole bivalves, iron staining on outer surfaces, and micro-borings. Scattered epifauna on surface, (e.g. corals), scattered, irregular small conduits. Some evidence for case hardening, as the exposed outer part is more indurated than inside, especially the outer 2 cm. |
| MOD-5 (Figs. 7.5B-C) | An overall well cemented sample compared to the others, it is cream grey with beige upper surface supporting micro-borings. Scattered bathymodiolin shells, some whole, others fragmented. Laminar carbonate crusts (5 – 10 mm thick) growing upon bivalves in vertical life orientation. |
| MOD-8 (Fig. 7.6B) | Calcareous chimney with massive interior and nodular exterior. Iron-stained on exterior surface; encrusting epifauna include bryozoans, serpulids and corals. |
| MOD-9 (Fig. 7.6C) | Muddy pale grey, tubular-shaped concretion with open central conduit about 1.5 cm in diameter. Cylinder is tapered from 10-15 cm over a distance of 15 cm. Scattered serpulid worm tube encrustations; also a group of profuse intertwined serpulids, 0.5-1.5 cm in diameter. |
| MOD-10 (Fig. 7.6D) | Bleb of highly indurated, muddy carbonate. Nearly central boring 2-3 cm in length. Exterior is iron-stained. |
| MOD-11 | Tubular feature, originally about 15-20 cm across but now relieved as many broken pieces. Body is well cemented siltstone, with exterior and conduit iron-stained and encrusting epifauna. Sample preserves partial conduit fill, similar to actual concretion. |

The samples appear to fall into two categories; these are shown in Table 7.3 and were later confirmed by XRD to be of two different mineralogies (see Section 7.5). These are aragonite and dolomite.

Table 7.3 Main characteristics of major modern seep-carbonate groups, as observed in hand sample.

| Characteristic | Aragonite | Dolomite |
|------------------------------------|-------------------------|--|
| Morphology | Nodules or slabs | Tubular or nodular with central conduits |
| Faunal assemblage within carbonate | Chemosymbiotic bivalves | - |
| Lithification | Porous and vuggy | Densely lithified |
| Borings | Minimal | Extensive on all samples |
| Other epifauna | - | Bryozoans, brittle stars, serpulids |
| Iron staining | - | On exterior of all samples |

Figure 7.3 shows the aragonitic samples, with some main features highlighted. These samples are MOD-1, -4, and -5 which are bioclastic and mainly relatively porous. Large vugs exist, especially in MOD-4, while MOD-1 has vugs are mostly filled with the encasing silty mudrock. MOD-5 includes quite fresh and articulated shells of bathymodiolin mussels within carbonate in life position, with a possible corrosion surface dividing the slab into two layers with visibly different cements. The vugs within MOD-4 are lined by creamy white carbonate crusts to 1 mm thick. In general MOD-5 has a much sandier texture than both MOD-1 and -4, which are composed primarily of a cemented fine grained mud.

Figure 7.4 displays a collection of dolomitic Ritchie Ridge samples (MOD-3, -8, -9, and -10). These samples are devoid of actual shell material, but all show evidence of borings. They all brittle stars, bryozoans, corals and coralline algae. Samples MOD-9 and -10 are muddy and relatively friable, while MOD-3 is indurated. A notable feature in both MOD-3 and -11 is a brown oxidised rind around outer edges, which also winds around into bored samples following the boring boundaries. While most of the sampled carbonates were in blocks or boulders, MOD-8 is different because it forms an elongated structure approximately 50 cm in length which appears to be composed of dark nodules.

The sample is relatively low in density, and rings with a hollow noise when struck with a hammer.

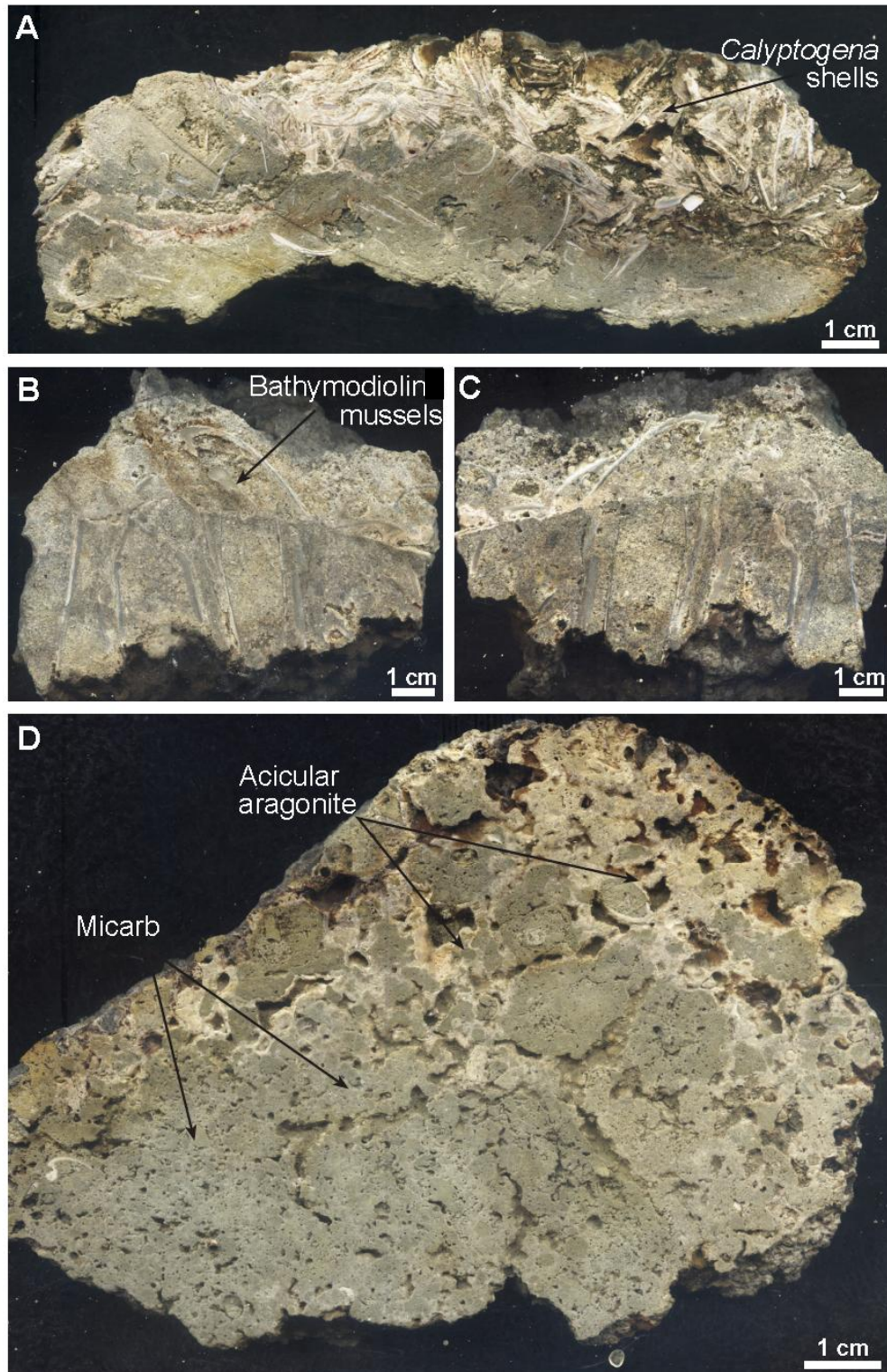


Figure 7.3 Ritchie Ridge modern aragonitic hand specimens. **A** – Sample MOD-1 - coquina of *Calyptogena* sp. in silty mudstone. Shells are disarticulated and specimen is poorly cemented and porous. **B** – Sample MOD-5 - slab from well cemented carbonate block revealing bathymodiolin mussel shells in life position. **C** – Sample MOD 5 – the other half of the dissected slab in B. **D** – Sample MOD-4 - porous slab of micarb, the

initial form of carbonate precipitation, which is evident in the image as peloidal or forms spherical aggregates. The white carbonate crusts forming on pore fringes are composed of acicular aragonite.

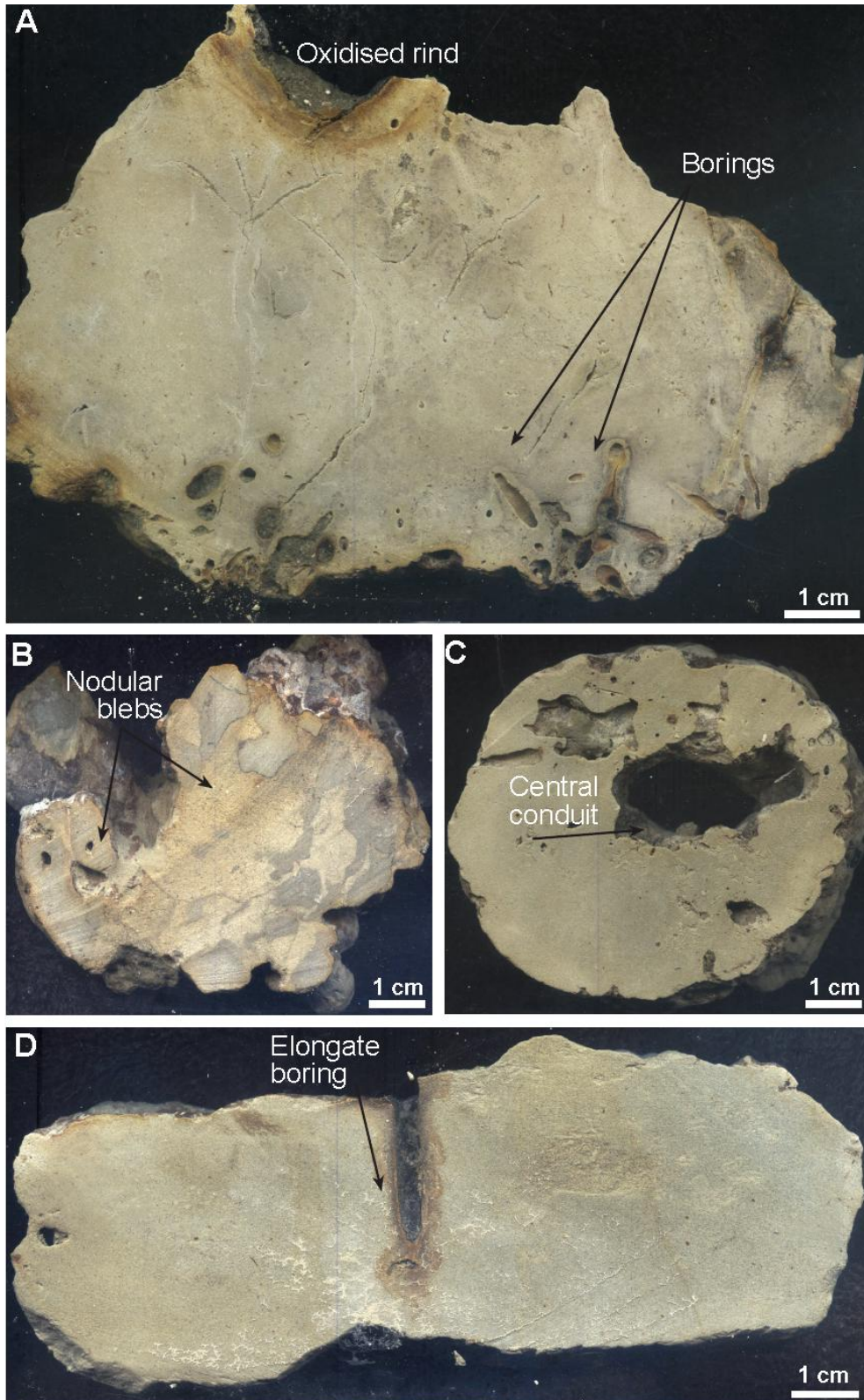


Figure 7.4 Modern Ritchie Ridge dolomitic hand specimens. **A** – Sample MOD-3 - highly lithified slab with oxidised weathering rim around edge and 2-3 types of borings. **B** – Sample MOD-8 – Cylindrical tube with a nodular exterior and texture. **C** – MOD-9 -

Grey muddy cylinder with central conduit. Sample is highly bored on its exterior surface. **D** – MOD-10 - Silty carbonate slab, with boring exhibiting iron oxidised rind. Slight variations in colour within the slab are indicative of fossilised bioturbation structures.

7.4 Petrographic Components

The Ritchie Ridge seep-carbonate thin sections were viewed using both plane polarised light (PPL) and cathodoluminescent light (CL) microscopy (see Section 4.3). Petrographic analysis has illustrated several similarities in fabric componentry with the Miocene TWP seep-carbonates (see Section 6.2), although there are two major differences. First, in the modern shell-bearing samples, which are entirely aragonitic, diagenetic overprinting has not occurred. Second, some of the abiotic modern samples are dominated by dolomitic cements, otherwise not found in the ancient samples from TWP. A key feature highlighted by microscopy and confirmed by XRD analysis is the carbonate mineralogy of the modern samples, which are either predominantly aragonitic or dolomitic. Which mineralogy a sample possessed had dramatic influence on subsequent laboratory results, as described further in Section 7.5.1.

7.4.1 Aragonitic micarb

The primary cement within most seep-carbonate samples studied herein is an aragonitic microcrystalline carbonate (micarb). The micarb is clotted in appearance and has a dirty brown–grey colour in clumps or nodules up to 2 mm across (Fig. 7.5A-B). In some situations, the micarb takes the shape of sub-spherical peloids averaging 0.2 mm size. The peloids are generally well-rounded and appear in groups of over 10 individual peloids (Fig. 7.5C-D). Under CL the micarb is a light blue colour, and appears to be devoid of any discernible internal structure.

7.4.2 Acicular aragonite cement

Acicular aragonite in the Ritchie Ridge samples may take several forms. Like the ancient TWP samples, acicular splays, spherulitic bundles and botryoids were found. Spatially, the aragonite either lines pore spaces or exploits minor cavities between sand grains and foraminifera. In areas where the aragonite lines clasts as acicular splays, the term acicular aragonite is used herein. In areas where the aragonite fills pore spaces, spherulitic or botryoidal aragonite has formed.

In the first case, the acicular aragonite appears as isopachous layers (0.5 – 2mm thick) radiating into the centre of voids and growing perpendicular to growth surfaces (Fig. 7.6A-D). These crystals may be up to 2 mm in length and their size depending on the amount of pore space available. They grew outwards either from the edges of large peloidal clusters and micarb clumps, or from disarticulated bivalve fragments (Fig. 7.6C-E).

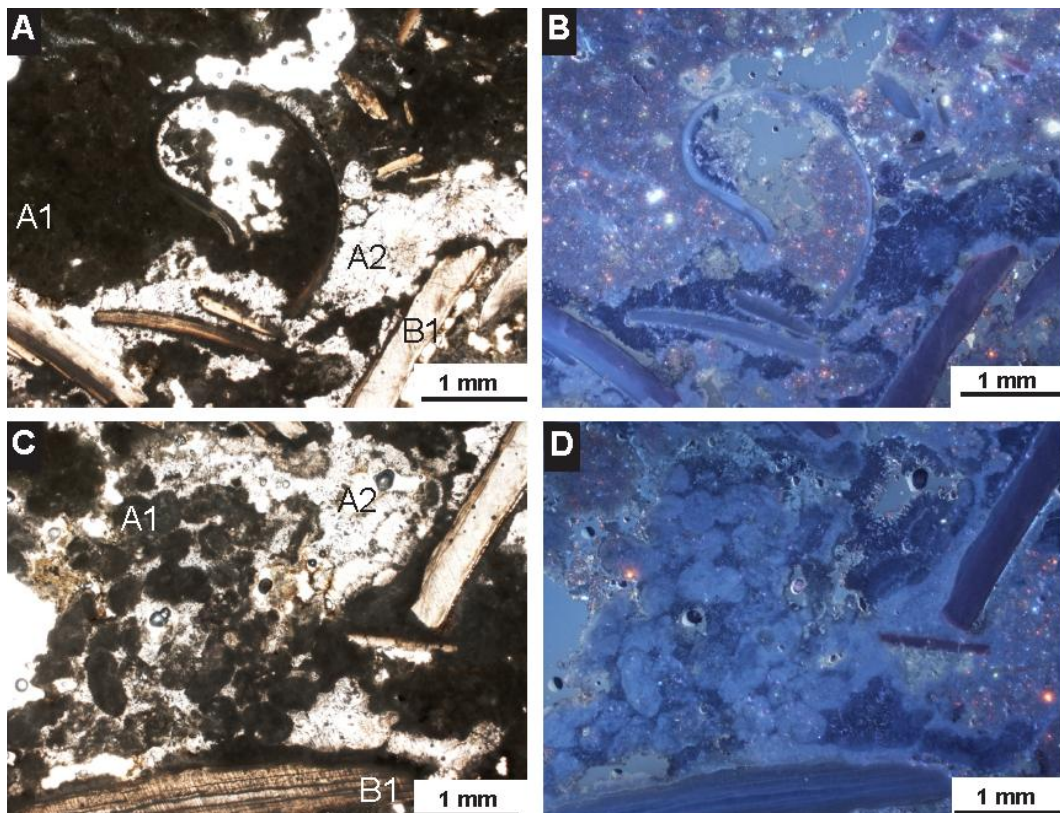


Figure 7.5: Photomicrograph pairs of Ritchie Ridge aragonitic seep-carbonates under PPL (left side) and CL (right side). **A** and **B** – Micarb (A1) and host sediments form a background in which cavities provide pore space for further carbonate precipitation such as acicular aragonite (A2) splays. Disarticulated bivalves (B1) also provide nucleation surfaces for the acicular aragonite (A2). **C** and **D** – Peloidal fabric (A1) has formed in a void space where acicular aragonite precipitated around it. Some botryoids of acicular aragonite (A2) have precipitated and grown into the cavity.

Where acicular aragonite grew within interparticle pore spaces, the needle growth may have been restricted due to a lack of void space, or enhanced if large voids or fractures existed. The latter is evident in Figure 7.7C-D where spherulitic aragonite with full rosettes has developed in a fracture cavity 1 mm thick. MOD-5 is an example where one half of the sample is characterised by bivalves in

growth position, which created a nucleating surface for the growth of splays of parallel, acicular aragonite needles. However, the other half of the sample is rich in quartz grains and foraminifera cemented by micarb. Where void space has

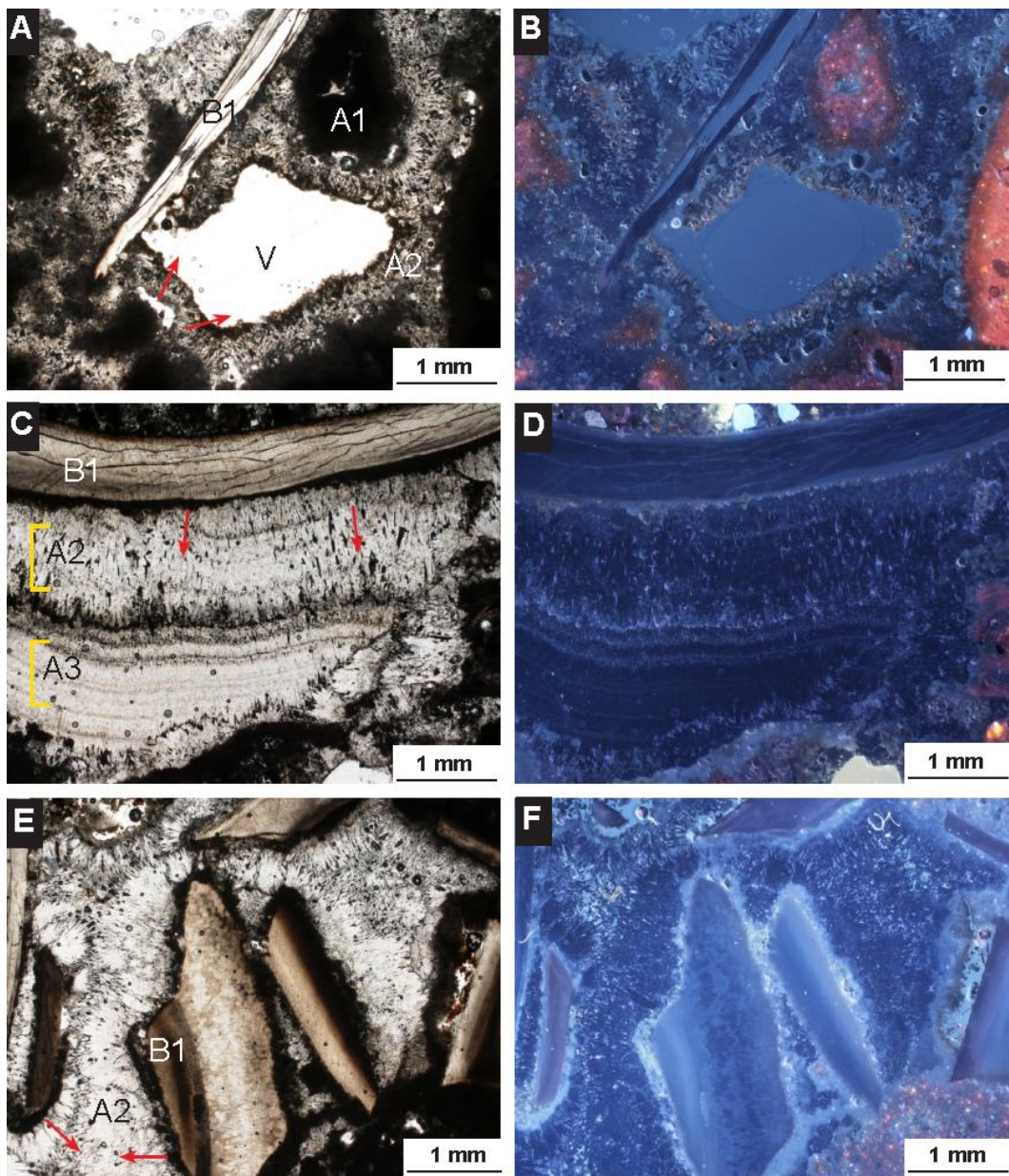


Figure 7.6: Photomicrograph pairs of modern Ritchie Ridge aragonitic seep-carbonate, under PPL (left side) and CL (right side). **A** and **B** – Example of acicular aragonite (A2) utilising bivalve clasts (B1) and micarb peloids (A1) as nucleation surfaces. Arrow indicates direction of growth into cavities. **C** and **D** – Splays of acicular aragonite (A2) and botryoidal aragonite (A3) precipitating from the edge of a bivalve clast. **E** and **F** – Disarticulated bivalve bioclasts (B1) provide a nucleation surface for splays of acicular aragonite (A2), which are growing into the centre of void spaces.

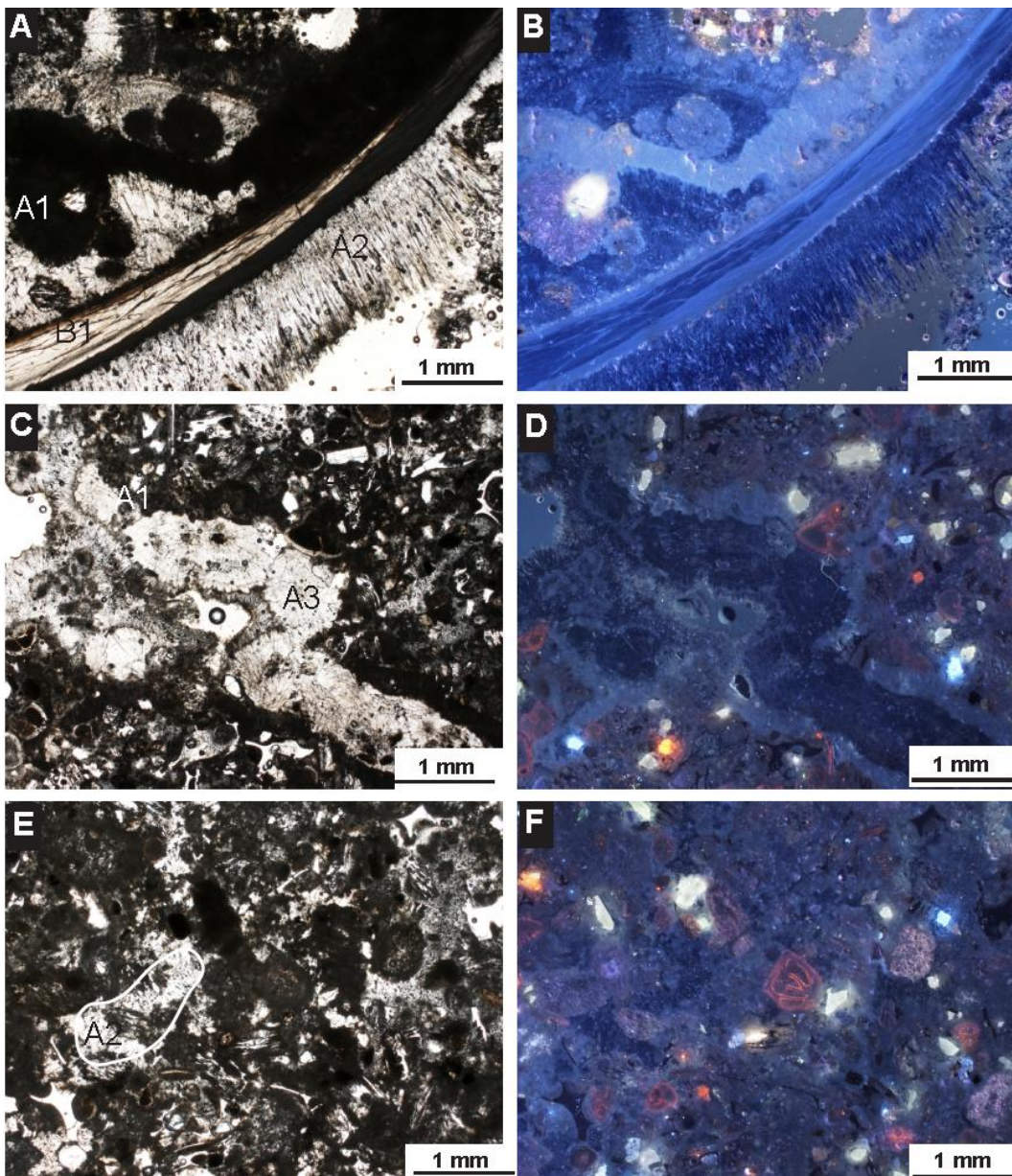


Figure 7.7: Photomicrograph pairs of modern Ritchie Ridge aragonitic seep-carbonates, under PPL (left side) and CL (right side). **A** and **B** – Bivalve (B1) with acicular aragonite (A2) growing from the outside the clast. The bivalve also acts as a sheltered zone in which micarb (A1) was precipitated. **C** and **D** – Spherulitic aragonite (A3) exploiting a fractured pore within a host sediment of foraminifera and quartz grains. **E** and **F** – Aragonitic cement amongst a ground mass of foraminifera and mineral grains; note small patches of spatially confined acicular aragonite (A2).

been created (perhaps by movement caused by ascending fluids) acicular aragonite has formed in small cavities 200µm wide (Fig. 7.7 E-F).

The aragonitic fabrics all have a luminescent pattern of varying blue hues under CL (e.g. Fig. 7.7A-B). In general the acicular aragonite appears to be a darker blue than the micarb fabrics. In Figure 7.6E-F a *Calyptogena* sp. bivalve shell luminesces bright blue (aragonitic shell), with a similar colour pattern of the acicular aragonite growing off its edge. However in Figure 7.5C-D, the acicular aragonite growing between the peloids is a far darker blue than the micarb. Variations in trace metal chemistry, not studied here, may have controlled CL colour differences (Pagel et al. 2003).

7.4.3 Dolomite

The majority of the modern dolomitic samples from Ritchie Ridge have a matrix of fine-grained silty mud plus varying amounts of foraminifera present. In general, the dolomitic samples are texturally less diverse than the aragonitic samples and also appear less sandy. Siliciclastic material is abundant and ranges from subrounded to angular, composed of grains of quartz and feldspar with minor amounts of other minerals. MOD-11 contains large amounts of pyrite dispersed between siliciclastic grains (Fig. 7.8A-B). In some samples pyrite is concentrated in veins, fractures or cavities such as foraminifera (Fig. 7.8E-F), perhaps utilising preferential fluid pathways or remnant bioturbation paths.

Under CL, the dolomitic samples range from a lilac pink to bright orange colour. As is evident from comparing Figures 7.8B and 7.9B, the CL colour varies quite a bit across the five samples.

In sample MOD-8 (Fig. 7.9), which has the highest iron content (see Section 7.5.4), dolomite rhombs are found dispersed between volcanic glass shards. In general MOD-8 has a brighter yellow CL pattern relative to the other dolomitic samples, and rhombs are clearly discernable (Figure 7.9C-D). The poor sorting of the glass shards appear to have provided a large amount of pore space in which the dolomite rhombs formed.

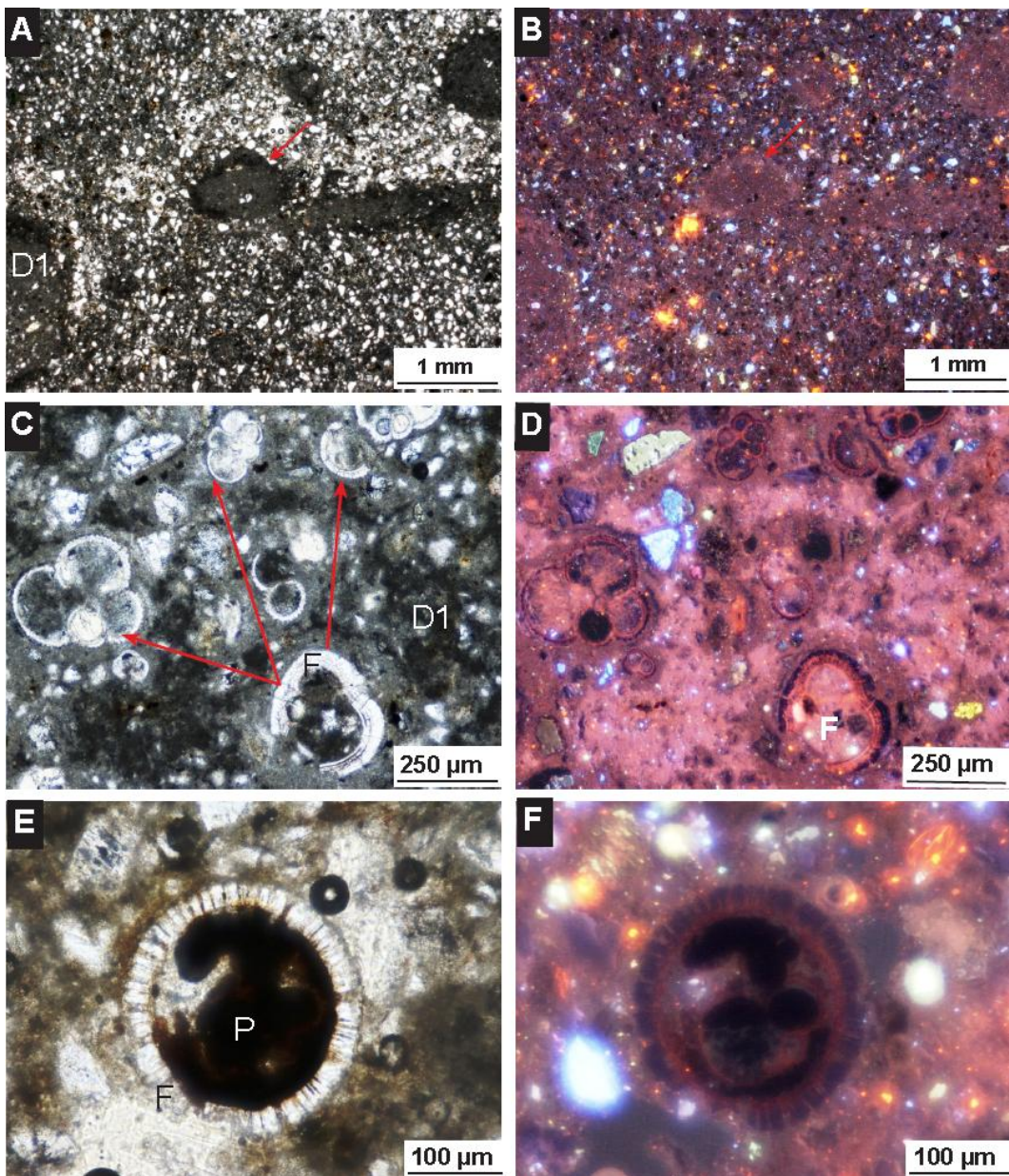


Figure 7.8 Photomicrograph pairs of modern Ritchie Ridge dolomitic seep-carbonates, under PPL (left side) and CL (right side). **A** and **B** – Siliciclastic-rich carbonate cement, with the different coloured zones defining areas of varying siliciclastic content, as well as disseminated pyrite (P) (e.g. red arrow). **C** and **D** – Foraminifera tests (F) (e.g. red arrows) in groundmass of siliciclastic rich dolomitic (or protodolomitic) cement (D1). **E** and **F** – Close up of foraminifera test with a fill of ankerite, as confirmed by GADDs analysis.

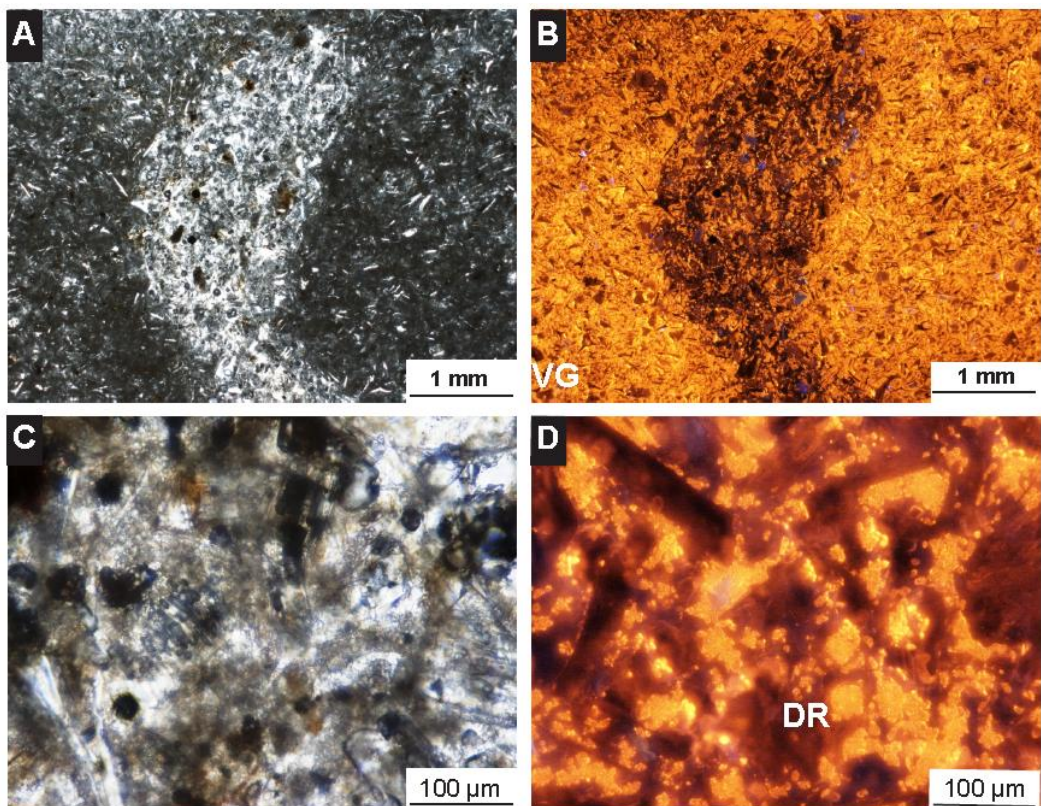


Figure 7.9 Photomicrograph pairs of modern Ritchie Ridge dolomitic seep-carbonates, under PPL (left side) and CL (right side). **A** and **B** – Sample MOD-8 is characterised by zones with varying CL patterns, perhaps attributed to bioturbation structures or varying fluid regimes. Characterised by volcanic glass shards cemented by dolomite (D1). **C** and **D** – Close up of A and B, the dolomite can be seen as brightly luminescent and zoned orange rhombs (D2).

7.4.4 Siliciclastic material

A feature common to all of the Ritchie Ridge seep-carbonate samples is their abundant siliciclastic component. Mineral grains identified include quartz as well as, feldspars, mica and clay minerals (Fig. 7.8A-B, Table 7.4). The varying amount of siliciclastic material within samples reflects variable cementation and the heterogeneity of the host sediment in which the carbonates formed (e.g. Orphan et al. 2004). Glauconite is seen in many samples and on the basis of colour appears to range from nascent to highly evolved (Middleton 2003). Ubiquitous, but scattered pyrite is also present.

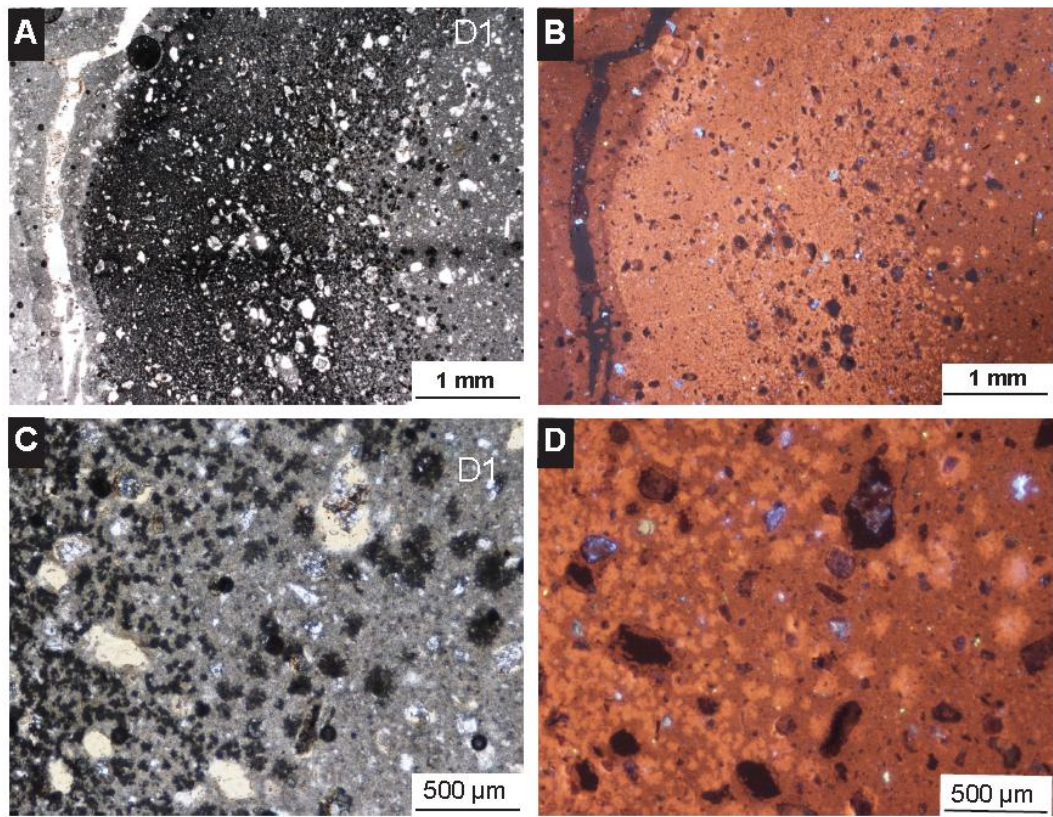


Figure 7.10: Photomicrograph pairs of modern Ritchie Ridge dolomitic seep-carbonates, under PPL (left side) and CL (right side). **A** and **B** – Variation within dolomite cement (D1) indicating varying elemental composition of the cement. **C** and **D** – Close up of transition zone of two dolomitic cements with apparent variations in chemistry resulting in different colours under CL.

7.4.5 Bioclasts

As is readily apparent in the hand specimens, the aragonitic samples tend to be bioclast rich (e.g. Fig. 7.3 and Fig. 7.6E-F). The most common bivalve shells are bathymodiolin mussels (e.g. MOD-5) and *Calyptogena* sp. (e.g. MOD-1). Benthic and planktic foraminifera are also a common constituent of the carbonate matrices. In MOD-5 the majority of the sample is composed of quartz grains and foraminiferal tests cemented by acicular aragonite. In dolomitic samples the foraminiferal tests may be filled with pyrite or ankerite (Fig. 7.8C-F).

7.5 Mineralogy and Elemental Composition

X-ray diffraction was utilised to determine the mineralogy of powdered bulk Ritchie Ridge samples, while the GADDs instrument analysed particular points of interest in polished thin sections.

7.5.1 Bulk mineralogy

XRD identified two main mineralogical groups among the modern samples, those that are dolomite rich and those with a dominant carbonate phase of aragonite (Table 7.4). All also have varying amounts of quartz, plagioclase feldspar and clay minerals.

Table 7.4 Relative abundance in mineralogy of bulk modern Ritchie Ridge samples determined by XRD. Key: Arag.- aragonite; LMC- low Mg calcite; HMC- high Mg calcite; Dolo.- dolomite; Qtz.- quartz; Plag.- plagioclase feldspar; Clay- various clay minerals; A- abundant; C- common; S- some; R- rare; (-) absent. Amounts are relative abundance as determined by graphed XRD peak intensities (see Chapter 4).

| Sample | Arag. | LMC | HMC | Dolo. | Qtz. | Plag. | Clay |
|--------|-------|-----|-----|-------|------|-------|------|
| MOD1 | A | C | - | - | S | - | R |
| MOD3a | - | R | - | A | C | S | S |
| MOD 4 | A | S | - | - | S | R | R |
| MOD 5a | A | C | - | - | C | S | R |
| MOD 8 | - | - | - | A | S | - | - |
| MOD 10 | - | S | - | A | A | S | R |
| MOD 11 | - | - | - | A | C | S | R |

7.5.2 Component specific mineralogy

Spot analysis was conducted on six Ritchie Ridge thin sections, three from aragonitic samples and three from dolomitic samples. Analysis confirmed the bulk mineralogies in Table 7.4. Also a fill that was previously presumed to be pyrite was found to be ankerite, an iron-rich mineral of the dolomite group. The fine component acicular carbonate fabrics in samples otherwise dominated by aragonite (from bulk XRD) were indeed shown by GADDs to comprise aragonite. Also matrices of the bulk dolomitic samples were confirmed to be dolomite. Appendix 3 has the full data set obtained from GADDs analysis.

7.5.3 Carbon content

MOD-1 and MOD-4 are bioclast rich with a fine-grained micarb matrix, while MOD-5 also contains bivalves but is dominated by a matrix of quartz grains. Dolomitic samples MOD-8 and MOD-10 are low in carbonate, approximately 50%. As is evident from Table 7.6 total organic carbon contents range from 0.173-1.0445 %.

Table 7.5 Carbonate content (%) for Ritchie Ridge samples.

| Sample | Carbonate (%) |
|---------|---------------|
| MOD 1 | 90 |
| MOD 3/A | 76 |
| MOD 4 | 83 |
| MOD 5A | 67 |
| MOD 8 | 54 |
| MOD 10 | 46 |
| MOD 11 | 74 |

Table 7.6 Total organic carbon content (%) for Ritchie Ridge samples.

| Sample | TOC (%) |
|--------|---------|
| MOD3C | 0.531 |
| MOD4 | 1.0445 |
| MOD8 | 0.173 |
| MOD9B | 0.532 |
| MOD10 | 0.31 |

7.5.4 Elemental chemistry

A summary of the results obtained from EPMA spot analyses on a representative group of thin sections from Ritchie Ridge samples is presented in Table 7.7.

The dolomite-rich samples were analysed for the character of their elemental components. Microprobe spot analysis illustrated that, relative to aragonitic samples, they were enriched in Si and Al in particular, probably from the siliciclastic components. Na was significantly less abundant in the dolomites than in the aragonites, and there were no detectable levels of Sr in the dolomites.

Aragonitic samples have Si, Al, Fe and Mn values that range from below detectable limits and 855 ppm, and there are minor amounts of K and Mg in several of the samples. Sr levels in the modern aragonites are moderately high, ranging from 1795 to 13284 ppm.

Figure 7.11 and 7.12 summarise microprobe results and variations of elemental content with mineralogy. It is clear that Fe, Mg and Mn are enriched in the dolomitic components relative to the aragonitic components. Also, Sr is enriched in the aragonites, but absent in the dolomites.

Table 7.7 Elemental content values as determined by EPMA analysis for selected components from modern Ritchie Ridge seep-carbonates. Note, b.d = below detectable limit.

| SAMPLE | Carbonate phase | Si | Al | Fe | Mn | Mg | Ca | Sr | Na ₂ | K ₂ |
|-----------|------------------|-------|-------|------|------|--------|--------|-------|-----------------|----------------|
| MOD-3Aa 1 | Dolomitic matrix | 25619 | 17517 | 4742 | b.d | 109884 | 193612 | b.d | 1335 | 7719 |
| MOD-3Aa 2 | Dolomitic matrix | 18887 | 7938 | 6063 | 77 | 89862 | 187823 | b.d | 816 | 2158 |
| MOD-3Aa 3 | Dolomitic matrix | 15942 | 8256 | 5208 | 1239 | 100356 | 187966 | b.d | 226 | 2407 |
| MOD-3Aa 4 | Dolomitic matrix | 3880 | 1958 | 777 | 155 | 119233 | 213124 | b.d | 742 | 1494 |
| MOD-3Aa 5 | Dolomitic matrix | 19588 | 7938 | 3809 | 232 | 103432 | 203975 | b.d | 2374 | 2905 |
| MOD-5Aa 1 | Bivalve | b.d | b.d | b.d | 310 | b.d | 380721 | 1795 | 5638 | 581 |
| MOD-5Aa 2 | Botryoidal arag. | b.d | b.d | b.d | b.d | b.d | 390726 | 6225 | 1187 | 581 |
| MOD-5Aa 3 | Acicular arag. | b.d | b.d | b.d | b.d | 241 | 387296 | 9874 | 2893 | 415 |
| MOD-5Aa 4 | Upper cement | b.d | b.d | 855 | b.d | 362 | 384652 | 13284 | 2152 | 664 |
| MOD-5Aa 5 | Lower cement | b.d | b.d | 233 | 542 | 422 | 385366 | 9963 | 2522 | 747 |

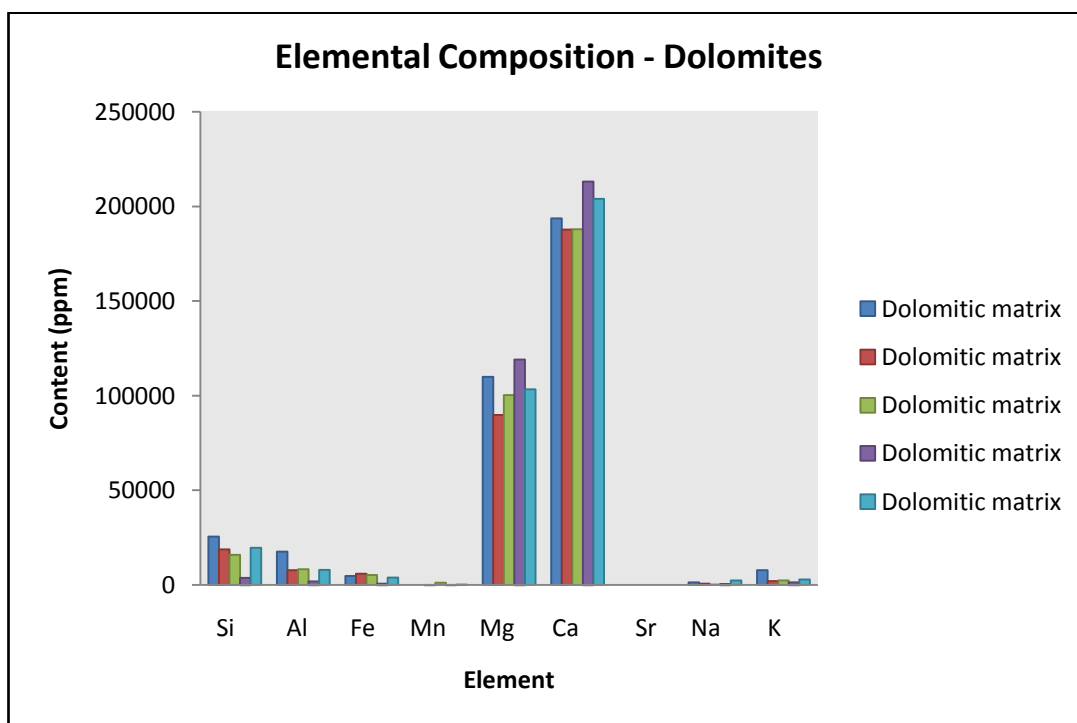


Figure 7.11 Elemental content for selected fabrics from modern dolomite thin sections. Mg and Ca are the two dominant elemental species, and Sr is absent. Si and Al contents likely reflect siliciclastic mineral “contamination”.

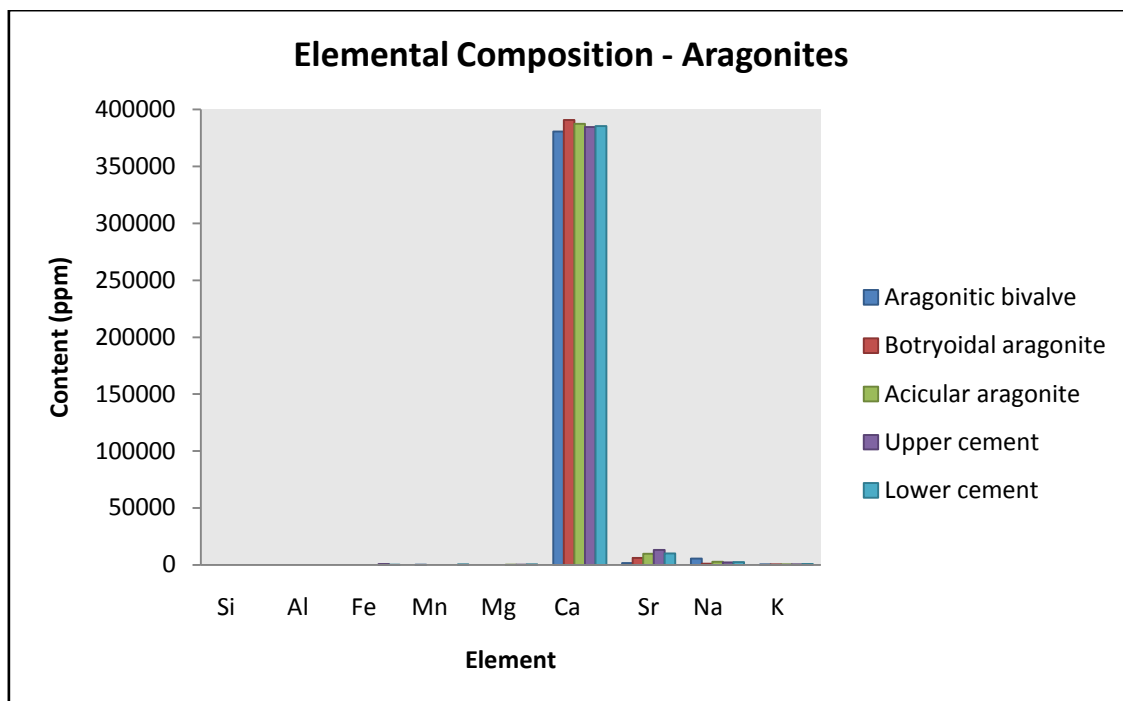


Figure 7.12 Elemental content for selected fabrics from modern aragonitic thin sections. Ca is dominant, while Sr and Na appear slightly enriched.

7.6 Stable isotopes

Bulk powders from the modern samples were used for stable isotope analysis, the results of which are displayed on Figure 7.13 and listed in Table 7.8. Aragonitic samples (Group 3) have $\delta^{18}\text{O}$ values ranging from +2.6 to +3‰ PDB and $\delta^{13}\text{C}$ values ranging between -34 to -41‰ PDB. The dolomites (Group 4) have $\delta^{18}\text{O}$ values that range from +5.29 to -6.74‰ PDB and $\delta^{13}\text{C}$ values ranging between -6.7 and -40‰ PDB.

Table 7.8 Stable $\delta^{18}\text{O}$ and $\delta^{13}\text{C}$ values for modern seep-carbonates. Sample MOD-3 is an average of sub-samples from a large dolomitic sample.

| Mineralogy | Sample | Location | $\delta^{13}\text{C } \text{\% PDB}$ | $\delta^{18}\text{O } \text{\% PDB}$ |
|------------|---------|-----------------|--------------------------------------|--------------------------------------|
| Dolomite | MOD-3* | Builders Pencil | -38.45 | 6.11 |
| Dolomite | MOD-8 | Rock Garden | -5.44 | 6.74 |
| Dolomite | MOD-9 A | Builders Pencil | -21.41 | 5.29 |
| Dolomite | MOD-10 | - | -20.27 | 5.45 |
| Dolomite | MOD-11 | Builders Pencil | -15.59 | 5.53 |
| Aragonite | MOD-1 | Builders Pencil | -37.08 | 3.64 |
| Aragonite | MOD-4 | Rock Garden | -41.57 | 3.75 |
| Aragonite | MOD-5 A | Rock Garden | -38.56 | 2.65 |

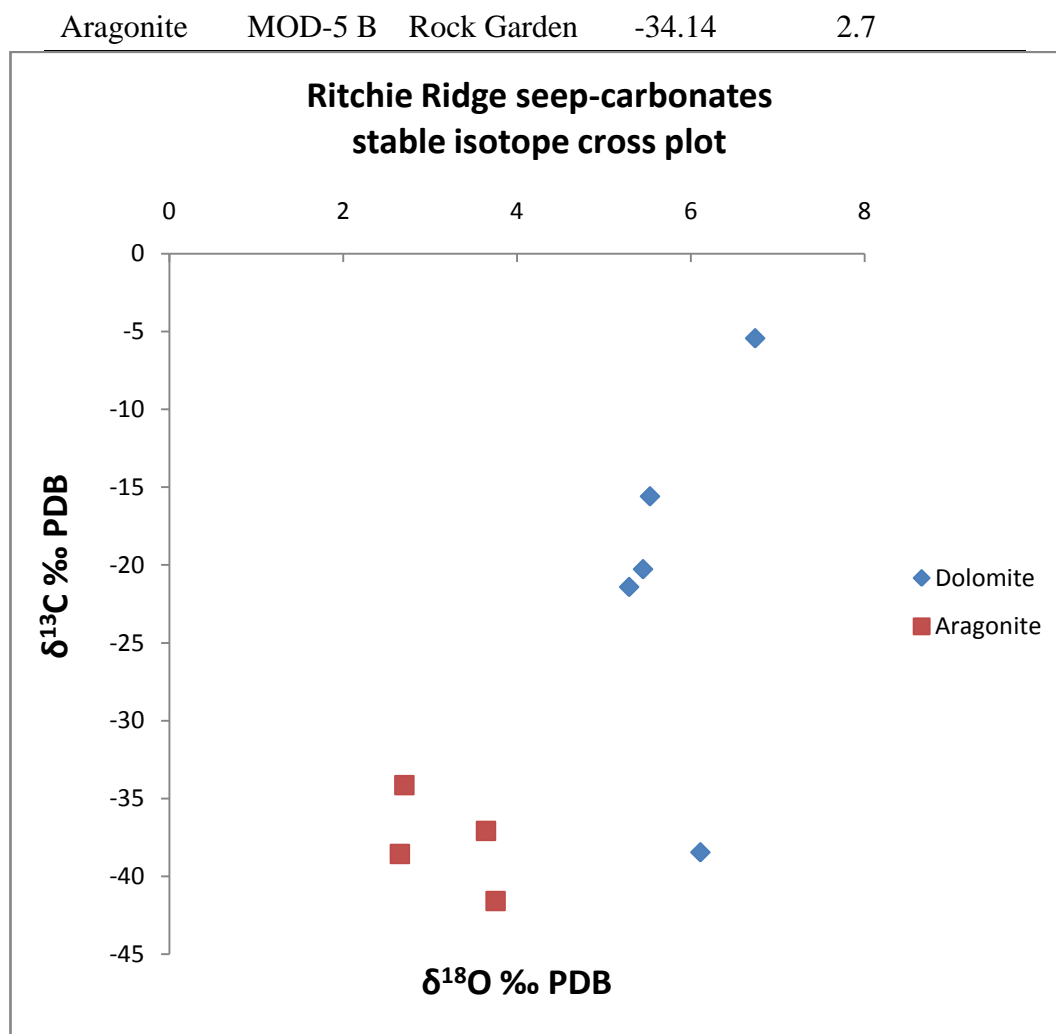


Figure 6.13 Cross plot of bulk stable $\delta^{18}\text{O}$ and $\delta^{13}\text{C}$ isotope values from Ritchie Ridge seep-carbonates.

7.7 Hydrocarbon Inclusions

Dark inclusions within the acicular aragonite needles were viewed under UV light to determine whether they were of an organic origin, and possibly hydrocarbons (e.g. Campbell et al. 2002). In thin sections, the dark inclusions were a pale green while the surrounding material did not fluoresce. Figure 6.14A-D shows that the hydrocarbons are found within the crystals or around the boundaries of needles. Spherulitic aragonite may have a layer of organic matter around the outer boundaries of the spherulites (Fig. 6.14B and 6.14D). It is evident that the material may also be present within the micarb or around its boundaries (Fig. 6.14E-F).

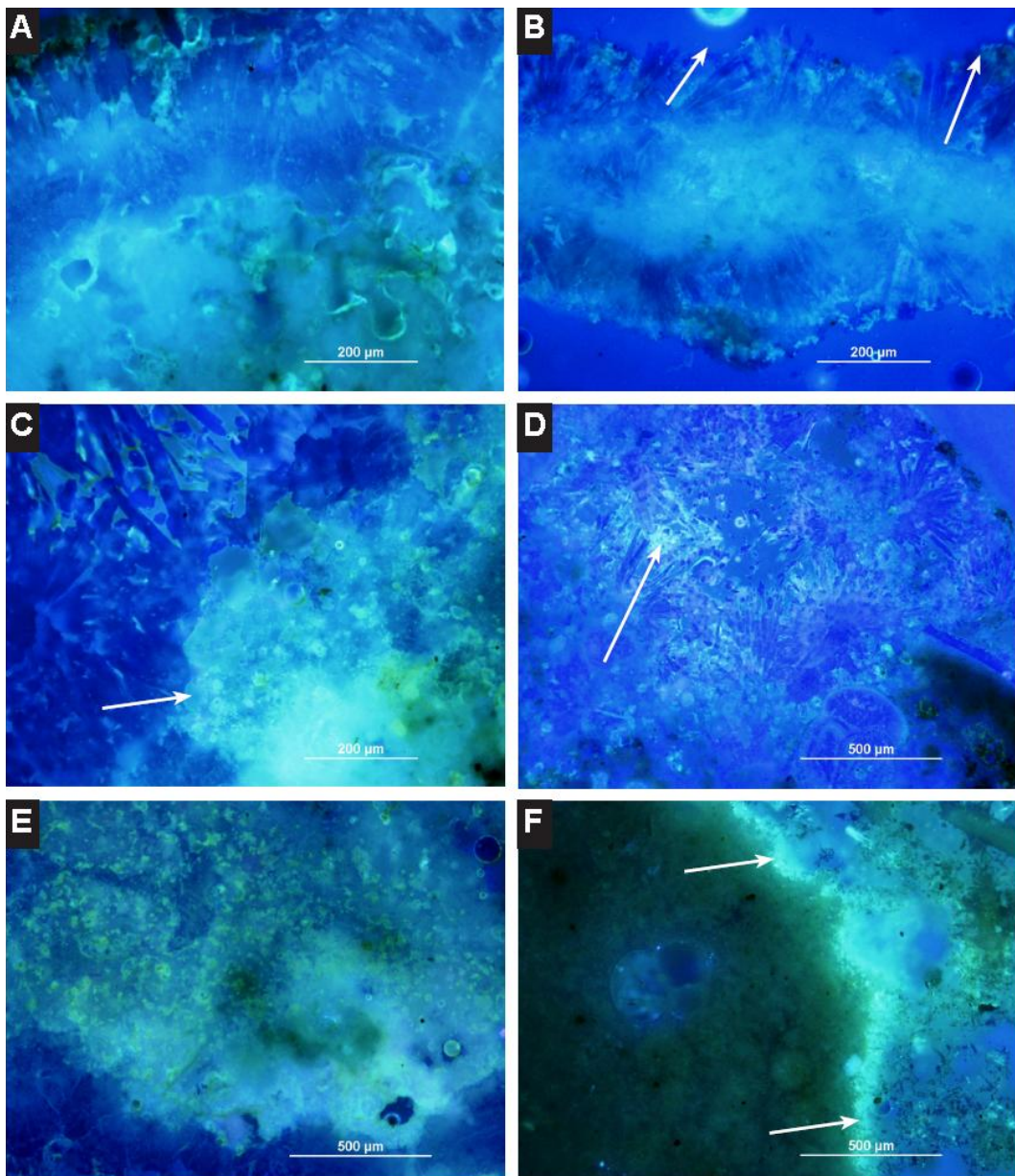


Figure 7.14 Photomicrographs of modern aragonitic thin sections under UV light.
A – D - Acicular aragonite with pale green zones of fluorescence around crystal terminations.
E – Both acicular aragonite and micarb is present with a large area of fluorescing mottled organic fluorescing material.
F – Micarb clasts with fluorescent layer around the edge. White arrows point out zones of intense fluorescence (**C-F**) or direction of crystals growth (**B**)

7.8 Discussion and Interpretation

Methane-rich fluids migrating through the subsurface and expelling at the seabed create a unique environment, forming a chemical gradient through the subsurface and into the seabed. This gradient produces different mineral formations and faunal assemblages in the seep system. The modern samples analysed in this study were from two areas offshore Hikurangi Margin (Fig. 7.1) and vary in mineralogy, fossil content, petrographic components and stable isotope values. There are variations in samples from the same site as well as between the two sites. The following section summarises the data in an attempt to form a synthesis of the results, and makes some comparisons with the literature available on some other modern seep-carbonates studied worldwide.

7.8.1 Bulk samples

Initial observations of the NIWA Ritchie Ridge samples are similar to descriptions from other studies of modern seep-carbonates worldwide (e.g. Greinert et al. 2001; Teichert et al. 2005; Campbell et al. in review; Han et al. 2008). Table 7.9 shows a comparison between the two study groups adapted from Table 7.3.

Table 7.9 Features of the two divisions of samples as grouped by mineralogy.

| Characteristic | Aragonite | Dolomite |
|-------------------------|-------------------------|------------------------------|
| Morphology | Nodules or slabs | Tubular or nodular |
| Faunal assemblage | Chemosymbiotic bivalves | - |
| Lithification | Porous and vuggy | Friable to densely lithified |
| Borings | Minimal | Extensive on all samples |
| Encrustations | Minimal | Extensive on most samples |
| Iron staining | - | On exterior of all samples |
| Other physical features | - | Central conduits |
| Carbonate (%) | 67 – 90 | 46 - 76 |
| Fabrics | Fibrous aragonites | Dolomite matrix and rhombs |
| Accessory minerals | - | Pyrite and ankerite |

Comparable kinds of morphological variants affiliated with mineralogy have been recorded elsewhere (Paull et al. 1996; Greinert et al. 2001; Campbell et al. in review; Han et al. 2008).

7.8.2 Paragenesis and formation environments

The paragenesis described for the aragonitic Ritchie Ridge seep-carbonates only includes a period of early diagenesis as the samples do not appear to have undergone significant burial or diagenetic alteration.

The onset of methane-rich fluid flow through the subsurface of the study sites has been attributed to the faulted setting of the imbricate wedge in which the seep-carbonates are found (Barnes et al. in review; Greinert et al. in review). Both Rock Garden and Builders Pencil sites are positioned above anticlinal folded ridges (Barnes et al. in review). The precipitation of a microbially induced aragonitic micarb into host sediments (comprising sandy muds and foraminifera) would have initially begun within the pore spaces of these sediments. As precipitation intensified due to an increase in fluid flux and/or an increase in alkalinity as a result of AOM (e.g. Luff et al. 2004; Reitner et al. 2005), the nodular precipitates would have increased in size, perhaps forming aggregates of micarb.

During periods of intense fluid flow, the initiation of which may have caused fracturing events, the micarb nodules were jostled and brecciated. The result is seen in thin sections where nodules of micarb are scattered through sample MOD-4. The primary fabric that formed within the samples is the aragonitic micarb. A microcrystalline carbonate comparable to micrite comprises the majority of nodular carbonate viewed in thin section. A combination of GADDs, microprobe and CL analysis leads to an interpretation that the fabric is aragonitic, and the product of rapid precipitation. The micarb is formed as a result of bacterial interaction with the migrating methane fluids, and thus may be classed as an ‘organomineral’ (Perry et al. 2008). Aloisi et al. (2002) reported biomarker analysis supporting evidence of bacterial tissue as a remnant in aragonitic seep structures. This micarb fabric seems to be the equivalent to the “cryptocrystalline aragonite” phase in Hydrate Ridge seep-carbonates (Teichert et al. 2005), and an observed micritic aragonite from the same location (Greinert et al. 2001, 2002). It is also likely to be the equivalent of the ‘gray micrite’ of Leefmann et al. (2008) who report this cement to be a mixture of both allochthonous organic and inorganic

material associated with AOM. Spatially, the micarb is found throughout the aragonitic samples. In hand specimen it constitutes the grey nodular material that may be seen as intraclasts.

The advective fluid flow would have fostered rapid precipitation of aragonite from solution, forming the acicular needles that line the nodules and clasts within samples MOD-1, -4, and -5. Samples with bathymodiolin mussels in life position are an important demonstration on how shells may be incorporated into the seep-carbonate crusts. After colonisation by the invertebrates and eventual waning of fluids, the dead shells provided nucleation surfaces for aragonitic crystals to grow (Jørgensen 1992; Greinert et al. 2002). The acicular aragonite is also intimately linked with microbial activity, and varying morphologies may be linked to variations in degree of microbial interaction (Leefmann et al. 2008).

Where pore space was slowly being filled with micarb precipitation, varying intensities of advective fluid flow through the crusts or pavements of carbonates led to minor fractures between the host sediment and the micarb, forming porosity which was cemented by further precipitation of acicular aragonite. In zones where these fractures were relatively large, the needles may have had sufficient space to form spherulites or botryoids.

It is likely that the aragonitic samples were precipitated within sediments between the shallow subsurface and the sediment-seawater interface. Initial observations of the hand specimens revealed a correlation with apparent porosity and dominant mineralogy. The aragonitic samples are contain many voids and cavities and thus are more porous than the dolomitic samples. To form a solid carbonate and still maintain these void spaces without compaction, it is assumed that the carbonate was being precipitated at shallow burial depths with minimal overburden to compress the underlying sediment. As mentioned above, the relationship between porosity and mineralogy has been previously documented (Greinert et al. 2001; Campbell et al. in review). Aragonitic cements also have been documented *in situ* in shallow depths in other offshore seep studies (Jørgensen 1992; Greinert et al. 2001; Aloisi et al. 2002; Teichert et al. 2005). This may be a result of the high sulphate levels in the shallow subsurface, which favour aragonite precipitation but

tend to inhibit the precipitation of calcite (Jørgensen 1992; Burton 1993; Savard et al. 1996; Aloisi et al. 2002; Orphan et al. 2004).

The dolomitic (or ‘protodolomite’) samples were characteristically well-cemented silty mudstones, with carbonate percentages ranging from 46 to 76%. The samples commonly had varying amounts of siliciclastic grains incorporated into the cement and were far less porous than the aragonites. Dolomites in other seep settings have been interpreted to form at greater depths than calcitic or aragonitic cements (Greinert et al. 2001; Campbell et al. in review). Favoured environments of deposition for dolomite are interpreted to be low in sulphate and have high Mg/Ca ratios (Von Rad et al. 1996; Greinert et al. 2001). The dolomitic samples analysed here appear to be consistent with other settings. The samples are densely lithified and compacted, supporting formation at depths that would eliminate or minimise pore spaces. The presence of bioencrustations on and boring into, these samples, as well as their iron stained and “weathered” appearance indicate that relative uplift of the sediment pile must have occurred to exhume and expose them on the modern seafloor (cf. Campbell et al. in review). The distinct morphological characteristics (e.g. tubular morphologies with central conduits) of the dolomites are indicative of seep plumbing systems (Léon et al. 2006; Nyman 2009), in deeper environments of formation than the aragonitic seafloor seep-carbonates.

The dominant carbonate mineralogies in the Ritchie Ridge samples are either dolomite or aragonite. The predominance of these minerals is not unexpected, although there is a paucity of some other accessory minerals documented from other modern seep-carbonates, such as barite from the Sea of Okhotsk (Derkachev et al. 2000; Greinert et al. 2002), siderite from Hydrate Ridge (Rodriguez et al. 2000) and pyrite (cf. Peckmann et al. 2001).

7.8.3 Fluid flow considerations

7.8.3.1 Stable $\delta^{13}\text{C}$ isotopes

The aragonitic samples have $\delta^{13}\text{C}$ values ranging between -41 and -34‰ PDB while the dolomites have values from -40 to -7‰ PDB (Fig. 7.13). The aragonite samples indicate that thermogenic methane was likely the primary methane source

of fluids precipitating carbonate, although there may be some mixing of microbial methane (see Fig. 2.11) (Roberts and Aharon 1994; Campbell et al. in review). However, it is evident that the dolomite fabrics have a spread between -40 and -7‰ PDB which may be interpreted as a mixing effect of thermogenic methane and seawater bicarbonate.

7.8.3.2 *Stable $\delta^{18}\text{O}$ isotopes*

The $\delta^{18}\text{O}$ stable isotope values of a seep-carbonate can provide information to determine the temperature of the fluids it was forming from and hence the processes occurring at formation. By using bottom water temperatures and estimates of standard sea water in an area, we can predict whether the carbonates were forming in equilibrium with normal sea water.

Bottom water temperatures recently measured at Rock Garden during the 2007 SONNE Cruise 191 were between 7.4 and 8.7°C (Campbell et al. in review). However these temperatures were only measured once and thus do not take into account any seasonal variation. From these temperatures, $\delta^{18}\text{O}$ values were estimated to range from -0.5 to +0.5‰ PDB. Had the cements of this study precipitated in equilibrium with these values then the measured $\delta^{18}\text{O}$ values should range from 0 to +1.5‰ PDB for aragonites (Fig. 7.15; Grossmann and Ku 1986) and +3.5 to +5‰ PDB for dolomites (Fig. 7.16; Fritz and Smith 1990).

Aragonitic samples from Ritchie Ridge have $\delta^{18}\text{O}$ values between +2.6 and +3.7‰ PDB. Based on aragonite equilibrium calculations (Fig. 7.15; Grossman and Ku 1986) and bottom water temperature estimates, these carbonates would have precipitated at temperatures less than 0°C, which is clearly unrealistic. This means that the aragonite cements are enriched in $\delta^{18}\text{O}$ by 2-3‰ PDB compared to the waters measured at Rock Garden today. This discrepancy could be due to the dissociation of gas hydrates. Upon formation, the clathrate molecule preferentially uses heavy oxygen, which is released upon dissociation (Davidson et al. 1983; Ussler and Paul 1995; Naehr et al. 2000; Hein et al. 2006). The release of these ^{18}O enriched waters may then be used in the formation of aragonitic seep-carbonates (cf. Campbell et al. in review).

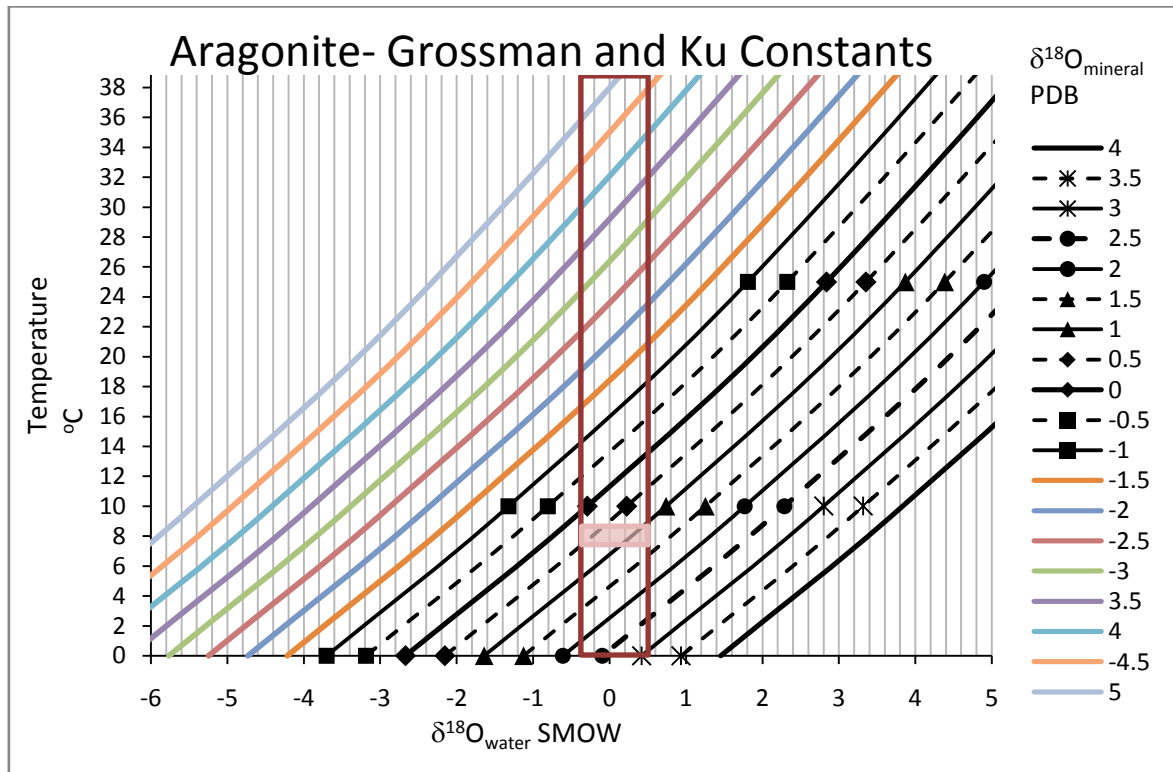


Figure 7.15 Equilibrium chart for argonite from Grossman and Ku (1986). Long red rectangle is field of $\delta^{18}\text{O}$ SMOW and PDB values with associated temperatures of formation. Small red rectangle encompasses values that aragonitic seep-carbonates that form in equilibrium with surrounding seawater would possess.

Dolomitic samples from Ritchie Ridge have $\delta^{18}\text{O}$ values between +5.29 and +6.74‰ PDB. Based on protodolomite equilibrium calculations (Fig. 7.16; Fritz and Smith 1990), these carbonates would have precipitated at temperatures between 0 and 6°C. However, dolomite precipitation is unlikely to occur at these low temperatures (Burton 1993). Thus, the carbonates are interpreted to be enriched by more than 2‰ PDB with respect to present sea water in the area of Rock Garden. This enrichment may be explained by the dissociation of gas hydrates.

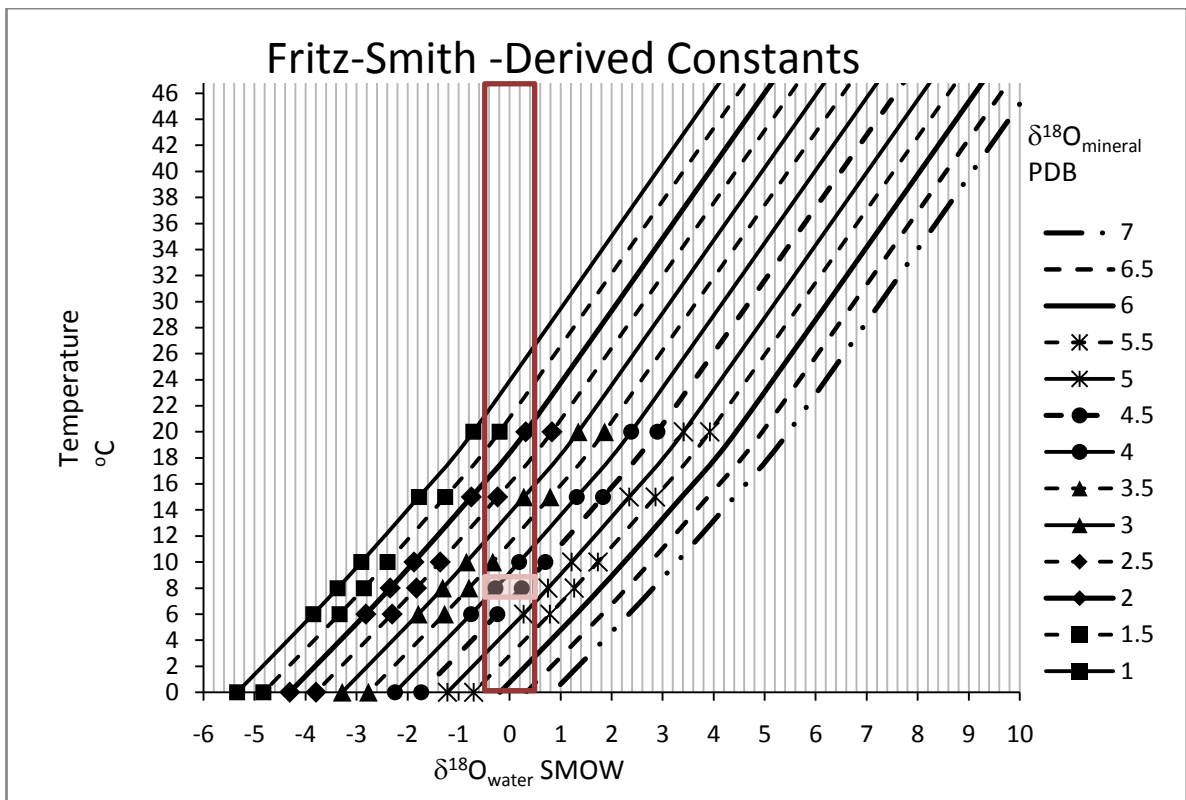


Figure 7.16 Equilibrium chart for protodolomite from Fritz and Smith (1971) Long red rectangle is field of $\delta^{18}\text{O}$ SMOW and PDB values with associated temperatures of formation. Small red rectangle encompasses values that aragonitic seep-carbonates that form in equilibrium with surrounding seawater would possess.

7.8.3.3 Gas hydrates

The Hikurangi Margin hosts extensive gas hydrates as indicated by strong BSRs in seismic profiles across the region (Pecher et al. 2004, 2007). The Rock Garden site and its associated gas hydrates have been the focus of several studies (Faure et al. 2006; Pecher et al. 2007; Crutchley et al. in review; Ellis et al. in review.), indicating that seep-carbonates in the area could have been influenced by their presence. The presence of gas hydrates in the cold seep system may affect the carbonates in several ways. Firstly, if the hydrates and seep-carbonates form in close spatial association, the former may be responsible for the brecciation or disturbance of both the interstitial sediments and the carbonate nodules (Greinert et al. 2001). Greinert et al. (2001) reported varying morphologies of seep-carbonates at Hydrate Ridge formed in association with lenses of gas hydrates. When the hydrate dissociates it may leave lensoidal pores in the micarb or mud substrate. This pattern is also documented in Oligocene seep-carbonates from the Carpathians which show a direct link with gas hydrates (Bojanowski 2007).

If methane is cyclically trapped and released by the process of gas hydrate formation and dissociation below or within the carbonates, the waters that migrate into the zones of carbonate precipitation (sulphate-reduction) will change in composition (Bohrmann et al. 1998; Aloisi et al. 2002; Nyman 2009). As discussed in Section 7.8.3.2 the Ritchie Ridge carbonates have enriched $\delta^{18}\text{O}$ values relative to seawater $\delta^{18}\text{O}$ estimates in the Rock Garden area, and are thus most likely to have originated from the enriched water molecules released during gas hydrate dissociation.

CHAPTER 8

Synthesis and Conclusions

8.1 OVERVIEW

Seep-carbonates from onshore and offshore the East Coast Basin, North Island, New Zealand, otherwise part of the so-called Hikurangi Margin, have been analysed in this study. The ancient onshore samples are from middle Miocene bathyal mudstones at Tauwhareparae (TWP) in the Raukumara Ranges, while offshore modern samples are from two sites on Ritchie Ridge, namely Builders Pencil (BPL) and Rock Garden (RGN) (Fig. 3.2 and Fig. 7.1). The Hikurangi Margin is known to be a region with a prolific cold-seep field that occurs across a subduction related accretionary wedge (Lewis and Marshall 1996; Pecher et al. 2007; Barnes et al. in review).

Field related analysis on the TWP deposit included stratigraphic and facies determination, coupled with extensive sampling. Laboratory analysis on the ancient and modern seep-carbonates included plane light petrography (PPL), cathodoluminescent light petrography (CL), stable isotope measurements ($\delta^{13}\text{C}$ and $\delta^{18}\text{O}$), EPMA microprobe, bulk mineralogy by XRD, component specific mineralogy by GADDs XRD, total organic carbon content (TOC), total carbon content (TC), carbonate content and UV light microscopy.

This chapter discusses the analytical results for the ancient and modern seep-carbonates in relation to each other, and compares and contrasts the key characteristics of each sample group. The synthesis should help identify when these differences were created by noting the changes occurring to seep-carbonates, from their development on the modern seafloor through their subsequent burial and late diagenetic phases recorded in the ancient examples. While this ideal is attempted, the small number of modern Ritchie Ridge samples (10) compared to the much larger number (100) from the ancient TWP site may mean that certain important trends have been missed for the modern Ritchie Ridge samples. See Appendix 1.1 and 1.2 for full sample lists.

8.2 MODERN vs ANCIENT COMPARISONS

8.2.1 Age

The samples from offshore Ritchie Ridge are termed ‘modern’, although this remains a relative term since no absolute dates are available for them. They are regarded as ‘modern’ because they are exposed on the modern seafloor. In the case of the dolomite-rich samples it has already been suggested that these are likely parts of the subsurface plumbing system of a cold seep and that they have been exhumed at the seabed by erosion following tectonic uplift and/or sea level fall. If true, they cannot be strictly modern.

If ages were determined, they may be used to link with tectonic events, or times of lowered sea level of similar correlative ages. Although a 100 m sea level fall would not expose samples in 800 m water depth, the change in pressure and depth around seep systems could lead to the dissociation of gas hydrates (clathrates). Such a process is known to result in sediment instability and erosion (Pecher et al. 2004, 2005; Crutchley et al. 2007, *in review*; Ellis et al. *in review*), capable of exposing subsurface dolomitic samples.

Aharon et al. (1997) dated extinct seeps from the modern setting of the Gulf of Mexico and obtained radiometric ages covering much of the late Pleistocene (195–13 ka). Until radiometric dates are available for the Ritchie Ridge samples, it is assumed that the fossiliferous seep-carbonates proper are probably of Holocene age, while the dolomitic ones are possibly older, perhaps as old as (late) Pleistocene.

The ancient onshore TWP samples are certainly of middle Miocene age, being biostratigraphically well dated by the slope mudstone in which they are encased (Mazengarb et al. 1991). The current tectonic regime on the Hikurangi Margin has been active since the early Miocene, and the envisioned depositional setting for the TWP deposit is similar to that of the modern Ritchie Ridge examples.

8.2.2 Componentry

The primary differences between the two sample groups have arisen from diagenetic processes including, burial, lithification, and alteration. These

processes are responsible for the transformation of the porous seep-carbonates into lithified ‘rocks’, and of primary aragonites into late-altered calcites. Table 8.1 summarises the major components of both the Ritchie Ridge and TWP sample groups in relation to each other, based on petrographical analysis (see Section 6.2 for details).

Table 8.1 Comparative components of modern and ancient seep-carbonates as ascertained by petrographical analyses.

| Component | MOD | TWP | Comment |
|----------------------------|-----|-----|---|
| Aragonitic micarb | Yes | Yes | Original fabric in Ritchie Ridge samples, and is preserved in many samples at TWP |
| Acicular aragonite | Yes | Yes | Common in most zones within the Ritchie Ridge group, especially nucleating off micarb clasts, most common as tube linings or shell fills at TWP |
| Spherulitic aragonite | Yes | Yes | Void filling in both cases, normally surrounded by acicular aragonite or micarb |
| Botryoidal aragonite | Yes | Yes | Ritchie Ridge examples are sparry, some are "structureless" and intact while in TWP they are split and have an internal acicular habit |
| Cellular calcite | - | Yes | Recrystallisation during late diagenesis leads to a cell texture, with rounded crystal faces throughout vein areas |
| Mottled calcite | - | Yes | Late stage veins that exploit discrete boundaries e.g. worm tube tests |
| Equant calcite | - | Yes | Dissolution and recrystallisation of aragonite species forms large equant calcite crystals, generally form in centre of worm tube fills |
| Siliciclastic rich calcite | - | Yes | Infilling of any cavities or pores in late stage diagenesis with carbonate saturated burial fluids |
| Dolomite matrix | Yes | - | Matrix of dolomitic samples, generally a fine grained siliciclastic rich groundmass |
| Dolomite rhombs | Yes | - | These rhombs form amongst siliciclastic grains and volcanic glass |
| Siliciclastic material | Yes | Yes | Variations in abundance and rounding, but common in all samples |
| Bioclasts | Yes | Yes | Found in most TWP facies, and aragonitic Ritchie Ridge examples, bioclasts are derived from chemosynthetic bivalves and tube worms |
| Pyrite | Yes | Yes | Generally found as fills in voids or fractures |

8.2.3 Mineralogy

Aragonite is the mineralogy common to both sample groups. Consequently, it is interpreted as the primary carbonate precipitate in the cold seep system. Dolomite

samples are included in the modern seep-carbonates but are likely of subsurface origin (see Section 7.8.2). Calcitic fabrics occur mainly within the TWP ancient examples.

Aragonitic fabrics are well-documented both in modern (Greinert et al. 2001; Aloisi et al. 2002; Teichert et al. 2005; Leefmann et al. 2008; Campbell et al. in review) and ancient seep-carbonates (Savard et al. 1996; Campbell et al. 2002, 2008; Buggisch and Krumm 2005; Peckmann et al. 2005; Himmller et al. 2008).

Calcite can also be found in both modern and ancient seep-carbonates. Modern examples include Hydrate Ridge, offshore southeastern North America (Pierre et al. 2000; Rodriguez et al. 2000; Greinert et al. 2001; Teichert et al. 2005), the South China Sea (Han et al. 2008), the Makran accretionary prism, offshore Pakistan (e.g. von Rad et al. 1996) and offshore California (Orphan et al. 2004; Hein et al. 2006). However, there are no dominant calcitic fabrics within the modern samples analysed in this study, although XRD picked up minor amounts of LMC in several samples (see Section 7.6). Due to the random method of sampling across the two sites, this may be a coincidence or a general trend of preferential aragonite formation in certain areas on the Hikurangi Margin. Campbell et al. (in review) examined samples from Rock Garden and found a dominance of aragonite rather than calcite within the porous ‘near surface’ samples.

In the TWP ancient samples, however, calcite is the co-dominant mineralogy with aragonite. The calcites are late stage phases interpreted to have formed during diagenesis, mostly by neomorphism of aragonite to calcite. This trend is typical of many ancient seep-carbonates (e.g. Kelly et al. 1995; Savard et al. 1996; Campbell et al. 2002; Buggisch and Krumm 2005; Himmller et al. 2008) and is identified by distinct morphological changes in crystal habits, coupled with variations in elemental and mineralogical data.

Dolomitic samples account for half of the modern Ritchie Ridge seep-carbonate examples, but no dolomite is present within the ancient TWP seep-carbonates. As discussed in Section 7.8.2, these dolomites are probably evidence of subsurface

plumbing or early pathways for fluid migration that formed in deeper zones than the aragonitic seep-carbonates (see Section 8.4.6) (e.g. Greinert et al. 2001; Nyman 2009). Their absence at TWP may be a result of the deeper samples not being exposed, or the opposite scenario, in which a localised event lead to the exposure of the plumbing system dolomites at the seafloor, resulting in exhumation and erosion, rather than burial and preservation with the aragonitic ancient seep-carbonates.

8.3 SUBSURFACE METHANE MIGRATION

Fluid flow regimes through cold seep systems are dynamic in nature. The fluids which migrate from depth originate from some source reservoir and may mix and entrain other pore fluids or sediments during their ascent (Judd and Hovland 2007). The seep-system itself has been identified as a significant sink for the sequestration of methane (Boetius et al. 2000; Parnell 2002; Judd 2003; Peckmann et al. 2004). Cold seep systems are typically ephemeral in nature, having features (e.g. pockmarks, gas hydrates and seep-carbonates) whose formation depends on the migration and expulsion of fluids for highly variable periods of time (Judd and Hovland 2007). If one flow condition encourages the precipitation of a certain carbonate fabric, then when this condition changes, a new fabric may begin to form in conjunction with, or superimposed upon, previous fabrics. The end result may be a seep-carbonate with varying amounts and types of carbonate cement, siliciclastic material and faunal assemblages. Hence, seep-carbonates form within a heterogeneous environment (Roberts et al. 1993; Levin et al. 2003) where conditions and products vary greatly from locality to locality.

Hovland (2002) reported that seep systems may undergo three distinct periods of fluid flow. He suggested that first, as seepage progresses the formation of bacterial mats begin and may be exposed at the seabed. Next, seep-carbonates or bioherms are formed, which are essentially self-sealing mechanisms which may create a waning seep. The third and final stage of the seep system is the cessation of fluid expulsion at the surface altogether. By assuming both this process of self-sealing seeps, and the dynamic nature of fluid flow through the system, it is logical to understand how overprinting and cyclic changes in fabrics can occur within a system.

8.4 SEEP-CARBONATE FORMATION

By combining the results obtained on both the modern and ancient seep-carbonates in this study, an attempt is made here to explain various processes occurring in seeps systems on the Hikurangi Margin at the present day and in the past through a series of schematic diagrams.

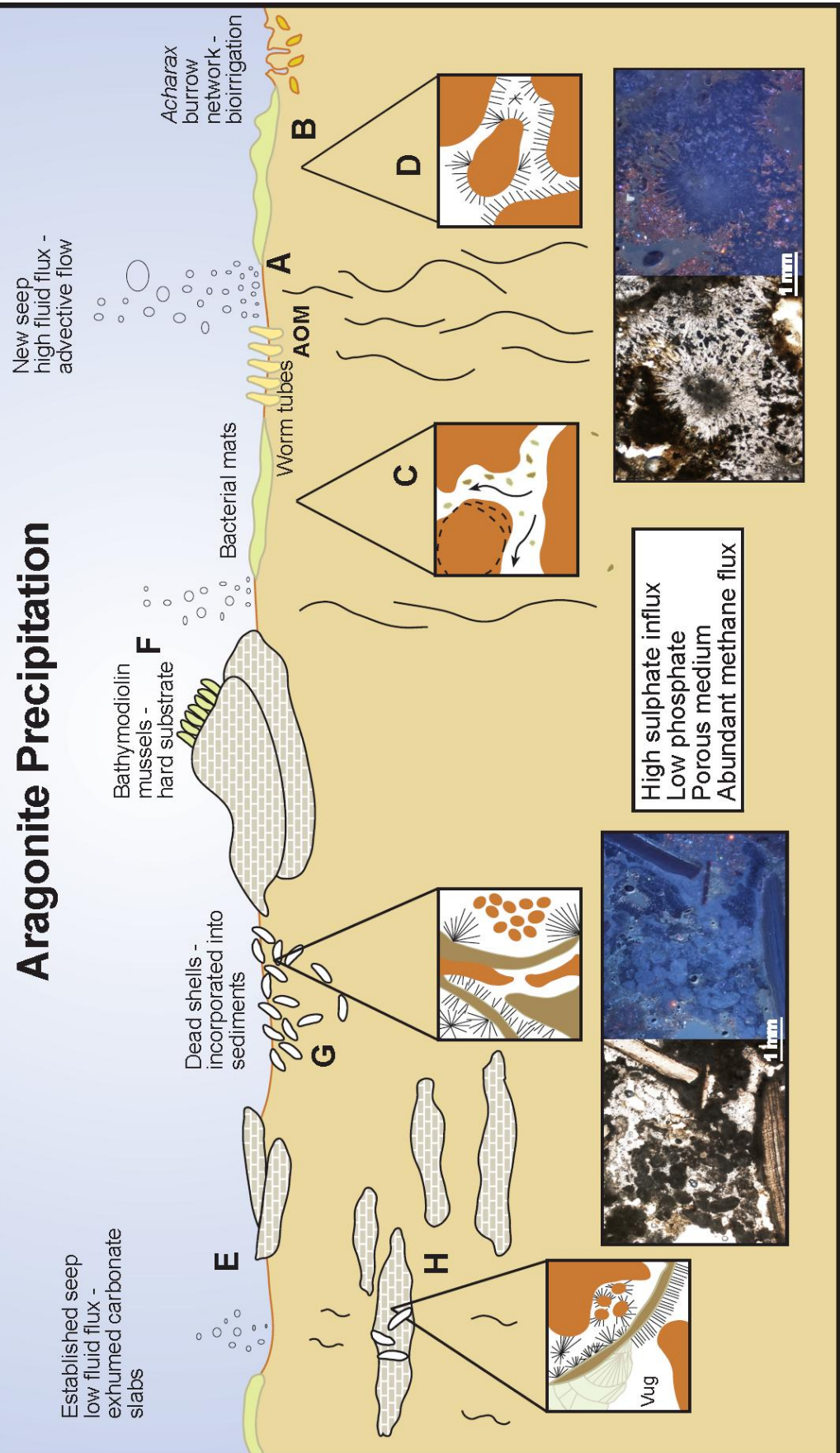
8.4.1 Aragonite precipitation

Aragonite is the mineralogy common to both the modern and ancient samples, and so is interpreted to be the primary carbonate phase precipitating within the matrix of the seafloor sediments at cold seep sites. Various conditions may exist in cold seep systems which encourage aragonite precipitation while tending to inhibit the precipitation of calcite (LMC or HMC) or dolomite. These conditions include, but are not be restricted to, high sulphate and low phosphate levels, a porous medium for carbonates to precipitate in pore spaces, an abundant methane flux, which under optimal conditions promote rapid precipitation (Jørgensen 1992; Burton 1993; Savard et al. 1996; Cavagna et al. 1999; Aloisi et al. 2002; Luff et al. 2004).

Figure 8.1 is a schematic model showing the environment of formation for aragonitic cements. In an area of early, advective seepage, with a high flux of methane, methanotrophic microbes will colonise the area in large populations to exploit the migrating methane (A in Fig. 8.1) (Boetius et al. 2000; Judd and Hovland 2007).

Figure 8.1: Schematic model for different kinds of aragonite precipitation in cold seep systems. Localities A through H are described in text. A – Area of fast advective seepage where aragonitic micarb is precipitated. B – Area of low bioirrigation where *Acharax* bivalves burrow through the sediment encouraging influx of sulphate from seawater. C – Jostling of micarb clasts by migrating fluids forms rounded ‘blebs’ or nodules’ of seep-carbonates. D – Clasts of micarb acts as nucleation surfaces for acicular aragonite splays. E – Established seeps are often characterised by slabs or exposed seep-carbonates at the seafloor. F – Exposed slabs may provide a hardground for Bathymodiolin mussels to attach to in areas of intermediate fluid flow. G – Dead bivalves are incorporated into seafloor sediments and subsequent seep-carbonates. H – Bioclasts provide nucleation surfaces for acicular aragonite. No Scale implied.

Aragonite Precipitation



The microbes form a consortium with sulphate reducing bacteria, which utilise the sulphate that occurs naturally in seawater (see Section 2.2) (Boetius and Suess 2004; Birgel and Peckmann 2008).



The *Acharax* sp. burrow into soft sediments to utilise the sulphide, although they may be found further away in areas of lower flow, i.e. the distal margins (**B** in Fig. 8.1), and in turn the burrows provide further pathways for seawater to transport sulphate into the sediments, also known as bioirrigation (Luff et al. 2004; Campbell et al. in review). Luff et al. (2004) reported that the process of bioirrigation is responsible for the downward migration of the zone of carbonate precipitation. Next, the sulphide may also be incorporated into FeS₂, or pyrite (e.g. Peckmann et al. 2001). Third, the reaction bicarbonate levels also rise which act as a catalyst for increased precipitation of carbonate species (Luff et al. 2004).

The precipitation of microcrystalline aragonitic carbonate (micarb) (**C** in Fig. 8.1) is microbially mediated, and the aragonite may be considered an organomineral (Perry et al. 2008). Leefmann et al. (2008) found that this precipitate is a mixture of organic and allochthonous material, formed by interaction with microbes. Teichert et al. (2005) described the same fabric as a cryptocrystalline carbonate. In thin section under PPL the micarb is a dark clotted material. In areas of high fluid flow two processes may affect the micarb. First, the micarb can become brecciated to form clasts that become rounded off as the migrating sediment-laden fluids jostle and wear away at the clasts (**C** in Fig. 8.1). Second, the fast fluid flux encourages precipitation of acicular aragonite, while the micarb clasts act as a nucleation surface (**D** in Fig. 8.1). In this situation, the acicular aragonite precipitates into pore spaces. The micarb may also occur as peloids, which may occur preferentially in sheltered environments. Peloidal fabrics have been reported in both modern (e.g. Campbell et al. 2002; Peckmann et al. 2002; Feng et al. 2008) and ancient seep carbonates (e.g. Cavalazzi et al. 2007; Jenkins et al. 2007) and are often attributed to microbially induced precipitation. Acicular aragonite also has been found to carry biomarkers which indicate that the

variation between aragonite morphologies may be related to the amount of microbial interaction within a seep-carbonate (Leefmann et al. 2004).

In established seeps (Hovland 2002), ROV images may show large carbonate slabs exhumed at the seafloor, often covered with layers of hemipelagic sediment (Fig. 7.2A-F) (e.g. Pecher et al. 2007). These may occur in areas where fluid flow is currently active or where seepage has waned (**E** in Fig. 8.1). In these areas, reactivation of fluid seepage may lead to large areas of bathymodiolin mussels, filter feeding molluscs that require a hard substrate to attach to, but also a relatively steady flux of methane (**F** in Fig. 8.1) (Sibuet and Olu 1998; Judd and Hovland 2007). In seeps where fluid flow has stopped for a period of time, resulting in the eventual death of the chemosynthetic communities, the scattered shells (**G** in Fig. 8.1) may then be incorporated into the subsurface sediment, and later integrated into seep-carbonate slabs. The process of incorporation of dead shells into new carbonate nodules was identified by Aloisi et al. (2002) as providing important nucleation sites for acicular aragonite (**H** in Fig. 8.1).

Figure 8.2 is an early diagenetic paragenetic sequence constructed from analysis of both the modern and ancient seep-carbonates. It covers events occurring from initial precipitation of early micarb at the onset of AOM to the end of seepage. It does not discuss late diagenesis, which is addressed later. The chart lists the relative order in which events and cement phases occur in the studied seep-carbonates. It is recognised that the dynamic nature of the seep systems may mean that these processes could become cyclic, or will vary slightly depending on local conditions.

8.4.2 Alternative fluid-flow scenarios

Figure 8.3 shows alternative scenarios for aragonite precipitation in which the end point remains, but the fluids that are feeding the seep-system are undergoing different processes. The two scenarios presented take into account the stable $\delta^{18}\text{O}$ and $\delta^{13}\text{C}$ isotope values for both the modern and ancient seep-carbonates.

Early Diagenesis

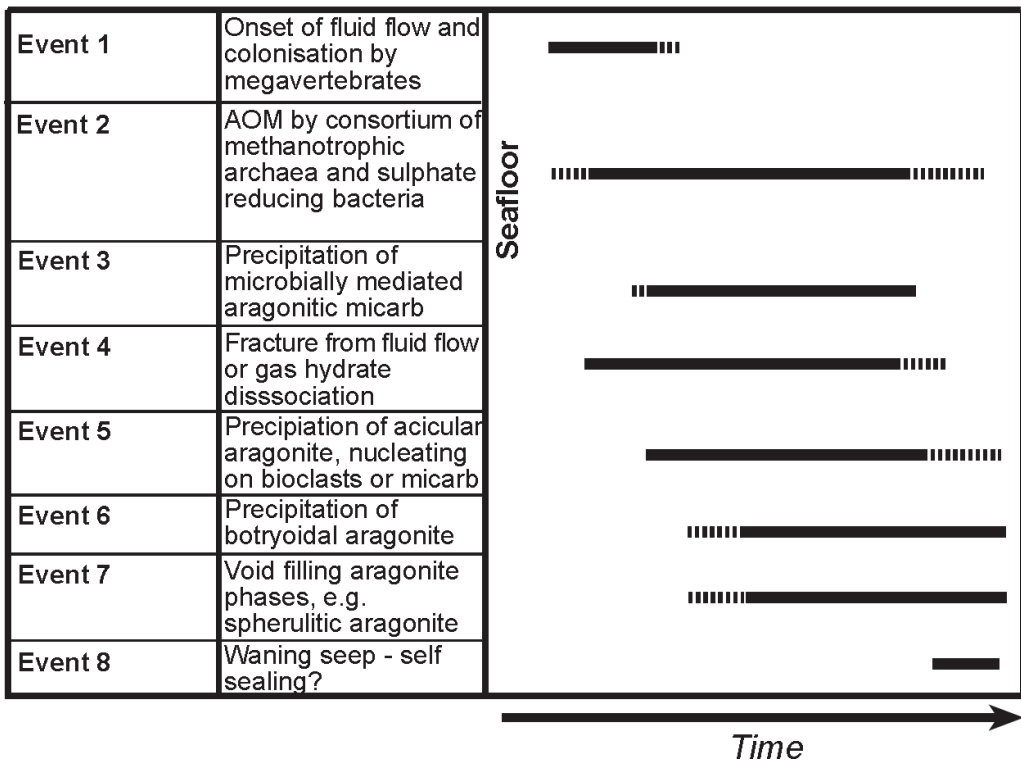


Figure 8.2: Relative timing diagram for early paragenetic events occurring within the seep system. This diagram links with the paragenesis table established in Chapter 6 based on the TWP samples (Fig. 6.13), although here a more detailed description of the earlier stages of seep formation and carbonate precipitation is noted.

There are a range of depleted $\delta^{18}\text{O}$ values (from -1.5 to -5‰ PDB) for the TWP seep-carbonates (both aragonite and calcite cements). Generally, these values would suggest burial at depths of (500-1200 m; see Section 6.9.3). While it is quite possible that these calcites formed at such depths, it seems unlikely that the aragonites would have the same isotopic signature from formation in environments at such depths (due to the conditions in which aragonite generally forms, e.g. Burton et al. 1993; Savard et al. 1996; Aloisi et al. 2002). In this case, the depleted values must be due to another process. One possibility is the migration of warmer fluids into the system. If the fluids rose at a sufficiently fast rate (i.e. fast enough to inhibit cooling to temperatures in equilibrium with surrounding pore waters) then any aragonite that was precipitated would have depleted $\delta^{18}\text{O}$ values, such as occur in some of the ancient cements. Another possibility is that the two groups of cements formed in different environments,

where the aragonites were forming from warmer fluids, and have retained that depleted isotopic signature when being altered to calcite.

8.4.3 Implicating gas hydrates

There are examples from both the modern and ancient sample groups in this study that are enriched in $\delta^{18}\text{O}$ relative to normal sea water, with values ranging from +2 to +6 ‰ PDB. These have been interpreted to form in areas of active gas hydrate (or clathrate) dissociation. When gas hydrates form, they preferentially use the heavy oxygen molecule, and upon dissociation this oxygen is released in an enriched water molecule. When the water is utilised in the process of carbonate precipitation the result is seep-carbonates with $\delta^{18}\text{O}$ values enriched relative to normal marine waters (Davidson et al. 1983; Ussler and Paul 1995; Kastner et al. 1998; Hein et al. 2006). Gas hydrates (clathrates) are a common phenomena worldwide, both within the sediment column of seep systems (see Section 2.3.4) (e.g. Wood et al. 2008), and within mud volcanoes associated with seeps (e.g. Milkov et al. 2004a,b).

Triggers which may induce the dissociation of gas hydrates include any event likely to disturb the sensitive boundaries of the gas hydrate stability zone (GSHZ), including changes to pressure, temperature, or fluid flux (Crutchley et al. 2007, 2008; Judd and Hovland 2007; Ellis et al. in review). The presence of gas hydrates on the Hikurangi Margin, and in particular at Rock Garden, is well documented (Pecher et al. 2004, 2005, 2007; Crutchley et al. 2008; Ellis et al. 2008). Furthermore, the phenomenon of gas hydrate dissociation at the site has been attributed to slope instability and erosive events (Pecher et al. 2005; Faure et al. 2006; Crutchley et al. 2008; Ellis et al. 2008). Considering the accepted presence of gas hydrates in the area, the inclusion of gas hydrate dissociation as a process occurring to affect the composition of seep-carbonates from the same area seems reasonable. Figures 8.3 and 8.4 illustrate the way in which the hydrates may affect the migration of fluids from depth in a generalised seep system in the presence of clathrate formation and dissociation.

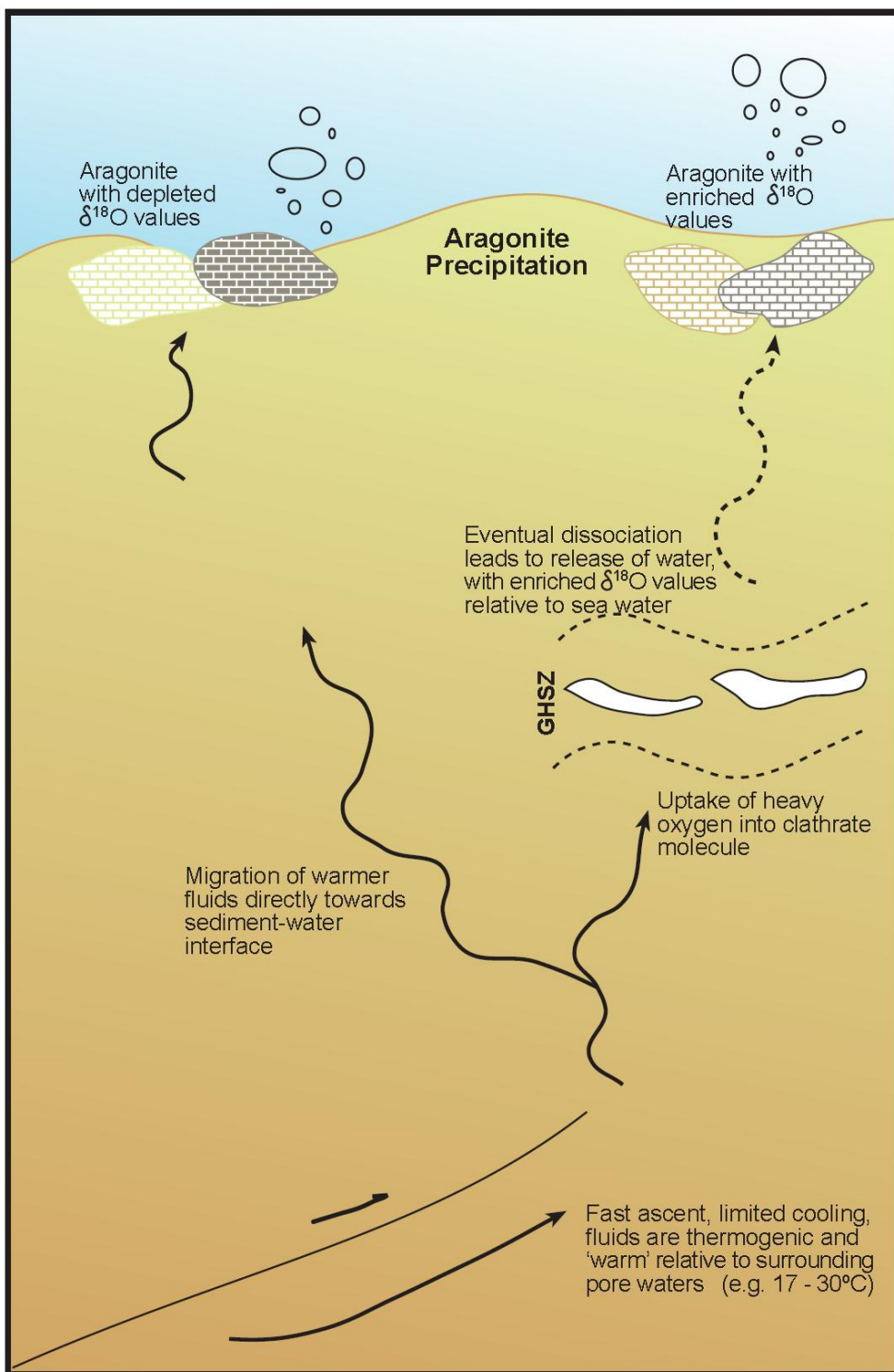


Figure 8.3: Schematic diagram to show two scenarios of fluid migration into the aragonite precipitation zone. The GHSZ is the gas hydrate stability zone, a narrow field in which temperature and pressure are optimal for the formation of gas hydrates. At times this area may be a narrow barrier to fluid flow, or it may incorporate rising fluids into the clathrate molecule. If fluid forming the aragonites was incorporated into the gas hydrate, then released as a heavy water molecule, the aragonites will have enriched $\delta^{18}\text{O}$ values relative to seawater. If the fluids bypass the GHSZ they may remain warm and the aragonites will have more depleted $\delta^{18}\text{O}$ values.

8.4.4 Waning seepage and reactivation

Established seep systems may be self-sealing after an extended period of fluid expulsion (Hovland 2002). This may occur after different periods of seepage, depending on local conditions. Several processes may occur that act to inhibit seepage, including high sedimentation rates (e.g. Luff et al. 2004), extensive carbonate formation that blocks ebullition sites (e.g. Hovland 2002), fault movement diverting fluids to another area, or simply that the reservoir supplying fluids to the system became emptied. The onset of burial and late diagenesis may be marked by waning seeps, followed by sedimentation in the area, or by tectonism causing burial and eventual uplift.

8.4.5 Calcite in seep-carbonates

The calcites in the TWP samples are interpreted to form during late diagenesis, either by late cementation by burial fluids, or by the neomorphic alteration of aragonite to calcite. These interpretations were formed from petrographic and elemental analysis. However, due to the depleted isotope values as discussed in Section 8.4.3, and their co-existence with depleted aragonite values, varying scenarios have been presented herein formed, to incorporate both petrographic results (Section 6.2) and isotopic results (Section 6.9.3).

Figure 8.4 illustrates one scenario in which late stage calcites may form following the reactivation of ‘dormant’ seeps. After seeps wane, there may be a period of quiescence until they are reactivated. Reactivation may occur following localised tectonic movement or an erosive period affecting the seafloor above the seeps. The fluids expelled during reactivation may also be of warmer temperatures (e.g. 17 – 30°C, see Section 6.9.3). If these encounter a horizon of gas hydrate, which is known to form natural barriers against fluid flow, then some of the fluids may cool while being held up below such a barrier. However, the calcitic cements do not have enriched ^{18}O values relative to sea water (either being depleted or in equilibrium $\delta^{18}\text{O}$ values ranging from -5 to +1‰ PDB). Effectively this means that, in this example, they were not included in gas hydrate formation. The ‘cooled’ fluids would eventually continue migrating upwards towards the surface. Fluids that bypass the GSHZ may continue to migrate until they come into contact with aragonitic seep-carbonates that have been buried to shallow depths by

sedimentation. The seep-carbonates, which are characteristically porous and contain abundant chemosynthetic bivalve shells, may be hydro-fractured and consequently filled with these migrating fluids that have entrained subsurface sediments. This phase of cementation is responsible for the appearance of dark silty fill seen in many worm tubes and shells (Fig. 5.2.7). If the carbonate blocks were buried to a depth where the sulphate flux from sea water was quite low, then calcite may be the major precipitate cementing the porous spaces (Burton 1993; Aloisi et al. 2002). Figure 8.6 is a paragenetic sequence for cements forming within the seep-carbonates following burial, although no depth parameters for burial have been set. Thus, in the above scenario the siliciclastic calcite phase could be occurring in depths of less than 10 m.

The neomorphic calcites are difficult to interpret given that the processes of neomorphism are currently not well understood, and there is a need for further elucidation of the process in the literature (e.g. Folk 1965; Maliva 1998; Maliva et al. 2000). Also, the calcites possess a combination of CL characteristics of ‘late’ cements (e.g. Figures 6.4-6.7) and ^{18}O isotopic values similar to ‘early’ cements that require near seabed conditions to form. However, certain interpretations regarding the altered components can be made. First, the neomorphic changes could be initiated with shallow burial of the porous aragonitic seafloor seep-carbonates, caused by high sedimentation rates in the area. If this occurs, the slight change to pressure and temperature in the subsurface, may be enough to initiate alteration of metastable aragonite to calcite (Fig. 8.5). This process may continue through time, regardless of burial depths, until a point where the carbonates are in equilibrium with their surrounds and are fully altered to calcite at which point, no further alterations may occur. This may mean that in terms of the controlling parameters on neomorphism, time may be more important than burial depth (although that would be dependent on local conditions).

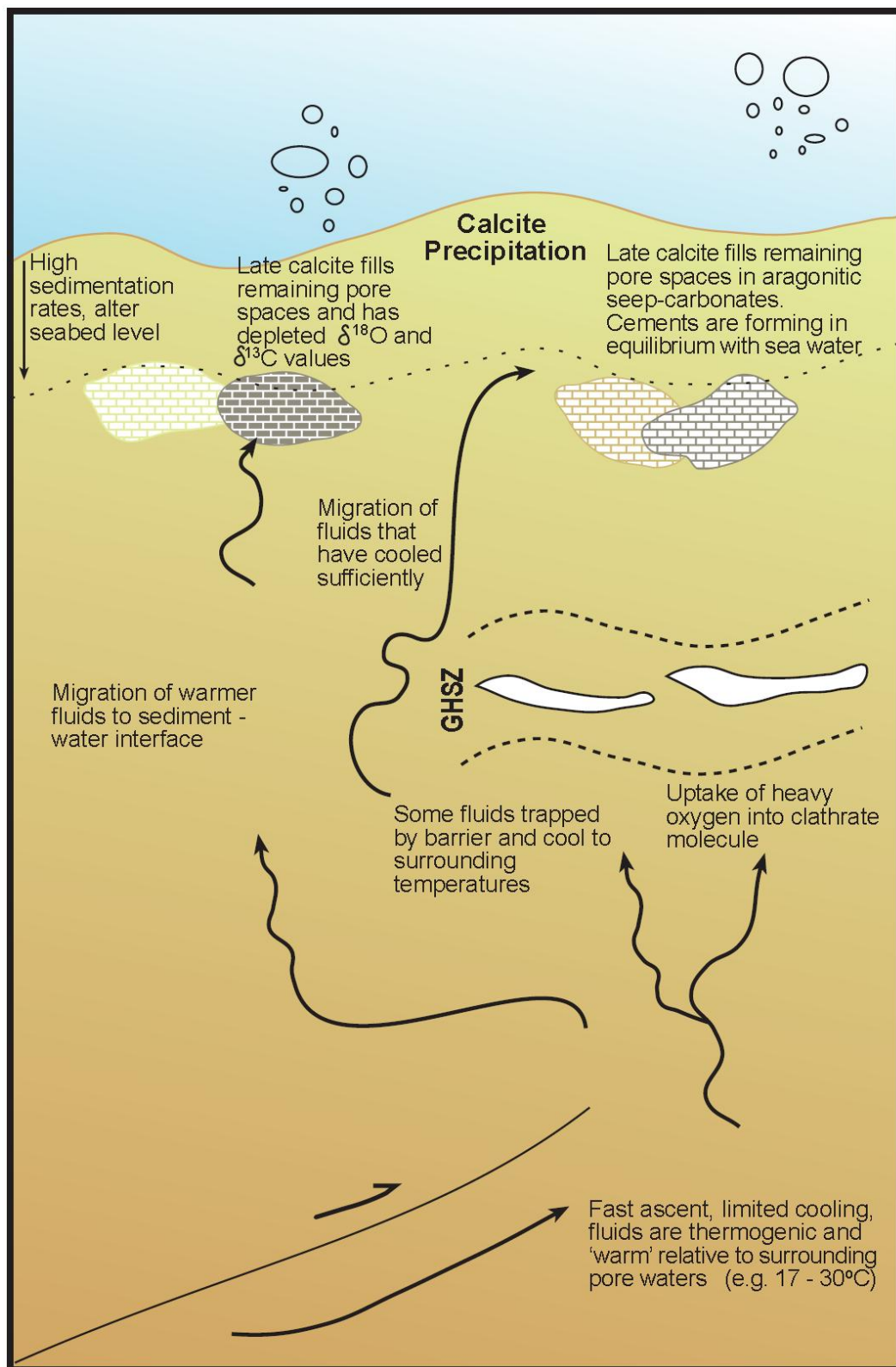


Figure 8.4: Schematic diagram to show the varying scenarios of fluid migration and the formation of calcites, as related to $\delta^{18}\text{O}$ and $\delta^{13}\text{C}$ isotopic signatures. In the ancient calcites samples have either depleted $\delta^{18}\text{O}$ values or near equilibrium with normal sea water, so while gas hydrates may have been present and formed a barrier effectively cooling the fluids, those particular fluids were probably not incorporated into the clathrate molecule.

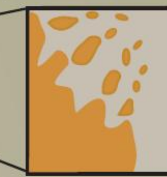
Aragonite Transformation - Calcite Formation



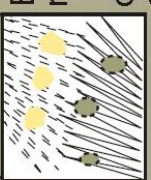
D-group 1
Early burial-pore fluids begin to circulate, aragonite dominates



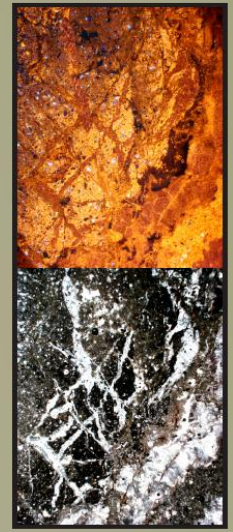
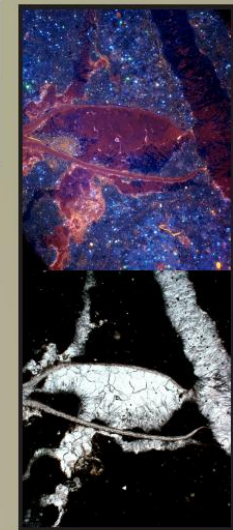
D-group 2
Initial and bioclastic neomorphism-dissolution of varied fabrics



D-group 3
Extensive neomorphism-dissolution and overprinting of all fabrics



Late tectonism-cementation of siliciclastics by burial fluids saturated in calcite



1 mm

Figure 8.5 Schematic diagram illustrating the processes of aragonite to calcite transformation within the ancient TWP seep-carbonates. Note that the various types and intensities of alterations may occur in patches across the deposit. Some samples have undergone only a minor amount of alteration in specific fabrics (e.g. left side photomicrograph pair, scale below = 1 mm) while others have been extensively altered (e.g. right side photomicrograph pair, scale below = 1 mm). G-groups 1-3 are diagenetic groups, formed from relative degree of alteration that has occurred in the samples (see Section 8.5.2).

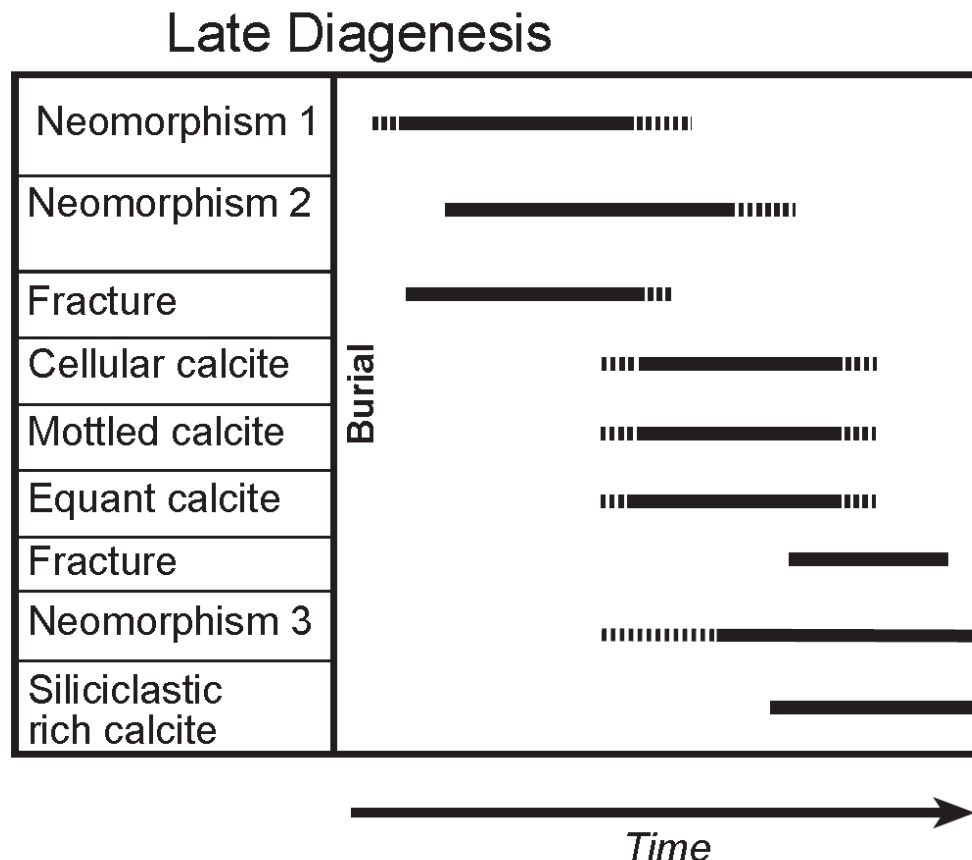


Figure 8.6 Relative timing diagram for burial diagenetic events as observed in selected TWP seep-carbonates. Refer to Section 6.2 for full descriptions of the phases, note that the three forms of neomorphism are, in order, initial neomorphism, bioclastic neomorphism and pervasive neomorphism. Full lines are where the process was occurring dominantly while dashed lines are where the process or event may have been occurring to a lesser degree.

8.4.6 Dolomite formation

The dolomite samples in the modern likely formed in a deeper environment relative to the aragonitic seep-carbonates (Fig. 8.7). The highly faulted nature of the Hikurangi Margin provides a dynamic setting in which subsurface plumbing features of seeps may become exposed via uplift, erosion and exhumation. This may be the reason why no dolomite has been detected at the TWP site, as the

dolomite present in the system may have been exhumed rather than buried properly with the aragonitic seep-carbonates to be preserved in the geologic record.

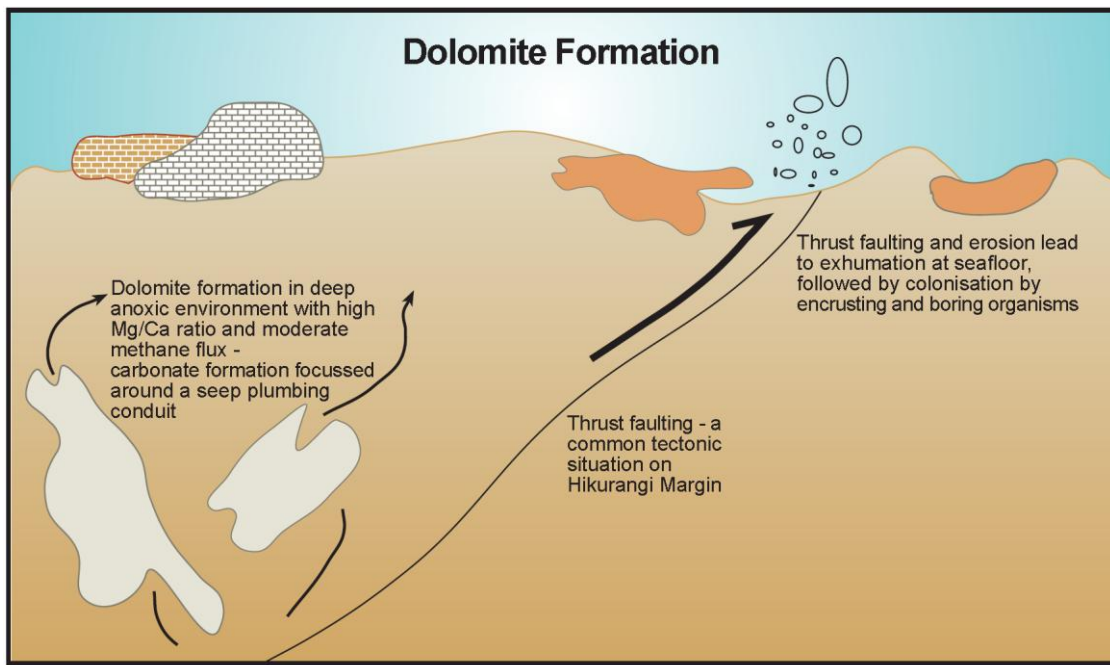


Figure 8.7 Schematic diagram illustrating the deeper environment in which the dolomites are interpreted to form. The dolomitic samples are likely subsurface plumbing features. Note that the thrust faulting regime pictured here is common on the Hikurangi Margin, which may be responsible for the uplift and exhumation of the dolomites, where they are exposed at the seafloor and may become bored and encrusted.

8.5 SEEP-CARBONATES THROUGH TIME

The diagenetic alterations that are responsible for the key differences in the modern and ancient sample groups (e.g. mineralogy, cements and elemental composition) are a factor of burial, but also time and local conditions (Folk 1965). The comparison of modern and ancient samples allows insight into these changes over time.

8.5.1 Modern seep-carbonates

It is clear that the modern aragonitic samples are unaltered and relatively pristine. This is evident from PPL and CL imaging of the internal fabrics (Section 7.3 and Fig. 8.8). Considering formation at the seafloor (or very shallow subsurface), followed by exhumation to be dredged by sampling sleds, there has been little time for alteration to the existing fabrics.

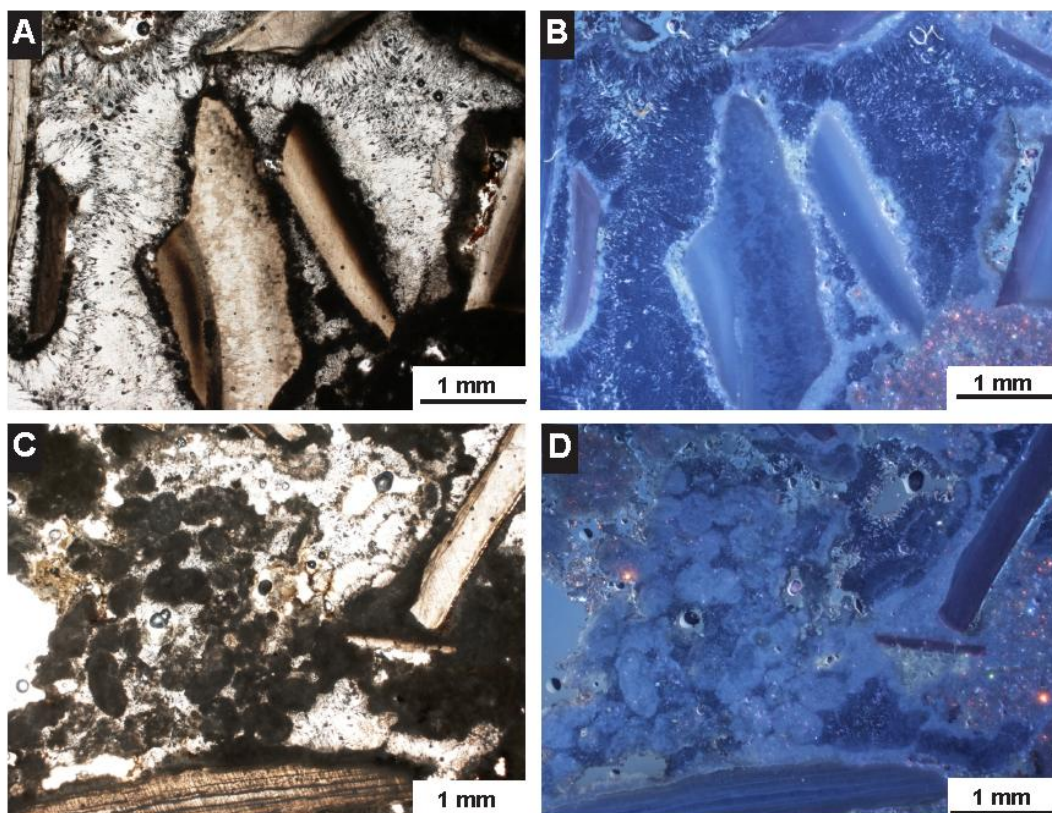


Figure 8.8 Photomicrograph pairs of modern seep-carbonates (under PPL – A and C; CL – B and D). **A** and **B** – Disarticulated bioclasts of *Calyptogena* sp. Shells are nucleation surfaces for splays of translucent aragonite. **C** and **D** – Group of dark, clotted spherical peloids which are growing between splays and botryoids of acicular aragonite. The CL colour of bright blue for both examples is indicative of little Mn within the material, in this case a recent unaltered aragonitic seep-carbonate.

8.5.2 Miocene seep-carbonates

The TWP samples have undergone different degrees of diagenetic alteration (cf. Fig. 8.5). This can be seen in CL patterns and neomorphic fabrics that vary across the deposit, and between ‘sampling zones’ or within facies. The ancient samples may be grouped into three broad diagenetic categories Diagenetic groups 1, 2 or 3 or simply D-Groups 1, 2 or 3.

D-group 1 samples show little apparent diagenetic alteration. Under CL, ‘fresh’ aragonites luminesce a dark blue–lilac (colour Fig. 8.10) and structures such as acicular needle splays and peloids are apparent. Within the aragonite fabrics of these samples, Sr values are enriched relative to other phases, and little or no calcite is identified on the XRD traces of the bulk samples.

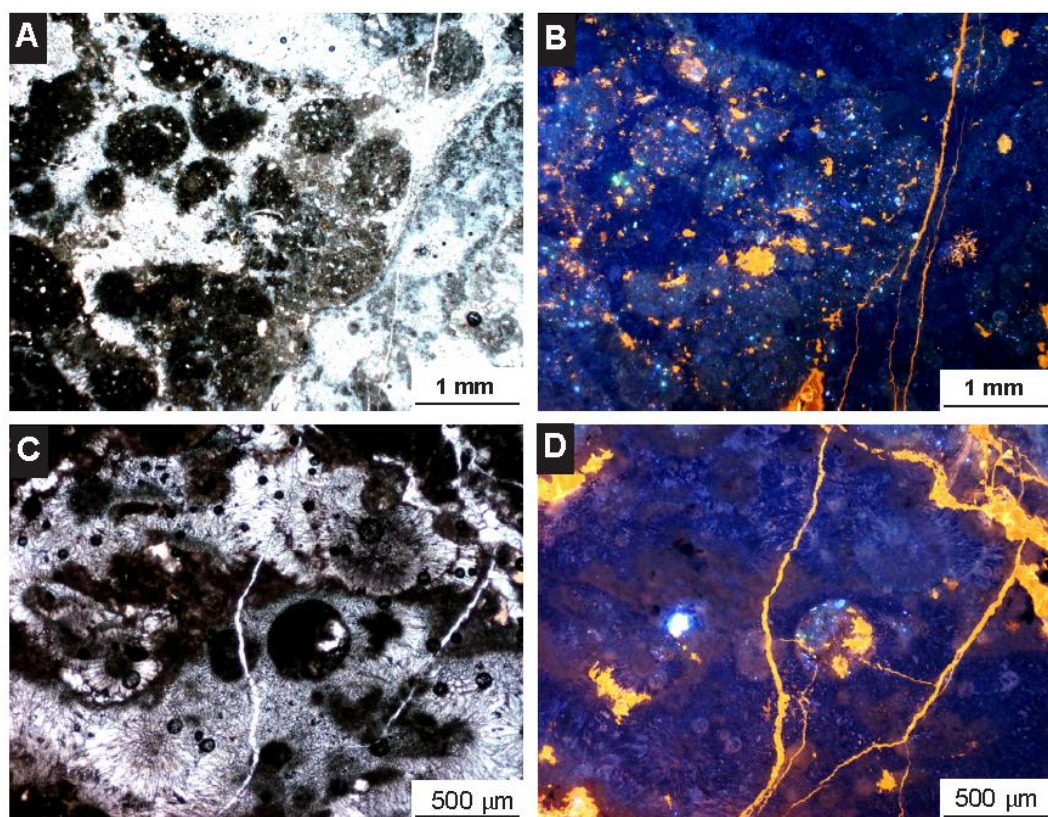


Figure 8.9 Photomicrograph pairs of TWP D-group 1 seep-carbonates (under PPL – A and C; CL – B and D). **A** and **B** – Dark, clotted peloidal fabric amongst a pore filling aragonite phase. Some bright yellow calcite is forming and is also found in the fenestrae cross-cutting the original micarb fabrics. **C** and **D** – Void fill of spherulitic aragonite is dominantly dark blue (non-luminescent) under CL but small pink zones with a mixed mineralogy of aragonite and calcite. The whole cavity is cross-cut by late yellow calcitic fenestrae.

D-group 2 samples have some evidence of diagenetic alteration, and may have evidence of initial or bioclastic neomorphic phases within their fabrics (see Section 6.2.12). CL colours range from zones of dark blue to lilac, with areas of bright yellows. Pink microspars and cerise equant calcites are common fabrics within these samples marking the morphological transformation of aragonites to calcites (Fig. 8.10). GADDs analysis identifies that these fabrics generally have mixed mineralogies of aragonite and calcite. These may be associated with fine fenestrae cross-cutting other fabrics.

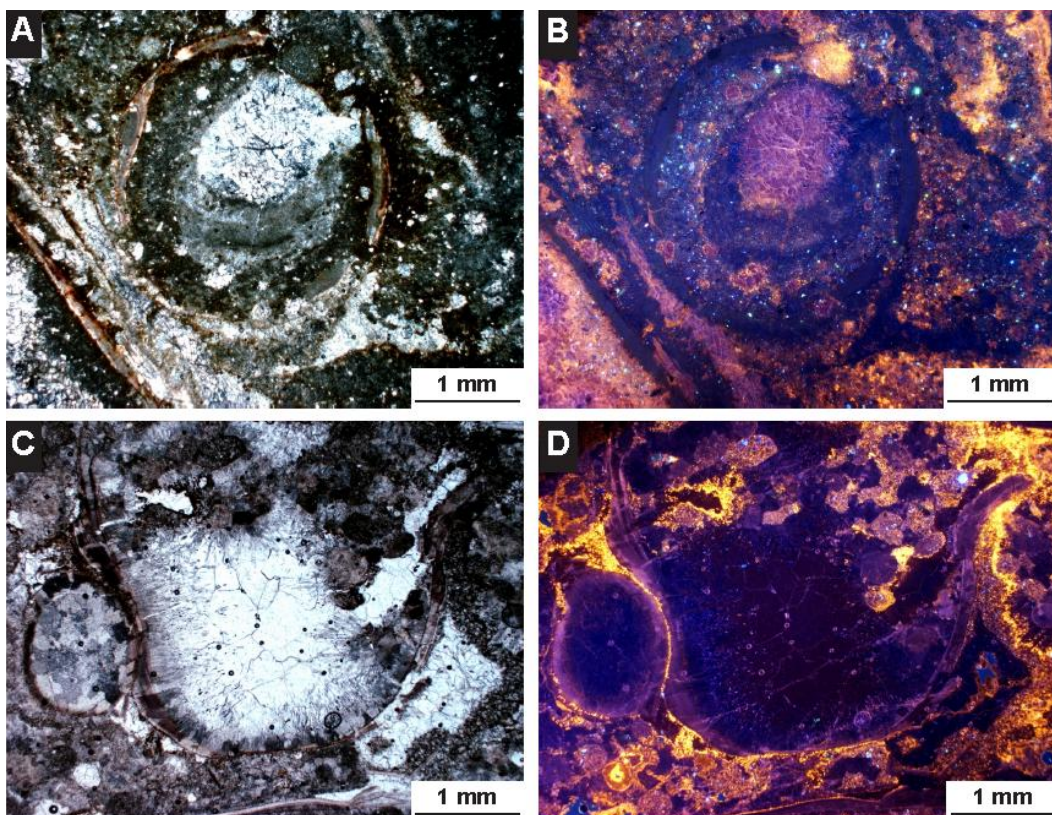


Figure 8.10: Photomicrograph pairs of TWP D-group 2 seep-carbonates (under PPL – A and C; CL – B and D). **A** and **B** – Worm tube in centre of image has been altered in concentric zones as is evident by the layers of colour variations within the worm. Under CL the microspar is pink, with a mineralogy that is a mix of calcite and aragonite. The central fabric within the worm tube is a recrystallised ‘flame’ fabric with rounded crystal faces. **C** and **D** – Worm tube surrounded by a zone of mottled late stage calcite which is forming on disarticulated bioclasts. The centre of the worm tube fill was originally an acicular aragonite, and is being neomorphosed from the centre out into an equant calcite.

D-group 3 samples are extensively diagenetically altered. In most cases there is little evidence of original aragonite fabrics, although elemental compositions may show remnant Sr within certain phases, associated with elevated Fe, Mg and Mn

from the circulating pore waters during burial. Under CL, fabrics appear structurally altered, with peculiar textures such as ‘flame’ or ‘cellular’ crystals; these crystals often have rounded edges, and are remnant or recrystallised structures (Fig. 8.11). CL colours range from deep oranges to yellows, a product of the increased Mn and Fe incorporated from burial fluids (see Fig. 6.20).

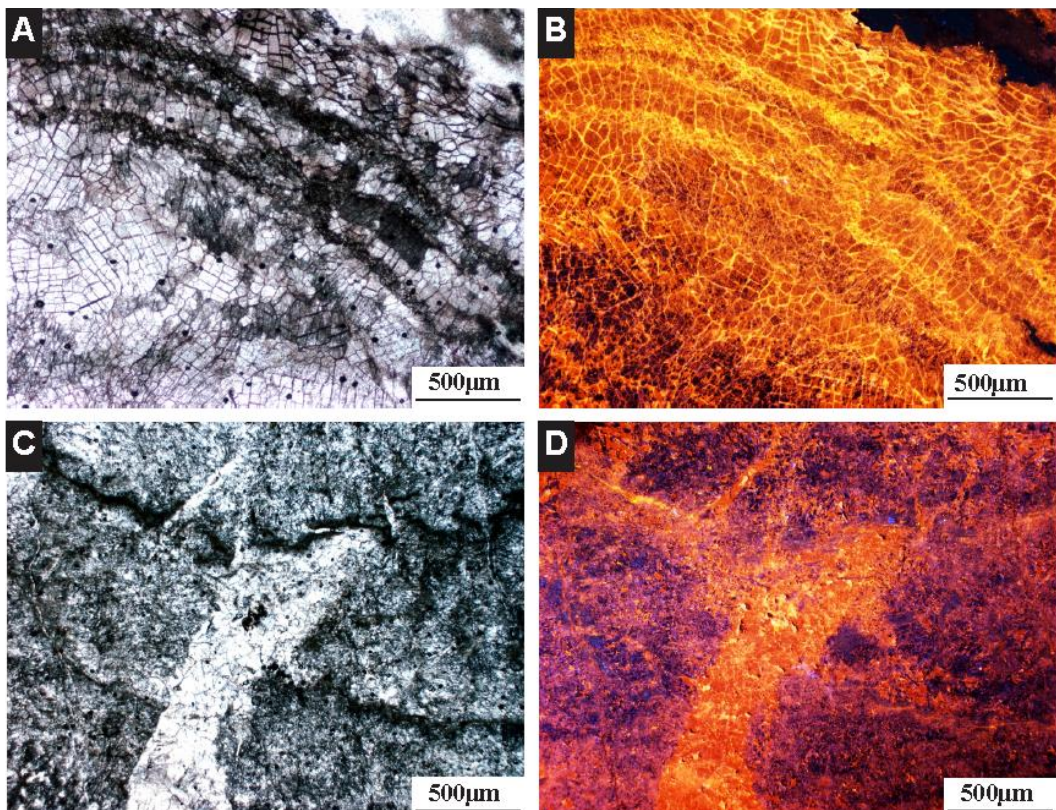


Figure 8.11: Photomicrograph pairs of TWP D-group 3 seep-carbonates (under PPL – A and C; CL – B and D). **A** and **B** – Extensively altered fabric, original acicular aragonite fabric is almost entirely gone except for some remnant needles in lower left corner. Calcite is dominant, and a ‘flame’ or ‘cellular’ structure typifies the crystal morphology. **C** and **D** – Drusy vug fill of an equant calcite pierces zone of altered acicular aragonite. The bright orange colours are typical of elevated Mn levels in a late burial environment.

The fabrics found in the D-group 3 seep-carbonates are comparable to examples in Campbell et al. (2002), a landmark paper reporting detailed petrographic analysis of Mesozoic examples from Paskenta, California. The Californian examples have incoherent, recrystallised structures under PPL and dark orange and red patterns under CL, these late stage changes being recorded in voids and fractures. However, the Californian Mesozoic samples are obviously far older than the TWP samples.

Therefore, at TWP there are a range of seep-carbonates that appear to have undergone varying degrees of diagenetic alteration. The samples range from having preserved primary fabrics as seen in the modern samples, to fabrics characteristic of late diagenesis, as seen in the Californian Mesozoic examples. This is a significant situation where the seep-carbonates have undergone patchy diagenesis as a whole, and may implicate ‘time’ as primary parameter in controlling the effects of neomorphism.

8.6 CONCLUSIONS

The field nature of the TWP seep-carbonates is varied, much like every facet of the seep-system. The subsurface plumbing system that fed the TWP paleoseep is encased in middle Miocene mudstone, and exposed locally at TWP in the form of tubular concretions. The basal mudstone is overlain by rehealed brecciated carbonate slabs, which highlight the high energy nature of the system, one that is commonly brecciated and hydrofractured. A faunal assemblage mostly composed of vestimentiferan worm tubes and bathymodioline mussels exists in stratigraphically higher facies. Faulting has affected the outcrop morphology of the TWP deposit and is linked to patchy diagenesis throughout the outcrop.

Modern seep-carbonates that form on the seafloor, are porous, rich in chemosynthetic fauna and dominated by aragonite. Dolomitic samples from within the seep-system are interpreted to be early, deep subsurface plumbing, a result of carbonate precipitation at depth in areas of high Mg/Ca ratio. The uplift and exposure of these at the seafloor result in samples that are bored and encrusted with epifauna and often iron stained.

Aragonites are the carbonate cement common to both modern Ritchie Ridge samples, and ancient TWP samples and is thus interpreted to be the initial carbonate to form in the shallow seep subsurface, where sulphate and methane flux are high. Calcites are a late stage fabric, occurring at least after shallow burial of the seep-carbonates. Dolomites may be forming concurrently with either mineralogy but at a greater depth, where higher temperatures and pressures encourage precipitation of the Mg rich carbonate.

Aragonitic microcrystalline carbonate (micarb) is interpreted as the initial carbonate cement to form in cold seep systems under specific local conditions. These conditions include pore water chemistries, fluid flux and sulphate exchange, and the presence of microbial communities carrying out the process of anaerobic oxidation of methane (AOM). Brecciation of the micarb clasts and megafauna shells provide nucleation sites for translucent splayes of acicular aragonite which may trap fluid inclusions of the migrating hydrocarbons.

A general paragenetic sequence exists in the seep-carbonates in which seafloor precipitation is dominated by various phases of aragonite cement including micarb, acicular aragonite, botryoidal aragonite and cavity filling aragonite (spherulitic aragonite). These cements are characterised by sparry, translucent cements under PPL that are dark blue-navy and non-luminescent under CL. Late diagenesis is marked by the cessation of initial seepage and thus waning of fluid expulsion during shallow burial. Late calcites fill in any remaining porosity within the seep-carbonate deposit and neomorphic alteration of metastable aragonites to calcite occurs. The process of neomorphism may not be so much a factor of depth of burial, but rather than duration of burial and age of the deposits.

In both the modern and ancient settings gas hydrates were likely to be forming and dissociating concurrently with carbonate precipitation. This process led to enriched $\delta^{18}\text{O}$ values in the carbonates, brecciated fabrics, and possible erosion of the seafloor exhuming the subsurface dolomitic concretionary bodies.

The most significant control on a cold seep is the nature of fluid flow through the system. The fluid flow regime of a cold seep system may be ephemeral, cyclic, short or long lived. The variations in fluid seepage result in the formation of a system that is heterogeneous and complex. Hence, seep system features such as seep-carbonates, tubular concretions, pock marks, and faunal assemblages are dynamic and variable. This is reflected in variations in carbonate fabrics, stable isotopic signatures, carbonate contents and the elemental chemistry of the seep-carbonates.

8.7 RECOMMENDATIONS FOR FURTHER STUDY

The following analyses would be beneficial if conducting a more in depth analysis of the seep-carbonates in this study.

- EPMA microprobe analysis
 - Only limited elemental analysis has been undertaken in this study. A much larger database is desirable to better relate elemental concentrations to the degree of neomorphism that samples have undergone.
- Scanning electron microscopy (SEM)
 - SEM would provide better structural detail of the fabrics identified within the seep-carbonates. SEM may also identify bacterial filaments in the fabrics (e.g. Barbieri and Cavalazzi 2005). Identifying these filaments would strengthen the argument of seep-carbonates forming through microbially induced precipitation.
- Lipid biomarker analysis
 - Biomarker analysis can help determine what processes were occurring at seeps when each fabric was cemented (e.g. whether AOM was occurring concurrently with cement precipitation). (e.g. Birgel and Peckmann 2008; Leefmann et al. 2008).
- Fluid inclusion analysis
 - Determining the composition of fluids trapped in fabrics such as acicular aragonite would provide useful insight into the nature of the fluid regimes forming the seep-carbonates.
- Radiometric dating (e.g. Aharon et al. 1997)
 - It would be beneficial to know when the ‘modern’ seep-carbonates actually formed, and if there are any differences in ages between the subsurface plumbing and seafloor carbonates.

References

- Aharon, P. 1994: Geology and biology of modern and ancient submarine hydrocarbon seeps and vents: An introduction. *Geo-Marine Letters* 14: 69-73.
- Aharon, P.; Schwarcz, H.P.; Roberts, H.H. 1997: Radiometric dating of submarine hydrocarbon seeps in the Gulf of Mexico. *Geological Society of America Bulletin* 109: 568-579.
- Aiello, I.W.; Garrison, R.E.; Moore, J.C.; Kastner, M.; Stokes, D.S.; 2001: Anatomy and origin of carbonate structures in a Miocene cold-seep field. *Geology* 29: 1111-1114.
- Aissaoui, D.M. 1985: Botryoidal aragonite and its diagenesis. *Sedimentology* 32: 345-361.
- Aloisi, G.; Bouloubassi, I.; Heijns, S.; Pancost, R.; Pierre, C.; Damsté, J. S.S.; Gottschal, J.C.; Forney, L.I.; Rouchy, J.M. 2002: CH⁴ -consuming microorganisms and the formation of carbonate crusts at cold seeps. *Earth and Planetary Science Letters* 203: 195-203.
- Barbieri, R.; Cavalazzi, B. 2005: Microbial fabrics from Neogene cold seep carbonates, Northern Apennine, Italy. *Palaeogeography, Palaeoclimatology, Palaeoecology* 227: 143-155.
- Barnes, E.M.; Lewis, K.B. 1991: Sheet slides and rotational failures on a convergent margin: the Kidnappers Slide, New Zealand. *Sedimentology* 38: 205-221.
- Barnes, P.M.; Lamarche, G.; Bialas, J.; Henrys, S.A.; Pecher, I.; Netzeband, G.L.; Greinert, J.; Mountjoy, J.J.; Pedley, K.; Crutchley, G. in review: Tectonic and geologic framework for gas hydrates and cold seeps on the Hikurangi subduction margin, New Zealand. Submitted to *Marine Geology*, special publication, methane seeps.
- Bathurst, R.C.G. 1975: Carbonate sediments and their diagenesis, pp 1-658. Elsevier, Amsterdam. 658 pp.
- Beauchamp, B.; Savard, M. 1992: Cretaceous chemosynthetic mounds in the Canadian Arctic. *Palaeos* 7: 434-450.

Bialis, J.; Greinert, J.; Linke, P.; Pfannkuche, O. 2007: FS SONNE Cruise Report SO 191, New Vents, IFM-GEOMAR Report 9/April 2007, 186 pp.

Birgel, D.; Peckmann, J. 2008: Aerobic methanotrophy at ancient marine methane seeps: A synthesis. Organic Geochemistry doi:10.1016/j.orggeochem.2008.01.023.

Black, R.D. 1980: Upper Cretaceous and Tertiary Geology of the Mangatu State Forest, Raukumara Peninsula. New Zealand Journal of Geology and Geophysics 23: 313-334.

Boetius, A.; Suess, E. 2004: Hydrate Ridge: a natural laboratory for the study of microbial life fueled by methane from near-surface gas hydrates. Chemical Geology 205: 291-310.

Boetius, A.; Ravenschlag, K.; Schubert, C.J.; Rickert, D.; Widdel, F.; Gieske, A.; Amann, R.; Jorgensen, B.B.; Witte, U.; Pfannkuche, O. 2000: A marine microbial consortium apparently mediating anaerobic oxidation of methane. Nature 407: 623-626.

Bohrmann, G.; Greinert, J.; Suess, E.; Torres, M. 1998: Authigenic carbonates from the Cascadia subduction zone and their relation to gas hydrate stability. Geology 26: 647-650.

Buggisch, W.; Krumm, S. 2005: Paleozoic cold seep carbonates from Europe and North Africa – an integrated isotopic and geochemical approach. Facies 51: 566-583.

Burton, E.A. 1993: Controls on marine carbonate cement mineralogy: review and reassessment. Chemical Geology 105: 163-179.

Bojanowski, M.J. 2007: Oligocene cold-seep carbonates from the Carpathians and their inferred relation to gas hydrates. Facies 53: 347-360.

Campbell, K.A. 1992: Recognition of a Mio-Pliocene cold seep setting from the Northeast Pacific convergent margin, Washington, USA. Palaios 7: 422-433.

Campbell, K.A. 2006: Hydrocarbon seep and hydrothermal vent paleoenvironments and paleontology: Past developments and future research directions. Palaeogeography, Palaeoclimatology, Palaeoecology 232: 362-407.

Campbell, K.A.; Bottjer, D.J. 1993: Fossil Cold Seeps. National Geographic Research and Exploration 9: 326-343.

Campbell, K.A.; Francis, D.A. 1998: Miocene methane-seep carbonates of the East Coast Basin, North Island. Geological Society of New Zealand Miscellaneous Publication 101A: 61.

Campbell, K.A.; Francis, D.A.; Collins, M. 1999: Hydrocarbon seepage in the East Coast Basin convergent margin (Miocene – Recent), New Zealand. American Association of Petroleum Geologists, Pacific Section Convention Program, Monterey, California, 24 pp.

Campbell, K.A.; Farmer, J.D.; Des Marais, D. 2002: Ancient hydrocarbon seeps from the Mesozoic convergent margin of California: carbonate geochemistry, fluids and palaeoenvironments. *Geofluids* 2: 63-94.

Campbell, K.A.; Francis, D.; Collins, M.; Gregory, M.R.; Nelson, C.S.; Greinert, J.; Aharon, P. 2008: Hydrocarbon seep-carbonates of a Miocene forearc (East Coast Basin), North Island, New Zealand. *Sedimentary Geology* 24: 83-105.

Campbell, K.A.; Nelson, C.S.; Alfaro, A.C.; Boyd, S.; Greinert, J.; Nyman, S.; Grosjean, E.; Logan, G.A.; Gregory, M.R.; Cooke, S.; Linke, P.; Milloy, S.; Wallis, I. in review: Geologic imprint of methane seepage on the seabed and biota of the convergent Hikurangi Margin, New Zealand: survey of core and grab carbonates. Submitted to *Marine Geology*, special publication, methane seeps.

Carney, R.S. 1994: Consideration of the oasis analogy for chemosynthetic communities at Gulf of Mexico hydrocarbon vents. *Geo-Marine Letters* 14: 149-159.

Cavagna, S.; Clari, P.; Martire, L. 1999: The role of bacteria in the formation of cold seep carbonates: geological evidence from Monferrato (Tertiary, NW Italy). *Sedimentary Geology* 126: 253-270.

Cavalazzi, B.; Barbieri, R.; Ori, G.G. 2007: Chemosynthetic microbialites in the Devonian carbonate mounds of Hamar Laghdad (Anti-Atlas, Morocco). *Sedimentary Geology* 200: 73-88.

Chafetz, H.S. 1986: Marine peloids: A product of bacterially induced precipitation of calcite. *Journal of Sedimentary Petrology* 56: 812-817.

- Clari, P.; Fornara, L.; Ricci, B.; Zuppi, G.M. 1994: Methane-derived carbonates and chemosymbiotic communities of piedmont (Miocene, northern Italy): An update. *Geo-Marine Letters* 14: 201-209.
- Collins, M. 1999: A biometric and taxonomic study of Miocene-age, hydrocarbon seep mussels from the East Coast of the North Island, New Zealand. MSc thesis, University of Auckland, 67 pp.
- Conti, S.; Fontana, D. 1999: Miocene chemoherms of the northern Apennines, Italy. *Geology* 27: 927-930.
- Conti, S.; Fontana, D. 2002: Sediment instability related to fluid venting in Miocene authigenic carbonate deposits of the northern Apennines (Italy). *International Journal of Earth Sciences* 91: 1030-1040.
- Conti, S.; Fontana, D. 2005: Anatomy of seep-carbonates: Ancient examples from the Miocene of the northern Apennines (Italy). *Palaeogeography, Palaeoclimatology, Palaeoecology* 227: 156-175.
- Conti, S.; Artoni, A.; Piola, G. 2007: Seep-carbonates in a thrust-related anticline at the leading edge of an orogenic wedge: The case of the middle-late Miocene Salsomaggiore Ridge (Northern Apennines, Italy). *Sedimentary Geology* 199: 233-251.
- Conti, S.; Fontana, D.; Lucente, C.C. 2008: Authigenic seep-carbonates cementing coarse-grained deposits in a fan-delta depositional system (middle Miocene, Marnoso-arenacea Formation, central Italy). *Sedimentology* 55: 471-486.
- Crutchley, G.J.; Gorman, A.R.; Fohrmann, M. 2007: Investigation of the role of gas hydrates in continental slope stability. *New Zealand Journal of Geology and Geophysics* 50: 357-364.
- Crutchley, G.J.; Pecher, I.A.; Gorman, A.R.; Henrys, S.A.; Greinert, J. in review: Seismic imaging of gas conduits beneath seafloor vent sites in a shallow marine gas hydrate province, Hikurangi Margin, New Zealand. Submitted to *Marine Geology*, special publication, methane seeps.
- Darby, D.; Ellis, S. 2003: Contrasting pressure regimes in sedimentary basins associated with a plate boundary, New Zealand. *Journal of Geophysical Exploration* 78-79: 149-152.

- Davidson, D.W.; Leaist, D.J.; Hesse, R. 1983: Oxygen-18 enrichment in water of a clathrate hydrate. *Geochimica et Cosmochimica Acta* 47: 2293-2295.
- De Boever, E.; Swennen, R.; Dimitrov, L. 2006: Lower Eocene carbonate cemented chimneys (Varna, NE Bulgaria): Formation mechanisms and the (a)biological mediation of chimney growth? *Sedimentary Geology* 185: 159-173.
- Derkachev, A.N.; Bohrmann, G.; Greinert, J.; Mozherovskii, A.V. 2000: Authigenic carbonate and barite mineralization in sediments of the Deryugin Basin (Sea of Okhotsk). *Lithology and Mineral Resources* 35: 568-585.
- Díaz-del-Río, V.; Somoza, L.; Martínez-Frias, J.; Mata, M.P.; Delgado, A.; Hernandez-Molina, F.J.; Lunar, R.; Martín-Rubí, J.A.; Maestro, A.; Fernández-Puga, M.C.; Léon, R.; Llave, E.; Medialdea, T.; Vázquez, J.T. 2003: Vast fields of hydrocarbon-derived carbonate chimneys related to the accretionary wedge/olistostrome of the Gulf of Cadiz. *Marine Geology* 195: 177-200.
- Ellis, S.; Pecher, I.; Kukowski, N.; Xu, W.; Henrys, S.; Greinert, J. in review: Testing proposed mechanisms for seafloor weakening at the top of gas hydrate stability, Rock Garden, New Zealand. Submitted to *Marine Geology*, special publication, methane seeps.
- Faure, K.; Greinert, J.; Pecher, I.A.; Graham, I.J.; Massoth, G.J.; De Ronde, C.E.J.; Wright, I.C.; Baker, E.T.; Olson, E.J. 2006: Methane seepage and its relation to slumping and gas hydrate at the Hikurangi Margin, New Zealand. *New Zealand Journal of Geology and Geophysics* 49: 503-516.
- Fearn, D.A.; Davies, P.J.; Pigram, C.J.; Symonds, P.A. 1991: Climatic evolution and control on carbonate deposition in northeast Australia. *Palaeogeography, Palaeoclimatology, Palaeoecology* 89: 341-361.
- Feng, D.; Chen, D.; Roberts, H.H. 2008: Petrographic and geochemical characterization of seep carbonate from Bush Hill (GC 185) gas vent and hydrate site of the Gulf of Mexico. *Marine and Petroleum Geology*, doi: 10.1016/j.marpetgeo.2008.07.001.
- Field, B.D.; Uruski, C.I.; and others 1997: Cretaceous-Cenozoic geology and petroleum systems of The East Coast Region, New Zealand. Institute of Geological and Nuclear Sciences monograph 19. 301 p, 7 enclosures. Lower Hutt, New Zealand: Institute of Geological and Nuclear Sciences Limited.

- Folk, R.L. 1959: Practical petrographic classification of limestones. American association o f Petroleum Geologists Bulletin 43: 1-38.
- Folk, R.L. 1962: Spectral subdivision of limestone types. *In:* Ham, W.E. *ed.* Classification of Carbonate Rocks. American Association of Petroleum Geologists, Tulsa, Oklahoma: 62-84.
- Folk, R.L. 1965: Some aspects of recrystallisation in ancient limestones. *In:* Pray, L.C.; Murray, R.C. *eds.* Dolomitization and Limestone Diagenesis: a Symposium – Society of Economic Paleontologists Mineralogists (SEPM), Special Publication 13: 14-48.
- Francis, D.; Bennett, D.; Courteney, S. 2004: Advances in understanding of onshore East Coast Basin structure, stratigraphic thickness and hydrocarbon generation. New Zealand Petroleum Conference Proceedings 2004.
- Francis, D.; Campbell, K.; Nelson, C. 2008: Geologic settings of methane seep-derived carbonates in the East Coast Basin. Geological Society of New Zealand Miscellaneous Publication 124A: 261.
- Friedman, I.; O'Neil, J.R. 1977: Compilation of stable isotope fractionation factors of geochemical interest. *In:* Fleisher, M. *ed.* U.S. Geological Survey Professional Paper, 440 pp.
- Fritz, P.; Smith, D.G.W. 1990: The isotopic composition of secondary dolomite. *Geochimica et Cosmochimica Acta* 34: 1161-1173.
- Gautier, D.L.; Claypool, G.E. 1984: Interpretation of methanic diagenesis in ancient sediments by analogy with processes in modern diagenetic environments. *In:* McDonald, D.A.; Surdam, R.C. *eds.* Elastic Diagenesis, American Association of Petroleum Geologists 37: 1-123.
- Gieskes, J.; Mahn, C.; Day, S.; Martin, J.; Greinert, J.; Rathburn, T.; McAdoo, J.B. 2005: A study of the chemistry of pore fluids and authigenic carbonates in methane seep environments: Kodiak Trench, Hydrate Ridge, Monterey bay, and Eel River Basin. *Chemical Geology* 220: 329-345.
- Goedert, J.L.; Thiel, V.; Schmale, O.; Rau, W.W.; Michaelis, W.; Peckmann, J. 2003: The late Eocene ‘Whiskey Creek’ methane-seep deposit (Western Washington State) Part 1: Geology, Palaeontology and Molecular Geobiology. *Facies* 48: 223-240.

- Gorman, A.R.; Pecher, I.A.; Henrys, S.A. 2004: Evidence for gas hydrate ‘sweet spots’ on the Hikurangi Margin and offshore Fiordland. New Zealand Petroleum Conference Proceedings.
- Greinert, J.; Bohrmann, G.; Suess, E. 2001. Gas hydrate-associated carbonates and methane-venting at Hydrate Ridge: Classification, distribution, and origin of authigenic lithologies. In: Parnell, C.K.; Dillon, K.P. eds. Natural Gas Hydrates: Occurrence, Distribution and Detection. Geophysical Monograph, 124: 99-113.
- Greinert, J.; Bollwerk, S.M.; Derkachev, A.; Bohrmann, G.; Suess, E. 2002: Massive barite deposits and carbonate mineralization in the Derugin Basin, Sea of Okhotsk: precipitation processes at cold seep sites. Earth and Planetary Science Letters 203: 165-180.
- Greinert, J.; Bialas, J.; Lewis, K.B.; Suess, E. in review: Methane migration and gas hydrates offshore New Zealand’s North Island: Compiling results from three cruises in 2006 and 2007. Submitted to Marine Geology, special publication, methane seeps.
- Grossman, E.L.; Ku, T.L. 1986: Oxygen and carbon isotope fractionation in biogenic aragonite temperature effects. Chemical Geology 59: 59-74.
- Han, M.W.; Suess, E. 1989: Subduction-induced pore fluid venting and the formation of authigenic carbonates along the Cascadia continental margin: Implications for the global Ca-Cycle. Palaeogeography, Palaeoclimatology, Palaeoecology 71: 97-118.
- Han, X.; Suess, E.; Huang, Y.; Wu, N.; Bohrmann, G.; Su, X.; Eisenhauer, A.; Rehder, G.; Fang, Y. 2008: Jiulong methane reef: Microbial mediation of seep carbonates in the South China Sea. Marine Geology 249: 243-256.
- Hein, J.R.; Normark, W.R.; McIntyre, B.R.; Lorenson, T.D.; Powell III, C.L. 2006: Methanogenic calcite, ^{13}C -depleted bivalve shells and gas hydrate from a mud volcano offshore southern California. Geology 34: 109-112.
- Himmler, T.; Freiwald, A.; Stollhofen, H.; Peckmann, J. 2008: Late Carboniferous hydrocarbon-seep carbonates from the glaciomarine Dwyka Group, southern Namibia. Palaeogeography, Palaeoclimatology, Palaeoecology 257: 185-197.

Hood, S.D. 2000: Subsurface stratigraphy and petrology of a non-tropical carbonate fracture reservoir – the Mid-Tertiary Tikorangi Formation, Taranaki basin, New Zealand. Unpublished PhD Thesis, University of Waikato, Hamilton, New Zealand.

Hovland, M. 2002: On the self-sealing nature of marine seeps. *Continental Shelf Research* 22: 2387-2394.

Hovland, M. 2003: Geomorphological, geophysical, and geochemical evidence of fluid flow through the seabed. *Journal of Geochemical Exploration* 78-79: 287-291.

Hovland, M.; Hill, A.; Stokes, D. 1997: The structure and geomorphology of the Dashgil mud volcano, Azerbaijan. *Geomorphology* 21: 1-15.

Hovland, M.; Svensen, H.; Forsberg, C.F.; Johansen, H.; Fichler, C.; Fossa, J.H.; Jonsson, R.; Rueslatten, H. 2005: Complex pockmarks with carbonate ridges off mid-Norway: Products of sediment degassing. *Marine Geology* 218: 191-206.

Irwin, H.; Curtis, C.; Coleman, M. 1977: Isotopic evidence for source of diagenetic carbonates formed during burial of organic rich sediments. *Nature* 269: 209-213.

Jenkins, R.G.; Kaim, A.; Hikida, Y.; Tanabe, K. 2007: Methane-flux-dependent lateral changes in a Late Cretaceous chemosymbiotic assemblage from the Nakagawa area of Hokkaido, Japan. *Geobiology* doi: 10.1111/j.1472-4669.2007.00106.x.

Jørgensen, N.O. 1992: Methane-derived carbonate cementation of marine sediments from the Kattegat, Denmark: Geochemical and geological evidence. *Marine Geology* 103: 1-13.

Judd, A.G. 2003: The global importance and context of methane escape from the seabed. *Geo-Marine Letters* 23: 147-154.

Judd, A.G.; Hovland, M. 2007: Seabed Fluid Flow: The Impact on Geology, Biology and the Marine Environment. Cambridge University Press, Cambridge. 475 pp.

- Kamp, P.J.J.; Nelson, C.S. 1988: Nature and occurrence of modern and Neogene active margin limestones in New Zealand. *New Zealand Journal of Geology and Geophysics* 31: 1-20.
- Kastner, M.; Kvenvolden, K.A.; Lorenson, T.D. 1998: Chemistry, isotopic composition and origin of a methane-hydrogen sulphide hydrate at the Cascadia subduction zone. *Earth and Planetary Science Letters* 156: 173-183.
- Kelly, S.R.A.; Ditchfield, P.W.; Doubleday, P.A.; Marshall, J.D. 1995: An upper Jurassic methane-seep limestone from the Fossil Bluff Group forearc basin of Alexander Island, Antarctica. *Journal of Sedimentary Research* 65: 274-282.
- King, P.R. 2000: Tectonic reconstructions of New Zealand: 40 Ma to the present. *New Zealand Journal of Geology and Geophysics* 43: 611-638.
- King, P.R.; Thrasher, G.P. 1996: Cretaceous-Cenozoic geology and petroleum systems of the Taranaki Basin, New Zealand. Institute of Geological and Nuclear Sciences, Monograph 13. 243 p. 6 enclosures. Institute of Geological and Nuclear Sciences, Ltd, Lower Hutt, New Zealand.
- Korbel, P.; Novak, M. 1999: The Complete Encyclopedia of Minerals. Rebo Publishers, the Netherlands, 296 pp.
- Krüger, M.; Treude, T.; Wolters, H.; Nauhaus, K.; Boetius, A. 2005: Microbial methane turnover in different marine habitats. *Palaeogeography, Palaeoclimatology, Palaeoecology* 227: 6-17.
- Kvenvolden, K.A.; Pettinga, J.R. 1989: Hydrocarbon gas seeps of the convergent Hikurangi margin, North Island, New Zealand. *Marine and Petroleum Geology* 6: 2-8.
- Leckie, D.A.; Morgans, H.; Wilson, G.J.; Edwards, A.R. 1995: Mid-Paleocene dropstones in the Whangai Formation, New Zealand – evidence of mid-Paleocene cold climate? *Sedimentary Geology* 97: 119-129.
- Leefmann, T.; Bauermeister, J.; Kronz, A.; Liebetrau, V.; Reitner, J.; Thiel, V. 2008: Miniaturized biosignature analysis reveals implications for the formation of cold seep carbonates at Hydrate Ridge (off Oregon, USA). *Biogeosciences* 5: 731-738.

Léon, R.; Somoza, L.; Medialdea, T.; Maestro, A.; Díaz-del-Río, V.; Carmen Fernandez-Puga, M. del. 2006: Classification of sea floor features associated with methane seeps along the Gulf of Cadiz continental margin. Deep-Sea Research II 53: 1464-1481.

Levin, L.A.; Ziebis, W.; Mendoza, G.F.; Growney, V.A.; Tyron, M.D.; Brown, K.M.; Mahn, C.; Gieskes, J.G.; Rathburn, A.E. 2003: Spatial heterogeneity of macrofauna at northern California methane seeps: influence of sulfide concentration and fluid flow. Marine Ecology Progress Series 265: 123-139.

Lewis, K.B.; Pettinga, J.R. 1993: The emerging, imbricate frontal wedge of the Hikurangi Margin. South Pacific Sedimentary Basins. *In: Ballance, P.F. ed. Sedimentary Basins of the World*, 2: 225-250. Elsevier Science, Amsterdam.

Lewis, K.B.; Marshall, B.A. 1996: Seep faunas and other indicators of methane-rich dewatering on New Zealand convergent margins. New Zealand Journal of Geology and Geophysics 39: 181-200.

Luff, R.; Wallmann, K.; Aloisi, G. 2004: Numerical modeling of carbonate crust formation at cold vent sites: significance for fluid and methane budgets and chemosynthetic biological communities. Earth and Planetary Sciences Letters 221: 337-353.

McKay, A. 1877: On the geology of East Auckland and the northern district of Hawkes Bay. New Zealand Geological Survey Reports of Geological Explorations during 1886-1887 18: 183-219.

Maliva, R.G. 1998: Skeletal aragonite neomorphism – quantitative modelling of a two-water diagenetic system. Sedimentary Geology 121: 179-190.

Maliva, R.G.; Missimer, T.M.; Dickson, J.A.D. 2000: Skeletal aragonite neomorphism in Plio-Pleistocene sandy limestones and sandstone, Hollywood, Florida, USA. Sedimentary Geology 136: 147-154.

Mazengarb, C. 1984: The Fernside Fault: an active normal fault, Raukumara peninsula, New Zealand. New Zealand geological Survey Record 3: 98-103.

Mazengarb, C. 1993: Cretaceous stratigraphy of Raukumara Peninsula. Institute of Geological and Nuclear Sciences Report 93/20.

- Mazengarb, C.; Francis, D.A. 1985: The occurrence of paramoudra concretions in the Gisborne District. Geological Society of New Zealand Newsletter 68: 52-53.
- Mazengarb, C.; Francis, D.A.; Moore, P.R. 1991: Sheet Y16 – Tauwhareparae. Geological map of New Zealand 1:50 000. Map (1 sheet) and notes (52 p.). Wellington, Department of Scientific and Industrial Research.
- Mazzini, A.; Svensen, H.; Hovland, M.; Planke, S. 2006: Comparison and implications from strikingly different authigenic carbonates in a Nyegga complex pockmark, G11, Norwegian Sea. Marine Geology 231: 89-102.
- Middleton, G.V. 2003: Encyclopedia of sediments and sedimentary rocks. Kluwer Publishers, United States, 858 pp.
- Milkov, A.V.; Dickens, G.R.; Claypool, G.E.; Lee, Y.J.; Borowski, W.S.; Torres, M.E.; Xu, W.; Tomaru, H.; Trehu, A.M.; Schultheiss, P. 2004a: Co-existence of gas hydrate, free gas, and brine within the regional gas hydrate stability zone at Hydrate Ridge (Oregon Margin): evidence from prolonged degassing of a pressurized core. Earth and Planetary Letters 222: 829-843.
- Milkov, A.V.; Vogt, P.R.; Crane, K.; Lein, A.Y.; Sassen, R.; Cherkashev, G.A. 2004b: Geological, geochemical, and microbial processes at the hydrate-bearing Hakon Mosby mud volcano: a review. Chemical Geology 205: 347-366.
- Moore, P.R. 1985: A revised Cretaceous-early Tertiary stratigraphic nomenclature for eastern North Island. New Zealand Geological Survey Report G104, 31 pp.
- Moore, P.R. 1988: Stratigraphy, composition, and environment of deposition of the Whangai Formation and associated Late Cretaceous-Paleocene rocks, eastern North Island, New Zealand. New Zealand Geological Survey Bulletin 100, 19 pp.
- Moore, P.R. 1989: Stratigraphy of the Waipawa Black Shale (Paleocene), eastern North Island, New Zealand. New Zealand Geological Survey Record 38, 82 pp.
- Morse, J.W.; Mackenzie, F.T. 1990: Geochemistry of Sedimentary Carbonates. Developments in Sedimentology 48. Elsevier, Amsterdam, 707 pp.

Naehr, T.H.; Rodriguez, N.M.; Bohrmann, G.; Paull, C.K.; Botz, R. 2000: Methane-derived authigenic carbonates with gas hydrate decomposition and fluid venting above the Blake Ridge Diapir. In: Paull, C.K.; Matsumoto, P.J.; Dillon, W.P. eds. Proceedings Ocean Drilling Project, Scientific Results, 164: College Station, TX, (Ocean Drilling Program).

Naehr, T.H.; Eichhubl, P.; Orphan, V.J.; Hovland, M.; Paull, C.K.; Ussler III, W.; Lorenson, T.D.; Greene, H.G. 2007: Authigenic carbonate formation at hydrocarbon seeps in continental margin sediments: A comparative study. Deep-Sea Research II 54: 1268-1291.

Nelson, C.S.; Cochrane, R.H.A. 1970: A rapid X-ray method for the qualitative determination of selected minerals in fine-grained and altered rocks. Tane 16: 151-162.

Nelson, C.S.; Healy, T.R. 1984: Pockmark-like structures on the Poverty Bay sea bed – possible evidence for submarine mud volcanism. New Zealand Journal of Geology and Geophysics 27: 225-230.

Netzeband, G.; Krabbenhoeft, A.; Zillmer, M.; Petersen, C.J.; Papenberg, C.; Bialas, J. in review: Seeps and the structures underneath – seismic evidence from the Wairarapa area. Submitted to Marine Geology, special publication, methane seeps.

Nyman, S.L. 2009: Tubular concretions from North Island, New Zealand: Evidence for hydrocarbon migration and the subsurface plumbing system of cold seeps. Unpublished PhD Thesis, University of Waikato, Hamilton, New Zealand.

Olu-Le-Roy, K.; Sibuet, M.; Fiala-Medioni, A.; Gofas, S.; Salas, C.; Mariotti, A.; Foucher, J.P.; Woodside, J. 2004: Cold seep communities in the deep eastern Mediterranean Sea: composition, symbiosis and spatial distribution on mud volcanoes. Deep-Sea Research I 51: 1915-1936.

Ongley, M.; Macpherson, E.O. 1928: The Geology of the Waiapu Subdivision, Raukumara Division. New Zealand Geological Survey Bulletin 30, 79 pp.

Orcutt, B.; Samarkin, V.; Boetius, A.; Joye, S. 2008: On the relationship between methane production and oxidation by anaerobic methanotrophic communities from cold seeps of the Gulf of Mexico. Environmental Microbiology 10: 1108-1117.

- Orphan, V.J.; Ussler III, W.; Naehr, T.H.; House, C.H.; Hinrichs, K.U.; Paull, C.K. 2004: Geological, geochemical, and microbiological heterogeneity of the seafloor around methane vents in the Eel River Basin, offshore California. *Chemical Geology* 205: 265-289.
- Orpin, A. 1997: Dolomite chimneys as possible evidence of coastal fluid expulsion, uppermost Otago continental slope, southern New Zealand. *Marine Geology* 138: 51-67.
- Pagel, M.; Barbin, V.; Blanc, P.; Ohnenstetter, D. 2003: Cathodoluminescence in Geosciences. Springerlink, Berlin. 514 pp.
- Parnell, J. 2002: Fluid seeps at Continental Margins: toward an Integrated Plumbing System. *Geofluids* 2: 57-61.
- Pecher, I.A.; Henrys, S.A.; Zhu, H. 2004: Seismic images of gas conduits beneath vents and gas hydrates on Ritchie Ridge, Hikurangi Margin, New Zealand. *New Zealand Journal of Geology and Geophysics* 47: 275-279.
- Pecher, I.A.; Henrys, S.A.; Ellis, S.; Chiswell, S.M.; Kukowski, N. 2005: Erosion of the seafloor at the top of the gas hydrate stability zone on the Hikurangi margin, New Zealand. *Geophysical Research Letters* 32: L24603, doi:10.1029/2005GL024687.
- Pecher, I.A.; Coffin, R.; Henrys, S.A.; CHARMNZ Working Group 2007: Tangaroa TAN0607 Cruise Report: Gas Hydrate exploration on the East Coast, North Island, New Zealand, GNS Science Report, 2007/29, 119 pp.
- Peckmann, J.; Thiel, V. 2004: Carbon cycling at ancient methane-seeps. *Chemical Geology* 205: 443-467.
- Peckmann, J.; Thiel, V.; Michaelis, W.; Clari, P.; Gaillard, C.; Martire, L.; Reitner, J. 1999: Cold seep deposits of Beauvoisin (Oxfordian; southeastern France) and Marmorito (Miocene; northern Italy): microbially induced authigenic carbonates. *International Journal of Earth Sciences* 88: 60-75.
- Peckmann, J.; Reimer, A.; Luth, U.; Luth, C.; Hansen, B.T.; Heinicke, C.; Hoefs, J.; Reitner, J. 2001: Methane-derived carbonates and authigenic pyrite from the northwestern Black Sea. *Marine geology* 177: 129-150.

- Peckmann, J.; Little, C.T.S.; Gill, F.; Reitner, J. 2005: Worm tube fossils from the Hollard Mound hydrocarbon-seep deposit, Middle Devonian, Morocco: Paleozoic seep-related vestimentiferans? *Palaeogeography, Palaeoclimatology, Palaeoecology* 227: 242-257.
- Perry, R.S.; McLoughlin, N.; Lynne, B.Y.; Sephton, M.A.; Oliver, J.D.; Perry, C.C.; Campbell, K.; Engel, M.H.; Farmer, J.D.; Brasier, M.D.; Staley, J.T. 2007: Defining biominerals and organominerals: Direct and indirect indicators of life. *Sedimentary Geology* 201: 175-179.
- Pettinga, J.G. 2003: Mud volcano eruption within the emergent accretionary Hikurangi margin, southern Hawkes Bay, New Zealand. *New Zealand Journal of Geology and Geophysics* 46: 107-121.
- Phillips, C.J. 1985: Upper Cretaceous and Tertiary Geology of the upper Waitahaia River, Raukumara Peninsula. *New Zealand Journal of Geology and Geophysics* 28: 595-608.
- Pierre, C.; Rouchy, J.M.; Gaudichet, A. 2000: Diagenesis in the gas hydrate sediments of the Blake Ridge: Mineralogy and stable isotope compositions of the carbonate and sulfide minerals. In: Paull, C.K.; Matsumoto, P.J.; Dillon, W.P. eds. *Proceedings Ocean Drilling Project, Scientific Results*, 164: College Station, TX, (Ocean Drilling Program).
- Reid, P.R.; Macintyre, I.G.; James, N.P. 1990: Internal precipitation of microcrystalline carbonate: a fundamental problem for sedimentologists. *Sedimentary Geology* 68: 163-170.
- Reitner, J.; Peckmann, J.; Blumenberg, M.; Michaelis, W.; Reimer, A.; Thiel, V. 2005: Concretionary methane-seep carbonates and associated microbial communities in Black Sea sediments. *Palaeogeography, Palaeoclimatology, Palaeoecology* 227: 18-30.
- Ridgway, N.M. 1969: Temperature and salinity of seawater at the ocean floor in the NZ region. *New Zealand Journal of Marine and Freshwater Research* 3: 57-72.
- Roberts, H.H.; Aharon, P.; Walsh, M.W. 1993: Cold-seep carbonates of the Louisiana Continental slope-to-basin floor. In: Rezak, R.; Lavoie, D.L. eds. *Carbonate Microfabrics*. Springer, Berlin, pp 95-104.

- Roberts, H.H.; Aharon, P. 1994: Hydrocarbon-derived carbonate buildups of the northern Gulf of Mexico continental slope: A review of submersible investigations. *Geo-Marine Letters* 14: 135-148
- Rodriguez, N.M.; Paull, C.K.; Borowski, W.S. 2000: Zonation of authigenic carbonates within gas hydrate-bearing sedimentary sections on the Blake Ridge: offshore southeastern North America. In: Paull, C.K.; Matsumoto, P.J.; Dillon, W.P. eds. *Proceedings Ocean Drilling Project, Scientific Results*, 164: College Station, TX, (Ocean Drilling Program).
- Rogers, K.M.; Collen, J.D.; Johnston, J.H.; Elgar, N.E.; A. 1999: A geochemical appraisal of oil seeps from the East Coast Basin, New Zealand. *Organic Geochemistry* 30: 593-605.
- Savard, M.M.; Beauchamp, B.; Veizer, J. 1996: Significance of aragonite cements around Cretaceous marine methane seeps. *Journal of Sedimentary Research* 66: 430-438.
- Sibson, R.H.; Rowland, J.V. 2003: Stress, fluid pressure and structural permeability in seismogenic crust, North Island, New Zealand. *International Journal of Geophysics* 54: 584-594.
- Sibuet, M.; Olu, K. 1998: Biogeography, biodiversity and fluid dependence of deep-sea cold-seep communities at active and passive margins. *Deep Sea Research II* 45: 517-567.
- Stakes, D.; Orange, D.; Paduan, J.B.; Salamy, K.A.; Maher, N. 1999: Cold-seeps and authigenic carbonate formation in Monterey Bay, California. *Marine Geology*, 159: 93-109.
- Strong, S.W.S. 1933: The Sponge Bay uplift, and the Hangaroa mud Blowout. *New Zealand Journal of Science and Technology* 15: 76-78.
- Suess, E.; Whiticar, M.J. 1989: Methane-derived CO₂ in pore fluids expelled from the Oregon subduction zone. *Palaeogeography, Palaeoclimatology, Palaeoecology* 71: 119-136.
- Teichert, B.M.A.; Bohrmann, G.; Suess, E. 2005: Chemoherms on Hydrate Ridge – Unique microbially-mediated carbonate build ups growing into the water column. *Palaeogeography, Palaeoclimatology, Palaeoecology* 227: 67-85.

Terzi, C.; Aharon, P.; Lucchi, F.R.; Vai, G.B. 1994: Petrography and stable isotope aspects of cold-vent activity imprinted on Miocene-age “calcare a Lucina” from Tuscan and Romagna Apennines, Italy. *Geo-Marine Letters* 14: 177-184.

Trehu, A.M.; Torres, M.E.; Moore, G.F.; Suess, E.; Bohrmann, G. 1999: Temporal and spatial evolution of a gas-hydrate bearing accretionary ridge on the Oregon continental margin. *Geology* 27: 939-942.

Torres, M.E.; Bohrmann, G.; Dubé, T.E.; Poole, F.G. 2003: Formation of modern and Paleozoic stratiform barite at cold methane seeps on continental margins. *Geology* 31: 897-900.

Townend, J. 1997: Estimates of conductive heat flow through bottom-simulating reflectors on the Hikurangi and southwest Fiordland continental margins, New Zealand. *Marine Geology* 141: 209-220.

Ussler III, W.; Paull, C.K. 1995: Effects of ion exclusion and isotopic fractionation on pore water geochemistry during gas hydrate formation and decomposition. *Geo-marine Letters* 15: 37-44.

Von Rad, U.; Rosch, H.; Berner, U.; Geyh, M.; Marchig, V.; Schulz, H. 1996: Authigenic carbonates derived from oxidized methane vented from the Makran accretionary prism off Pakistan. *Marine Geology* 136: 55-77.

Wood, W.T.; Hart, P.E.; Hutchinson, D.R.; Dutta, N.; Snyder, F.; Coffin, R.B.; Gettrust, J.F. 2008: Gas and gas hydrate distribution around seafloor seeps in Mississippi Canyon, Northern Gulf of Mexico, using multi-resolution seismic imagery. *Marine and Petroleum Geology* 25: 952-959.

Appendix 1

Sample Data

Appendix A1.1 Full sample list of seep-carbonates from TWP paleo-seep, and some brief field descriptions. The ‘UoW’ number is the sample number logged in the PET database.

| Sample number | UoW number | Description |
|---------------|------------|---|
| TWP-A/1 | 2009 0001 | Concretionary material from host mudstone. |
| TWP-A/2 | 2009 0002 | Muddy long tube from host mudstone, plus several long pieces. |
| TWP-A/3 | 2009 0003 | Dark grey bleb, cut in half by thick creamy vein, and creamy carbonate crust |
| TWP-A/4 | 2009 0004 | Concreted layer in pipe, zone A, veining present and crystals growing on edge of rock, some brecciated clasts. |
| TWP-A/5 | 2009 0005 | Highly veined material, at base of large vein network. |
| TWP-A/6 | 2009 0006 | Right flank, large chunk of highly veined material, at different stages of fill, fine grey dark micrite. |
| TWP-A/7 | 2009 0007 | Centre of Zone A, brecciated micrite. |
| TWP-A/8 | 2009 0008 | Right flank, midway, pale colours, and some dark, highly veined. |
| TWP-A/9 | 2009 0009 | Right flank, from long 3 m slab bottom corner. |
| TWP-A/10 | 2009 0010 | Left flank, in zone of intense brecciation, below large slab. |
| TWP-A/11 | 2009 0011 | Carbonate clasts from area of worm tubes and mussels. |
| TWP-A/12 | 2009 0012 | Slab of highly cemented carbonate, dark grey micrite, weathered exterior, yellow calcite and crystals indicate a joint face. |
| TWP-A/13 | 2009 0013 | From lower section, near mudstone contact, blue/grey and oxidising ring, some vugs and minor veining. |
| TWP-A/14 | 2009 0014 | Clasts from top of section. |
| TWP-A/15 | 2009 0015 | Blue/grey brecciated material. |
| TWP-A/16 | 2009 0016 | Brecciated clasts from top right flank. |
| TWP-A/17 | 2009 0017 | Brecciated and bioturbated, blue grey and creamy infill, fibrous aragonite veins in areas, crystals are pink and elongate. |
| TWP-A/18 | 2009 0018 | Concretionary material in trench on A side. |
| TWP-B/1 | 2009 0019 | Left of boulder, oxidised ring of orange, blue/grey inner material is slightly fractured with several stages of lighter fill. |
| TWP-B/2 | 2009 0020 | From top edge of boulder highly burrowed, slightly concreted burrow or bleb. |
| TWP-B/3 | 2009 0021 | Bottom right of boulder, zonation from slightly fractured to intense brecciation and bioturbation. |
| TWP-B/4 | 2009 0022 | North facing edge of boulder highly burrowed, slightly concreted burrow or bleb. |

| | | |
|----------|-----------|--|
| TWP-B/5 | 2009 0023 | Blue/grey bleb with vugs and minor veining. |
| TWP-B/6 | 2009 0024 | Fine grained blue/grey clasts, lots of vugs and veining |
| TWP-B/7 | 2009 0025 | Large bleb of concretion on mudstone interface. |
| TWP-B/8 | 2009 0026 | Small pipe from zone of disseminated carbonate and mudstone. |
| TWP-B/9 | 2009 0027 | Highly veined carbonate from base of boulder. |
| TWP-B/10 | 2009 0028 | Concretionary material from trench, spongiform, burrows? Bioturbation? |
| TWP-C/1 | 2009 0029 | Fossiliferous boulder from between Zone C and E, similar to sample E/15, is this same bed of Bathymodiolin mussels? |
| TWP-C/2 | 2009 0030 | Further boulders from above C/1, similar, full of mussels. |
| TWP-C/3 | 2009 0031 | Weathered, brown micrite white aragonite veining. |
| TWP-C/4 | 2009 0032 | Worm tubes, latitudinal and longitudinal worm section. |
| TWP-C/5 | 2009 0033 | Quite weathered, brown micrite patches, worm tubes are infilled with cream white crystalline cement or dark micrite. |
| TWP-C/6 | 2009 0034 | Brown, grey matrix, and creamy crusts, infilled tubes. |
| TWP-C/7 | 2009 0035 | Creamy matrix well cemented worm tubes, infilled by dark micrite, some grey host rock left, mussels reappearing. |
| TWP-C/8 | 2009 0036 | Very brown sample, micrite fill, weathered worm tubes. |
| TWP-C/9 | 2009 0037 | Grey tortoise shell colour, creamy marble swirls or cement, worm tubes are lined by creamy carbonate crusts and infilled with dark detrital material or micrite. |
| TWP-C/10 | 2009 0038 | Light tan, some mussel indentations, worm tubes are filled with micrite, some zones of siliciclastics. |
| TWP-C/11 | 2009 0039 | Light tan, worm tubes, micrite and siliciclastic fill, slightly more coarser grained than C/8. |
| TWP-C/12 | 2009 0040 | Light tan, grey small drusy vugs, worm tubes, some host sediment clasts, rip up clasts? |
| TWP-C/13 | 2009 0041 | Creamy white, brown micrite, few infills of micrite, longer worm tubes, up to 4 cm long, seem to be arranged in similar orientation. |
| TWP-C/14 | 2009 0042 | Light- dark grey Microbrecciation and siliciclastic infill, some grains visible, vugs present, veining through sample. |
| TWP-C/15 | 2009 0043 | Grey tan, large worm tube and vugs and Microbrecciation along veins, Bathymodiolin mussels. |
| TWP-C/16 | 2009 0044 | Very hard and lithified, full of mussel shells, Bathymodiolin, matrix is dark-grey brown, coarse grained, mussels are up to 5 cm long. |
| TWP-C/17 | 2009 0045 | Long thin worm tubes, coarse grained cf. C/15 dark micrite fill in tubes, matrix is a creamy brown. |
| TWP-C/18 | 2009 0046 | Long, white mussels on edge, vary dark micrite internally, matrix has several worm tubes. |
| TWP-C/19 | 2009 0047 | Creamy brown some orange, weathering, <i>Calyptogena</i> ? Veining-oxidised, very brown matrix. |
| TWP-D/1 | 2009 0048 | From top boulder with mussel stuck firm, fluting or drilling marks on boulders, micritic or siliciclastic brown matrix, large Bathymodiolins up to 5 cm long, worm tubes are present, 1 boring into a mussel → exhumation and bioturbation post cementation? |

| | | |
|----------|-----------|--|
| TWP-D/2 | 2009 0049 | Pink/brown matrix, full of vugs and mussels, some shells have calcite ring and micrite infill, worm tubes less common. |
| TWP-D/3 | 2009 0050 | Many pink crystals, vugs lined with micrite rings, some odd weathering effects. |
| TWP-D/4 | 2009 0051 | Grey/brown matrix and worm tubes, micrite fill, carbonate lignin, some worm tubes are up to 4 mm thick. |
| TWP-D/5 | 2009 0052 | Dark brown micrite, plus creamy oatmeal matrix, some worm tubes are present, white and creamy vugs. |
| TWP-D/6 | 2009 0053 | Dark brown micrite, several patches. |
| TWP-D/7 | 2009 0054 | Marble cake layer, brown tan coloured matrix, some scattered worm tubes. |
| TWP-D/8 | 2009 0055 | Pink crystals, aragonite veins, dark micrite patches, infilled worm tubes. |
| TWP-D/9 | 2009 0056 | Smaller sample, similar to D/8, pink and grey micrite blebs, coarse grained. |
| TWP-D/10 | 2009 0057 | Pink matrix and crystalline grey zones, swirled through sample. Crystals and drusy vugs are common. |
| TWP-D/11 | 2009 0058 | Similar colouring to D/10, full of Bathymodiolin mussels, small scattering of worm tubes and vugs. |
| TWP-D/12 | 2009 0059 | Long calcareous worm tubes with crystalline pink infills, micrite interspersed with pink aragonite. |
| TWP-D/13 | 2009 0060 | Spongiform present, micritic blebs, slightly pinkish, some crystals, veining present. |
| TWP-D/14 | 2009 0061 | Marble oatmeal grey tan, cream more veined than other D samples, several worm tubes. |
| TWP-D/15 | 2009 0062 | Heaps of vugs, and worm tubes, vugs not really infilled with micrite, have a crystalline interior instead. |
| TWP-D/16 | 2009 0063 | A lot of worm tubes, some are in groups together, others are scattered or isolated, micrite matrix around tubes. |
| TWP-D/17 | 2009 0064 | A lot of little worm tubes, and larger ones infilled with micrite, most have calcareous lining, some zones of micrite infill and calcareous cement around them. |
| TWP-D/18 | 2009 0065 | Tube worms quite large, and filled with micrite cement, some calcareous tubes are creamy, others have crystalline pink fill. |
| TWP-D/19 | 2009 0066 | Oatmeal fabric and tubes filled with crystals, large pink infill crystals in shells and mussels. |
| TWP-D/20 | 2009 0067 | Micrite mottled with pink zones, also some dark laminae. |
| TWP-D/21 | 2009 0068 | Highly weathered carbonate clasts, blebs of micrite in creamy cement with worm tubes. |
| TWP-D/22 | 2009 0069 | Small sample, pink-brown cement. |
| TWP-E/1 | 2009 0070 | Large sample of creamy carbonate veins, with clasts of host mudstone. Some dark micrite zones and a large amount of worm tubes. Has large vugs with a yellow crystalline lining. |
| TWP-E/2 | 2009 0071 | Abundant worm tubes, similar to E/1, less micrite present, although worm tubes are partially infilled with dark micrite and partially with a pink crystalline cement. |
| TWP-E/3 | 2009 0072 | From top of section, abundant mussel fossils, large sparry vugs. |
| TWP-E/4 | 2009 0073 | Crystalline material, with some weathered patches and dark micrite in burrows. |

| | | |
|----------|-----------|--|
| TWP-E/5 | 2009 0074 | Large vuggy patches, sparry blebs and dark micrite. |
| TWP-E/6 | 2009 0075 | Heavily veined, weathered piece, worm tubes are infilled, veins are thin, and surrounded by a siliciclastic infill. |
| TWP-E/7 | 2009 0076 | Highly weathered block, vugs present. |
| TWP-E/8 | 2009 0077 | Worm tube rich facies. |
| TWP-E/9 | 2009 0078 | Aragonite veins though a micritic nodule. |
| TWP-E/10 | 2009 0079 | Aragonitic, crystalline veined example. |
| TWP-E/11 | 2009 0080 | Crystalline, pink-grey sample, with many druses. Matrix is coarse grained. |
| TWP-E/12 | 2009 0081 | Highly weathered and highly veined sample. |
| TWP-E/13 | 2009 0082 | Aragonitic rich facies with dark micrite injections. |
| TWP-E/14 | 2009 0083 | Micritic slab with mussels. |
| TWP-E/15 | 2009 0084 | Light grey, mussel fossils, and worm tubes. Infill's of dark micrite. |
| TWP-E/16 | 2009 0085 | Large, low angled slab, pink-grey micrite above E section. |
| TWP-E/17 | 2009 0086 | Mussel rich facies. |
| TWP-E/18 | 2009 0087 | Veined sample with rehealed carbonate. |
| TWP-E/19 | 2009 0088 | Micritic sample, many vugs. |
| TWP-E/20 | 2009 0089 | Large veined sample, multi-generations of cement – aragonite layers with pink laminae interspersed with dark microbial laminae? And injection zones of siliciclastic or detrital material. |
| TWP-E/21 | 2009 0090 | Rehealed carbonate slab. |
| TWP-E/22 | 2009 0091 | Aragonitic crusts in micritic sample. |
| TWP-E/23 | 2009 0092 | Aragonitic dominated hand specimen with zones of patchy micrite. |

NOTE: *Images of slabbed samples and hand samples are available on the Appendices disk.*

Appendix A1.2 Full sample list of seep-carbonates analysed from NIWA Cruise TAN0616. The ‘UoW’ number is the sample number logged in the PET database. Note that Dashed (-) lines are in places where data is unavailable for the samples, and that blue shaded samples were analysed in this study.

| Sample | UoW number | Stratum | NIWA sample |
|--------|------------|------------------|-------------|
| MOD-1 | 2009 0100 | Builders Pencil | - |
| MOD-2 | 2009 0101 | East Uruti Ridge | 1047 |
| MOD-3a | 2009 0102 | Builders Pencil | 730 |
| MOD-3b | 2009 0103 | Builders Pencil | 730 |
| MOD-4 | 2009 0104 | Rock Garden | - |
| MOD-5 | 2009 0105 | Rock Garden | - |
| MOD-6 | 2009 0106 | South Tower | 1201 |
| MOD-7 | 2009 0107 | South Tower | 1162 |
| MOD-8 | 2009 0108 | Rock Garden | 216 |
| MOD-9 | 2009 0109 | Builders Pencil | 730 |
| MOD-10 | 2009 0110 | - | - |
| MOD-11 | 2009 0111 | Builders Pencil | 473 |
| MOD-12 | 2009 0112 | - | - |
| MOD-13 | 2009 0113 | North Tower | - |

Appendix A1.3 Further information for samples studied in detail, i.e. samples from northern areas.

| Sample | Location | Sample Station | Depth Range (m) |
|---------|-----------------|----------------|-----------------|
| MOD-1* | Builders Pencil | - | - |
| MOD-3 | Builders Pencil | 38 | 815-819 |
| MOD-4 | Rock Garden | 12 | 749-787 |
| MOD-5 | Rock Garden | 12 | 749-787 |
| MOD-8 | Rock Garden | 10 | 700-760 |
| MOD-9 | Builder Pencil | 38 | 815-819 |
| MOD-10^ | - | - | - |
| MOD-11 | Builders Pencil | 25 | 786-810 |

* **Note:** MOD-1 was donated by a fisherman, so exact sampling data is not available, but sample is believed to be form around Builders Pencil area.

^ **Note:** MOD-10 had lost its identification in the NIWA storage facility, but the sample was amongst others from Builders Pencil and Rock Garden.

Appendix A1.4 Cruise data for sample transects (sample stations) where studied samples were obtained. Cruise data is courtesy of NIWA. (Cruise TAN0616). Note that Latitude and longitude measurements are in degrees and minutes.

| Transect Station | Location | Samples acquired | Depth Range (m) | Heading (°) | Sampling Method |
|------------------|-----------------|------------------|-----------------|-------------|-----------------|
| 10 | Rock Garden | MOD-8 | 700 - 760 | 54 | Grab |
| 12 | Rock Garden | MOD-4, -5 | 749 - 787 | 141 | Grab |
| 25 | Builders Pencil | MOD-11 | 786 - 810 | 42 | Grab |
| 38 | Builders Pencil | MOD-3, -9 | 815 - 819 | 264 | Grab |

| Transect Station | Transect Start | | Transect Finish | | Distance (km) |
|------------------|----------------|-----------|-----------------|-----------|---------------|
| | Latitude | Longitude | Latitude | Longitude | |
| 10 | 400239 | 1780855 E | 400222 | 1780886 E | 0.29 |
| 12 | 400242 | 1780867 E | 400265 | 1780891 E | 0.29 |
| 25 | 393828 | 1781971 E | 393264 | 1781992 E | 0.24 |
| 38 | 393260 | 1782019 E | 393265 | 1781962 E | 0.44 |

Appendix 2

Tauwharepareae Laboratory Data

Appendix A2.1 Stable $\delta^{13}\text{C}$ and $\delta^{18}\text{O}$ isotope data for TWP seep carbonate components.

| Sample | $\delta^{13}\text{C}\text{\% PDB}$ | $\delta^{18}\text{O}\text{\% PDB}$ | Component |
|----------|------------------------------------|------------------------------------|-----------------------|
| TWP-A5a | -38.805 | -2.944 | Neomorphosed phase |
| TWP-A5b | -42.977 | 0.695 | Siliciclastic calcite |
| TWP-A6a | -38.87 | -4.241 | Neomorphosed phase |
| TWP-A6b | -41.706 | -2.913 | Neomorphosed phase |
| TWP-A6c | -28.371 | -3.574 | Siliciclastic calcite |
| TWP-A6d | -45.207 | 0.547 | Neomorphosed phase |
| TWP-A6e | -42.291 | -4.675 | Neomorphosed phase |
| TWP-A10a | -46.724 | 1.388 | Neomorphosed phase |
| TWP-A10b | -40.03 | -1.771 | Aragonitic micarb |
| TWP-A10c | -24.338 | -4.333 | Siliciclastic calcite |
| TWP-A12a | -38.625 | -4.201 | Siliciclastic calcite |
| TWP-A12b | -36.244 | -4.691 | Neomorphosed phase |
| TWP-A12c | -32.942 | -5.156 | Siliciclastic calcite |
| TWP-A16a | -39.197 | -3.628 | Aragonitic micarb |
| TWP-A16b | -38.592 | -4.242 | Aragonitic micarb |
| TWP-A16c | -44.104 | 1.234 | Acicular aragonite |
| TWP-A16d | -38.502 | -5.009 | Siliciclastic calcite |
| TWP-A16e | -43.525 | 0.536 | Siliciclastic calcite |
| TWP-E4a | -37.445 | -5.045 | Botryoidal aragonite |
| TWP-E4b | -38.27 | -5.05 | Aragonitic micarb |
| TWP-A17a | -49.991 | 0.693 | Neomorphosed phase |
| TWP-A17b | -41.157 | -3.373 | Siliciclastic calcite |
| TWP-A17c | -42.205 | 0.695 | Acicular aragonite |
| TWP-B9a | -36.898 | -3.405 | Neomorphosed phase |
| TWP-B9b | -47.129 | 1.682 | Neomorphosed phase |
| TWP-B9c | -30.055 | -4.556 | Siliciclastic calcite |
| TWP-B10a | -50.567 | 1.871 | Acicular aragonite |
| TWP-B10b | -38.506 | -1.749 | Neomorphosed phase |
| TWP-B10c | -35.373 | -2.848 | Siliciclastic calcite |
| TWP-C2a | -28.996 | 0.607 | Shell |
| TWP-C2b | -44.457 | 0.932 | Aragonitic micarb |
| TWP-C2c | -45.018 | 0.729 | Acicular aragonite |
| TWP-C2d | -48.141 | 2.08 | Acicular aragonite |
| TWP-C13a | -45.738 | -4.158 | Acicular aragonite |
| TWP-C13b | -41.26 | -4.958 | Siliciclastic calcite |
| TWP-C13c | -41.051 | -4.599 | Siliciclastic calcite |

| | | | |
|----------|---------|--------|-----------------------|
| TWP-C13d | -48.385 | 1.104 | Acicular aragonite |
| TWP-C16a | -45.172 | -1.866 | Acicular aragonite |
| TWP-C16b | -48.427 | 1.602 | Acicular aragonite |
| TWP-C16c | -41.86 | -2.84 | Siliciclastic calcite |
| TWP-C16d | -29.194 | 1.684 | Shell |
| TWP-D4a | -46.684 | 1.453 | Spherulitic aragonite |
| TWP-D4b | -47.691 | 1.516 | Aragonitic micarb |
| TWP-D4c | -42.348 | -4.213 | Siliciclastic calcite |
| TWP-D15a | -8.97 | 0.53 | Siliciclastic calcite |
| TWP-D15b | -40.7 | -4.01 | Acicular aragonite |
| TWP-D20a | -32.23 | -4.34 | Botryoidal aragonite |
| TWP-D20b | -37.74 | -4.09 | Siliciclastic calcite |

Appendix A2.2 XRD bulk mineralogy results. Key: A- abundant; C- common; S- some; R- rare; (-) absent. Amounts are relative abundance as determined by graphed XRD peak intensities (see Chapter 4).

| Sample | Aragonite | LMC | HMC | Quartz | Plagioclase | Clays |
|----------|-----------|-----|-----|--------|-------------|-------|
| TWP-A/10 | S | A | - | C | S | R |
| TWP-A/12 | R | A | - | S | R | S |
| TWP-A/14 | C | C | - | C | S | R |
| TWP-A/16 | C | C | - | C | C | R |
| TWP-A/17 | C | A | - | R | R | C |
| TWP-A/4 | - | A | - | A | R | R |
| TWP-B/1 | S | A | - | C | R | S |
| TWP-B/9 | C | A | S | S | S | S |
| TWP-C/1 | A | A | - | S | R | S |
| TWP-C/13 | A | C | S | S | S | R |
| TWP-C/14 | A | C | - | S | R | R |
| TWP-C/17 | A | C | - | S | S | R |
| TWP-C/18 | A | A | - | C | S | S |
| TWP-C/2 | A | C | - | C | S | C |
| TWP-C/5 | A | C | - | C | R | - |
| TWP-C/7 | C | C | - | C | C | R |
| TWP-C/9 | C | A | - | S | C | R |
| TWP-D/1 | A | C | - | S | R | - |
| TWP-D/15 | - | A | - | C | S | S |
| TWP-D/16 | A | C | - | S | S | - |
| TWP-D/20 | C | A | - | C | S | - |
| TWP-D/4 | A | C | - | S | R | - |
| TWP-E/14 | C | A | - | R | - | - |
| TWP-E/4 | R | A | - | R | - | - |
| TWP-E/8 | C | A | - | S | S | R |

NOTE:

A representative selection of XRD graphs from TWP seep-carbonates are found below, for the entire selection of the ancient XRD graphs refer to TWP folder on the Appendices Disk.

Figure A2.1 XRD graph for sample TWP-A/4 showing characteristic mineralogy peaks; Q – Quartz; P – Plagioclase; C – Calcite.

Figure A2.2 XRD graph for sample TWP-C/7 showing characteristic mineralogy peaks; Q – quartz; P – Plagioclase; C – Calcite; A – Aragonite.

Figure A2.3 XRD graph for sample TWP-D/4 showing characteristic mineralogy peaks; Q – Quartz; C – Calcite.

Figure A2.4 XRD graph for sample TWP-C/16 showing characteristic mineralogy peaks; Q – Quartz; C – Calcite; A – Aragonite.

Appendix A2.3 Results from GADDs component specific mineralogical analysis.

| Thin Section | Point | Mineralogy |
|---------------------|--------------|-------------------------|
| TWP-D/4b | D/4b-1 | Calcite |
| | D/4b-2 | Calcite |
| | D/4b-3 | Aragonite |
| | D/4b-4 | Aragonite |
| TWP-C/9b | C/9b-1 | Calcite |
| TWP-A/6a | A/6a-1 | Calcite |
| | A/6a-2 | Calcite |
| | A/6a-3 | Calcite |
| TWP-D/20 | D/20a-1 | Calcite + clays |
| | D/20a-2 | Altered aragonite |
| | D/20a-3 | Aragonite minor |
| TWP-C/2b | C/2b-1 | Calcite + quartz |
| | C/2b-3 | Aragonite + calcite |
| | C/2b-4 | Quartz + calcite + clay |
| | C/2b-6 | Aragonite |
| | C/2b-5 | Aragonite |
| | C/2b-2 | Calcite + quartz |
| TWP-C/1 | C/1-1 | Aragonite |
| | C/1-2 | Aragonite |
| | C/1-3 | Calcite |
| | C/1-4 | Aragonitic micarb |
| | C/1-5 | Calcite |
| TWP-D/4a | D/4a-1 | Aragonite |
| | D/4a-2 | Aragonite |
| | D/4a-3 | Calcite |
| | D/4a-4 | Aragonite |
| | D/4a-5 | Aragonitic micarb |
| | D/4a-6 | Calcite |

NOTE:

A representative selection of GADDs XRD graphs from TWP seep-carbonates are found below, for the entire selection of the ancient XRD graphs refer to TWP folder on the Appendices Disk. Also available on the disk are the images of the point analysis.

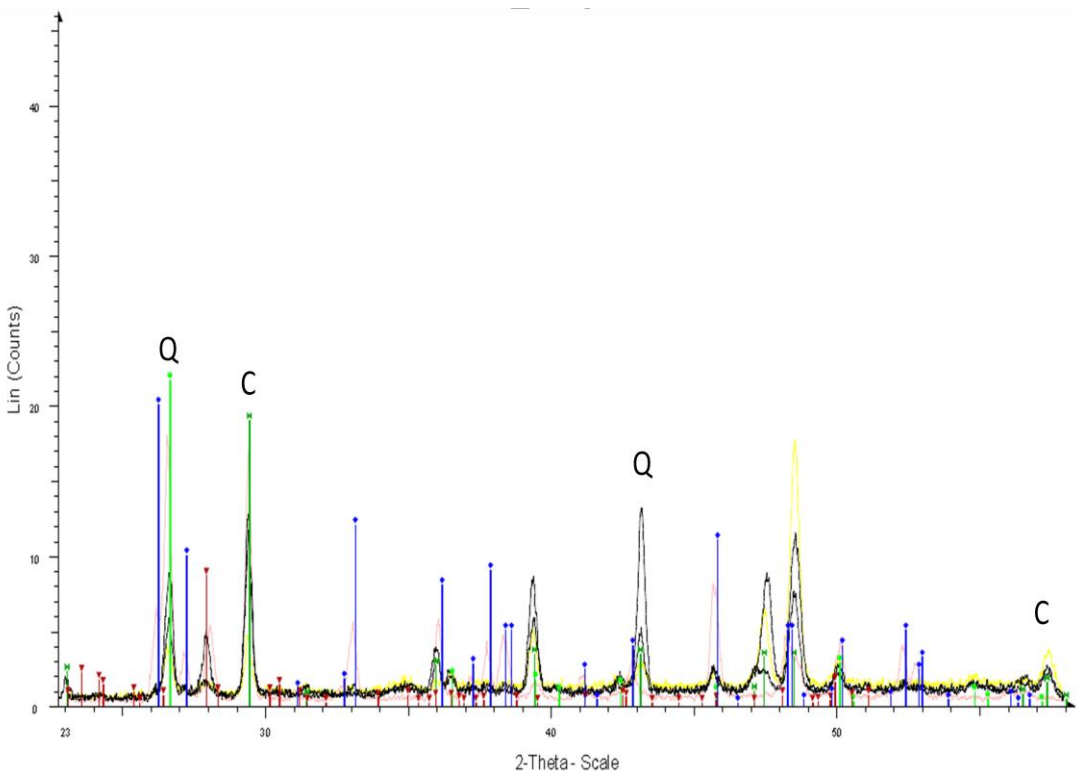


Figure A2.5 Mineralogy peak graph obtained from GADDs analysis on siliciclastic calcite phases in TWP seep-carbonates; C – Calcite; Q – Quartz.

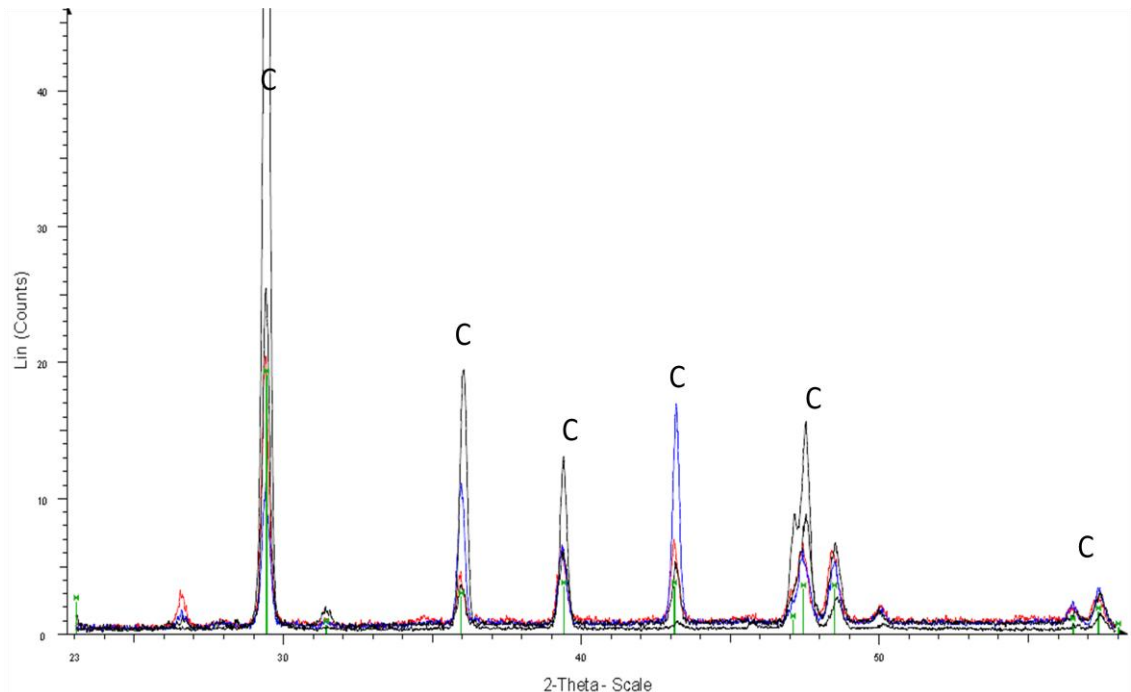


Figure A2.6 Mineralogy peak graph obtained from GADDs analysis on calcite phases in TWP seep-carbonates; C – Calcite.

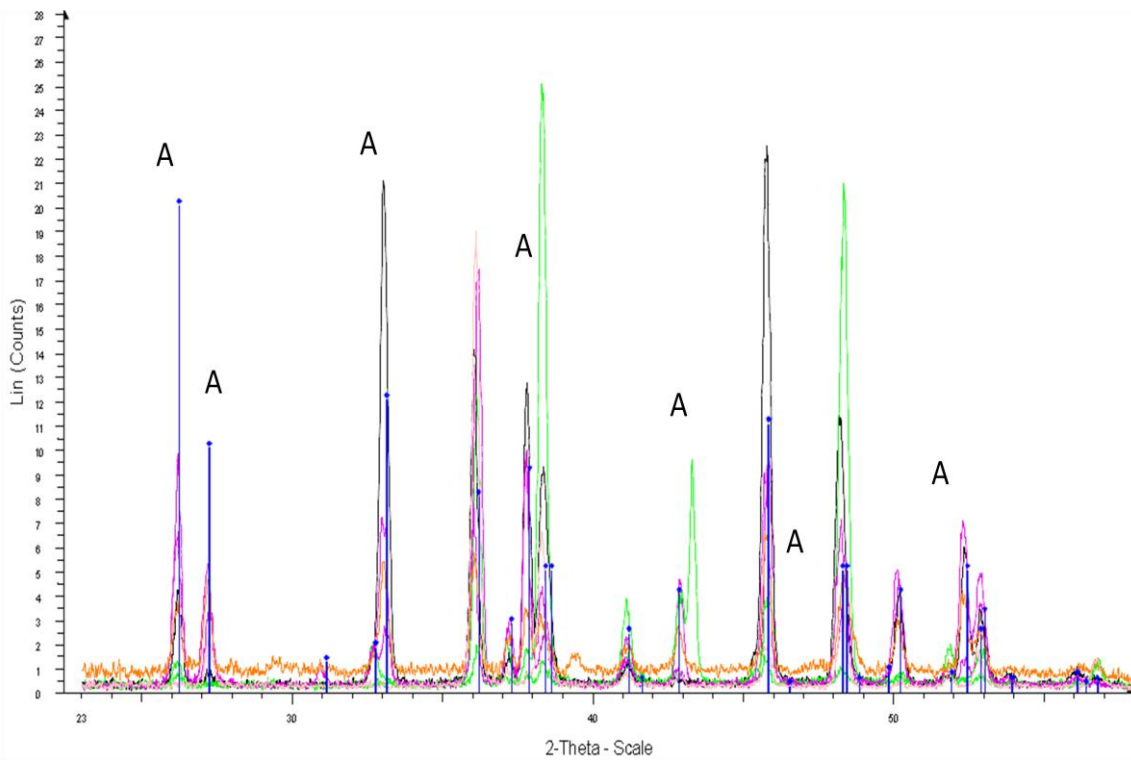


Figure A2.7 Mineralogy peak graph obtained from GADDs analysis on aragonite phases in TWP seep-carbonates; A – Aragonite.

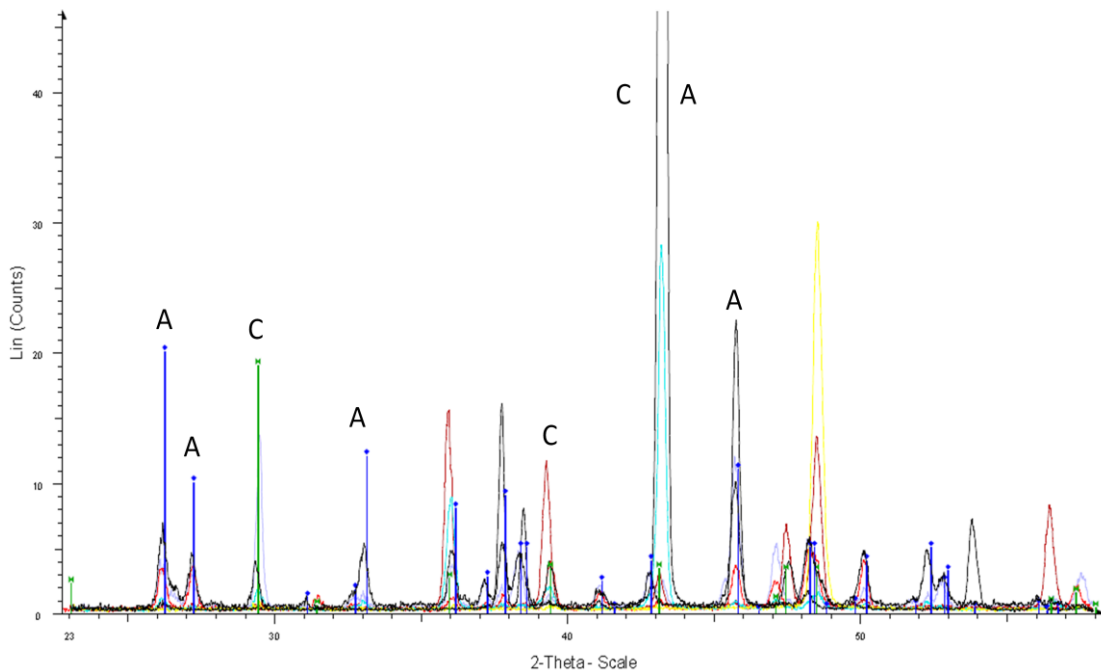


Figure A2.8 Mineralogy peak graph obtained from GADDs analysis on neomorphosed aragonite phases in TWP seep-carbonates; A – Aragonite; C – Calcite.

Appendix A2.4 Microprobe analysis, raw data as weight (%) oxides for selected phases from the TWP seep-carbonates.

| SAMPLE | PHASE | SiO ₂ | Al ₂ O ₃ | FeO | MnO | MgO | CaO | SrO | Na ₂ O | K ₂ O | Cl |
|-------------|-----------------------|------------------|--------------------------------|-------|-------|-------|-------|-------|-------------------|------------------|-------|
| TWP-C/1 1 | Acicular aragonite | - | -0.07 | -0.02 | 0.04 | 0.82 | 53.49 | 0.06 | 0.22 | 0.09 | 0.03 |
| TWP-C/1 2 | Acicular aragonite | - | 0.01 | 0.14 | 0.05 | 0.04 | 54.54 | 1.22 | 0.30 | 0.06 | -0.03 |
| TWP-C/2b 1a | Acicular aragonite | - | -0.05 | -0.02 | -0.10 | -0.01 | 53.27 | 0.89 | 0.39 | 0.04 | 0.03 |
| TWP-C/2b 1b | Detrital calcite | 1.56 | 0.36 | 0.65 | 0.13 | 0.82 | 51.21 | - | 0.12 | 0.19 | -0.02 |
| TWP-C/2b 1c | Detrital calcite | 0.37 | 0.10 | 0.56 | 0.13 | 0.79 | 53.06 | - | 0.10 | 0.13 | 0.03 |
| TWP-C/2b 2a | Detrital calcite | - | -0.07 | 0.13 | 0.03 | -0.03 | 53.71 | 1.07 | 0.19 | 0.05 | 0.03 |
| TWP-C/2b 3a | Arag micarb peloid | 3.79 | 2.59 | 0.56 | -0.01 | 0.29 | 47.47 | - | 0.10 | 0.61 | 0.08 |
| TWP-C/2b 3b | Arag micarb peloid | 4.36 | 2.22 | 0.64 | -0.04 | 0.39 | 45.20 | - | 0.34 | 0.58 | 0.11 |
| TWP-C/9b 1 | Cellular calcite | 6.13 | 2.39 | 0.64 | 0.12 | 0.76 | 45.33 | - | 0.32 | 0.37 | 0.05 |
| TWP-C/9b 2 | Equant calcite | - | 0.00 | 0.02 | -0.01 | 0.06 | 48.79 | 1.56 | 0.20 | 0.09 | 0.06 |
| TWP-D/4b 1 | Acicular aragonite | - | -0.08 | -0.05 | -0.03 | 0.10 | 55.00 | 1.18 | 0.30 | 0.06 | -0.03 |
| TWP-D/4b 2 | Neomorphism | 0.52 | 0.24 | 0.32 | 0.00 | 1.24 | 53.01 | - | 0.01 | 0.16 | -0.03 |
| TWP-D/4b 3 | Neomorphic front | - | -0.13 | 0.25 | 0.03 | 1.14 | 54.18 | - | 0.01 | 0.07 | 0.02 |
| TWP-D/4b 4 | Equant calcite | - | 0.00 | 0.05 | 0.05 | 1.15 | 54.82 | 0.05 | -0.02 | 0.06 | 0.06 |
| TWP-D/4b 5 | Burrow | - | -0.05 | 0.03 | -0.05 | 0.77 | 54.27 | 0.27 | 0.12 | 0.01 | 0.03 |
| TWP-D/4b 8 | Aragonitic micarb | - | 3.94 | 0.09 | 0.01 | 0.22 | 49.70 | 1.15 | 0.28 | 0.23 | 0.07 |
| TWP-D/4b 6 | Acicular aragonite | - | 0.00 | 0.11 | -0.02 | 1.15 | 53.64 | 0.17 | 0.05 | 0.11 | 0.00 |
| TWP-D/4b 7 | Aragonitic micarb | - | -0.05 | 0.14 | -0.08 | -0.04 | 55.06 | 0.93 | 0.26 | 0.09 | -0.01 |
| TWP-D/20 1 | Botryoidal aragonite | - | 0.04 | -0.02 | -0.11 | 0.55 | 54.12 | 0.11 | 0.15 | 0.03 | 0.01 |
| TWP-D/20 2 | Detrital calcite | - | 0.03 | 0.33 | -0.07 | 1.21 | 54.02 | 0.24 | 0.01 | 0.09 | 0.02 |
| TWP-D/20 3 | Acicular aragonite | - | -0.03 | 0.23 | -0.02 | 0.99 | 55.70 | 0.33 | 0.00 | 0.06 | 0.01 |
| TWP-A/6a 1 | Cellular calcite | - | 0.01 | 0.03 | -0.04 | 0.96 | 54.87 | -0.01 | 0.15 | 0.04 | 0.01 |
| TWP-A/6a 2 | Pervasive neomorphism | 3.24 | 1.54 | 0.42 | -0.01 | 0.69 | 50.19 | - | 0.14 | 0.31 | 0.01 |
| TWP-A/6a 3 | Pervasive neomorphism | - | -0.04 | 0.18 | -0.06 | 0.87 | 55.41 | 0.06 | 0.09 | 0.01 | -0.04 |

Appendix 3

Modern Laboratory Data

Appendix A3.1 Stable $\delta^{13}\text{C}$ and $\delta^{18}\text{O}$ isotope values for modern Ritchie Ridge seep-carbonates. Note that samples that are shaded in blue were analysed in this study.

| Sample No | Location | $\delta^{13}\text{C} \text{ ‰ PDB}$ | $\delta^{18}\text{O} \text{ ‰ PDB}$ |
|-----------|------------------|-------------------------------------|-------------------------------------|
| MOD-1 | Builders Pencil | -37.08 | 3.64 |
| MOD-2A | East Uruti Ridge | -47.13 | 2.87 |
| MOD-2 B | East Uruti Ridge | -47.18 | 2.87 |
| MOD-2 C | East Uruti Ridge | -46.88 | 2.71 |
| MOD-3 A | Builders Pencil | -39.08 | 6.21 |
| MOD-3 B | Builders Pencil | -37.35 | 6.06 |
| MOD-3 C | Builders Pencil | -38.45 | 6.01 |
| MOD-3 D | Builders Pencil | -38.29 | 6.1 |
| MOD-3 E | Builders Pencil | -39.06 | 6.17 |
| MOD-4 | Rock Garden | -41.57 | 3.75 |
| MOD-5 A | Rock Garden | -38.56 | 2.65 |
| MOD-5 B | Rock Garden | -34.14 | 2.7 |
| MOD-6 | South Tower | -45.76 | 3.15 |
| MOD-7 | South Tower | -46.06 | 3.83 |
| MOD-8 | Rock Garden | -5.44 | 6.74 |
| MOD-9 A | Builders Pencil | -21.41 | 5.29 |
| MOD-10 | Builders Pencil | -20.27 | 5.45 |
| MOD-11 | Builders Pencil | -15.59 | 5.53 |
| MOD-13 | North Tower | -49.75 | 4.27 |

Appendix A3.2 XRD bulk mineralogy results for modern Ritchie Ridge seep-carbonates, blue shaded sample were analysed in detail in this study. Key: A- abundant; C- common; S- some; R- rare; (-) absent. Amounts are relative abundance as determined by graphed XRD peak intensities (see Chapter 4).

| Sample | Aragonite | LMC | HMC | Dolomite | Quartz | Plagioclase | Clays |
|--------|-----------|-----|-----|----------|--------|-------------|-------|
| UoW1 | A | C | - | - | S | - | S |
| UoW2a | A | C | - | - | S | R | S |
| UoW2b | A | S | - | - | S | - | S |
| UoW2c | A | S | - | - | S | - | S |
| UoW3a | - | R | - | A | C | S | S |
| UoW3b | - | - | - | A | C | S | S |
| UoW3c | - | R | - | A | C | S | S |
| UoW3d | - | R | - | A | C | S | S |
| UoW3e | - | R | - | A | C | S | S |
| UoW4 | A | S | - | - | S | R | S |
| UoW5a | A | C | - | - | S | S | S |
| UoW5b | A | - | - | - | - | R | S |
| UoW6 | A | - | - | R | C | C | S |
| UoW7 | - | S | C | R? | C | C | S |
| UoW8 | - | - | - | A | S | - | S |
| UoW9a | - | C | S | A | C | S | S |
| UoW10 | - | - | - | A | A | S | S |
| UoW11 | - | - | - | A | C | S | S |
| UoW13 | - | A | C | - | C | S | S |

NOTE:

A representative selection of XRD graphs from the Ritchie Ridge seep-carbonates are found below, for the entire selection of the modern XRD graphs refer to MOD folder on the Appendices Disk.

Figure A3.1 XRD graph for sample MOD-1 showing characteristic mineralogy peaks; Q – Quartz; A – Aragonite; C – Calcite.

Figure A3.2 XRD graph for sample MOD-5A showing characteristic mineralogy peaks; A – Aragonite; P – Plagioclase.

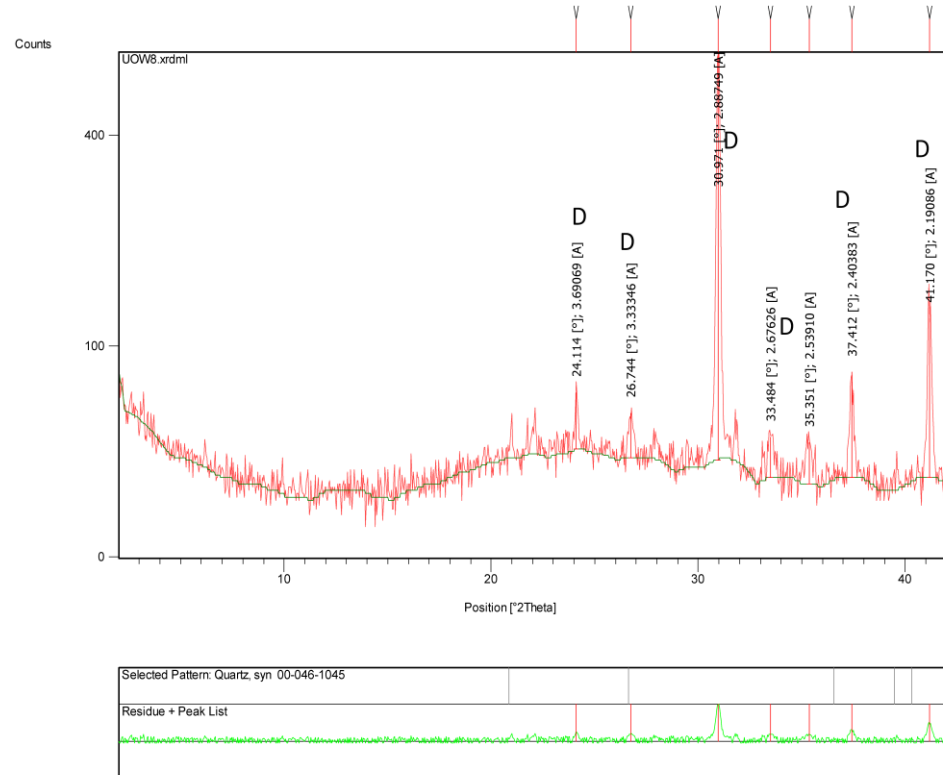


Figure A3.3 XRD graph for sample MOD-8 showing characteristic mineralogy peaks; D – Dolomite.

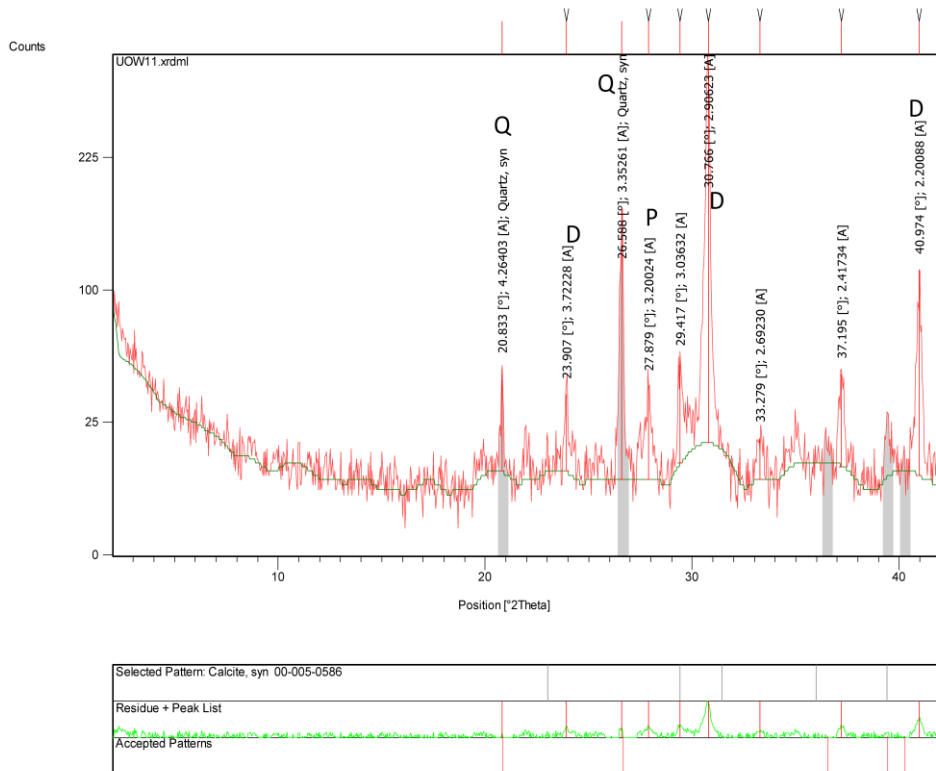


Figure A3.4 XRD graph for sample MOD-11 showing characteristic mineralogy peaks – D – Dolomite; Q – Quartz; P – Plagioclase.

Appendix A3.3 GADDs component specific mineralogical results.

| Sample | Mineralogy |
|---------|------------|
| MOD5a1 | Aragonite |
| MOD5a2 | Aragonite |
| MOD1b1 | Aragonite |
| MOD1b2 | Aragonite |
| MOD1b3 | Aragonite |
| MOD3Ab1 | Dolomite |
| MOD3Ab2 | Dolomite |
| MOD3Ab3 | Dolomite |
| MOD3Ab4 | Dolomite |
| MOD8-1 | Dolomite |
| MOD8-2 | Dolomite |
| MOD8-3 | Dolomite |
| MOD4a1 | Aragonite |
| MOD4a2 | Aragonite |

| | |
|---------|------------------|
| MOD4a3 | Calcite |
| MOD4a4 | Aragonite |
| MOD10a1 | Dolomite + clays |
| MOD10a2 | Dolomite + clays |
| MOD10a3 | Ankerite |

NOTE:

A representative selection of GADDs XRD graphs from the Ritchie Ridge seep-carbonates are found below, for the entire selection of the modern graphs refer to MOD folder on the Appendices Disk. Also available on the disk are the images of the point analysis.

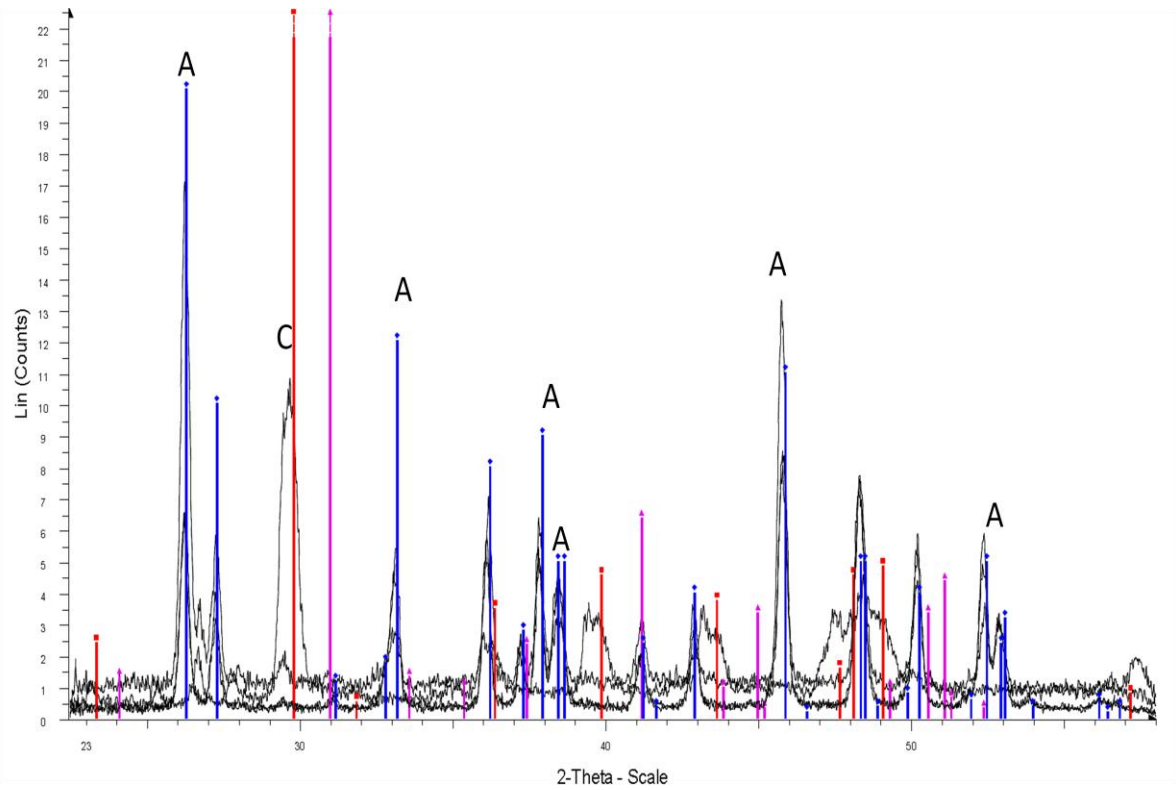


Figure A3.5 Mineralogy peak graph obtained from GADDs analysis on aragonitic Ritchie Ridge seep-carbonates; A – Aragonite, blue vertical lines; C – Calcite, red vertical lines.

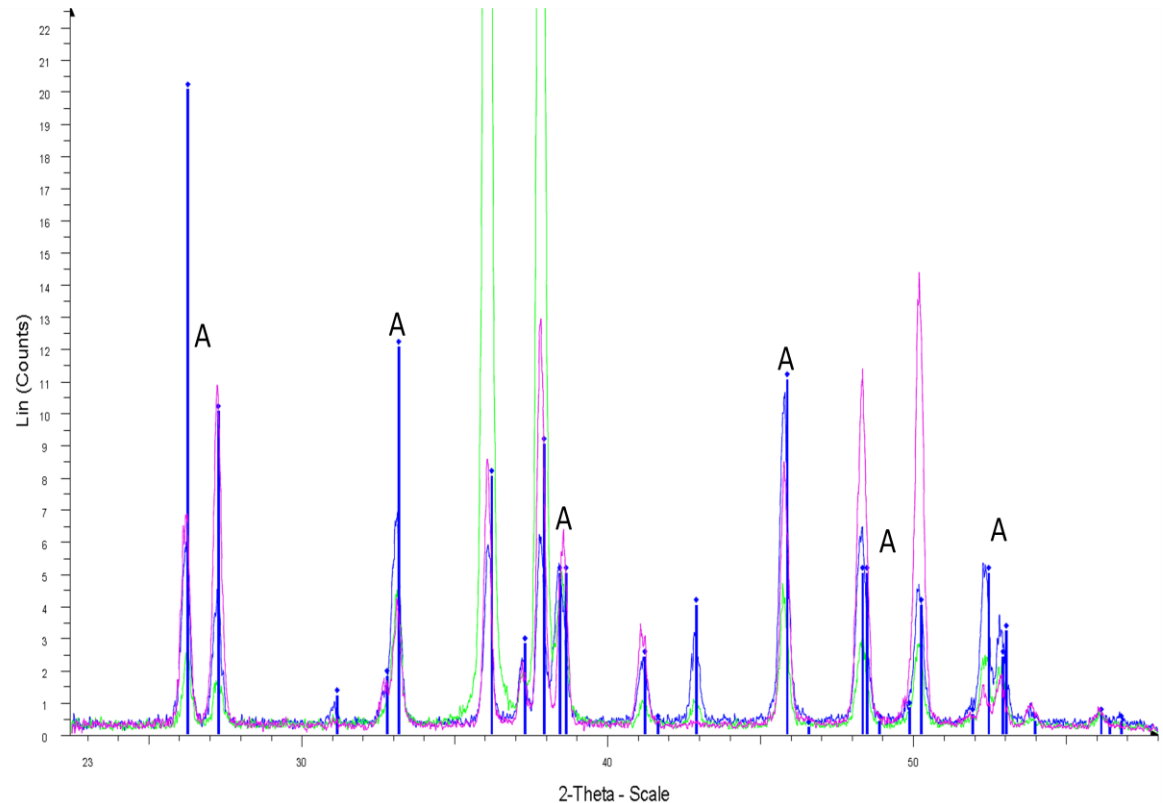


Figure A3.6 Mineralogy peak graph obtained from GADDs analysis on aragonitic Ritchie Ridge seep-carbonate; A – Aragonite, blue vertical lines.

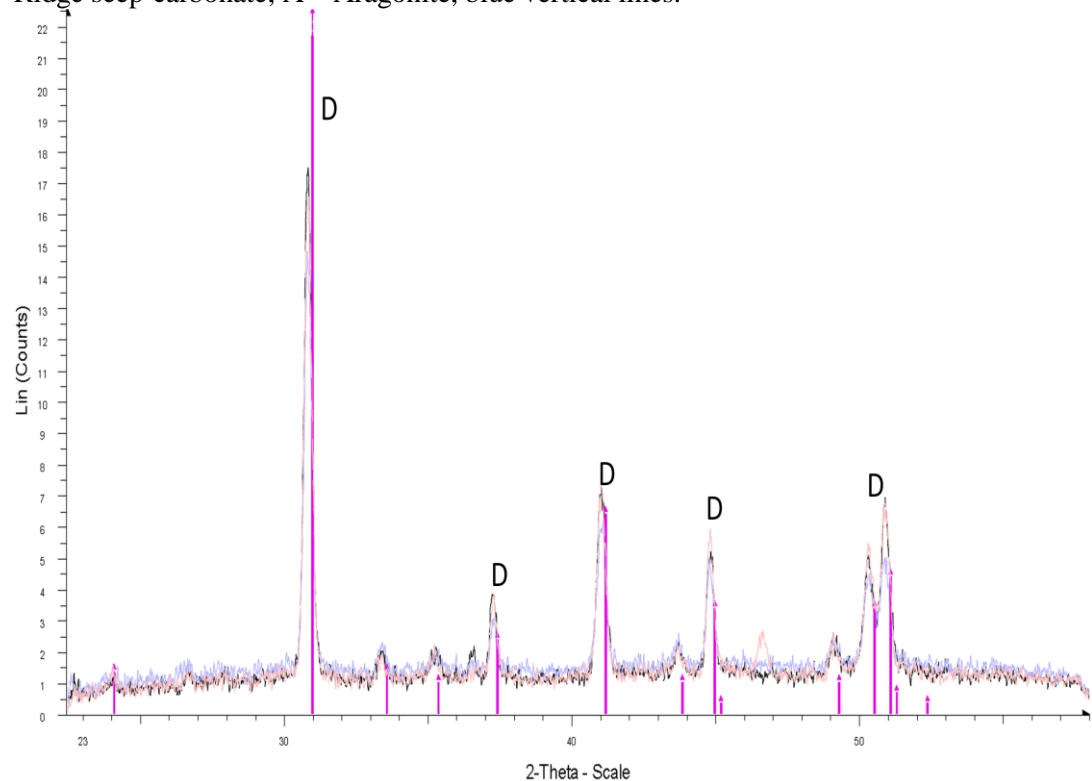


Figure A3.7 Mineralogy peak graph obtained from GADDs analysis on dolomitic Ritchie Ridge seep-carbonates; D – Dolomite, cerise vertical lines.

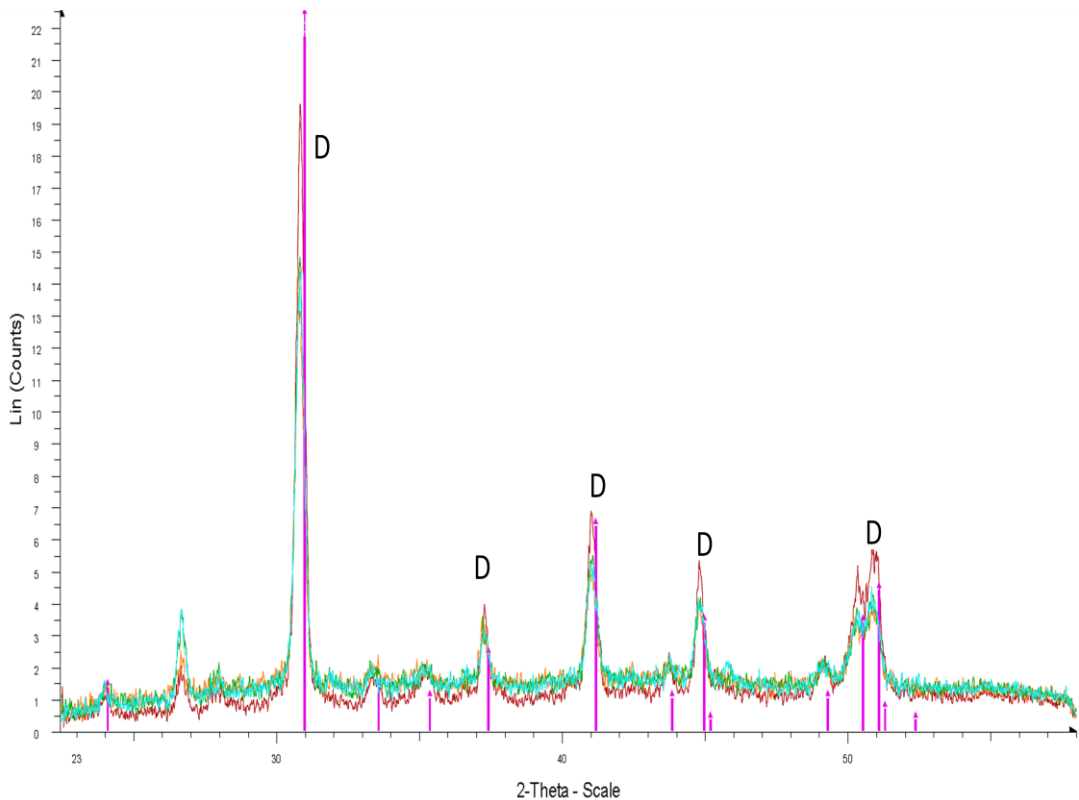


Figure A3.8 Mineralogy peak graph obtained from GADDs analysis on dolomitic Ritchie Ridge seep-carbonates; D – Dolomite, cerise vertical lines.

Appendix A3.4 Microprobe analysis, raw data as weight (%) oxides for selected fabrics of modern Ritchie Ridge seep-carbonates.

| Phase | SiO ₂ | Al ₂ O ₃ | FeO | MnO | MgO | CaO | SrO | Na ₂ O | K ₂ O | Cl | Total |
|-----------|------------------|--------------------------------|-------|-------|-------|-------|------|-------------------|------------------|-------|-------|
| Dolomite | 5.48 | 3.31 | 0.61 | -0.01 | 18.22 | 27.09 | - | 0.18 | 0.93 | 0.01 | 55.82 |
| Dolomite | 4.04 | 1.5 | 0.78 | 0.01 | 14.9 | 26.28 | - | 0.11 | 0.26 | 0.22 | 48.1 |
| Dolomite | 3.41 | 1.56 | 0.67 | 0.16 | 16.64 | 26.3 | - | 0.3 | 0.29 | 0.17 | 49.5 |
| Dolomite | 0.83 | 0.37 | 0.1 | 0.02 | 19.77 | 29.82 | - | 0.1 | 0.18 | 0.14 | 51.33 |
| Dolomite | 0.83 | 0.37 | 0.1 | 0.02 | 19.77 | 29.82 | - | 0.1 | 0.18 | 0.14 | 51.33 |
| Dolomite | 4.19 | 1.5 | 0.49 | 0.03 | 17.15 | 28.54 | - | 0.32 | 0.35 | 0.25 | 52.82 |
| Aragonite | - | -0.05 | -0.04 | 0.04 | -0.05 | 53.27 | 0.2 | 0.76 | 0.07 | 0.14 | 54.34 |
| Aragonite | - | -0.12 | 0 | -0.05 | -0.01 | 54.67 | 0.73 | 0.16 | 0.07 | -0.01 | 55.44 |
| Aragonite | - | -0.06 | -0.03 | -0.04 | 0.04 | 54.19 | 1.1 | 0.39 | 0.05 | -0.02 | 55.62 |
| Aragonite | - | -0.05 | 0.11 | -0.03 | 0.06 | 53.82 | 1.48 | 0.29 | 0.08 | 0.03 | 55.79 |
| Aragonite | 0.08 | 0.04 | 0.07 | 0.01 | 0.17 | 0.35 | - | 0 | -0.19 | -0.05 | 0.48 |
| Aragonite | - | -0.05 | 0.03 | 0.07 | 0.07 | 53.92 | 1.11 | 0.34 | 0.09 | 0.08 | 55.66 |

Appendix 4

Additional Information

Appendix A4.1 Additional seep-carbonate deposits in the East Coast Basin of the North Island. Grid reference (GR) are given, and landowner information, as well as information about the seep-phenomena at the site.

| Site | GR | Nature/Description | Landowners |
|-----------------------------|----------------------|---|--|
| Bexhaven | Y16 | Scattered boulders on left | N/A |
| BXH | 2955810E 6333127N | hand side of road. Common marble cake texture, plus fossil beds. | |
| Karikarihuata Stream | Y16 2965700E | Large carbonate mound high on cliff, with mudstone and carbonate beds up stream. | Forest Block - Managers Leigh and Sheree Phillips Gate - 56.5km along road |
| KKH | 6335100N | | |
| Moonlight North | Y16 | Large volume of material, 2 main sites. Outcrop \leq 10 m thick. Micritic marble cake, plus fine micrite dominates. | Olsen Forestry 06 |
| MLN | 2943343E 6314003N | Odd fossil beds. | 8685426 396 Childers Rd, Gisborne |
| Rocky Knob | Y16 | large amounts of ls, varying facies. Cross | Olsen Forestry |
| RKN | 2941200E 6310300N | bedding present, plus several dominant fossil types. Largest outcrop in NZ. | 06 8685426 396 Childers Rd, Gisborne |
| Tauwhareparae | Y16 | Carbonate mound underlain by plumbing tubes and host | Scotty and Margo |
| TWP | 2946283E 6324166N | mudstone. Shows prevalent bioturbation, brecciation and fossil beds. | Wallace 06 8638944 |
| Totaranui | Y16 | Several small outcrops of | Olsen Forestry |
| Upper Waiau River | 2960605E 6319160N | seep-carbonate, difficult access however. | 06 8685426 396 Childers Rd, Gisborne |
| TTN | | | |
| Turihaua | Y18 | Small fossiliferous | Hamish and Angela |
| | 2958065E 6274500N | boulders. | Williams. 06 868 8421 |

| | | | |
|----------------------------------|-----------------------------|---|---|
| Waitangi | Y17 2938359E 6306206N | Series of 6 oil seeps along a fault along hill side. Seepage varies, dependent on water table level and activity in region. Source: Whangai Fm - marine source. | N/A |
| Haunui HAU | 2807322E 6104425N | Large pine covered mound, abundant fossil material. Siliciclastic rich facies, with varying amounts of micritic cements. Large amounts of burrows present at this site. | James and Sue Hewitt 348 Haunui Epae Rd 06 8554947 |
| Ngawaka NGW | 2803946E 6107468N | Several outcrops across 4 adjoining paddocks. Fossil material varies spatially. Main outcrop has undergone high amount of brecciation, and evidence of veining is seen throughout. | Ngawaka North - Richard Barrett 06 8554846 Ngawaka South - Marcus and Jeanette Louisson 06 8554738 |
| Ugly Hill North | 2809905E 6107090N | Collection of boulders in valley below house. Mix of facies, fossil rich. Some boulders display a variety of cement phases and crystal rich vugs. | Maggie and Tim Simcock Ugly Hill Road 06 8554731 |
| Ugly Hill South | 2809402E 6107203N | Outcrops are restricted to small boulders on higher areas, and small quarry in pines. Whale bones in several samples. | Paul Deardon Epae Rd 06 8554878 |
| Wanstead | 2813331E 6111065N | Strewn boulders right down through valley. Coral and bioclastic rich facies. | Tim Hodge 2413 Porangahau Rd 06 8554841 |
| Wilder Road WLD | 2806268E 6102668N | Small zones of boulders throughout a back paddock, possible oil seep and further boulders on ridge above paddock. Fossil poor, but thrombolites are abundant. | Rod and Emma Bremer Wilder Rd, Porangahau 06 8555370 |

Appendix A4.2 Abbreviations used in the Thesis (in alphabetical order).

| Code | Full description |
|--------------------------------|--|
| Seep-carbonate deposits | |
| BXH | Bexhaven, northern seep-carbonate site |
| BPL | Builders Pencil, northern offshore sampling area |
| HAU | Haunui, southern seep-carbonate site |
| KKH | Karikarihuata, northern seep-carbonate site |
| MNL | Moonlight North, northern seep-carbonate site |
| MOD | Modern sample group |
| NGW | Ngawaka, southern seep-carbonate site |
| RGN | Rock Garden, southern offshore sampling area |
| TRH | Turihaua, northern seep-carbonate site |
| TTN | Totaranui, northern seep-carbonate site |
| TWP | Tauwhareparae, onshore sampling area and samples |
| UGH-n | Ugly Hill North, southern seep-carbonate site |
| UGH-s | Ugly Hill South, southern seep-carbonate site |
| WAN | Wanstead, southern seep-carbonate site |
| WLD | Wilder Rd, southern seep-carbonate site |
| WPU | Waipu, northern seep-carbonate site |
| WPR | Waapiro Stream, northern seep-carbonate site |
| Miscellaneous | |
| BSR | Bottom simulating reflector |
| GHSZ | Gas hydrate stability zone |
| ROV | Remoted operated vehicle |
| Laboratory Techniques | |
| CL | Cathodoluminescent light |
| PPL | Plane polarised light |

Appendix A4.3 Abstracts from presenting some data from this thesis.

Ewen, S.; Campbell, K.; Nelson, C.; Hood, S.; Francis, D. 2007: Petrology of some Miocene cold seep limestones in Raukumara Peninsula, East Coast Basin: Geologic evidence for past seabed hydrocarbon seepage. Geological Society of New Zealand Miscellaneous Publication 123A: 47.

Ewen, S.; Nelson, C.; Hood, S.; Campbell, K.; Orpin, A. 2008: Petrology of some modern and ancient cold seep-carbonates, East Coast Basin, New Zealand. Geological Society of New Zealand Miscellaneous Publication 124A: 258.
[<http://www.victoria.ac.nz/geosciences08/symposia.html>]

Hood, S.; Nelson, C.; Campbell, K.; Ewen, S.M. 2008: Insights into paragenetic complexities within Miocene hydrocarbon seep limestones in East Coast Basin, New Zealand. Geological Society of New Zealand Miscellaneous Publication 124A: 265.
[<http://www.victoria.ac.nz/geosciences08/symposia.html>]

PETROLOGY OF SOME MIOCENE COLD-SEEP LIMESTONES IN RAUKUMARA PENINSULA, EAST COAST BASIN: GEOLOGIC EVIDENCE FOR PAST SEABED HYDROCARBON SEEPAGE

**Sarah Ewen¹, Kathleen Campbell², Campbell Nelson¹, Steven Hood¹
& David Francis³**

Cold seeps mark sites of focused fluid migration and subsequent expulsion at the sea floor. Often these fluids are rich in hydrocarbons such as methane. Anaerobic oxidation of methane (AOM) acts as a major biogeochemical driving force behind carbonate precipitation at seeps sites and is responsible for the presence of chemosynthesis-based communities that thrive in such environments. The ensuing biological activity and precipitation of methane-derived authigenic carbonate (MDAC) at seep sites, results in chemoherm build-ups, which upon burial may be preserved in the rock record as a unique variety of limestone.

In recent years, ancient seep limestones have been increasingly reported, many of which were originally misinterpreted, and their identification may be aided by recognising diagnostic characteristics of modern MDACs. Features include the precipitation of carbonate in a variety of morphologies (e.g., crusts, pillars, slabs, pavements and blebs), mineralogies and crystal fabrics, very light carbon isotopic signatures, and assemblages of unusual chemosynthesis-based biota.

In the Raukumara Peninsula of North Island, several occurrences of discrete limestone bodies are known to be enclosed within deep-water mudstones of Miocene age. While their previous interpretation has been inconclusive it is now apparent that many of the anomalous features in these limestones are consistent with an MDAC origin as exemplified by modern seeps. Reconnaissance field and petrologic studies at three of the limestone localities (Rocky Knob, Karikarihuata and Tauwhareparae) demonstrate that rapid vertical and lateral changes in lithofacies occur both on a macro- and microscopic scale, likely reflecting the dynamic nature of fluid ascent and expulsion at the sea floor and the subsequent evolution of the seep system as a whole. Early petrographic results reveal a complex diagenetic history involving brecciation, veining and multi-phase carbonate precipitation of isopachous fibrous aragonite, calcitic spar and micrite cements. Ongoing more detailed petrological and geochemical analysis of the limestones should enable an assessment of the type and origin of migrating fluids, the evolving nature of the fluid migration pathways, and the changes in fluid dynamics which result from carbonate precipitation and the consequent restriction of fluid expulsion.

This study is part of a wider collaborative project examining the occurrence of cold seep systems in North Island. It aims to construct a conceptual model of seabed fluid seepage during the Neogene, and ultimately apply the results to modern fluid escape along the Hikurangi Margin, and to evaluate implications for the East Coast Basin petroleum system.

PETROLOGY OF SOME MODERN AND ANCIENT COLD SEEP-CARBONATES, EAST COAST BASIN, NEW ZEALAND

**Sarah Ewen¹, Campbell Nelson¹, Steven Hood¹, Kathleen Campbell²
& Alan Orpin³**

Cold seeps mark areas of focussed methane rich fluid expulsion at the sea floor. They correspond to oases of diverse biological, chemical and geological processes, including common precipitation of carbonates from the interaction of hydrocarbon fluids with a consortium of methanotrophic bacteria and archaea.

This study is the first detailed petrographic analysis of New Zealand's cold seep-carbonates. The inclusion of both modern and ancient samples into the study allows a comparison on the effect of early diagenetic influences and overprinting of fabrics in the carbonates. Ancient samples come from Tauwhareparae, a moderate sized, middle Miocene (Lillburnian) carbonate mound 70 km inland from Tolaga Bay in East Coast Basin. Modern samples are sourced from Ritchie Ridge on the Hikurangi Margin (NIWA Collection: Tangaroa Cruise, TAN0616).

The seep carbonates range from fossil absent to fossil rich, where they include chemosynthetic species of Bathymodioline mussels and Vesicomyid clams and varying amounts of planktic and benthic foraminifera. The Tauwhareparae deposit is especially fossil rich, with abundant mussels and worm tubes. Various burrowing and boring fabrics are conspicuous in the mound-like carbonates.

Laboratory analysis of the carbonate samples included standard and cathodoluminescent petrography, carbonate percentage determinations, XRD mineralogy, and stable carbon ($\delta^{13}\text{C}$) and oxygen ($\delta^{18}\text{O}$) isotopes.

Petrographic fabrics are often complex and there is much variation between and within samples, highlighting their dynamic paragenesis of the seep carbonates. Not uncommonly their evolution has involved several phases of carbonate-siliciclastic sedimentation, carbonate precipitation and cementation, fracturing or brecciation, fluid injection and veining, reworking and resedimentation, and diagenetic alteration or replacement.

Mineralogically, aragonite is the dominant carbonate species in both the modern and ancient samples, with subordinate calcite. Dolomite is also common in several of the modern samples, possibly due to sea floor exhumation of former subsurface deposits.

Isotopically, the carbonates fall within the range $\delta^{13}\text{C}$ -27 to -45‰ PDB, supportive of formation from thermogenic methane, which is characteristic of many seep carbonates. Positive $\delta^{18}\text{O}$ values to suggest the formation and disassociation of gas hydrates may have been implicated in the precipitation of the carbonates.

INSIGHTS INTO PARAGENETIC COMPLEXITIES WITHIN MIOCENE HYDROCARBON SEEP LIMESTONES IN EAST COAST BASIN, NEW ZEALAND

Steven Hood¹, Campbell Nelson¹, Kathleen Campbell² & Sarah Ewen¹

Miocene cold seep limestones in East Coast Basin forearc, New Zealand, archive paleohydrocarbon seafloor seepage, and represent a previously little-documented, volumetrically small but unique and important carbonate rock type in the New Zealand stratigraphic record. They occur in two main geographic areas, one northwest of Gisborne in Raukumara Peninsula and the other east of Dannevirke in southern Hawke's Bay. The limestones are hosted within Miocene slope mudstones and are commonly characterised by chemosynthesis-based fossils, including lucinid, vesicomyid, and/or mytilid bivalves, together with non-chemosynthetic corals, gastropods, brachiopods, and worm tubes.

In outcrop the seep limestones are commonly rather bland in appearance, yet extraordinary once slabbed revealing a truly complex array of textures, fabrics, and mineralogies. Fossils, along with variable amounts of siliciclastics, are cemented by typically pristine methane-derived authigenic carbonates (MDACs) with minimal alteration and distinctly negative $\delta^{13}\text{C}$ isotopic signatures (-20 to -30‰ PDB) indicative of formation via microbially mediated, anaerobic oxidation of methane (AOM). Major textural complexities arise through a combination of sequential mineralisation episodes punctuated by multiple hydrofracturing and brecciation, recementation, and local corrosion events, which collectively dramatically altered rock fabrics and poroperm characteristics.

A host of primary and secondary mineral types formed during early (at or near seafloor) through later (burial) diagenetic phases. Many important spatial and temporal relationships are emerging despite the overwhelming fabric complexity, enabling recognition of a broadly based paragenetic sequence. Generally dark cathodoluminescent, early authigenic peloidal aragonitic micarb ("micrite") is associated with seepage inception and diffuse flow, while radiating acicular to botryoidal isopachous bands of often hydrocarbon-bearing inclusion-rich aragonite alternating with laminated microbial fabrics and digitate thrombolites formed during more advective fluid flow. Vacated worm tubes provided additional preferential conduits for aragonite mineralisation. The bacterially mediated sea bed diagenesis resulted in early lithification and local firm or hardground formation, as evidenced by burrows and bores.

Once in the burial realm, later diagenetic precipitates developed more slowly from diffuse flow forming generally brightly luminescent Mn-rich calcitic phases and recrystallised micarb fabrics, coarse variably coloured and complexly zoned red through purple late stage dentate/equant carbonate minerals often infilling skeletal pores and corrosion cavities. Authigenic quartz and possibly barite also occur.

